Report 1896

DEPARTMENT OF THE NAVY

HYDROMECHANICS

o

AERODYNAMICS

o

STRUCTURAL MECHANICS

o

APPLIED MATHEMATICS

o

ACOUSTICS AND VIBRATION

A STUDY OF THE BULK CAVITATION CAUSED BY UNDERWATER EXPLOSIONS

by

R. R. Walker and J. D. Gordon

Distribution of this document is unlimited.

STRUCTURAL MECHANICS LABORATORY
UNDERWATER EXPLOSIONS RESEARCH DIVISION
PORTSMOUTH, VIRGINIA

RESEARCH AND DEVELOPMENT REPORT

35

September 1966 Report 1896

A STUDY OF THE BULK CAVITATION CAUSED BY UNDERWATER EXPLOSIONS

by

R. R. Walker and J. D. Gordon

September 1966

Report 1896
DASA Web No. 14.055

TABLE OF CONTENTS

LIST OF TABLES

LIST OF FIGURES

ABSTRACT

The detailed theoretical models of bulk cavitation derived in studies conducted by the Engineering-Physics Company of Rockville, Maryland, under contract of the Office of Naval Research and bulk cavitation data obtained from tests conducted by the David Taylor Model Basin are used to develop simple calculations for predicting bulk cavitation phenomena. Several reasonable mathematical approximations describing these phenomena are derived. The mathematical treatments have, as a foundation, concepts derived in the theoretical study; however they are modified and simplified in this study where experimental results indicate that such modifications and simplifications are justified. With these approximate mathematical models, estimations can be made of the boundaries, depths and durations of cavitation as well as the motion of the water surface for a wide variety of conditions without employing a computer.

Other findings derived from the experimental test data are: (1) for the closer regions extending even beyond the ring of first impact, the bubble expansion causes the water below the closure depth to rise and thus causes closure to occur at a much earlier time, since the layer does not have to fall to its original position; (2) when the draft of a floating structure is small compared to the thickness of the water layer, the bodily motions of that structure are essentially the same as the water layer, and these motions are relatively independent of the cross sectional shape of the structure; and (3) negative reflections from the bottom strong enough to produce cutoff are quite possible even with relatively large pressure amplitudes, and are capable of considerably modifying the region of cavitation.

ADMINISTRATIVE INFORMATION

The work described in this report was sponsored under DASA Web No. 14.055. The detailed theoretical models of bulk cavitation derived in studies conducted by the Engineering-Physics Company, Rockville, Maryland, for the office of Naval Research under Contracts NONR-3389(00) and NONR-3709(00) and bulk cavitation data obtained from tests conducted by David Taylor Model Basin under Subproject S-F013 04 03, Task 1755, are used to develop simple calculations for predicting bulk cavitation phenomena.

INTRODUCTION

When the shock wave produced by an underwater explosion impinges upon a boundary, such as the top surface, having a lower specific acoustic impedance than the characteristic impedance of the water, tensile reflections are generated which can lead to rupture of the water throughout a very large volume. This process of rupture is referred to as bulk cavitation of the water. The response of surface ships to underwater explosions of large charges is greatly influenced by the bulk cavitation occurring under the water surface. A complete understanding of the shock motions experienced by a surface ship under such attacks requires a knowledge of the phenomena involved in the bulk cavitation.

To advance the knowledge concerning these phenomena, the Underwater Explosions Research Division of the David Taylor Model Basin conducted a series of explosions tests in the Chesapeake Bay during June, 1962. Concurrent with the planning for this test series a theoretical study of the bulk cavitation phenomena was also conducted.[1,2] Prior to these two studies, one primarily experimental and the other theoretical, little emphasis had been placed on the understanding of these particular phenomena.

This report describes the experimental investigation and presents an analysis of the data obtained from the tests based on the theoretical model which was evolved from the theoretical study. The theoretical study provides a comprehensive description of the formation and collapse of the cavitated regions. The mathematical treatments comprised in the analysis of this report have, as a foundation, the concepts presented in the theoretical study but contain modifications and simplifications where the experimental results indicate that such modifications and simplifications are justified. With these approximate mathematical models, estimations for other explosive weights and test geometries can be made of the boundaries, depths, and durations of cavitation as well as of the motion of the water surface without resorting to the use of a computer. A procedure not requiring a computer is particularly desirable for field work where such calculations and estimations must be made at the test site.

[1] References are listed on page 24.

THE EXPERIMENTAL PROCEDURE

TEST CONFIGURATION

The bulk cavitation series comprised eight explosion tests. The principal charge detonated during each of these tests was 10,000 lb of HBX-1 in a cylindrical container having a height to diameter ratio of one. Four of these charges were detonated at a depth of 50 ft, three at a depth of 100 feet. One, because of a premature failure of its supporting float, was fired while on the bottom; the data from this test were not considered in the analysis and therefore no further reference is made to it.

These charges were fired against an anchored test array attached to the starboard bow of the UEB-1, a floating test facility of the David Taylor Model Basin. This array, shown schematically in Figure 1, was composed primarily of eight instrumented stations at 100-ft intervals on the water surface in a direct line between the charge and the UEB-1. The burst depths and horizontal ranges of the principal charge from its nearest instrumented station (Station 1) are given for each test in Table 1. These were the primary parameters varied through the test series.

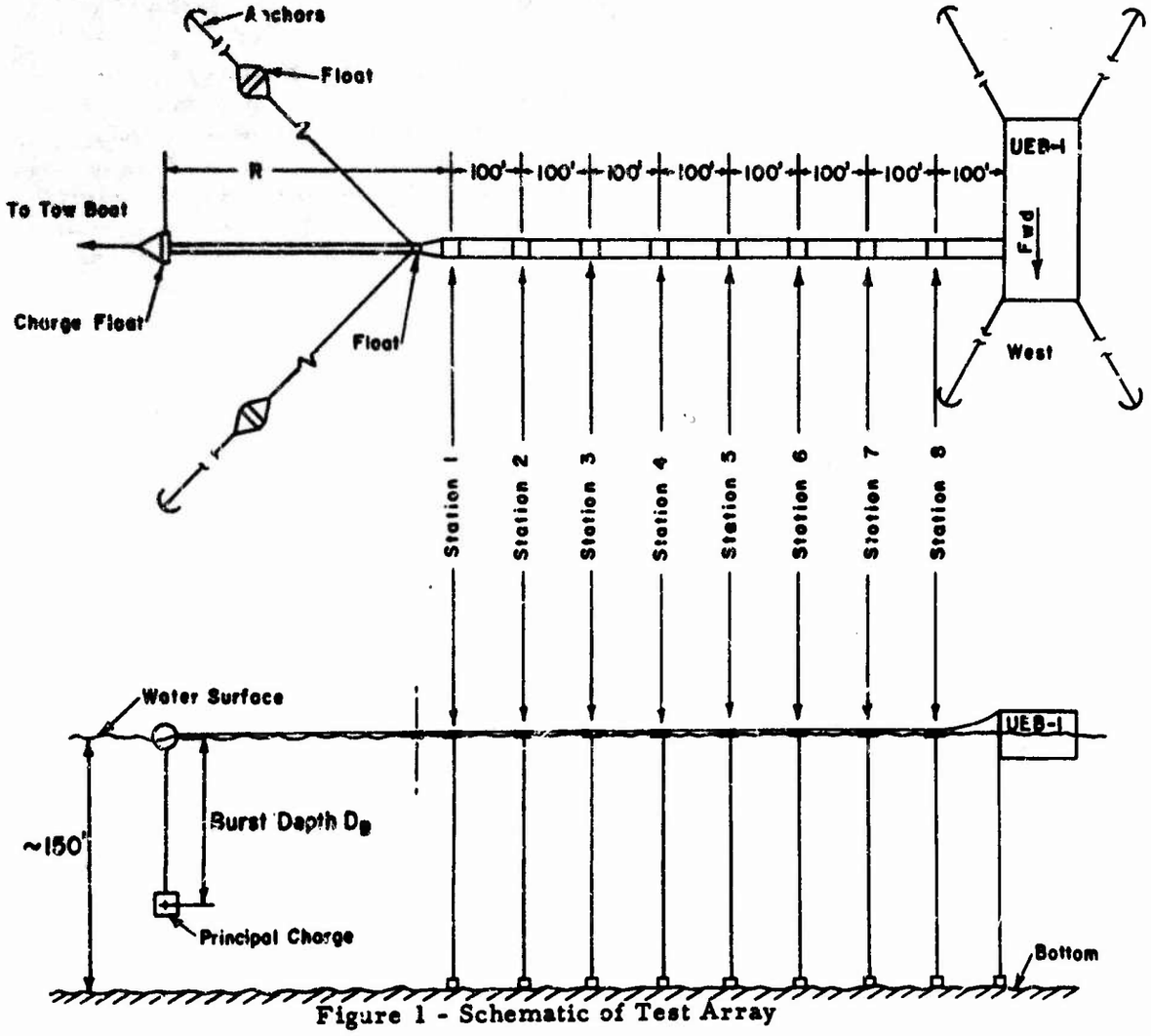

Figure 1 - Schematic of Test Array

TABLE 1
Test Geometries

UERD Shot No.	Test No.	Burst Depth (D_B) (ft)	Horizontal Standoff to Station 1 (R) (ft)
5440	1	50	400
5446	2	50	1200
5449	3	100	400
5451	4	50	600
5452	5	100	1200
5455	6	50	200
5457	7	100	200

Work platforms which also supported the instrumentation cables were located at each of the instrumented stations. These platforms were constructed so as to provide no contact with the water surface except on the two sides parallel to the test array. Thus the water surface motions near the center of the platforms were not significantly influenced by the platforms themselves. The interiors of these platforms were therefore suitable for mooring instrumented targets.

Two types of targets were used within the platforms. One type consisted of ballasted wooden models of ship sections; the other type was a very light wooden float having a draft of only 2 or 3 inches. One of the light wooden floats within a work platform is shown in Figure 2; it is being hoisted for placement in the water.

Figure 2 - Light Wooden Float Within Work Platform

One of the ship models was of an EC-2 type hull in way of the engine room. This model, of course, had an essentially rectangular cross section as can be seen in Figure 3. The other model corresponded to a section very far forward on a CGN hull, and had a very definite V-shaped cross section. Both models were about 6 ft long and the wooden float was about 6 ft square. Thus all targets had very nearly the same surface area, although they differed greatly in cross section. All targets were held in place within the platforms during the tests only with very light elastic cords so that they might move freely and independently of the platforms.

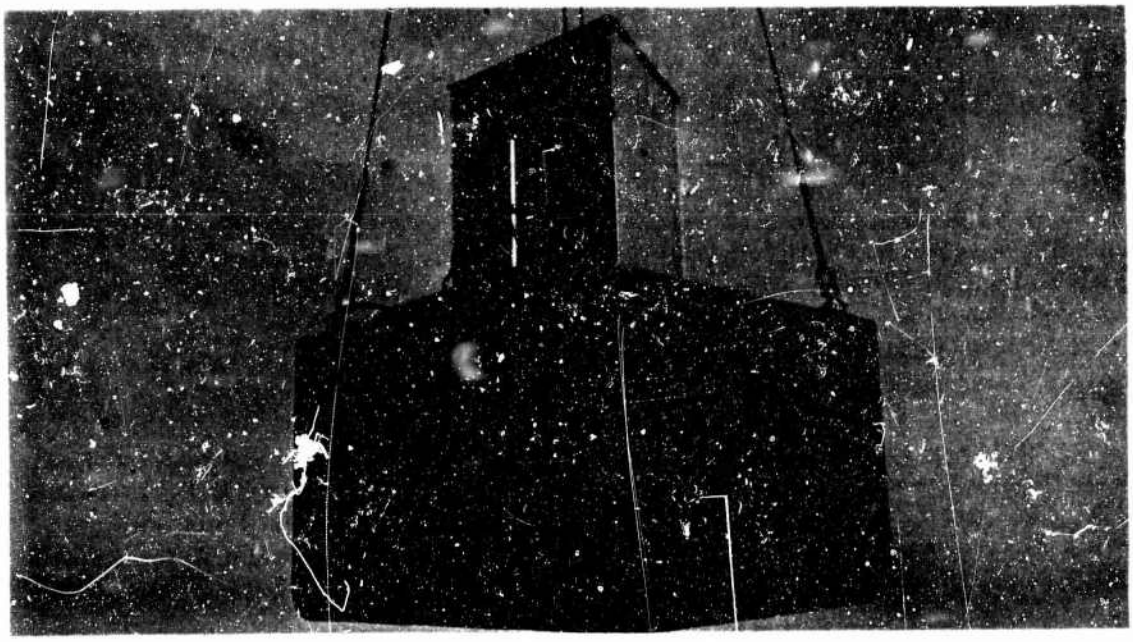

Figure 3 - The EC-2 Model

The entire array in position, as seen from the UEB-1, is shown in Figure 4. The plumes resulting from two of the tests are shown in Figures 5 and 6.

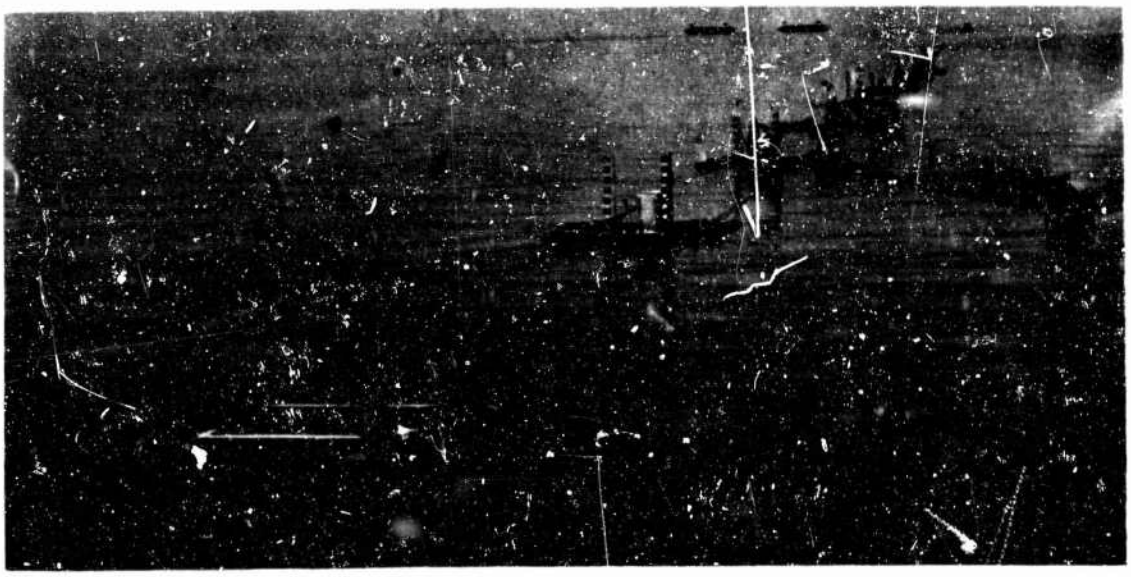

Figure 4 - View of Test Array from UEB-1

Figure 5 – Plume of 50-Ft Burst

Figure 6 - Plume of 100-Ft Burst

INSTRUMENTATION

In this test series emphasis was placed on the measurement of underwater pressure. At each of the test stations, supported by the work platform, a heavily weighted cable was extended almost to the bottom. From 2 to 10 pressure gauges (PE) were distributed along each of these 8 cables to provide a total of 48 pressure measurements for each test.

The pressure measurements were designed to perform a dual purpose. In addition to providing pressure versus time histories at each location which resulted from the principal charge, they also indicated the pulses resulting from firing small signal charges during each test. A signal charge capable of being detonated at a precise delay interval after the detonation of the principal charge was located near the end of the cable from each even-numbered station. These signal charges, which had weights ranging from 10 lb to 2 oz, were selected to produce at the gauges of interest peak pressures about 10 percent of that produced by the principal charge. Each signal charge was used only with the pressure gauges at the adjacent lower-numbered station and was timed to provide a pressure pulse at that station at the time cavitation was presumed to be most severe. The concept behind the use of the signal charges was that since the propagation velocity should be different in the cavitated region, the arrival time of the signal at each of the pressure gauges, if indeed the signal penetrated that far, should indicate the presence or absence of cavitation in that region.

The locations of each of the pressure gauges and signal charges are given in Table 2. The weights of the signal charges and the time delays between the detonation of the principal charge and that of each of the signal charges are given in Table 3.

TABLE 2

Pressure Gauge and Signal Charge Locations

Test 1								
Depth*	Station 1	Station 2	Station 3	Station 4	Station 5	Station 6	Station 7	Station 8
2	PE-1		PE-11		PE-21		PE-31	
4	PE-2		PE-12		PE-22		PE-32	
5	PE-9	PE-41	PE-19	PE-43	PE-29		PE-39	
8	PE-3		PE-13		PE-23		PE-33	
10						PE-45		PE-47
15	PE-4		PE-14		PE-24		PE-34	
30	PE-5		PE-15		PE-25		PE-35	
40	PE-10	PE-42	PE-20		PE-30		PE-40	
45				PE-44				
50						PE-46		PE-48
60	PE-6		PE-16		PE-26		PE-36	
90	PE-7		PE-17		PE-27		PE-37	
120	PE-8	Signal Charge #1	PE-18		PE-28		PE-38	
130				Signal Charge #2		Signal Charge #3		Signal Charge #4

Tests 2 - 7								
Depth*	Station 1	Station 2	Station 3	Station 4	Station 5	Station 6	Station 7	Station 8
4	PE-2		PE-12		PE-22		PE-32	
15	PE-4		PE-14		PE-24		PE-34	
30	PE-5		PE-15		PE-25		PE-35	
45	PE-10	PE-41	PE-20	PE-43	PE-30	PE-45	PE-40	PE-47
60	PE-6		PE-16		PE-26		PE-36	
75	PE-9		PE-19		PE-29		PE-39	
90	PE-7	PE-42	PE-17	PE-44	PE-27	PE-46	PE-37	PE-48
105	PE-1		PE-11		PE-21		PE-31	
120	PE-8		PE-18		PE-28		PE-38	
130	PE-3	Signal Charge #1	PE-13	Signal Charge #2	PE-23	Signal Charge #3	PE-33	Signal Charge #4

*Feet below water surface.

TABLE 3

Signal Charge Data

Signal Charge No.		1		2		3		4	
UERD Shot No.	Test No.	Weight (lb)	Delay* (msec)	Weight (lb)	Delay* (msec)	Weight (lb)	Delay* (msec)	Weight (lb)	Delay* (msec)
5440	1	1.0	87.78	1.0	89.38	0.125	151.4	0.125	186.7
5446	2	0.125	223.5	0.125	264.8	0.125	305.4	0.125	344.5
5449	3	10.0	66.12	1.0	106.4	1.0	145.1	1.0	186.1
5451	4	1.0	105.8	1.0	144.5	1.0	185.9	0.125	225.6
5452	5	0.125	226.4	0.125	265.8	0.125	305.5	0.125	344.8
5455	6	10.0	30.41	10.0	64.42	1.0	103.1	1.0	142.0
5457	7	10.0	30.31	10.0	64.79	1.0	103.4	1.0	142.7

*Time delay between detonation of principal charge and signal charge.

Figure 7 - Subsurface Unit

In addition to the pressure instrumentation at each station, each of the models and floats contained instrumentation designed to measure its motions. Each of these targets contained a velocity meter (VM) and a seismic displacement gauge (SD) for measuring the absolute bodily velocity and displacement histories respectively. Also, during some tests, in an effort to determine layer motions below the surface, a reinforced flat plate was suspended at certain stations about 12 ft below the surface from a pipe elastically supported from the float above. This subsurface unit, shown in Figure 7, had the same area as the wooden float and was fairly light in weight. This unit had a relative displacement gauge (MD) to measure the relative displacement between the surface float and the subsurface unit and also a velocity meter for measuring the absolute vertical velocity of the subsurface unit.

A completely instrumented float is shown in position for testing in Figure 8. All surface motion gauge locations are given in Table 4.

All the transducers were electromechanical in nature and produced electrical signals as outputs. These signals were transmitted by means of electrical cables back to the recording centers located aboard the UEB-1. All gauges with the exception of 16 pressure gauges were recorded on magnetic tape; these were recorded on 35mm film by drum cameras photographing cathode ray oscilloscopes.

DATA OBTAINED

The measurement effort was successful; satisfactory records were obtained for nearly all of the instruments used in each test. The interest of the study of this report is fairly specific. However, the experimental data represent a very comprehensive documentation of the pressure field and surface phenomena for the geometries studied and since they have not been published elsewhere, the majority of them are presented in the appendix of this report.

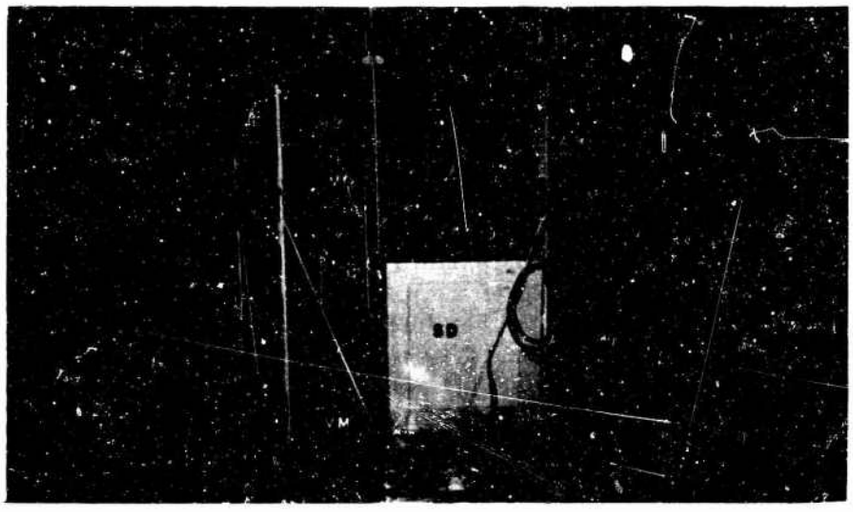

Figure 8 - An Instrumented Float in the Test Array

TABLE 4
Surface Motion Gauge Locations

Gauge Designation	Station	Location
VM-1	2	Float 1
VM-2	3	Float 2
VM-3	4	Float 3
VM-4	6	Float 4
VM-5	7	Float 5
VM-6	1	EC-2 Model
VM-7	5	CGN Model
VM-16	1	EC-2 Model
VM-17	5	CGN Model
SD-1	2	Float 1
SD-2	3	Float 2
SD-3	4	Float 3
SD-4	6	Float 4
SD-5	7	Float 5
SD-6	1	EC-2 Model
SD-7	5	CGN Model
MD-1	2	Float 1
MD-2	3	Float 2
MD-3	4	Float 3
MD-4	6	Float 4
MD-5	7	Float 5

DATA ANALYSIS

For the purpose of analysis, the data from all shots of the same burst depth but varying ranges were treated as if they had come from a single explosion with a longer array and more gauges. Agreement evidenced among the various test data obtained at comparable locations validates this approach.

BOUNDARIES OF THE CAVITATED REGION

Examination of the pressure histories for both the 50-ft and 100-ft bursts shows that in all cases the bottom reflections were negative. This unexpected behavior was due to the particular bottom consistency which probably was somewhat gaseous as a result of the decomposition of organic matter trapped in the mud. Thus cutoff resulted from the bottom as well as from the top surface. This fact presents an additional complication to the analysis in that this bottom reflection can also cause cavitation. With two possible sources for cavitation, the effects of each must be isolated and attributed to the proper source wherever possible. Therefore, before attempting any further interpretation of the pressure histories, the theoretical extent of cavitation for the charge size and test geometries used in the actual tests is discussed, considering a negative reflection from the bottom as well as the surface. Linear shock-wave propagation theory and surface cutoff time derived from the plane-wave approximation are used in the mathematical analysis.

Theoretically Derived Cavitation Boundaries

Figure 9 shows a hypothetical pressure history at the borderline depth (x) between cavitated water and uncavitated water. At this depth surface cutoff

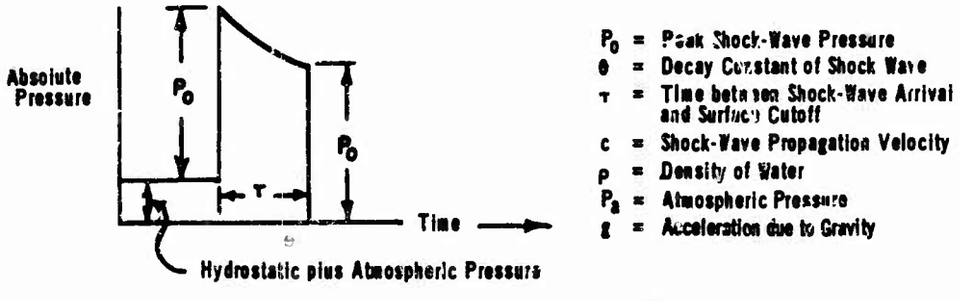

Figure 9 - Hypothetical Pressure History

must drop the pressure to essentially zero (vapor pressure) if the water is considered to be unable to support tension. This mathematically stated for reflection from the top surface is:

$$P_0 - P_0 \exp(-\tau/\theta) = \rho g x + P_a .$$

For a plane wave making an angle β with the surface as in Figure 10,

$$\tau = \frac{2x \cos\beta}{c} .$$

Therefore

$$\frac{P_o}{\rho g}\left[1 - \exp\left(-x/k\right)\right] = x + \frac{P_2}{\rho g}$$

where

$$k = \frac{c\theta}{2\cos\beta} .$$

The values for P_o and θ were obtained from a nomogram for HBX-1,[3] and $P_o/(\rho g)$ and k were calculated at various standoffs for each of the two bursts. The equations were then solved for (x) at each standoff. The boundaries thus derived are shown in Figures 11 and 12 for the 50-ft and 100-ft bursts respectively.

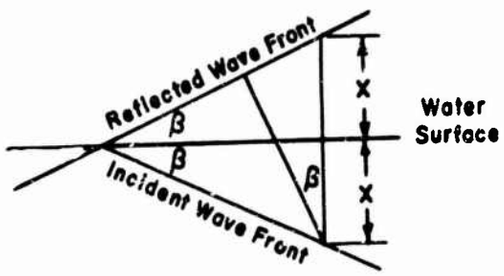

Figure 10 - Nomenclature of
Surface Reflections

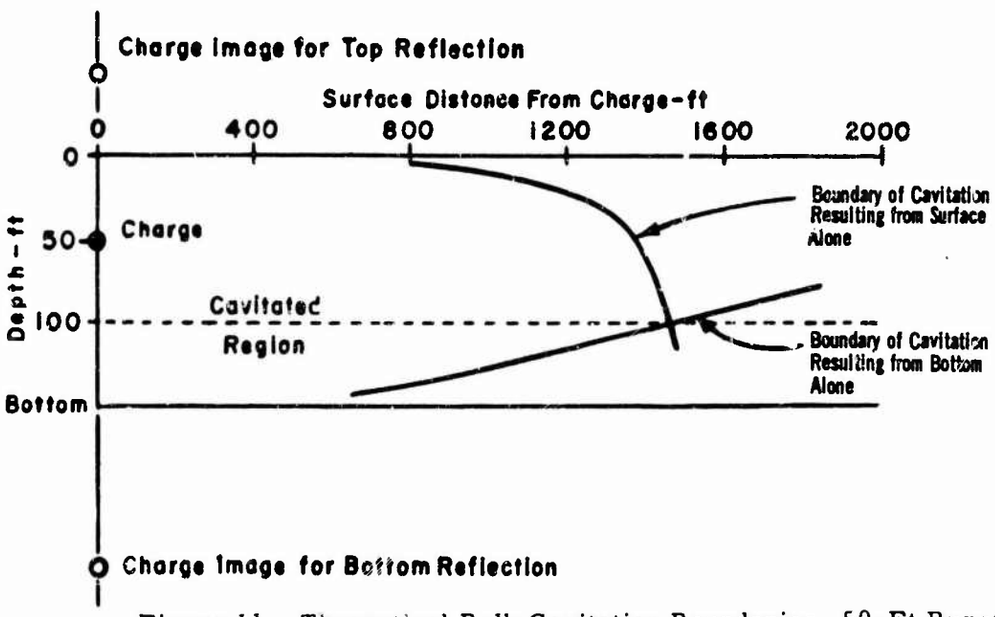

Figure 11 - Theoretical Bulk Cavitation Boundaries, 50-Ft Burst

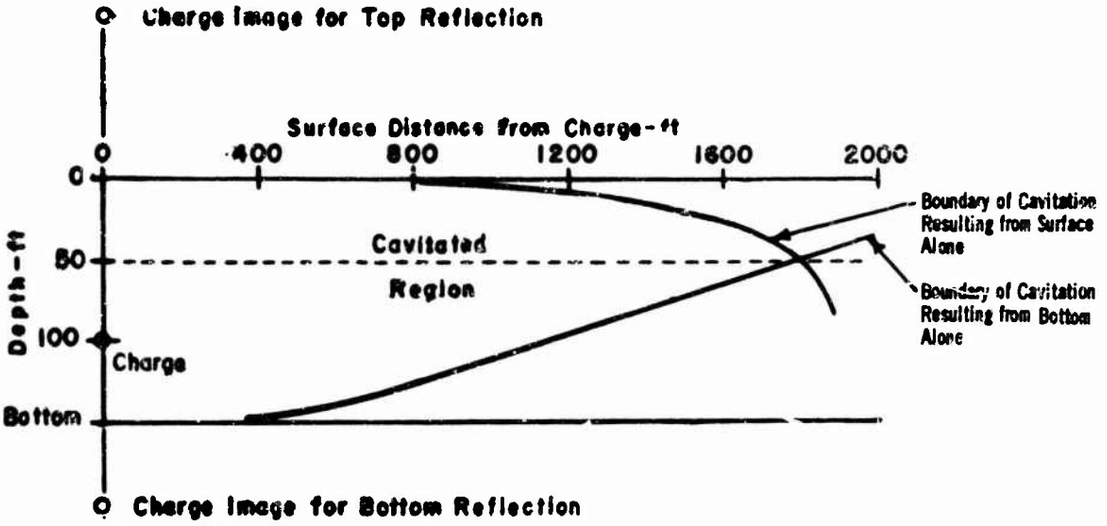

Figure 12 - Theoretical Bulk Cavitation Boundaries, 100-Ft Burst

The theoretical cavitation boundary which would result from the negative bottom reflection alone is obtained if (x) is measured from the bottom, which is 150-ft deep, and β is considered to be the angle the plane wave makes with the bottom. If d_w is the water depth, the equation previously derived now becomes

$$\frac{P_o}{\rho g}\left[1 - \exp\left(-x/k\right)\right] = \frac{P_a}{\rho g} + d_w - x$$

provided we assume full amplitude reflection from the bottom. The boundaries derived from this equation using the same procedures as before are also plotted in Figures 11 and 12.

Figures 11 and 12, therefore, are graphs of theoretical cavitation boundaries from surface cutoff and from bottom cutoff for each of the two experimental burst depths. The dotted lines in the two figures are drawn halfway between the two image charges for each burst depth and represent lines of demarcation of influence. Above these lines, cutoff occurs first from the surface; below the lines, cutoff occurs first from the bottom. Along the lines, the reflected waves from the surface and bottom arrive simultaneously.

Consider first the behavior of a column of water in the region between the charge and the intersection of the two boundary curves. As the reflected wave from the surface moves down the water column, the water is cavitated and the water particles are kicked off in the upward direction in the region above the demarcation lines. Conversely, the water below the line is being kicked downward by the negative reflection from the bottom. When the reflected wave fronts arrive simultaneously at the demarcation line, each can propagate no further since each has reached water already in cavitation. Since the water particles on either side of the dotted line are moving away from those on the other side, cavitation along the line should be quite pronounced. Thus in the region between the charge and the intersection of the two curves, little interaction would be expected between the cavitation resulting from the surface reflection and that from the bottom reflection. In this region then, cavitation effects on or near the top surface would not be significantly influenced by the fact that the bottom reflections are negative.

Consider now the behavior of a water column at ranges beyond the intersection of the two curves. As the surface reflection moves down the water column and the bottom reflection moves up the water column no cavitation results because of their respective cutoffs until the simultaneous arrival of both reflections at the demarcation line. Since at this time the water on neither side of the line is cavitated, the two reflected wave fronts propagate through each other causing two cutoffs, one from the surface and one from the bottom. The two cutoffs reinforce each other and thus extend considerably the area in which cavitation can exist.

Experimentally Derived Cavitation Boundaries

The pressure histories obtained for each of the two bursts depths are given in Appendix A. Although these histories indicate that the pressure at surface cutoff sometimes goes slightly below absolute zero, the accuracy of the measurement does not allow the conclusion to be drawn that the water may withstand tension. A judgment of the existence or nonexistence of cavitation at border depths is made by considering the flatness of the pressure history immediately after cutoff as well as the zero absolute pressure condition; flatness is an indication that no disturbance is being transmitted to the gauge and therefore that cavitation does exist. The cavitation boundaries determined in this manner are presented for each of the burst depths in Figures 13 and 14. The experimental data are shown as vertical lines on these plots to indicate the uncertainty within which the boundary could be determined from the pressure records.

In the theoretical study, cavitation from the bottom and top are treated separately; thus the superposition of both cavitation sources are not taken into consideration. Consequently, predictions are valid only in the regions where interaction does not occur. Since the interaction is observed at 800 ft for the bursts at the 50-ft depth and 1000 ft for the bursts at the 100-ft depth, the predictions based on the models apply up to these ranges. Beyond these ranges, bottom effects become influential and introduce noticeable deviations.

At ranges beyond 800 ft for bursts at the 50-ft depth and 1000 ft for bursts at the 100-ft depth, the two cutoffs predicted in the preceding section are evident on the pressure records. Reinforcement of the two cutoffs opens the boundary curves and extends the range of cavitation considerably beyond the last range at which data are available. At closer ranges than these only the one cutoff from the surface or bottom can be found, and the border depth separating surface and bottom cavitation occurs at about the predicted depth. Furthermore, in most cases the pressures from the signal charges propagate through the cavitated water and are seen on the pressure histories except at about 100 ft deep and 50 ft deep for the 50-ft and 100-ft bursts depths respectively.

Figures 13 and 14 indicate that if reinforcement of the two cutoffs did not begin to take effect, the upper and lower boundaries would apparently meet at about 900 ft from the 50-ft bursts and 1100 ft from the 100-ft bursts. These ranges are considerably less than predicted.

The discrepancy between the theoretically predicted cavitation boundaries and those obtained from the pressure histories can be attributed to several effects, each of which tends to indicate smaller extents than would be predicted. First, the depths experimentally determined are those at which cavitation almost certainly exists, since it would be very difficult to determine that an area is just within a cavitated

region. By the time cavitation can be recognized as such on a pressure record, it probably would be well within the region actually cavitated. Also the theoretical predictions are based on the premise that the sea water can support no tension. Any tensile strength the water possesses would tend to reduce the extent of the cavitated region to less than that predicted. Other factors ignored in the theoretical treatment are the possibilities of incomplete reflection from the surfaces and the attenuation of the reflected wave due to the greater distance traveled, each of which would also tend to reduce the actual extent of cavitation.

The experimental data, therefore, support the conclusion that in the case of the bursts 50 ft deep, cavitation phenomena occurring at depths less than 100 ft and at ranges less than 800 ft are adequately described by considering reflections only from the top surface. Similarly, in the case of the bursts 100 ft deep, phenomena occurring at depths less than 50 ft and at ranges less than 1000 ft are adequately described by considering reflections only from the top surface. Outside these regions, bottom reflections are quite influential and can cause appreciable deviations.

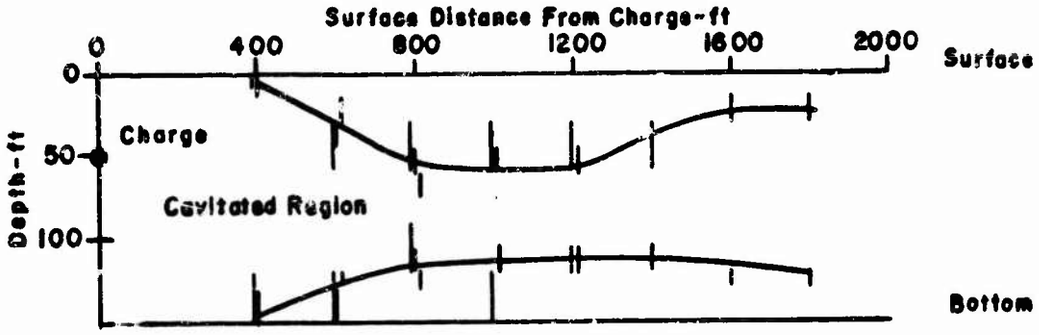

Figure 13 - Bulk Cavitation Boundaries Determined from Experimental Data, 50-Ft Burst

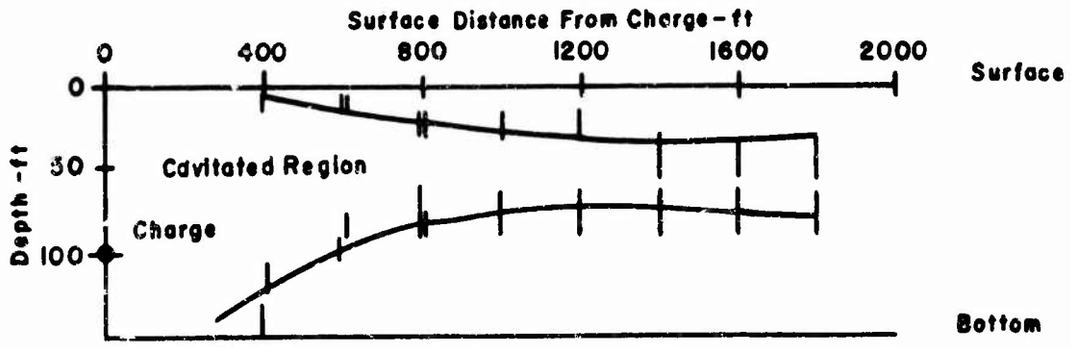

Figure 14 - Bulk Cavitation Boundaries Determined from Experimental Data, 100-Ft Burst

CLOSURE OF THE CAVITATION

The records of the velocity meters and displacement gauges on the wooden floats give surface velocity and surface displacement histories for various ranges for both burst depths. A comparison of the velocity and displacement records from the CGN and EC2 models with each other and with those from the floats show that the bodily surface effects from cavitation are essentially alike for all; therefore, the analysis treats model data on an equal basis with float data.

In the theoretical study,[1] it was shown that a solid water layer is kicked off above the cavitated region. The resultant motion of this water layer is characterized by a high initial deceleration, which drops off rapidly and approaches a constant value as the water layer increases in thickness from below. Eventually, the velocity of this uncavitated water layer is decreased to zero by the force of atmospheric pressure and gravity: the water layer falls until the time of the closure,* which then imparts a positive change in velocity to the water.

This theoretical model is confirmed by the measurements. Inspection of the surface velocity histories at various ranges from the charge reveals that except for the initial portion of the histories immediately after shock-wave arrival, a fairly constant negative acceleration exists to the time of cavitation closure on practically all the records.

The thickness of the water layer at the time of cavitation closure (depth of closure) may be calculated from the negative acceleration of the water layer at the time of closure. Consider a column of uncavitated water having density (ρ), sectional area (S), and depth (d) with cavitation existing beneath. The force on the water column due to atmospheric pressure (P_a) and gravity (g) is

$$P_a S + \rho S d g.$$

This force must equal the mass of the water multiplied by its downward acceleration, a; therefore

$$P_a S + \rho S d g = \rho S d a$$

or

$$d = \frac{P_a}{\rho(a - g)}.$$

The acceleration of the water layer may be obtained from the negative slope of the velocity history at the time just prior to closure.

The falling water layer must first hit in a ring at some specific distance from the charge and this closure must then propagate inward and outward from there. The nearest instrumented point to this initial closure would show cavitation closure

*Closure, as used in this report, refers to the final impact in a given column of an uncavitated waterlayer upon the water below it, which by that time has also become uncavitated.

disturbance in the shortest time. The time at which cavitation closure occurs at locations to either side of this point of first closure would increase with the distance from the point of first closure.

The rapidity with which the water surface approaches a constant deceleration suggests that the majority of the growth of the water layer thickness is completed shortly after shock-wave arrival. Therefore a good approximation of the layer motion is obtained if the water layer is considered to move with its final thickness for the entire time between shock-wave arrival and closure. These conclusions, reached from an examination of the surface velocity histories, allow relatively simple mathematical relationships to be derived which yield approximate theoretical surface velocity and displacement histories and approximate theoretical cavitation closure depths and times, all of which may be compared with those experimentally measured.

Figure 15 illustrates the approach for obtaining the water column cavitation approximation. To obtain approximate relationships of cavitation from the surface, all water particles in the column are considered to receive an initial velocity at the time of shock-wave arrival at the surface of the column. The magnitude of this velocity is determined by the change in pressure at cutoff at the given particle's depth. Atmospheric pressure is considered to instantly form an uncavitated water layer of depth d, so that the uncavitated water layer is kicked off with an initial momentum equal to the sum of the momenta of the individual particles within it. The entire uncavitated water layer then moves as a single body with a constant negative acceleration resulting from atmospheric pressure and gravity. The individual cavitated particles beneath the uncavitated water layer fall with the acceleration of gravity to their original position and thus end their cavitated state. The deeper water particles have smaller initial velocities than the shallower particles and fall back sooner. Consequently, an uncavitated region builds up from the bottom of the water column. Finally, the uncavitated water built up from the bottom is struck by the falling surface uncavitated water layer and closure occurs.

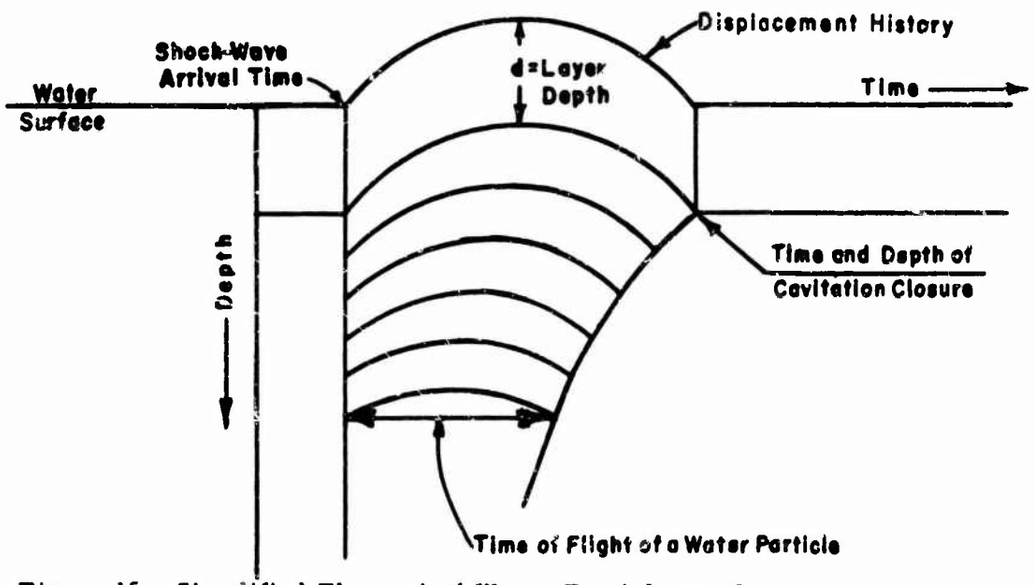

Figure 15 - Simplified Theoretical Water Particle Displacement Histories as a Function of Depth

For the mathematical analysis let:

$\bar{v}$ = Initial surface water layer kickoff velocity

$U(x)$ = Individual cavitated water particle velocity at depth x due to the shock-wave pressure at the time of surface cutoff.

ρ = Density of water, and

d = Thickness of surface water layer or depth of cavitation closure.

Then by equating surface water layer momentum with the sum of the individual momenta of the particles contained therein we obtain

$$d\rho\bar{v} = \int_0^d \rho\, U(x)dx \qquad \text{or} \qquad \bar{v} = \frac{1}{d}\int_0^d U(x)dx. \tag{1}$$

Also let:

P_a = Pressure of the atmosphere

t = Time after shock-wave arrival at the surface of the water column

g = Acceleration due to gravity

$V(t)$ = Velocity of water layer any time after kickoff, and

T_c = Time between shock-wave arrival and cavitation closure.

Then the velocity history of the water layer can be described as follows

$$V(t) = \bar{v} - \left(g + \frac{P_a}{\rho d}\right)t .$$

If such effects as bubble expansion are ignored, at cavitation closure

$$t = T_c \text{ and } V(T_c) = -\bar{v};$$

therefore

$$-\bar{v} = \bar{v} - \left(g + \frac{P_a}{\rho d}\right) T_c \ . \tag{2}$$

Combining Equations (1) and (2), we obtain the following:

$$\frac{2}{d}\int_o^d U(x)dx = \left(g + \frac{P_a}{\rho d}\right) T_c \cdot \tag{3}$$

If we let $V_1(t)$ = Velocity after shock-wave arrival of the cavitated water particles at a depth d directly under the uncavitated surface water layer, the velocity history of this uppermost cavitated water particle is $V_1(t) = U(d) - gt$, and at cavitation closure $t = T_c$ and $V_1(T_c) = -U(d)$.

Therefore

$$-U(d) = U(d) - gT_c$$

or

$$2U(d) = gT_c. \tag{4}$$

Equations (3) and (4) solved simultaneously yield the depth and time of closure.

For a plane wave of velocity c, peak pressure P_o and exponential time constant θ making an angle β with the surface, the change in pressure at cutoff at a depth x from the surface is approximately $P_o \exp[(-2x \cos\beta)/(c\theta)]$ when hydrostatic plus atmospheric pressure is small compared to the shock-wave pressure just prior to cutoff. The cavitated particle kickoff velocity at a depth x from the surface then becomes

$$U(x) = \frac{2P_o \cos\beta}{\rho c} \exp\left(-\frac{2x\cos\beta}{c\theta}\right).$$

Using this particle kickoff velocity, and solving Equations (3) and (4) simultaneously, we obtain

$$\exp(d/k) = 1 + \frac{d}{k} + \frac{P_a}{\rho g k} \quad \text{and} \quad \frac{T_c}{\theta} = \frac{2P_o}{\rho g (k + d) + P_a} \tag{5}$$

where

$$k = \frac{c\theta}{2\cos\beta} \tag{6}$$

Figure 16 provides a quick solution to these equations.

After T_c, the time of flight of the water layer, and $\bar{v}$, the initial kickoff velocity of the uncavitated surface water layer, have been calculated, comparisons may be made between the theoretical velocity histories of the water layer and the actual histories experimentally measured. In addition, h(t), the vertical displacement of the water layer anytime after kickoff, can be calculated from the expression

$$h(t) = \bar{v}t - \frac{1}{2}\left(1 + \frac{P_a}{\rho g d}\right) g t^2 .$$

These calculations, of course, can also be compared with the experimentally measured displacement histories.

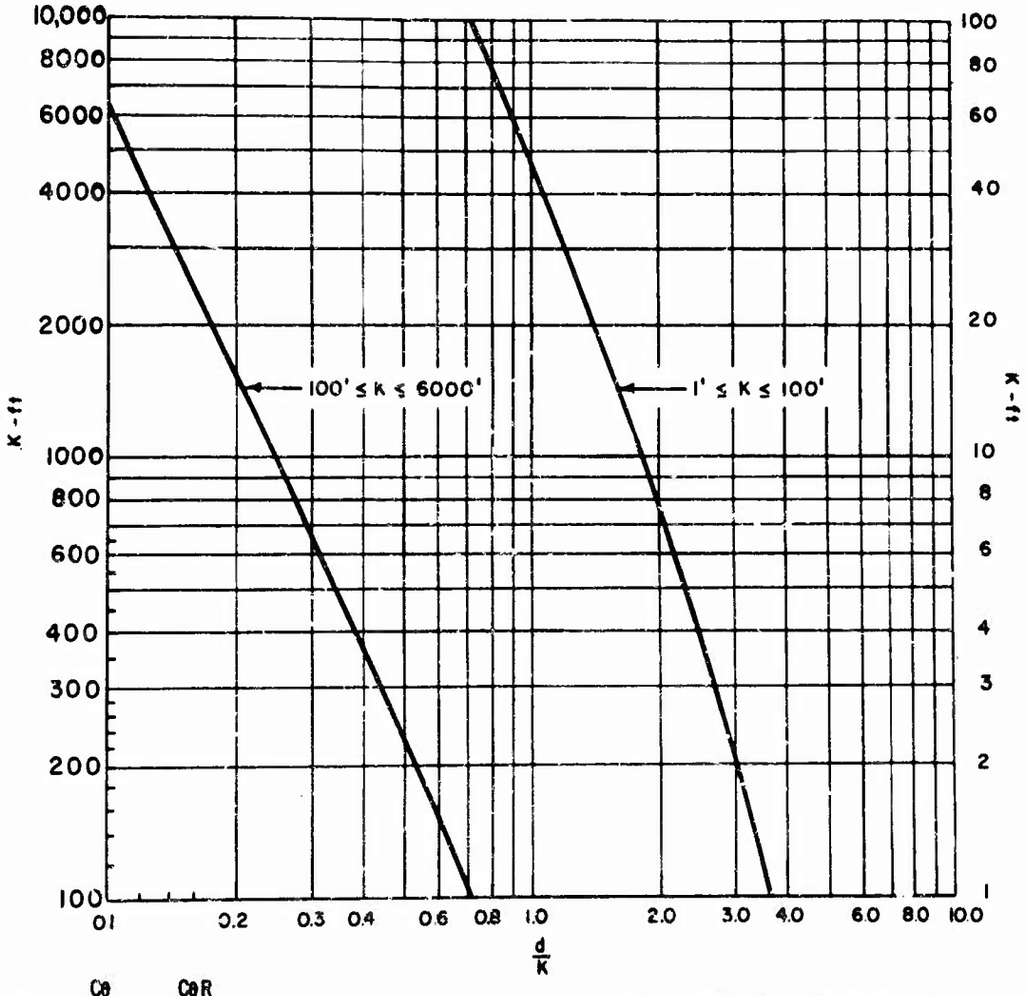

$$K = \frac{C\theta}{2\cos\beta} = \frac{C\theta R}{2D_B}$$

$$\frac{T_c}{\theta} = \frac{2P_0}{\rho g(\theta + K) + P_a}$$

T_c = Time Between Shock-Wave Arrival & Cavitation Closure
ρ = Density of Water
g = Acceleration due to Gravity
d = Depth of Cavitation Closure

C = Shock-Wave Propagation Velocity
θ = Shock-Wave Decay Constant
β = Angle Between Plane Wave Front & Surface
R = Slant Range from Charge to Surface over Point of Interest
D_B = Depth of Burst
P_0 = Peak Shock-Wave Pressure at R
P_a = Atmospheric Pressure

Figure 16 - Estimation of Cavitation Closure Depth and Closure Time for Plane Shock Wave

Plots of all the vertical velocity and displacement histories measured on the surface at the various ranges for both burst depths are given in Appendix A. The theoretical velocity and displacement histories calculated using the approach just described are also indicated by means of dashed lines on each corresponding measurement for all ranges up to 1000 feet. The calculated initial surface particle kick-off velocity $U(o) = (2 P_o \cos\beta)/(\rho c)$ is also indicated (by a small dot at the primary shock wave) on those same velocity records. It is evident that the predicted uncavitated surface water layer histories are in good agreement with the measured velocity histories.

The theoretical curves plotted on the measured surface displacement histories give reasonable estimations of surface displacement prior to closure but tend to be small since they do not take into account the high initial velocity of the surface.

Graphs of closure depths versus range illustrating both the theoretical and the experimental data are presented in Figures 17 and 18. For each of the burst depths, the experimental closure depths determined from the pressure histories and from the slopes of the velocity histories are clustered together without much scatter out to the range at which interaction of bottom and surface cutoffs are first observed. Since the theoretical closure depth curve is derived for cavitation from the top surface cutoff only, it only applies when it gives closure depths above the line of simultaneous reflected wave arrivals and at ranges shorter than the nearest range at which reflected wave interaction is seen. Dashed lines therefore are used in the graphs for the theoretical curves beyond these regions.

Since the bottom reflection for this particular test series causes a component of particle velocity toward the bottom, the surface velocity decreases at ranges where interaction occurs after the bottom reflection reaches the surface. The resulting surface velocity histories at those ranges, therefore, have a steeper negative acceleration which is not indicative of closure depth.

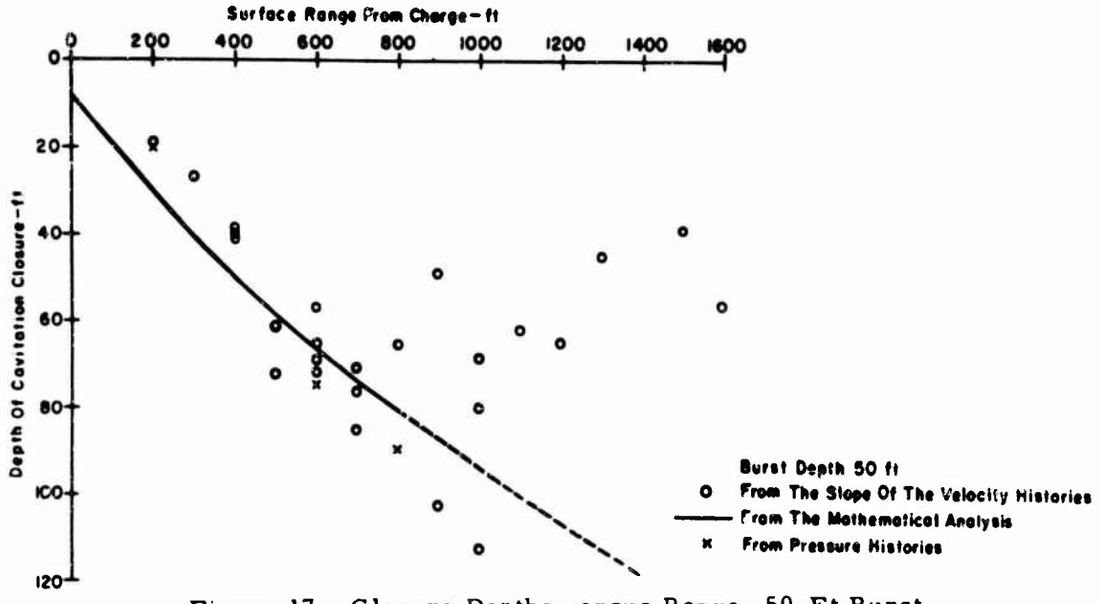

Figure 17 - Closure Depths versus Range, 50-Ft Burst

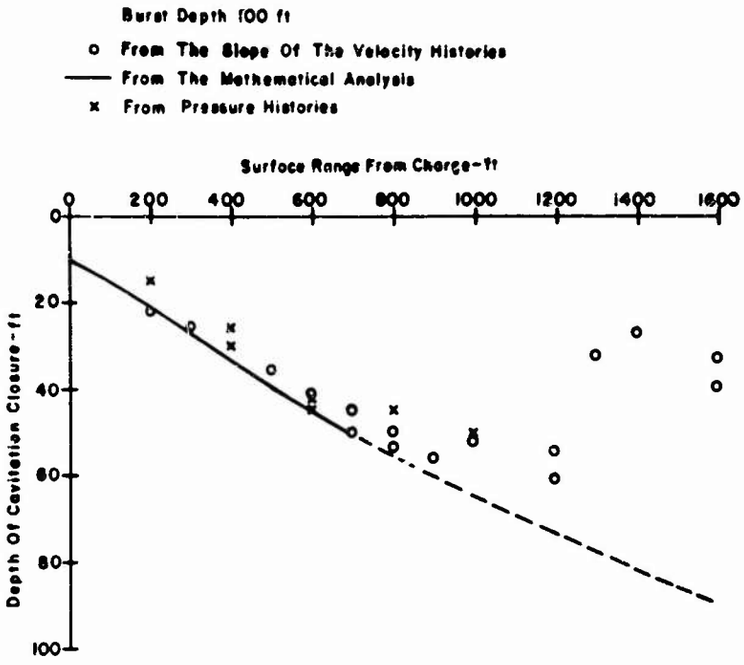

Figure 18 - Closure Depths versus Range, 100-Ft Burst

The times at which the closure pulse reached the surface at each of the stations are plotted versus range for each burst depth in Figures 19 and 20. The range at which the minimum time occurs is the range at which closure is first initiated. For the bursts at 50-ft depth, the experimental data indicate that the initial impact occurred at a range of about 300 feet. Similarly, the first impact for the burst at 100-ft depth occurred at a range of about 400 feet. A study of the slope of the closure pulse arrival time curve for each of the burst depths shows that after the initial closure, closure propagates outward away from the charge with a supersonic velocity becoming asymptotic to the speed of sound in water at large standoffs. After the initial closure, closure propagates inward toward the charge supersonically at first but then becomes subsonic at standoffs close to the charge. Also plotted in Figures 19 and 20 are the theoretical closure times derived from the mathematical analysis assuming that closure occurs when the surface water layer returns to its original position. These theoretical closure time curves of course, do not apply beyond the ranges of application of the theoretical closure depth curves. The discrepancy between the calculated closure time and closure pulse arrival at the surface at short ranges from the charge is largely due to bubble expansion effects. Examination of the displacement records indicates that at close standoffs the water layer does not fall back to its original position prior to closure as assumed in the mathematical analysis. The bubble expanding and pushing the water up under the water layer causes the impact to occur sooner than it would if the water layer had fallen back all the way to its original position. This upward motion of the water below the surface layer has a relatively large effect on the closure time and on the range at which closure is initiated.

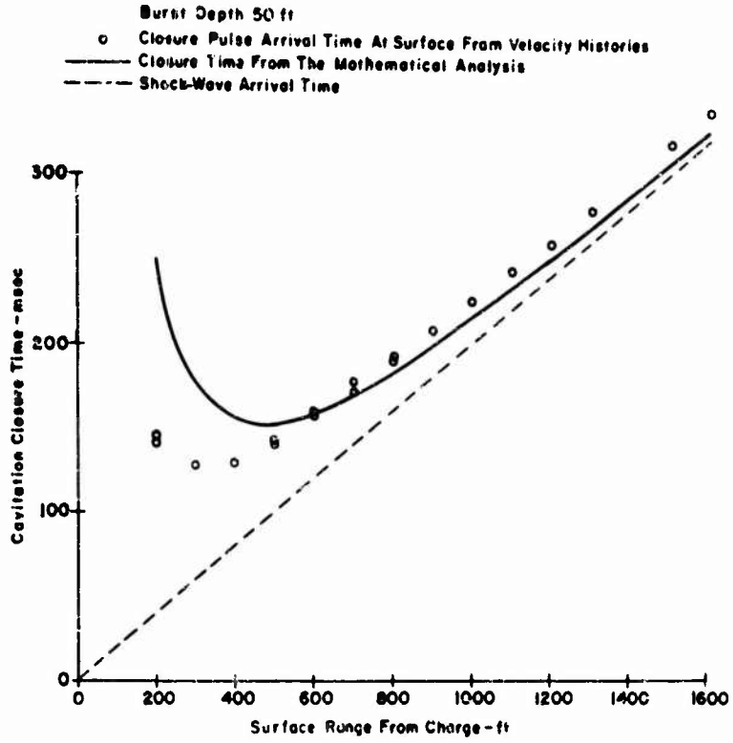

Figure 19 - Closure Times versus Range, 50-Ft Burst

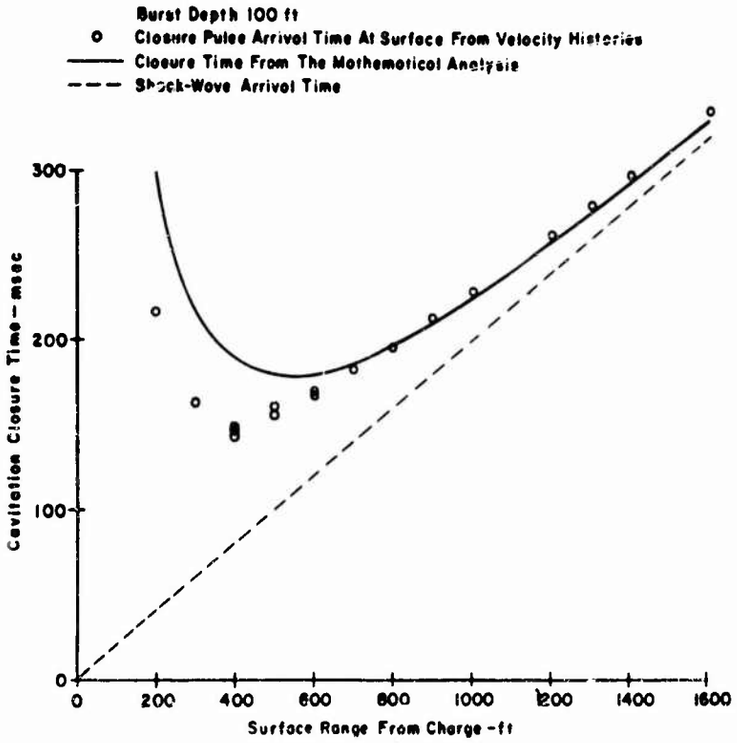

Figure 20 - Closure Times versus Range, 100-Ft Burst

SUMMARY AND COMMENTS

The experimental study has provided very extensive and comprehensive data for the two test geometries investigated. Likewise, these data have provided much guidance toward the determination of the relative importance of the many parameters which influence the cavitation phenomena. As a result, several reasonable mathematical approximations which describe these phenomena, and which are readily calculated without the aid of a computer, have been derived from the more detailed and comprehensive theoretical studies. Consequently, generally adequate predictions for other geometries and charge sizes can now be readily made for the following:

1. Boundaries of the cavitated region,
2. Depth at which cavitation closure occurs,
3. Time at which cavitation closure occurs,
4. Velocity history of the surface until cavitation closure occurs, and
5. Displacement history of the surface until cavitation closure occurs.

Although these calculations have been compared in detail only with the experimental data herein, spot checks of other data indicate that these relationships are valid for a surprisingly wide range of charge sizes and geometries. The limits of validity, however, have yet to be established for both charge size and geometry.

For the closer regions extending even beyond the ring of first impact, the displacement measurements indicate quite clearly that the bubble expansion causes the water below the closure depth to rise and thus causes closure to occur at a much earlier time, since the layer does not have to fall to its original position. The closure pulse pressure can, of course, also be considerably affected by this motion due to bubble expansion.

The experiments indicated that when the draft of a floating structure is small compared to the thickness of the water layer, the bodily motions of that structure are essentially the same as the water layer, and these motions are relatively independent of the structure's cross sectional shape.

This test series also demonstrated that negative reflections from the bottom strong enough to produce cutoff are quite possible even with relatively large pressure amplitudes, and are capable of considerably modifying the region of cavitation.

ACKNOWLEDGMENTS

The assistance provided and contributions made to the theoretical phase of the work presented in this report by Dr. Vincent J. Cushing of the Engineering-Physics Company of Rockville, Maryland, and Dr. H. M. Schauer of the Underwater Explosions Research Division of the David Taylor Model Basin are gratefully acknowledged by the authors.

REFERENCES

1. Cushing, Vincent, "Study of Bulk Cavitation and Consequent Water Hammer," Engineering-Physics Company Final Report on Contract NONR-3389(00) EPCO Project No. 106 (Oct 31, 1961) UNCLASSIFIED.

2. Cushing, Vincent et al., "Three-Dimensional Analysis of Bulk Cavitation," Engineering-Physics Company Interim Report on Contract NONR-3709(00), EPCO Project No. 106 (Sept 24, 1962) UNCLASSIFIED.

3. "Revised Similitude Equations for the Underwater Shockwave Performance of Pentolite and HBX-1," U. S. Naval Ordnance Laboratory, White Oak, NAVWEPS Report 7380 (1 Feb 1961) UNCLASSIFIED.

APPENDIX A
EXPERIMENTAL TEST DATA

CONTENTS

APPENDIX A

EXPERIMENTAL TEST DATA

While the interest of the study presented as the text of this report is fairly specific, the data of the experimental test series represent a very comprehensive documentation of the pressure field and surface phenomena for the geometries studied. Since these data could be useful for further study and they have not been published elsewhere, the majority of the records obtained are given in this appendix, even including those with obvious errors (such as a shift or drift in the base line).

Pressure, velocity and displacement histories are presented for the bursts at 50-ft and 100-ft depths according to range from the burst. In the pressure and velocity records, the primary shock wave is labeled and the signal charge shock waves are labeled where their occurrences are certain. The theoretical velocity and displacement histories calculated are shown as dashed lines on each corresponding measurement for all ranges up to and including the 1000-ft range. The calculated initial surface particle kickoff velocity is also indicated (by a small dot at the primary shock wave) on velocity records in the 200 to 1000-ft range. The base line of the pressure record represents the depth of the gauge, although the history is plotted with pressure as the ordinate. Some of the pressure records are magnified to show details that are small in comparison with the primary shock wave, and in these cases the full amplitude of the shock wave is not shown.

The time scales of all the records are shown with respect to detonation of the primary charge. The time scales of the pressure records in some of the figures, however, are not exactly the same. In each of these, the time scale at the top applies to the top record and ticks are applied at 10-millisecond intervals above each of the other records in that figure. The records are approximately aligned and hence the ticks in a column correspond to the same time with respect to detonation of the primary charge. The records in figures which show no time ticks have identical time scales.

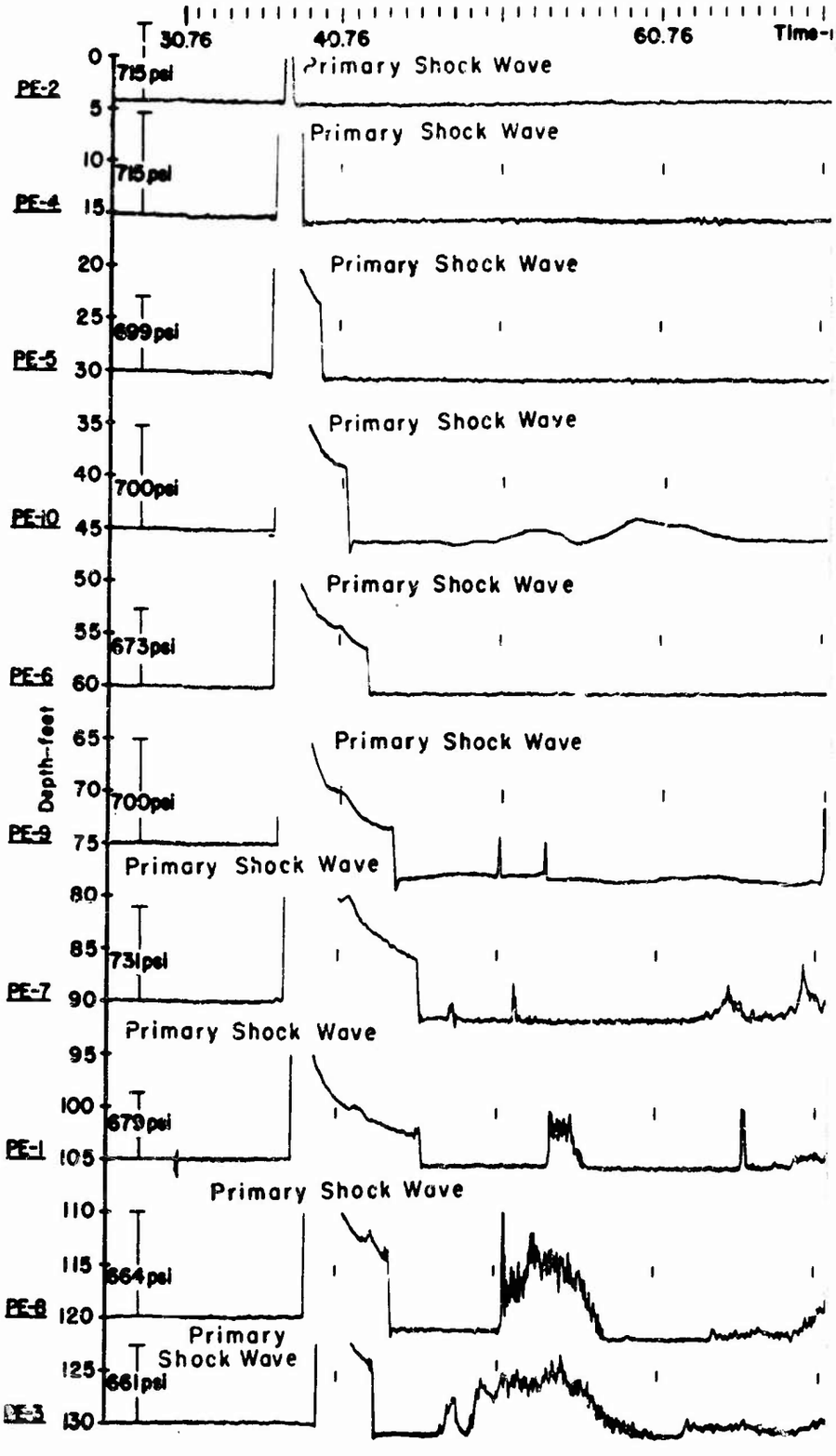
30.76
40.76
60.76
Time-
Depth-feet
PE-2
715 psi
Primary Shock Wave
PE-4
715 psi
Primary Shock Wave
PE-5
699 psi
Primary Shock Wave
PE-10
700 psi
Primary Shock Wave
PE-6
673 psi
Primary Shock Wave
PE-9
700 psi
Primary Shock Wave
PE-7
731 psi
Primary Shock Wave
PE-1
673 psi
Primary Shock Wave
PE-8
664 psi
Primary Shock Wave
PE-3
661 psi

A

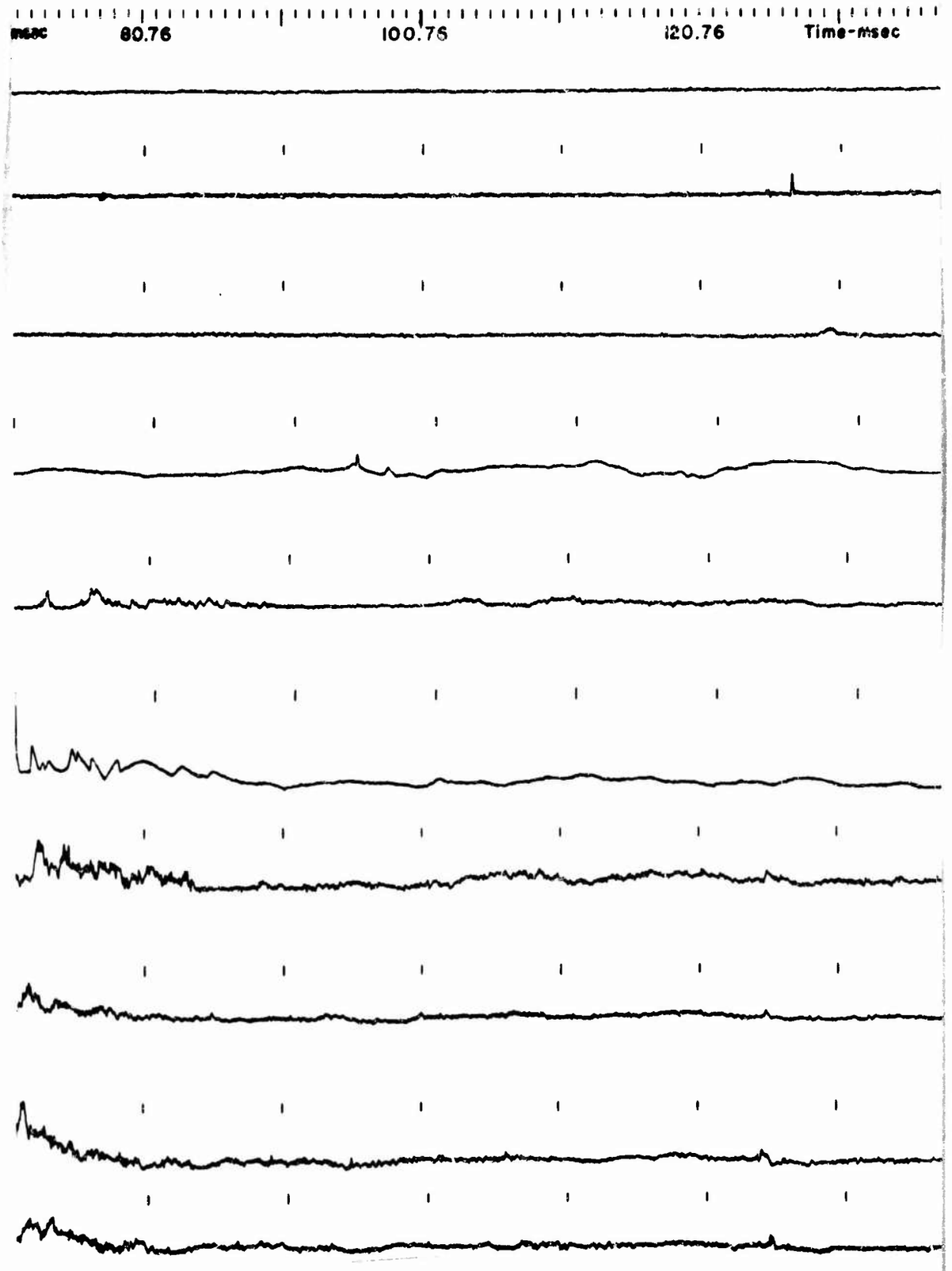

B

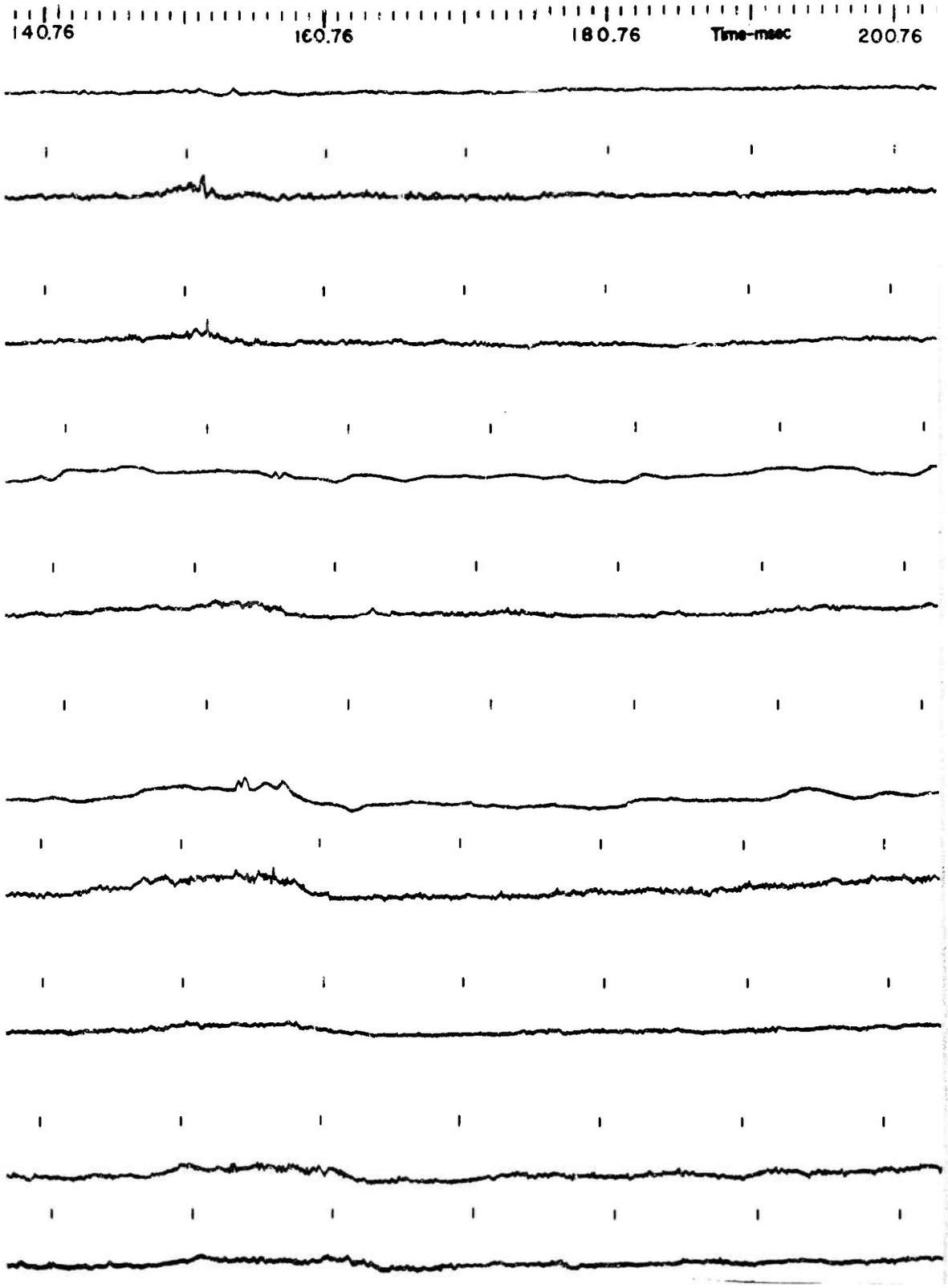

C

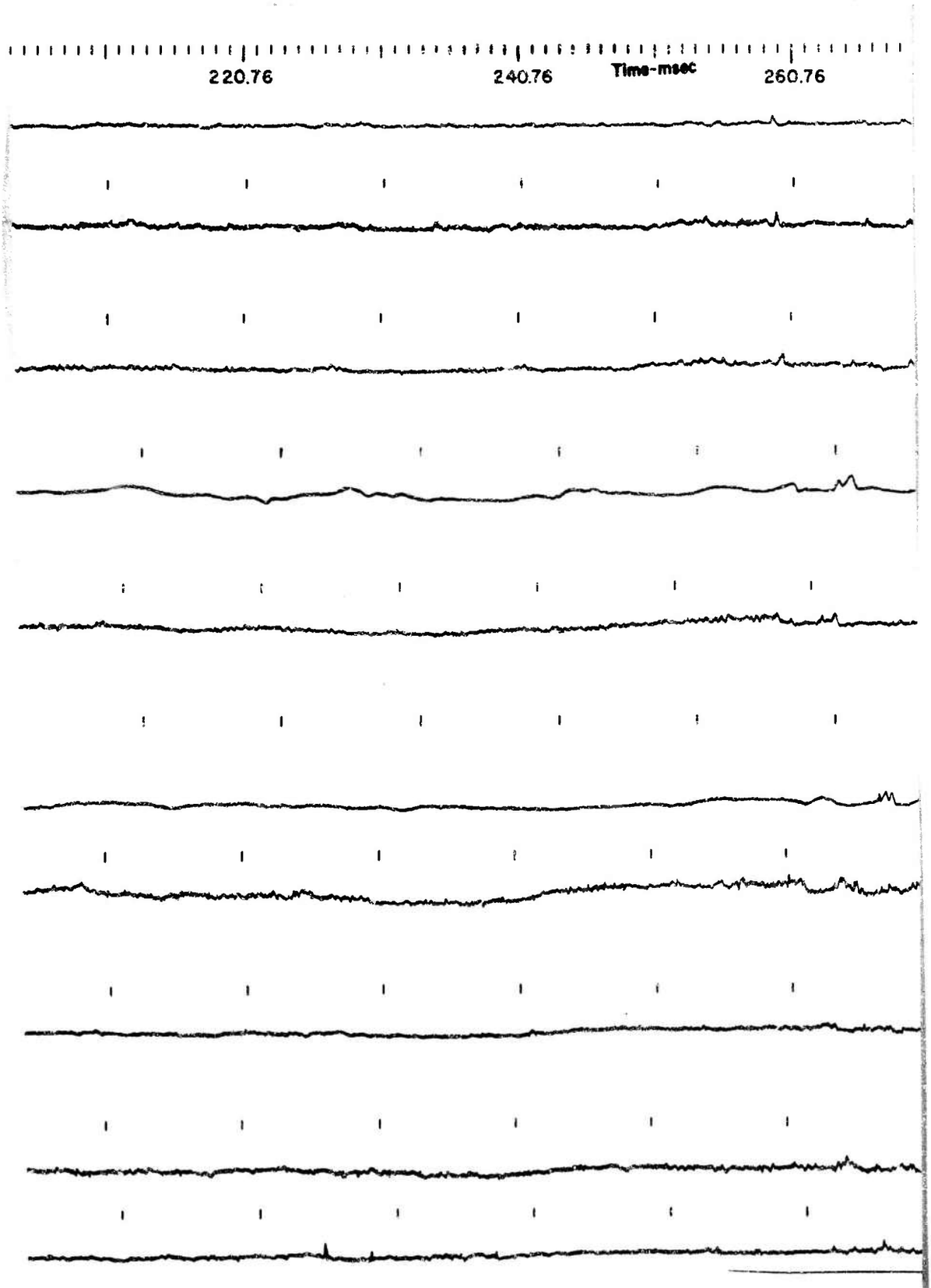

Figu

D

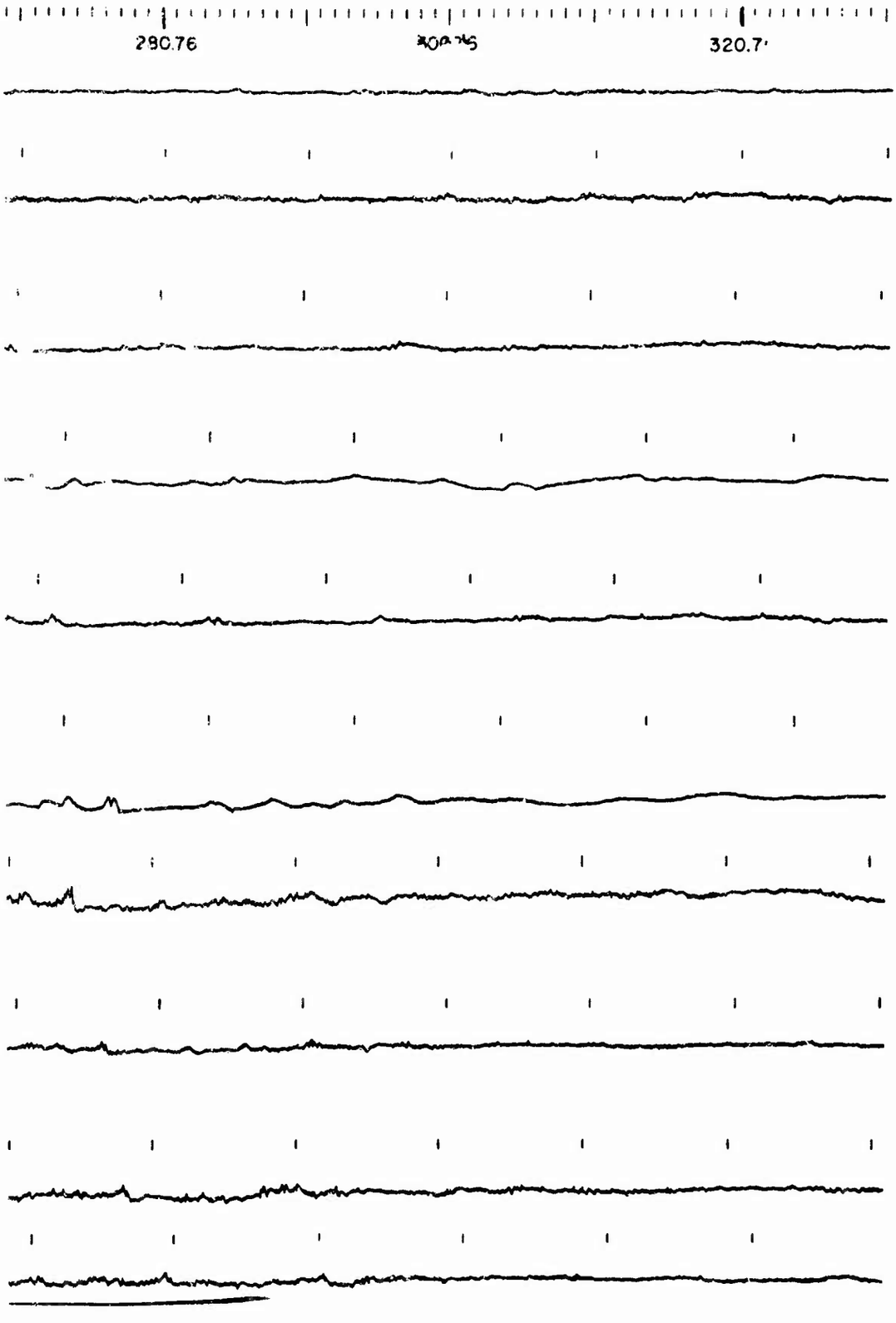

ıre A1 - Pressure Histories - 200-Ft Range from Burst at 50-Ft Depth (Station 1, Test 6)

E

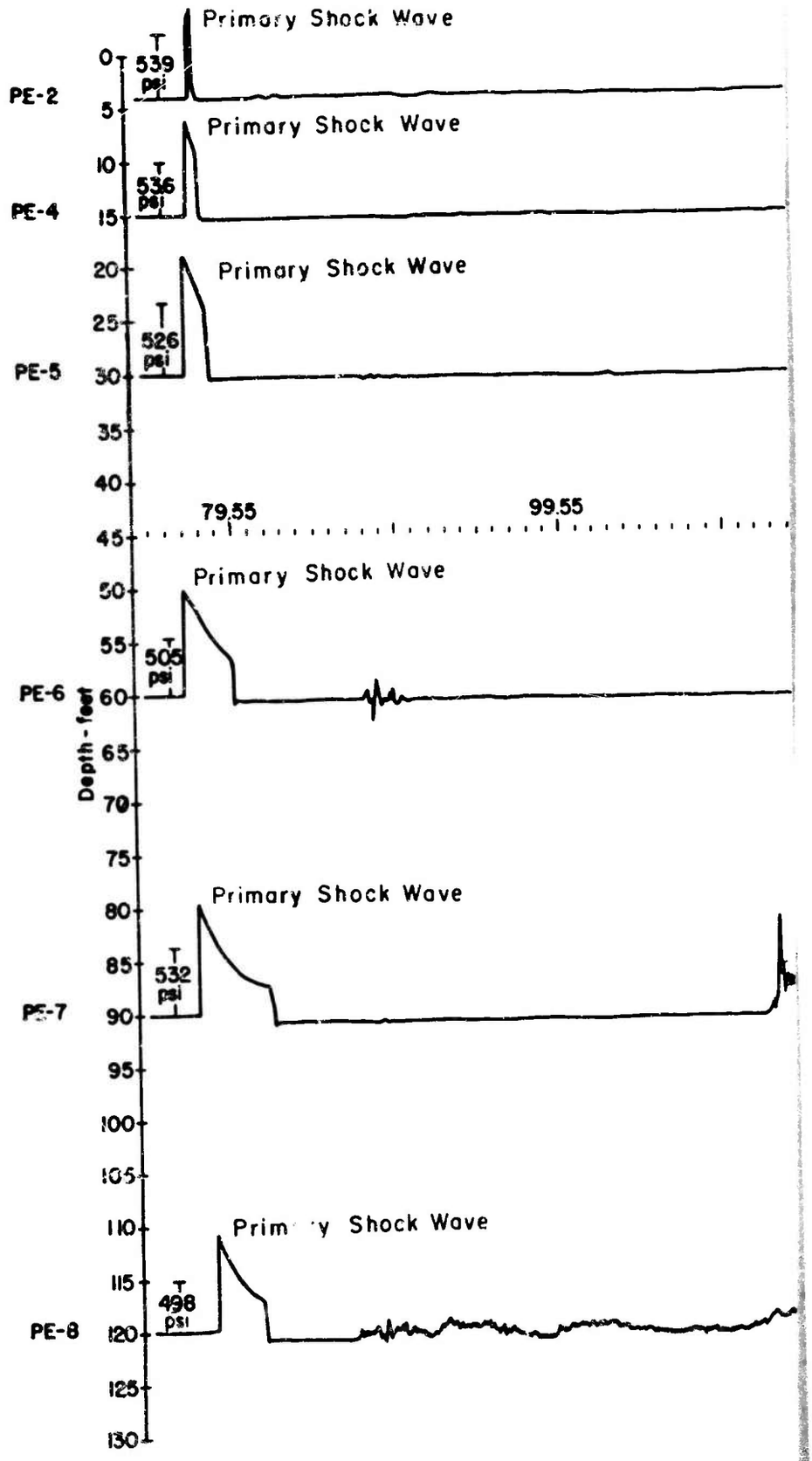
Primary Shock Wave
T
539
psi
PE-2
Primary Shock Wave
T
536
psi
PE-4
Primary Shock Wave
T
526
psi
PE-5
79.55
99.55
Primary Shock Wave
T
505
psi
PE-6
Depth - feet
Primary Shock Wave
T
532
psi
PE-7
Prim y Shock Wave
T
498
psi
PE-8
0
5
10
15
20
25
30
35
40
45
50
55
60
65
70
75
80
85
90
95
100
105
110
115
120
125
130

A

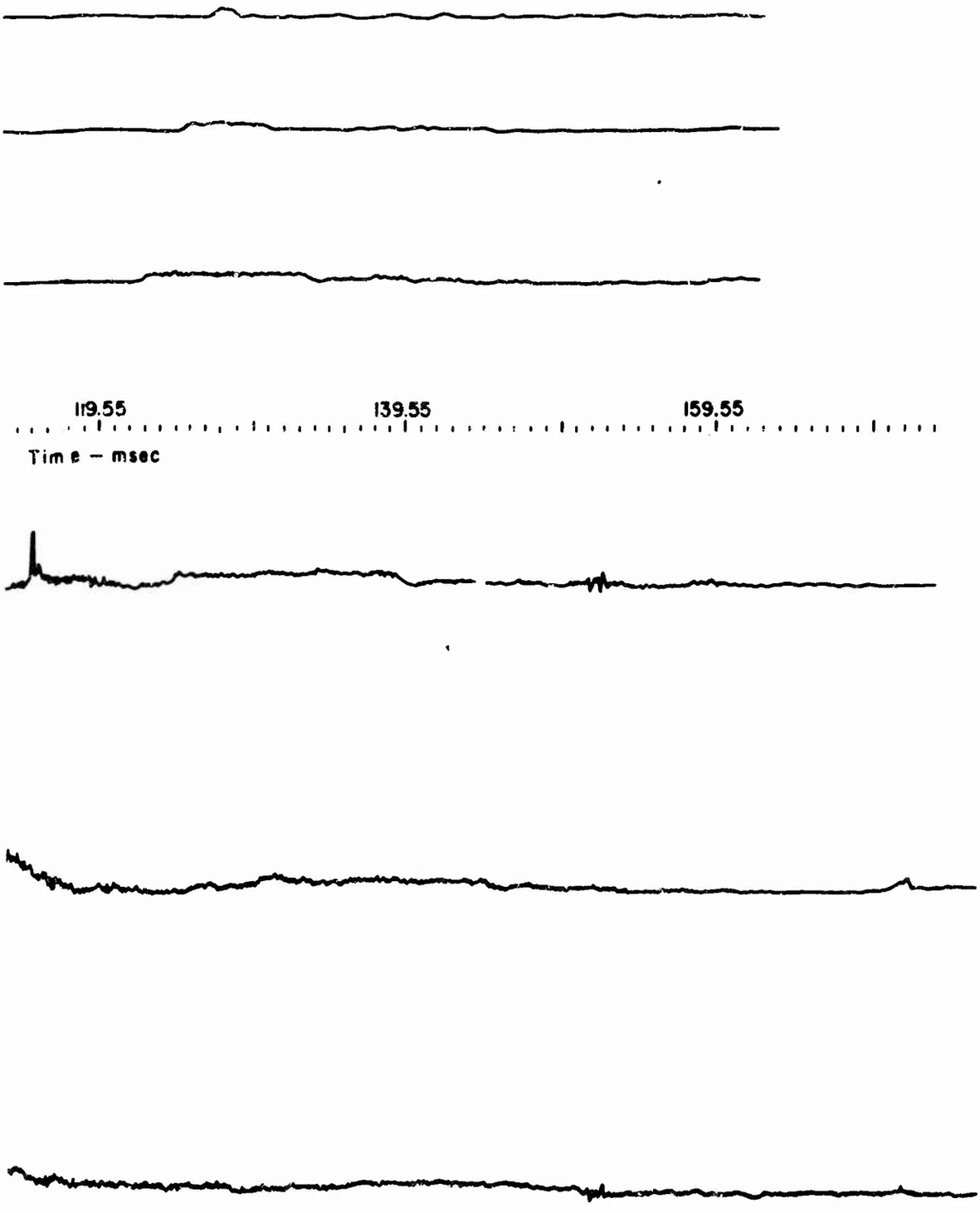

Figure A2 - Pressure Histories - 400-Ft Range from Burst at 50-Ft Depth (Station 1, Test 1)

B

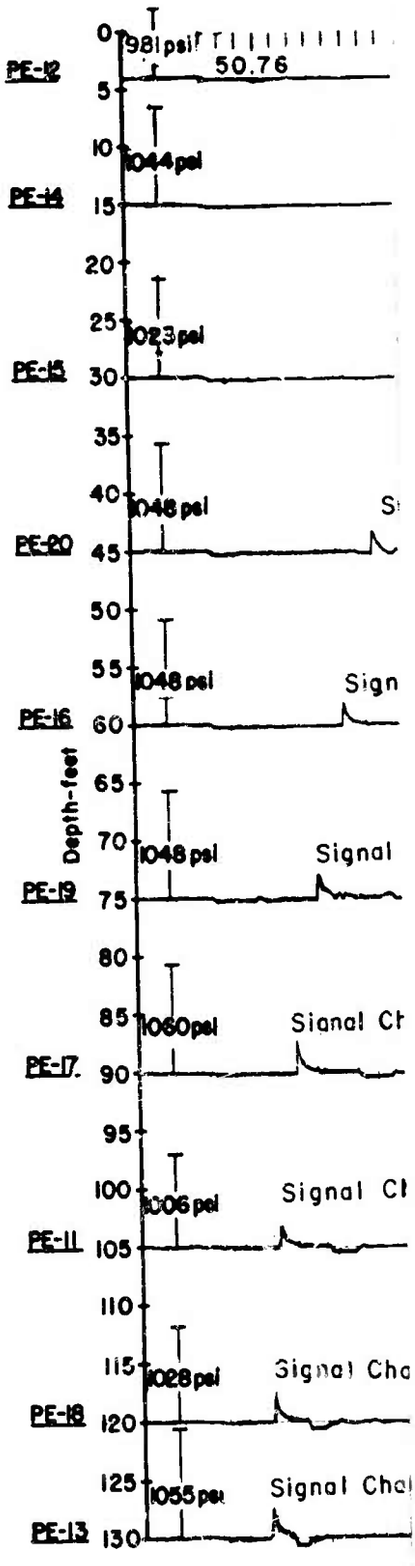
981 psi
50.76
PE-12
1044 psi
PE-14
1023 psi
PE-15
1048 psi
PE-20
1048 psi
Sign
PE-16
Depth-feet
1048 psi
Signal
PE-19
1060 psi
Signal Ch
PE-17
1006 psi
Signal Ch
PE-11
1028 psi
Signal Cha
PE-18
1055 psi
Signal Cha
PE-13
0
5
10
15
20
25
30
35
40
45
50
55
60
65
70
75
80
85
90
95
100
105
110
115
120
125
130

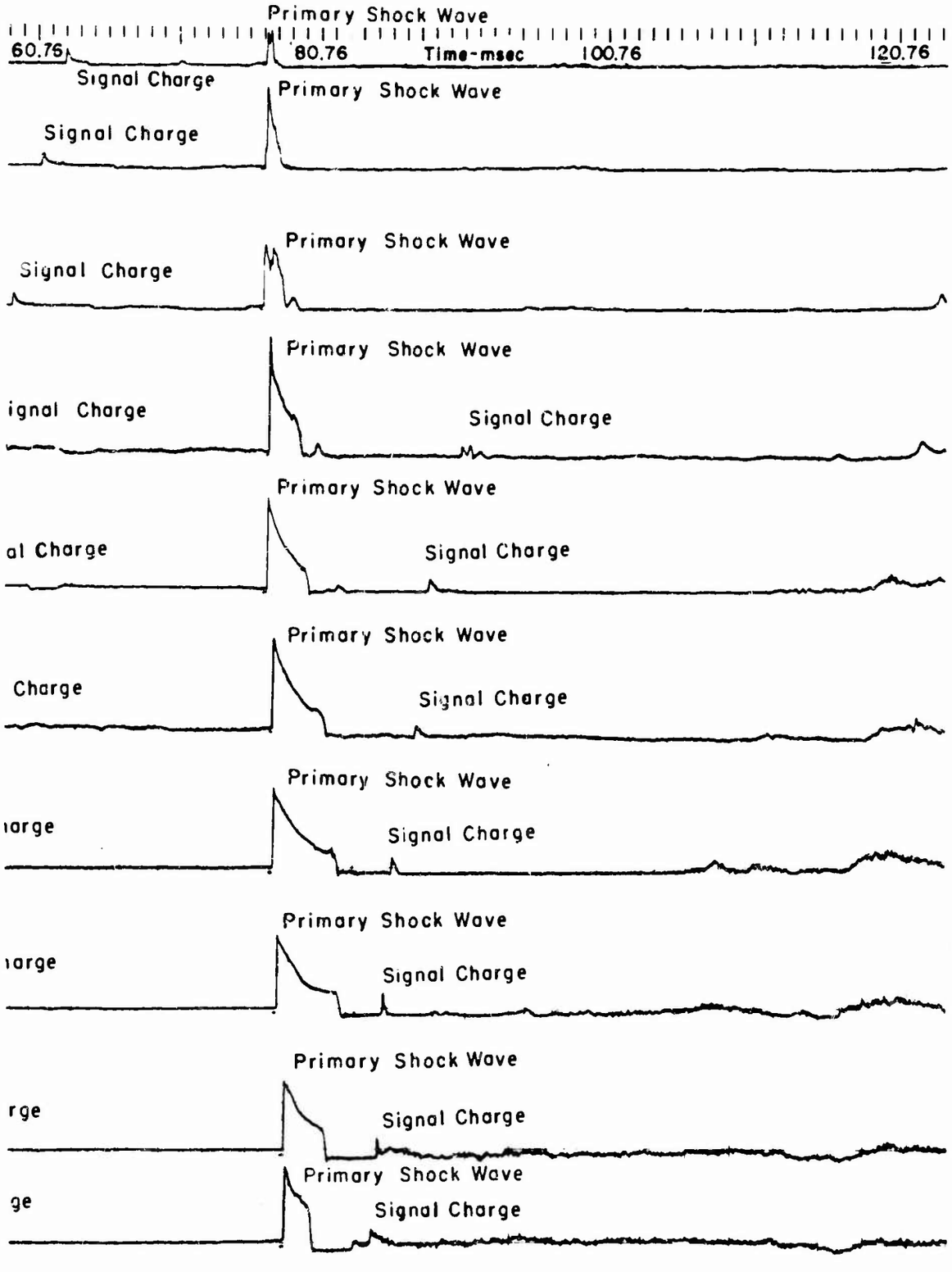
Primary Shock Wave
60.76
80.76
Time-msec
100.76
120.76
Signal Charge
Primary Shock Wave
Signal Charge
Primary Shock Wave
Signal Charge
Primary Shock Wave
ignal Charge
Signal Charge
Primary Shock Wave
al Charge
Signal Charge
Primary Shock Wave
Charge
Signal Charge
Primary Shock Wave
harge
Signal Charge
Primary Shock Wave
harge
Signal Charge
Primary Shock Wave
rge
Signal Charge
Primary Shock Wave
ge
Signal Charge

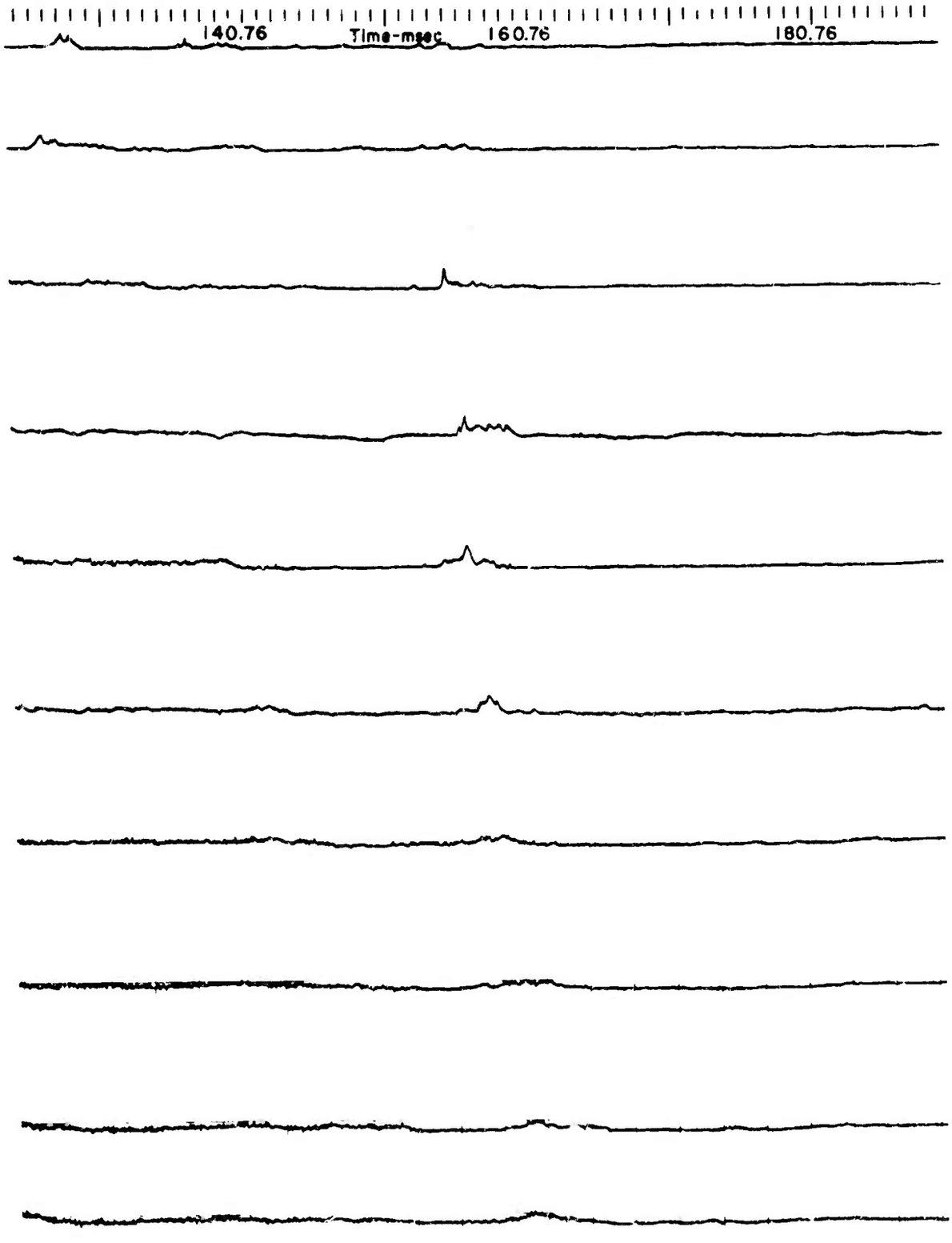

Fig

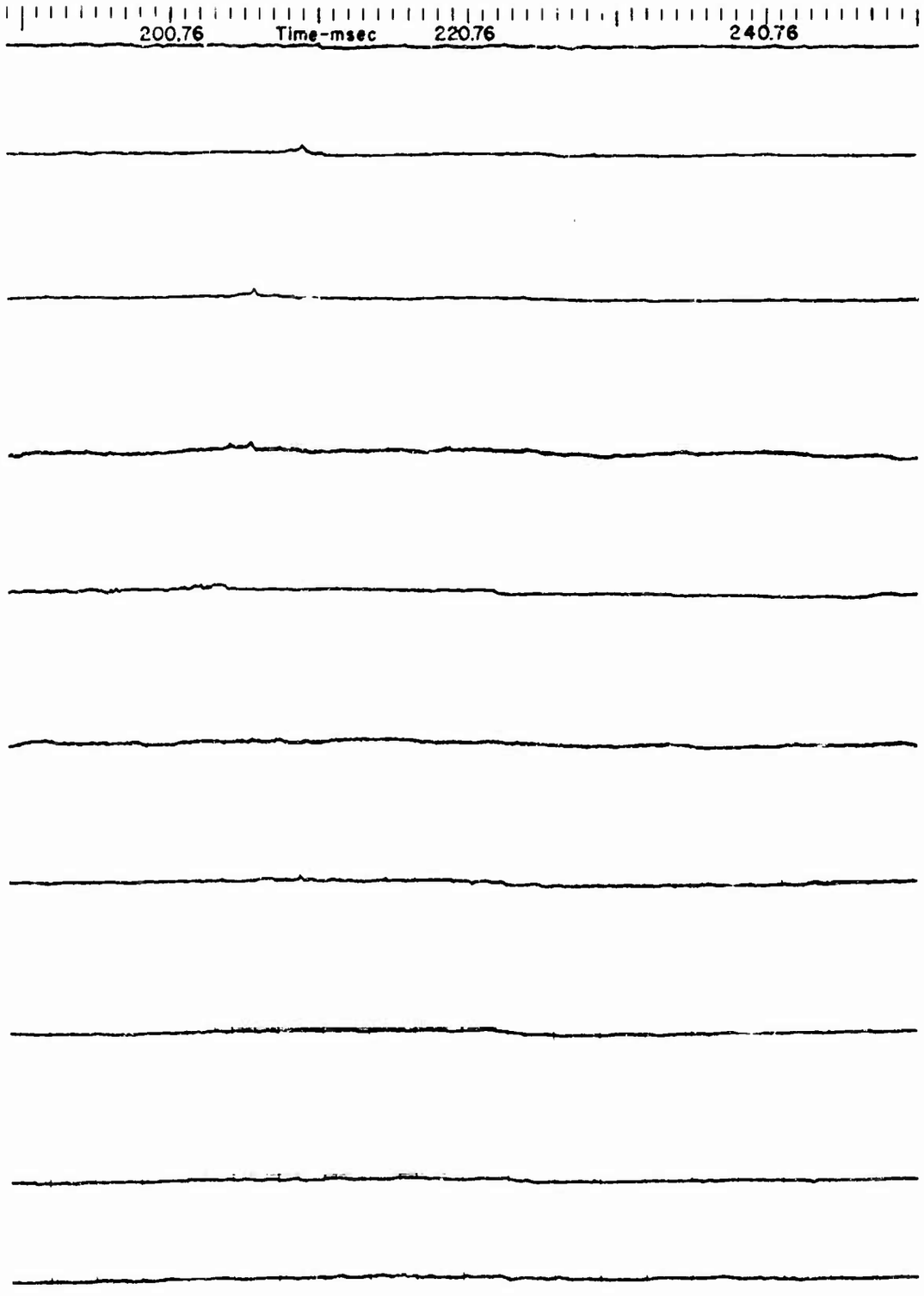

ıre A3 - Pressure Histories - 400-Ft Range from Burst at 50-Ft Depth (Station 3, Test 6)

D

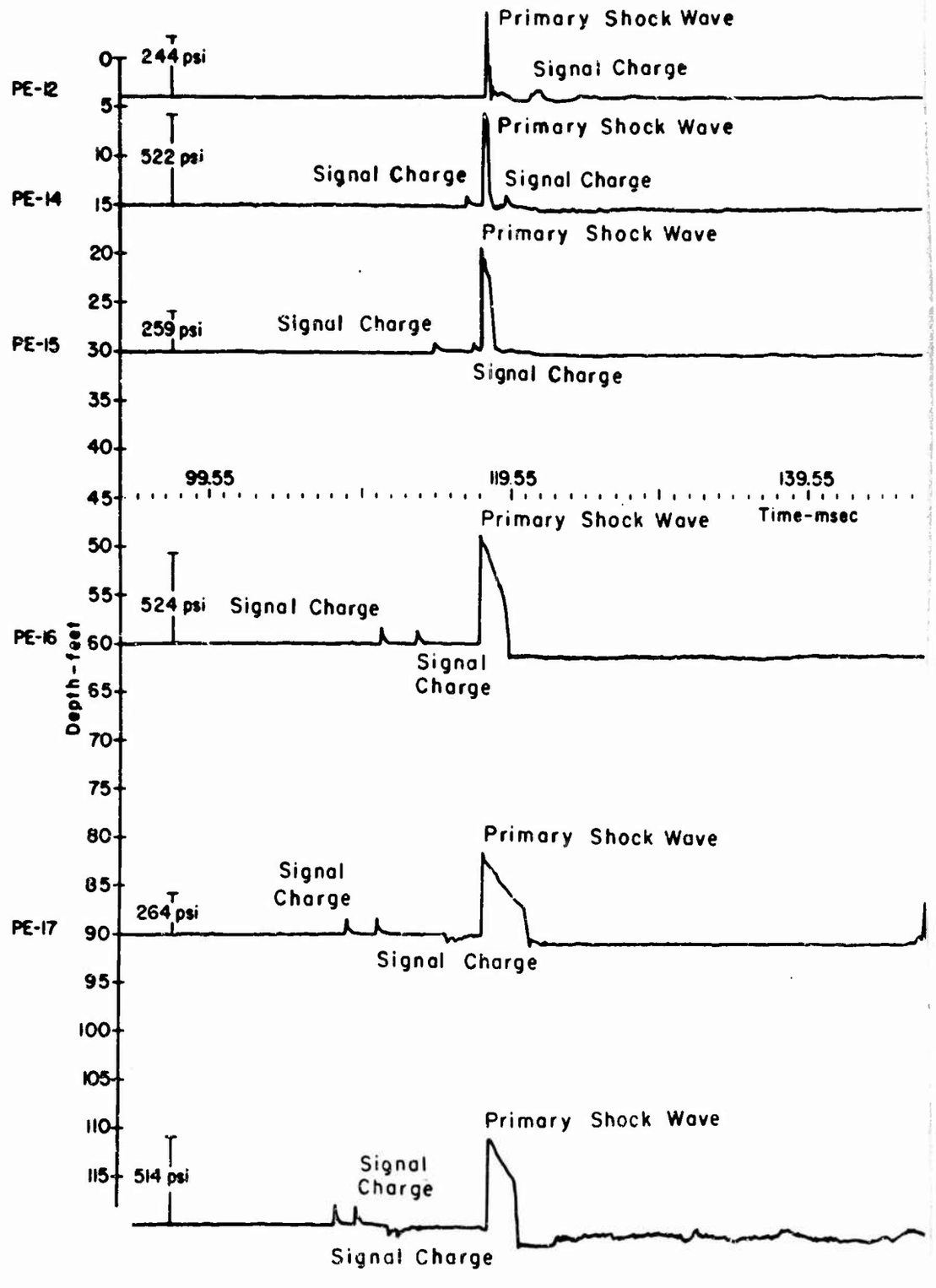
Primary Shock Wave
Signal Charge
244 psi
PE-12
Primary Shock Wave
522 psi
Signal Charge
Signal Charge
PE-14
Primary Shock Wave
259 psi
Signal Charge
PE-15
Signal Charge
99.55
119.55
139.55
Time-msec
Primary Shock Wave
524 psi
Signal Charge
PE-16
Signal Charge
Depth-feet
Primary Shock Wave
Signal Charge
264 psi
PE-17
Signal Charge
Primary Shock Wave
Signal Charge
514 psi
Signal Charge

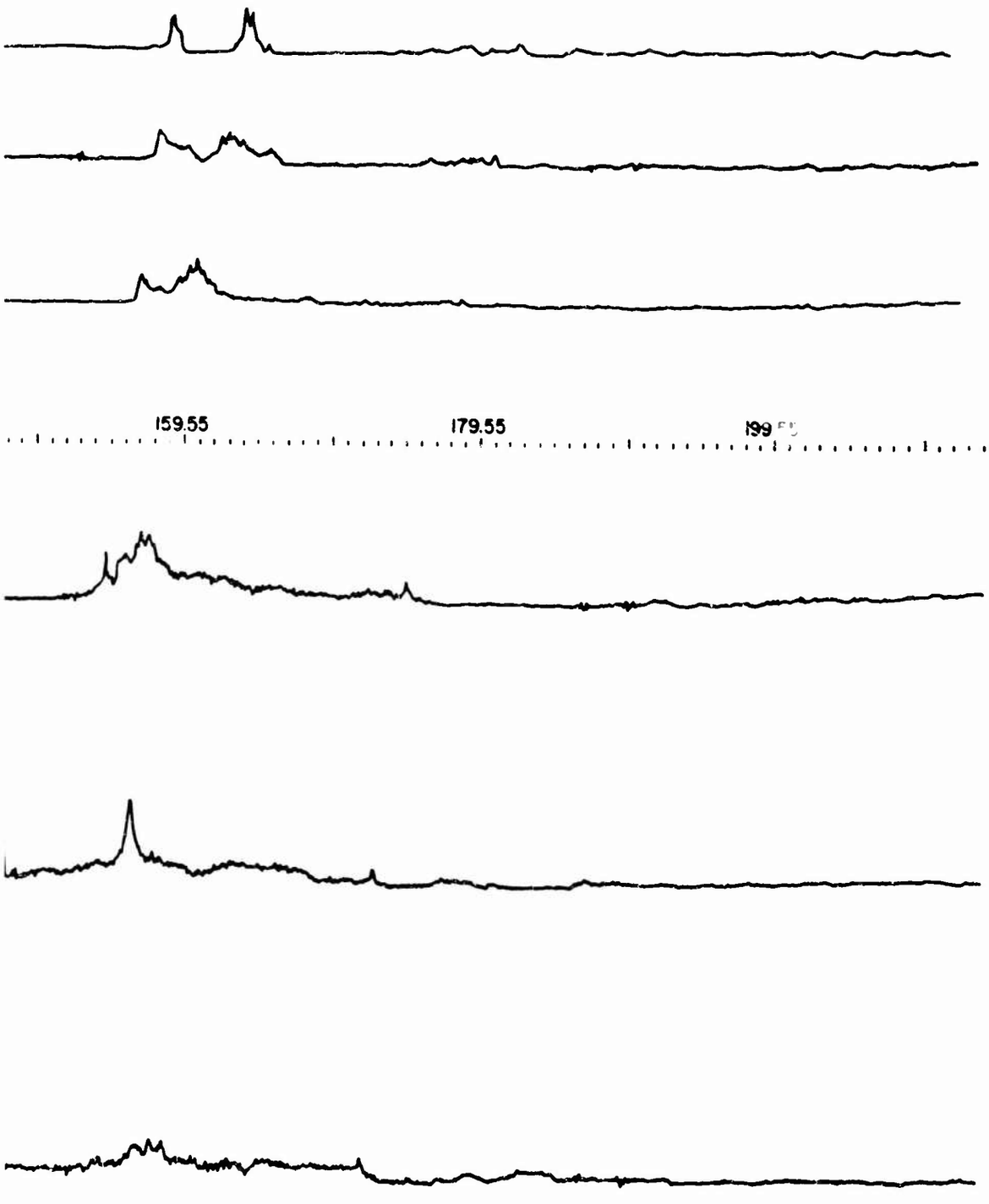

Figure A4 - Pressure Histories - 600-Ft Range from Burst at 50-Ft Depth (Station 3, Test 1)

B

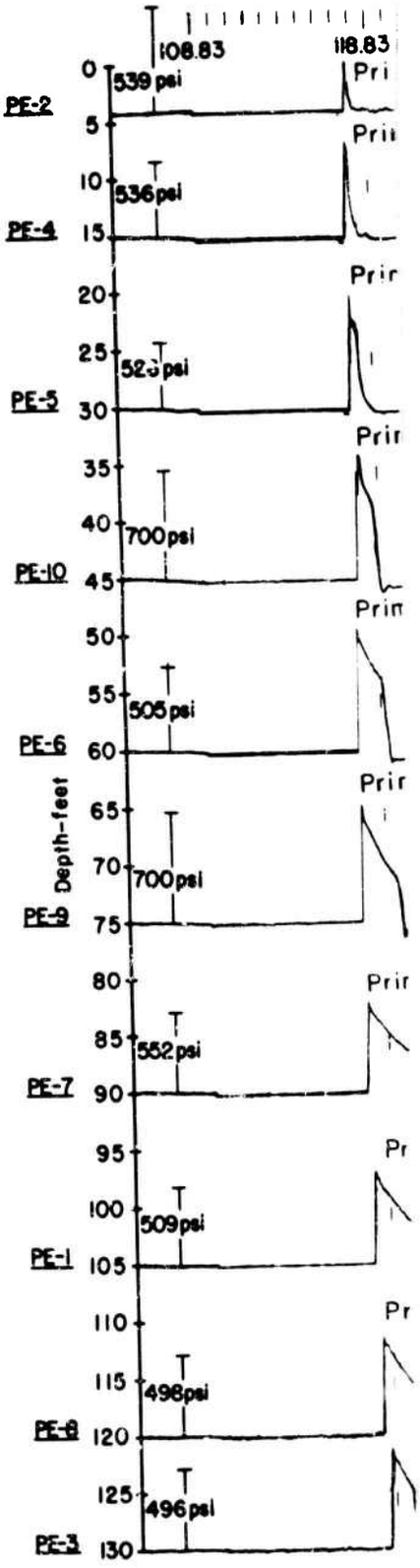
108.83
118.83
0
539 psi
PE-2
5
10
536 psi
PE-4
15
20
25
PE-5
30
35
700 psi
PE-10
40
45
50
55
505 psi
PE-6
60
Depth-feet
65
70
700 psi
PE-9
75
80
85
552 psi
PE-7
90
95
100
509 psi
PE-1
105
110
115
498 psi
PE-8
120
125
496 psi
PE-3
130

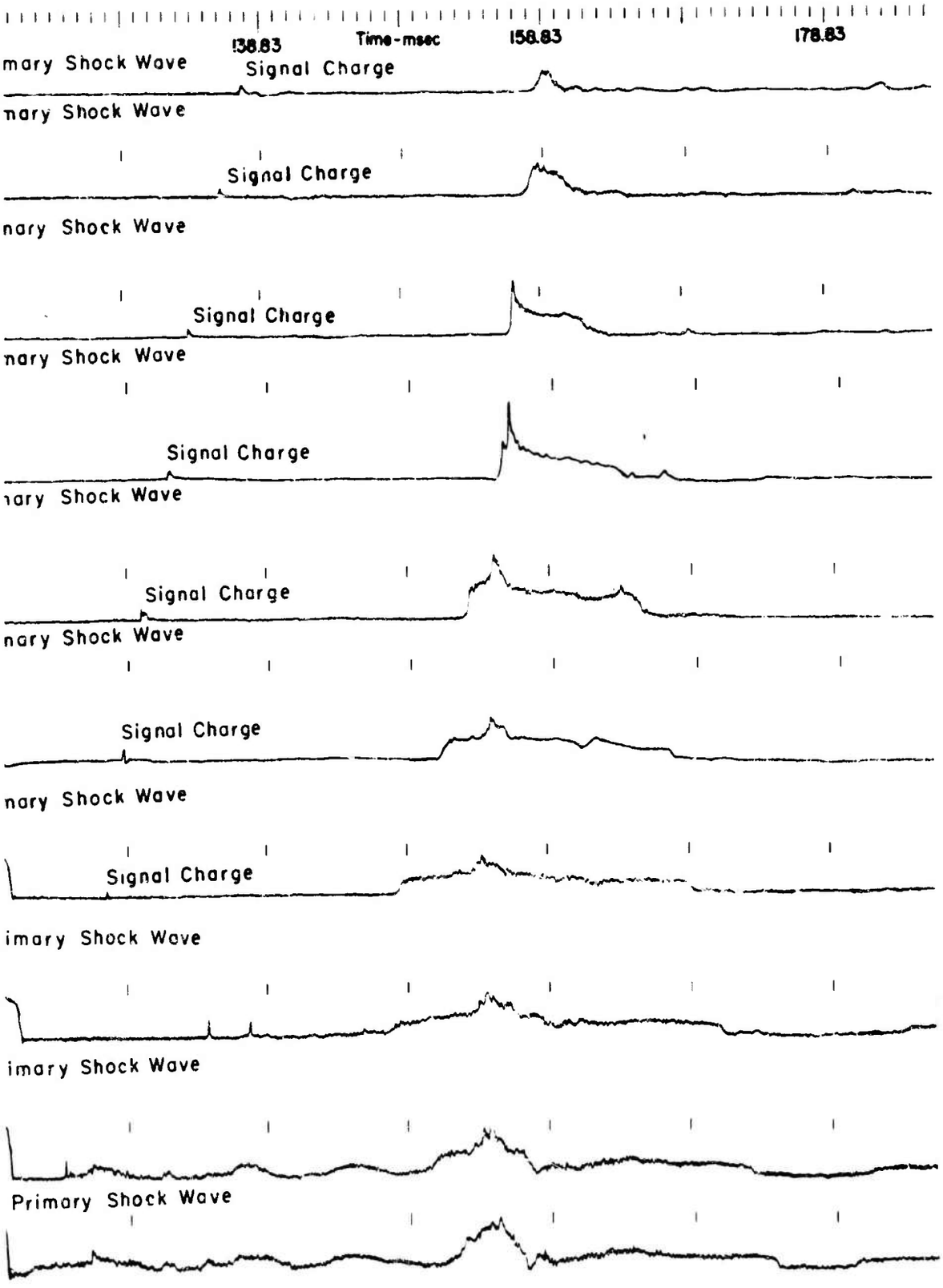
138.83
Time - msec
158.83
178.83
mary Shock Wave
Signal Charge
nary Shock Wave
Signal Charge
nary Shock Wave
Signal Charge
nary Shock Wave
Signal Charge
nary Shock Wave
Signal Charge
nary Shock Wave
Signal Charge
nary Shock Wave
Signal Charge
imary Shock Wave
imary Shock Wave
Primary Shock Wave

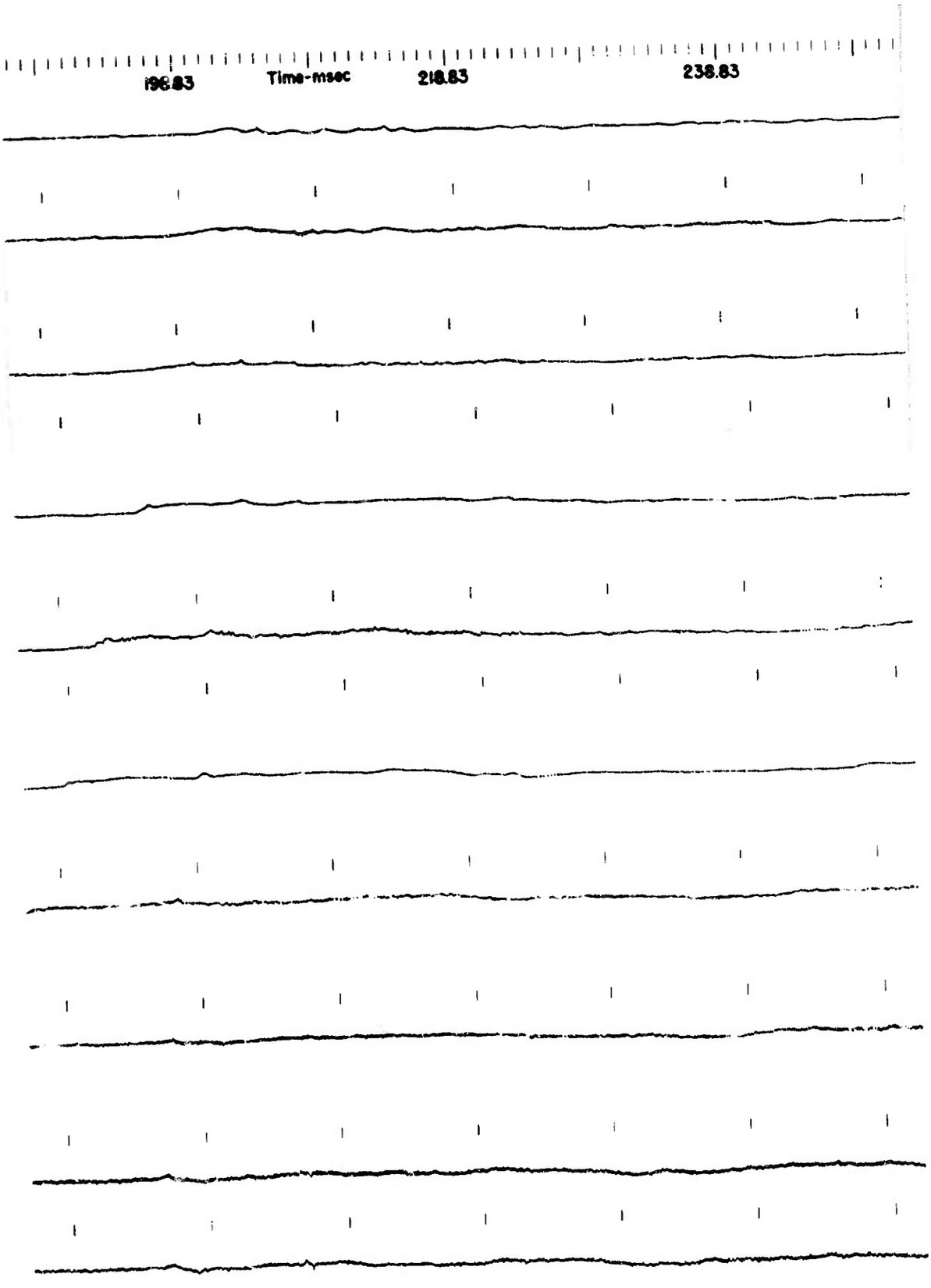

Figu

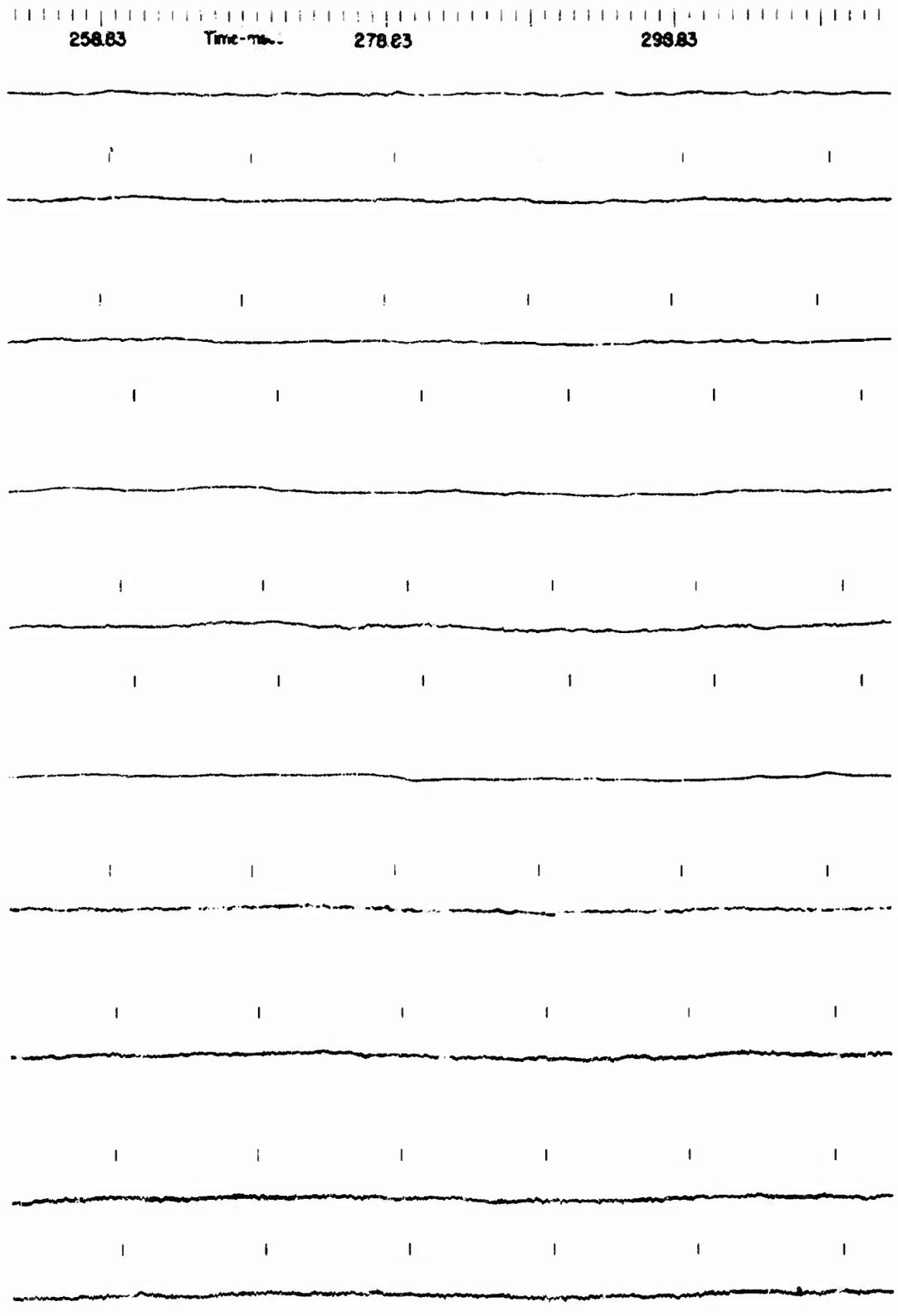

re A5 - Pressure Histories - 600-Ft Range from Burst at 50-Ft Depth (Station 1, Test 4)

D

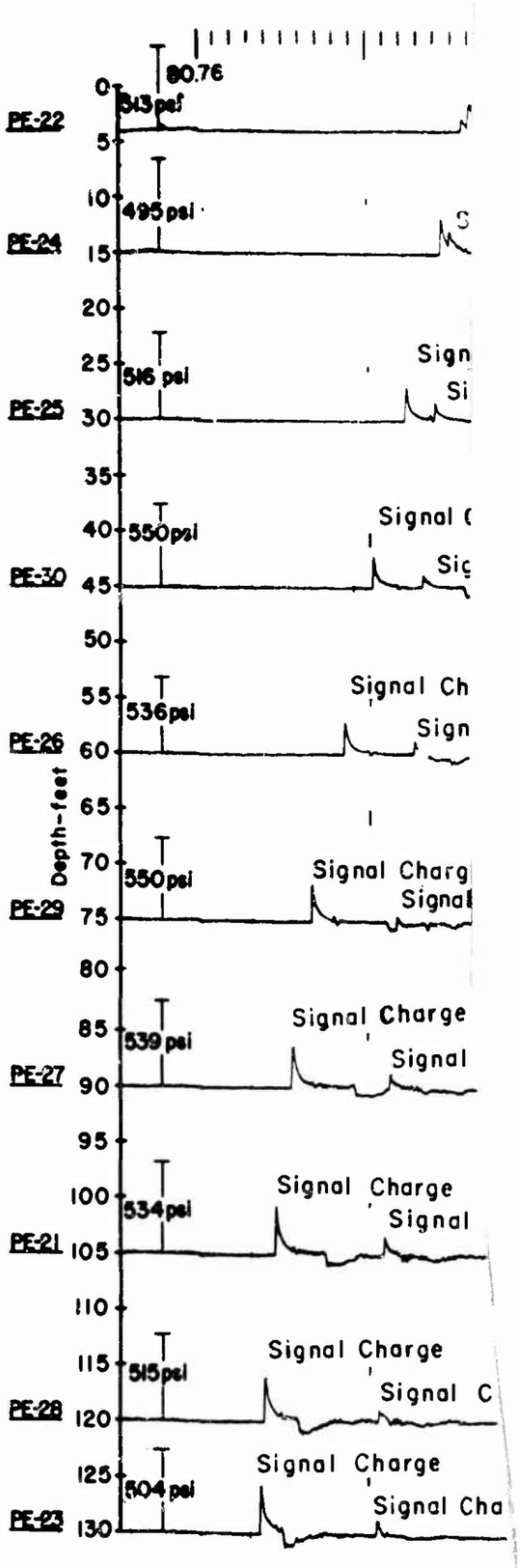
80.76
PE-22
513psi
PE-24
495 psi
PE-25
516 psi
Sign
PE-30
550psi
Signal
PE-26
536psi
Signal Ch
Sign
Depth-feet
PE-29
550psi
Signal Charg
PE-27
539 psi
Signal Charge
Signal
PE-21
534psi
Signal Charge
Signal
PE-28
515psi
Signal Charge
Signal C
PE-23
504 psi
Signal Charge
Signal Cha

A

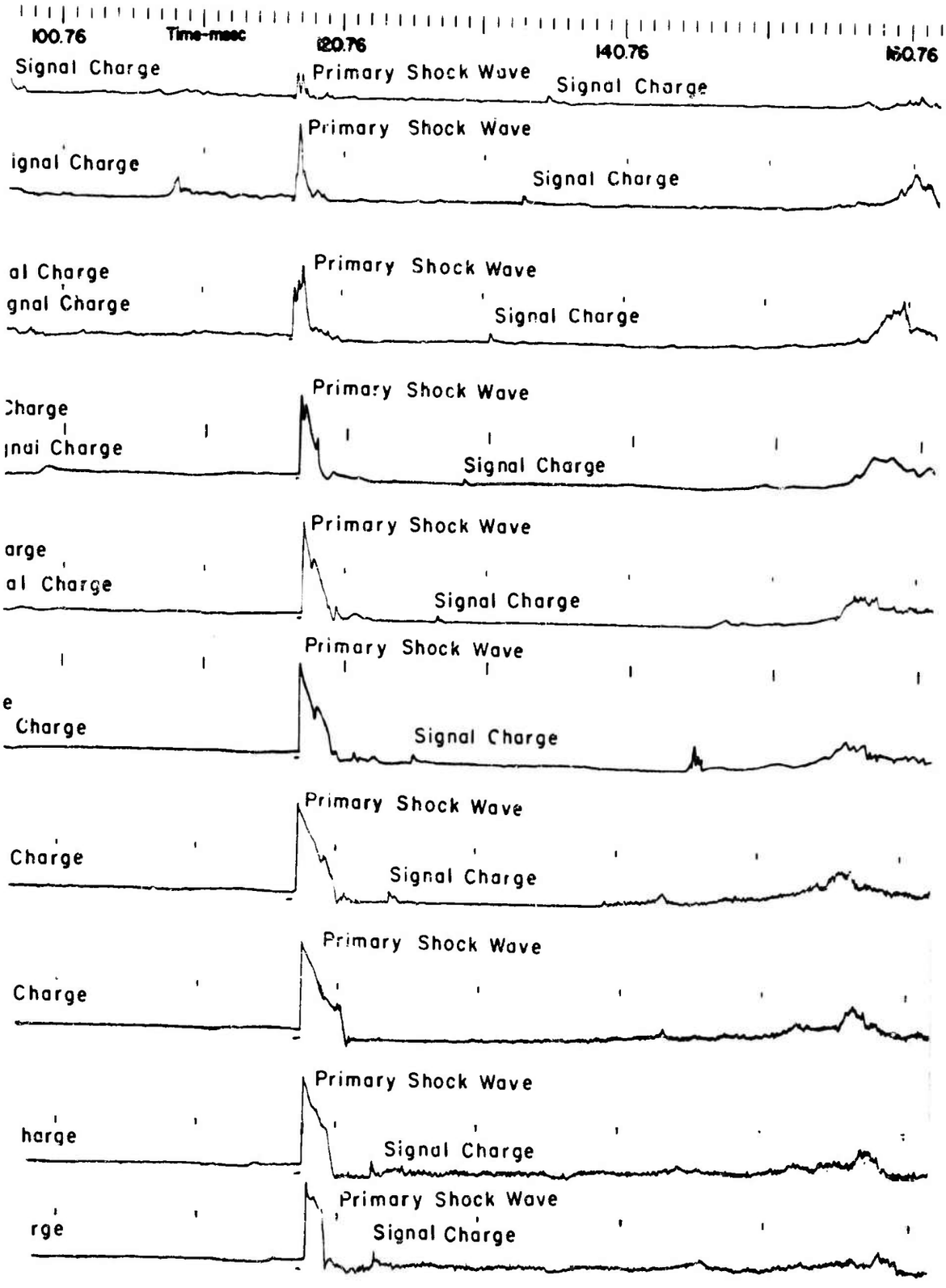
100.76
Time-msec
120.76
140.76
160.76
Signal Charge
Primary Shock Wave
Signal Charge
Primary Shock Wave
ignal Charge
Signal Charge
al Charge
gnal Charge
Primary Shock Wave
Signal Charge
Charge
gnal Charge
Primary Shock Wave
Signal Charge
arge
al Charge
Primary Shock Wave
Signal Charge
e
Charge
Primary Shock Wave
Signal Charge
Charge
Primary Shock Wave
Signal Charge
Charge
Primary Shock Wave
Signal Charge
harge
Primary Shock Wave
Signal Charge
rge
Primary Shock Wave
Signal Charge

B

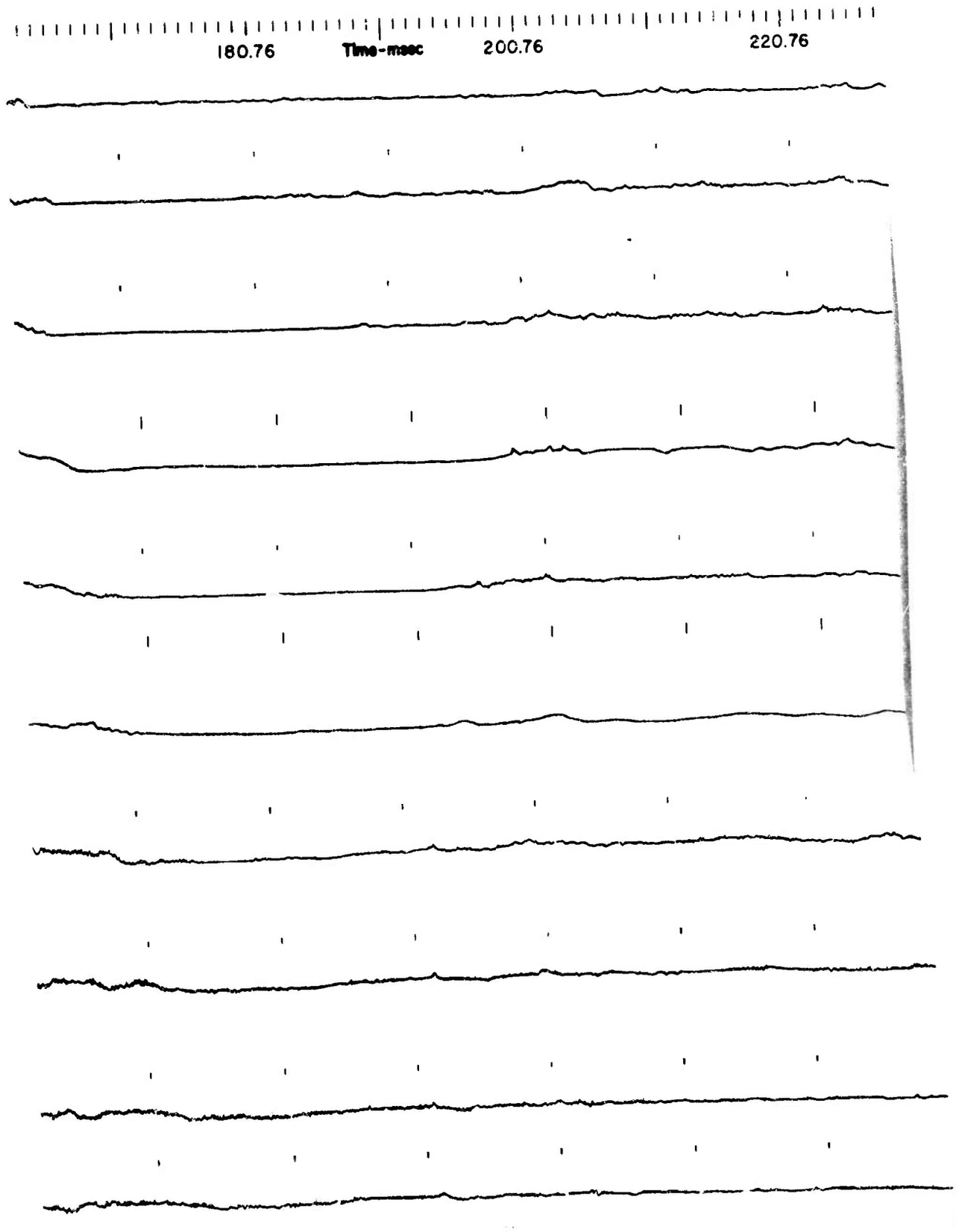

Figure

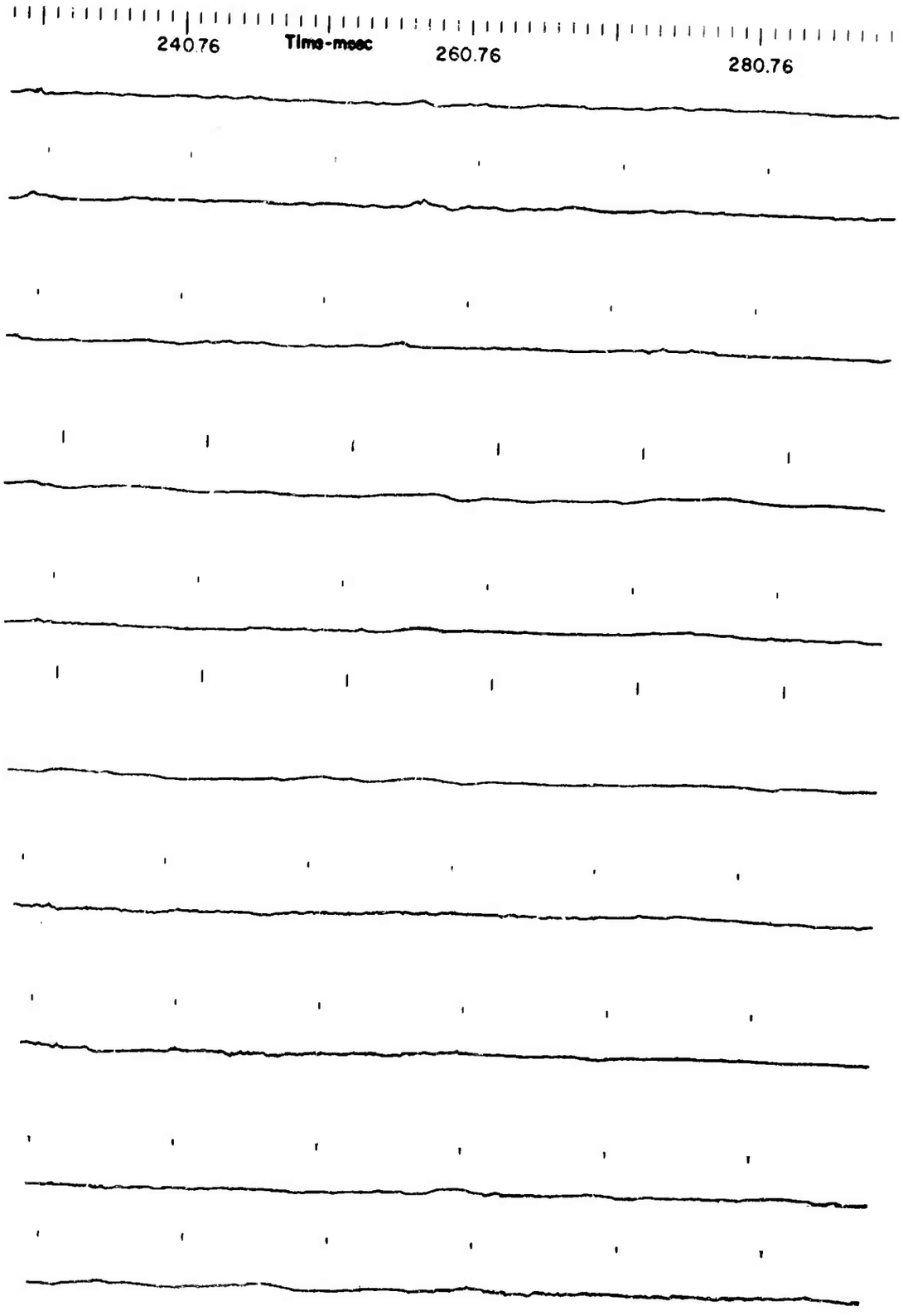

A6 - Pressure Histories - 600-Ft Range from Burst at 50-Ft Depth (Station 5, Test 6)

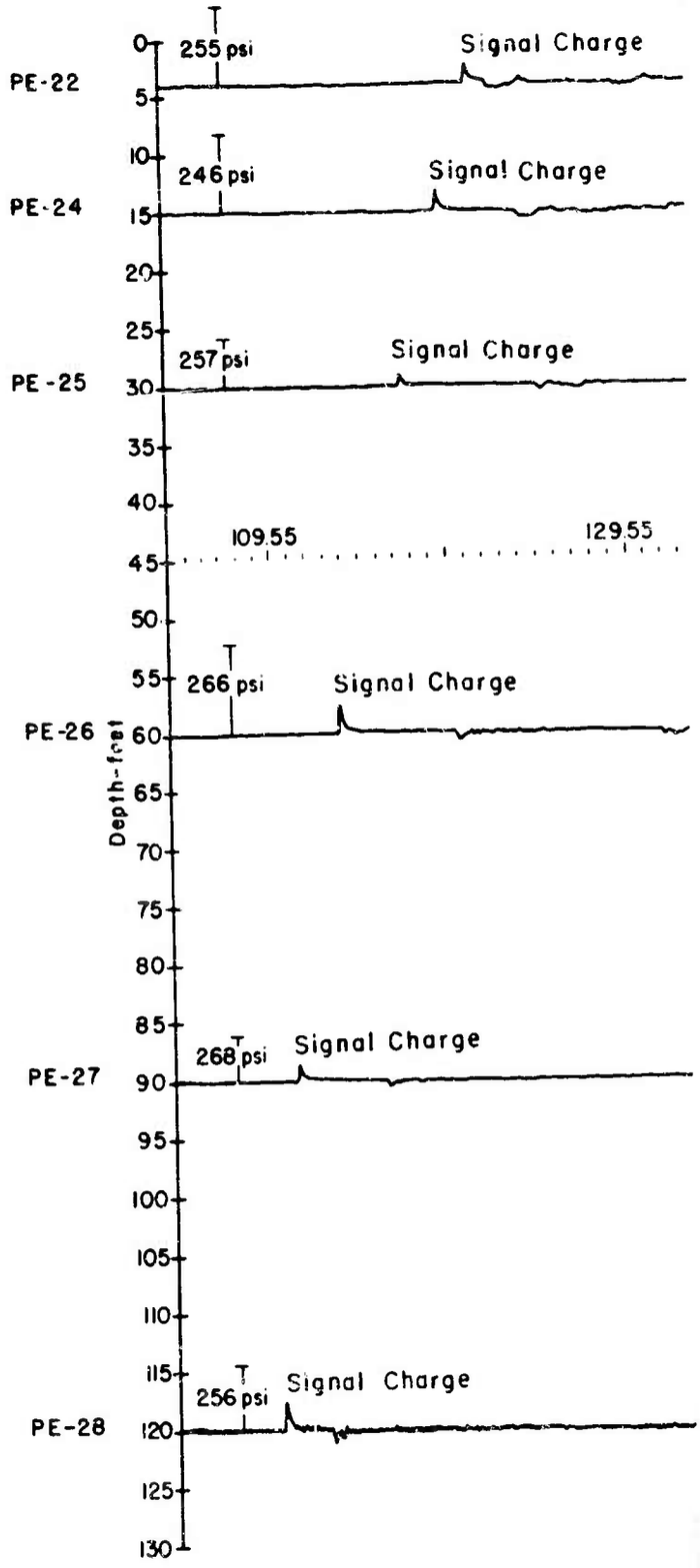
255 psi
Signal Charge
PE-22
246 psi
Signal Charge
PE-24
257 psi
Signal Charge
PE-25
109.55
129.55
266 psi
Signal Charge
PE-26
Depth-feet
268 psi
Signal Charge
PE-27
256 psi
Signal Charge
PE-28
0
5
10
15
20
25
30
35
40
45
50
55
60
65
70
75
80
85
90
95
100
105
110
115
120
125
130

A

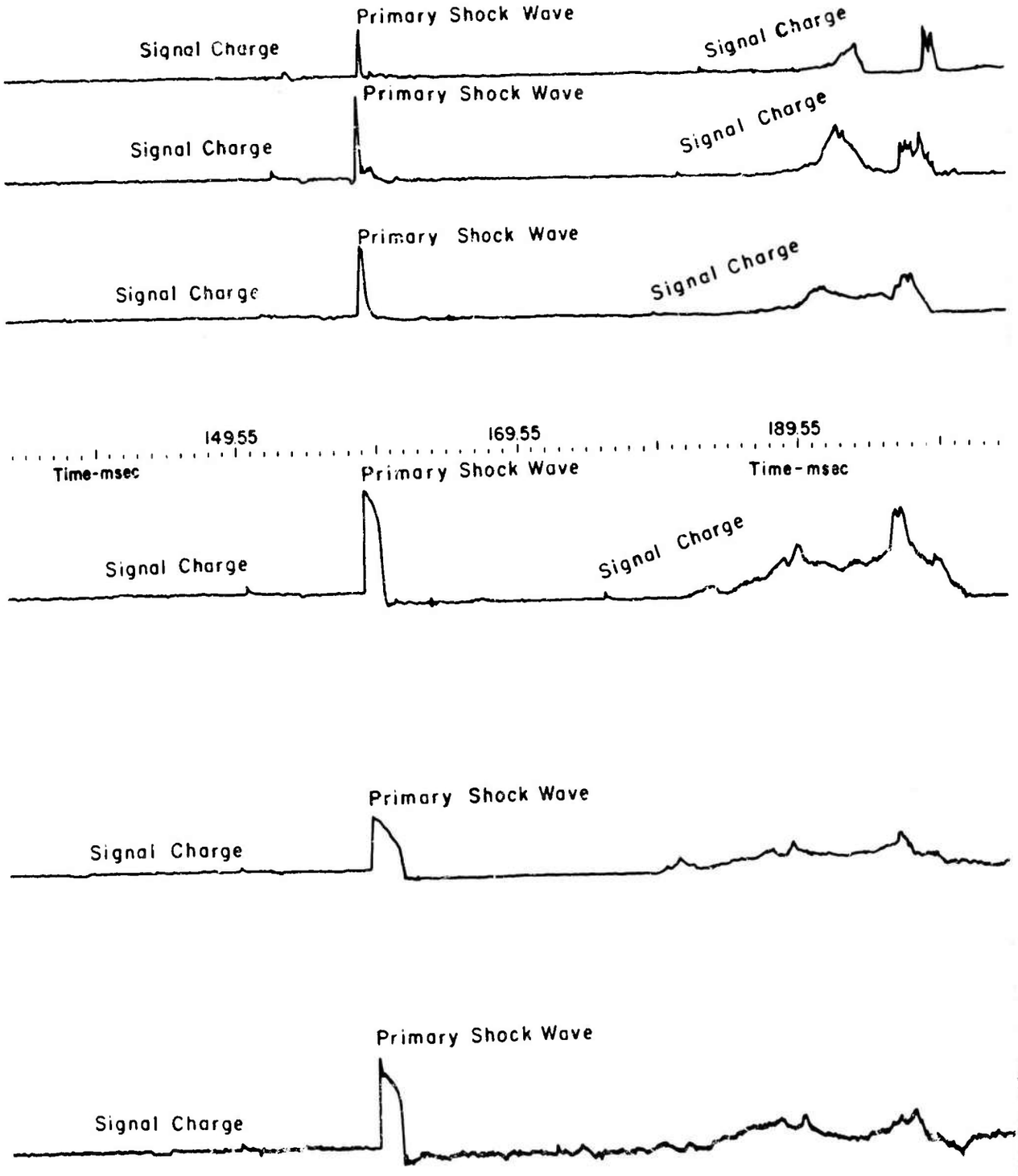
Primary Shock Wave
Signal Charge
Signal Charge
Primary Shock Wave
Signal Charge
Signal Charge
Primary Shock Wave
Signal Charge
Signal Charge
149.55
169.55
189.55
Time-msec
Time-msec
Primary Shock Wave
Signal Charge
Signal Charge
Primary Shock Wave
Signal Charge
Primary Shock Wave
Signal Charge

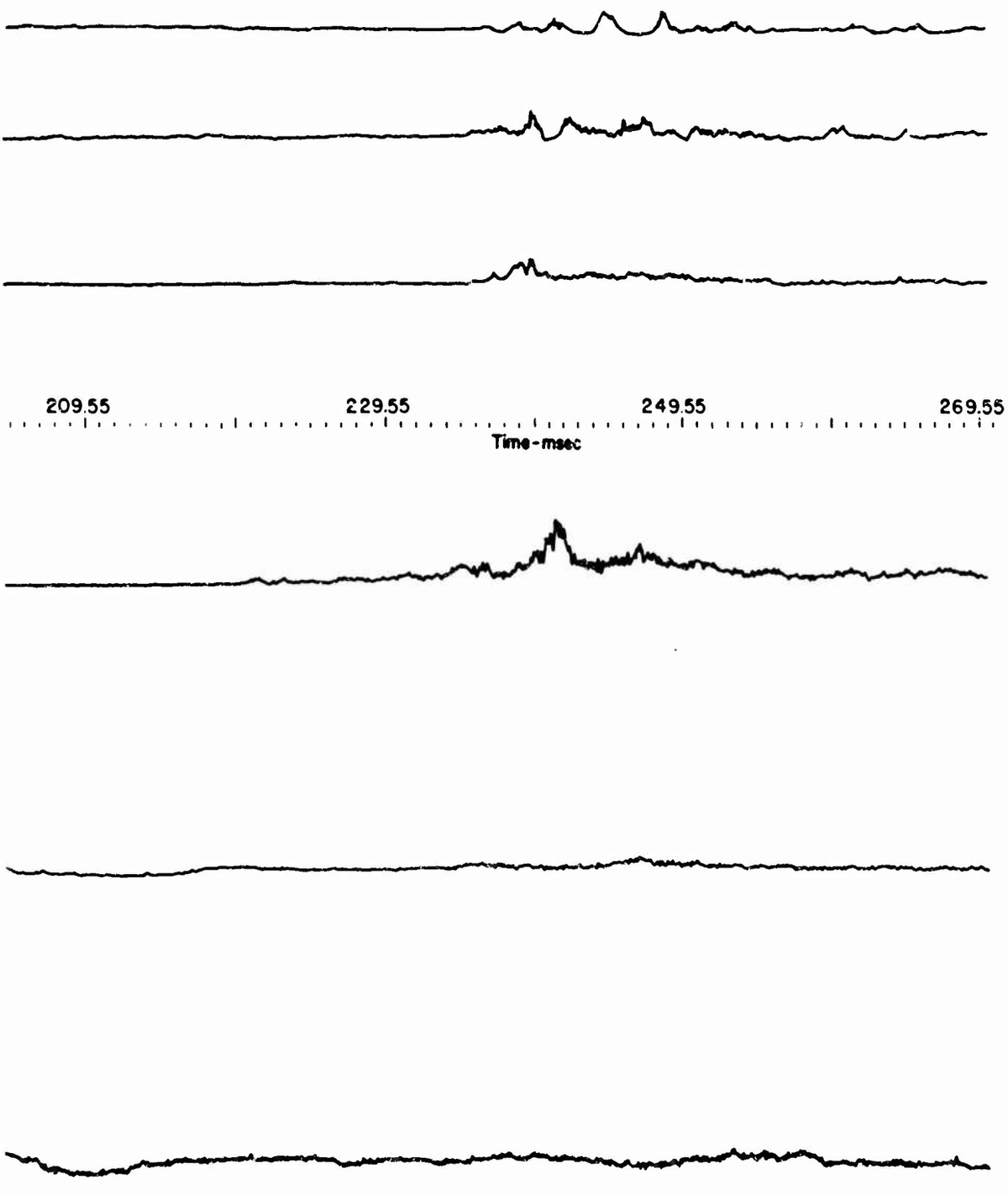

Figure A7 - Pressure Histories - 800-Ft Range from Burst at 50-Ft Depth (Station 5, Test 1)

C

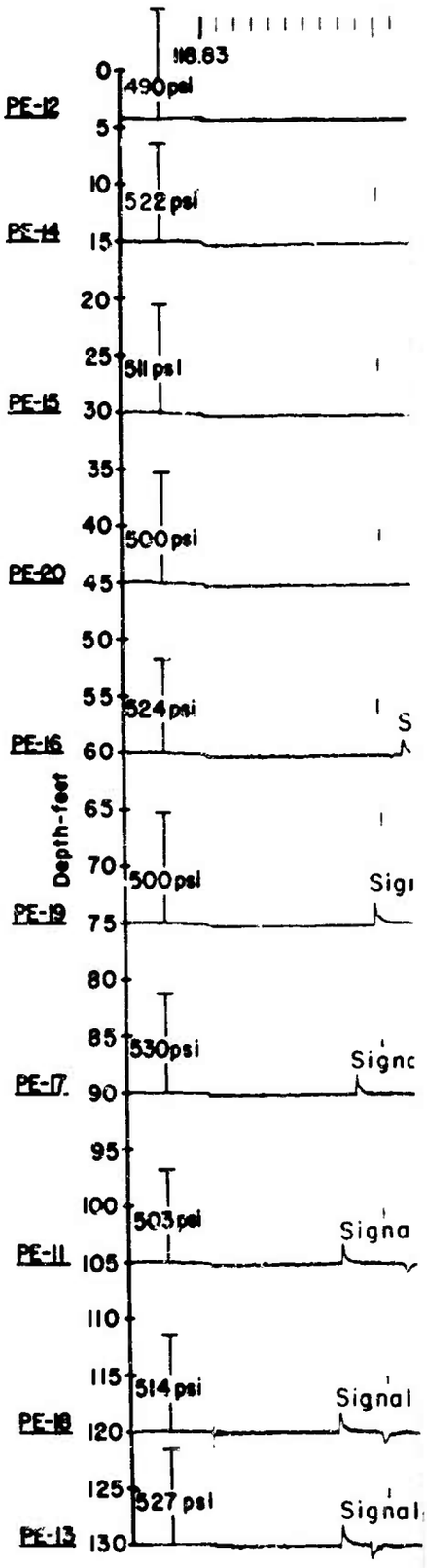
118.83
0
490 psi
PE-12
5
10
522 psi
PE-14
15
20
25
511 psi
PE-15
30
35
40
500 psi
PE-20
45
50
55
524 psi
S
PE-16
60
Depth-feet
65
70
500 psi
Sig
PE-19
75
80
85
530 psi
Signc
PE-17
90
95
100
503 psi
Signa
PE-11
105
110
115
514 psi
Signal
PE-18
120
125
527 psi
Signal
PE-13
130

A-

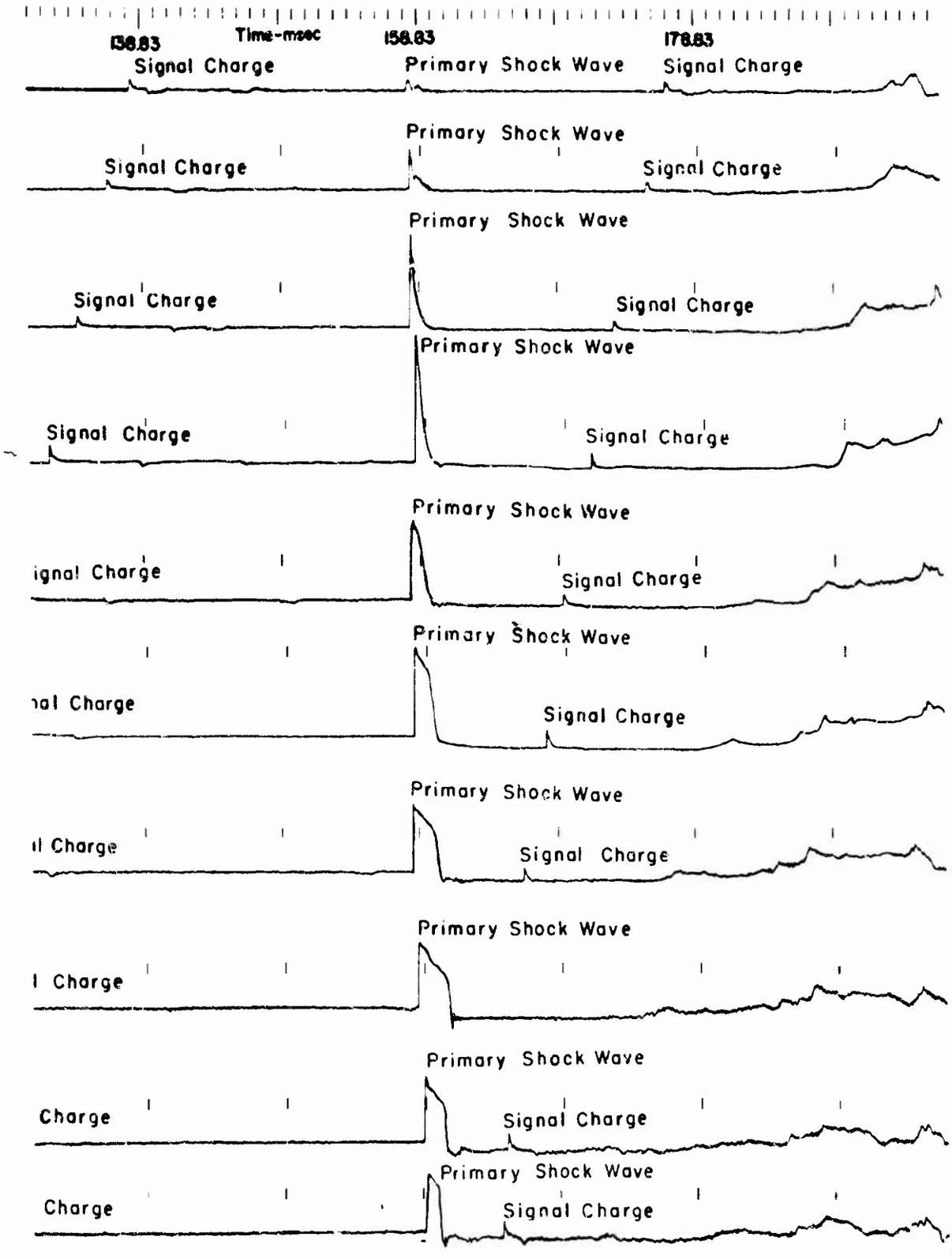
138.83
Time-msec
158.83
178.83
Signal Charge
Primary Shock Wave
Signal Charge
Primary Shock Wave
Signal Charge
Signal Charge
Primary Shock Wave
Signal Charge
Signal Charge
Primary Shock Wave
Signal Charge
Signal Charge
Primary Shock Wave
ignal Charge
Signal Charge
Primary Shock Wave
al Charge
Signal Charge
Primary Shock Wave
l Charge
Signal Charge
Primary Shock Wave
l Charge
Primary Shock Wave
Charge
Signal Charge
Primary Shock Wave
Charge
Signal Charge

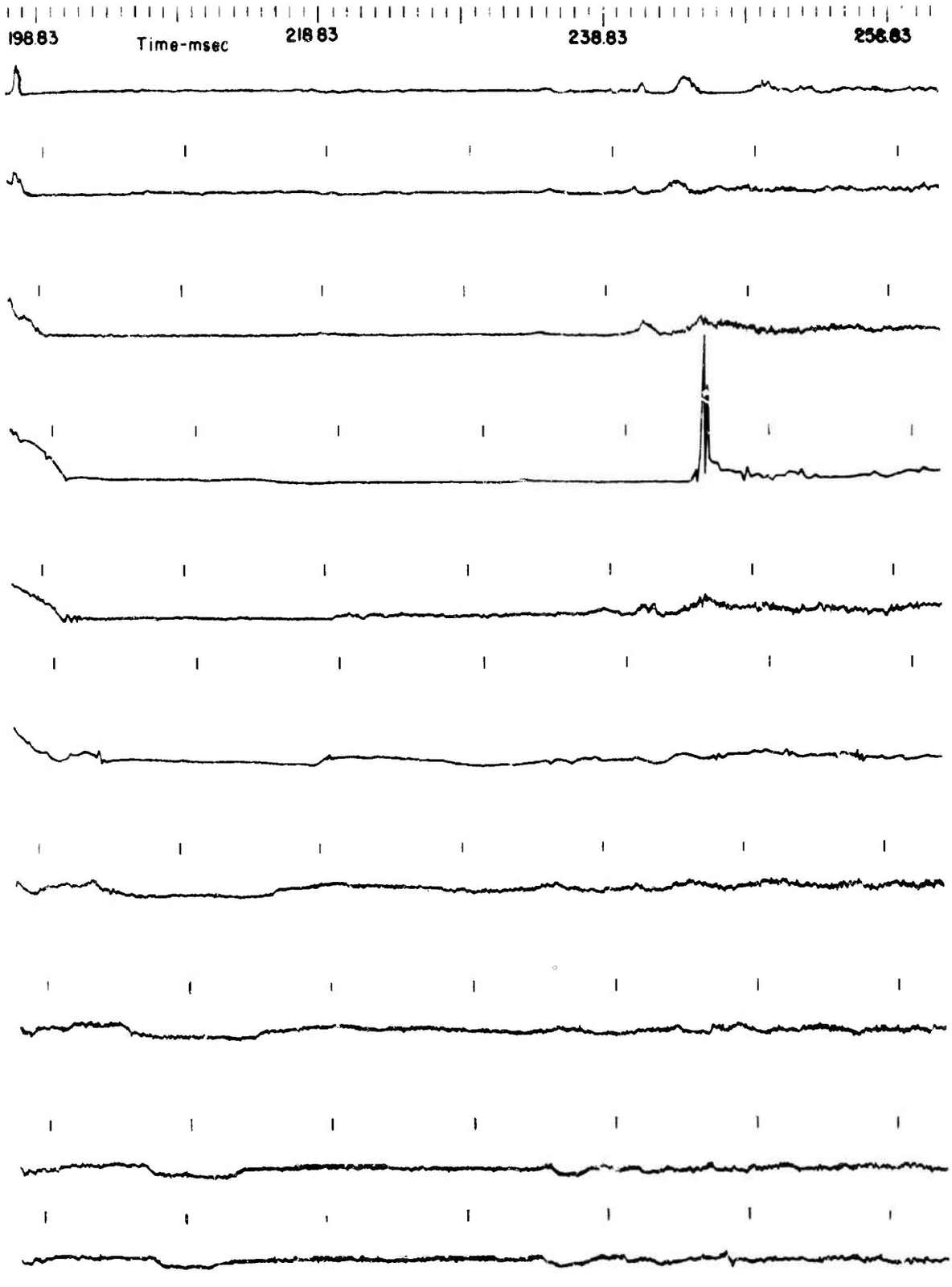

Fig

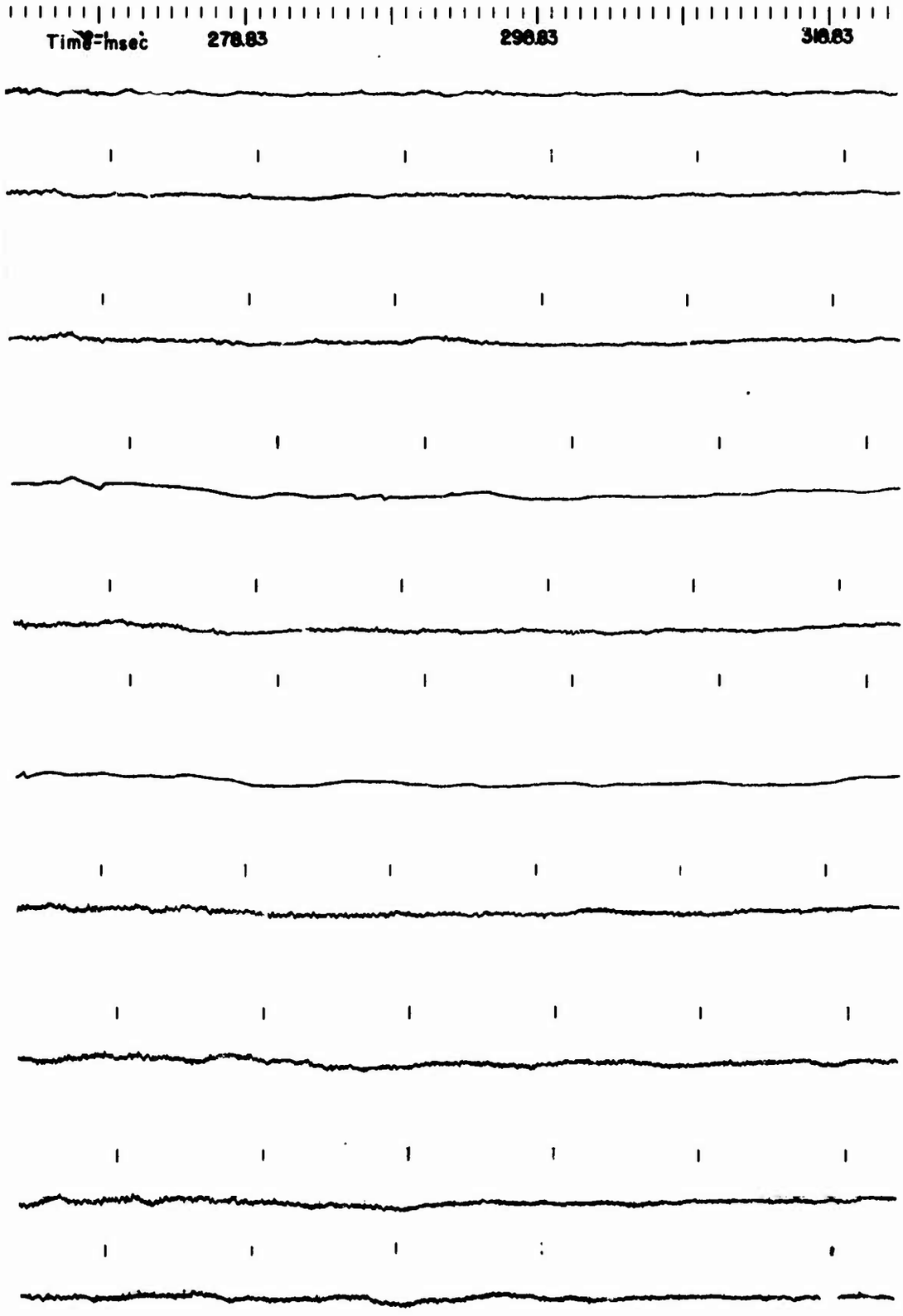

ıre A8 - Pressure Histories - 800-Ft Range from Burst at 50-Ft Depth (Station 3, Test 4)

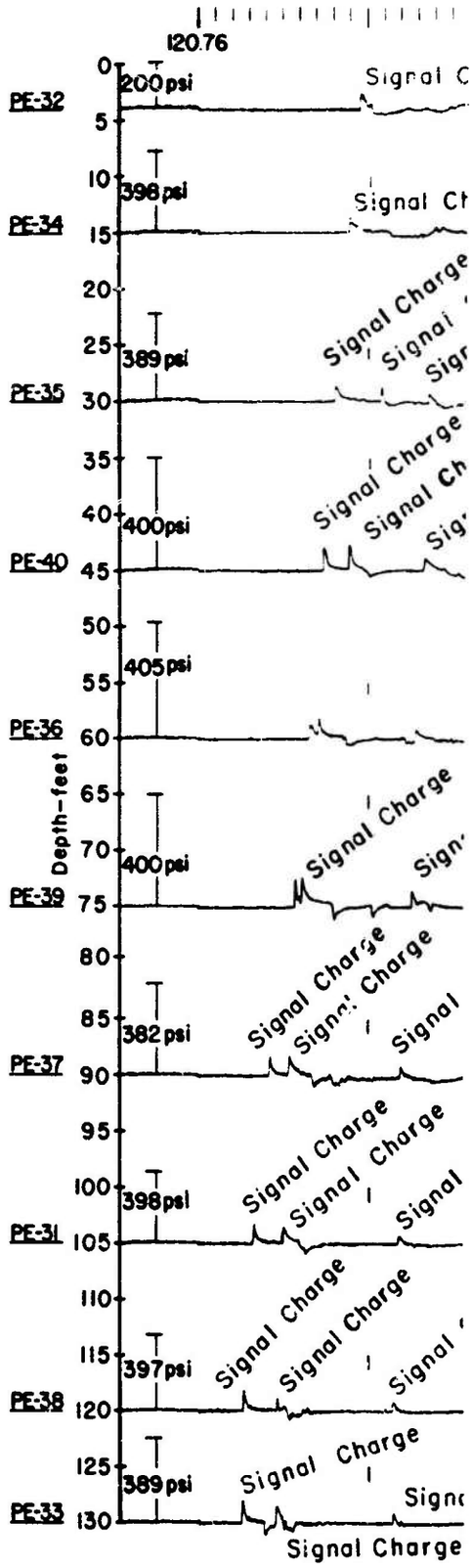
120.76
200psi
PE-32
398psi
PE-34
389psi
PE-35
400psi
PE-40
405psi
PE-36
400psi
PE-39
382psi
PE-37
398psi
PE-31
397psi
PE-38
389psi
PE-33
Depth-feet
0
5
10
15
20
25
30
35
40
45
50
55
60
65
70
75
80
85
90
95
100
105
110
115
120
125
130
Signal Charge

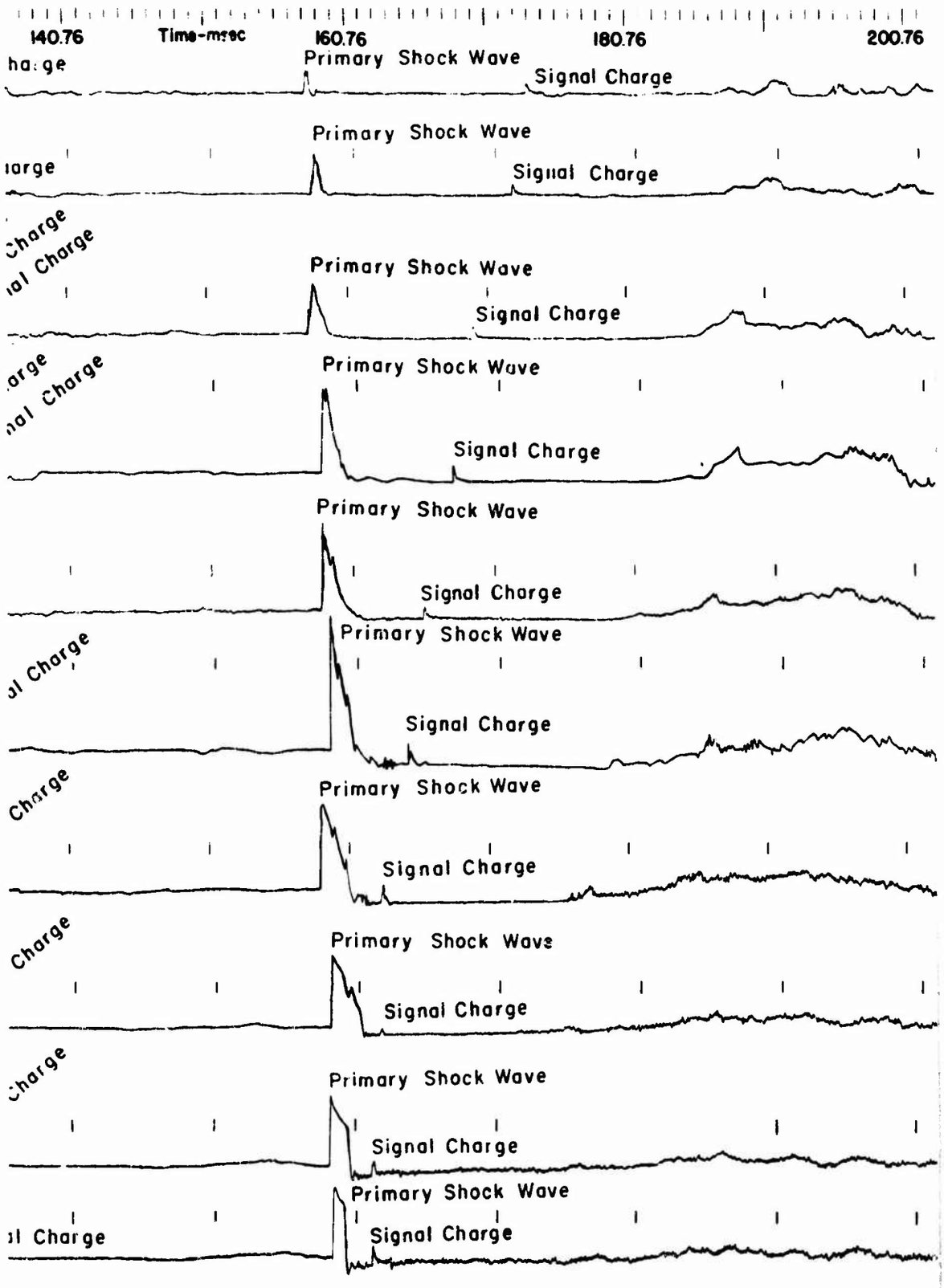
140.76
Time-msec
160.76
180.76
200.76
Primary Shock Wave
Signal Charge

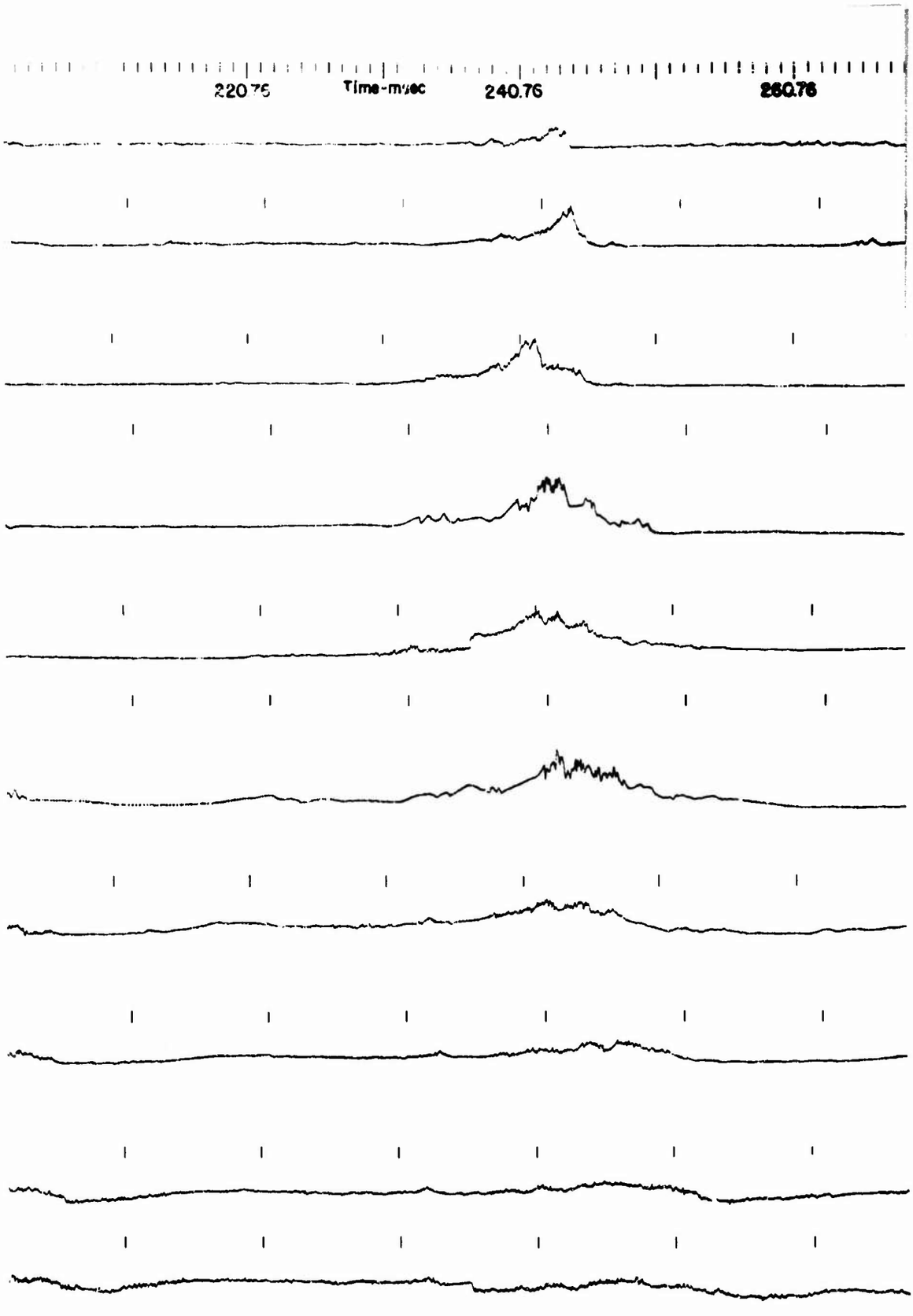

Fig

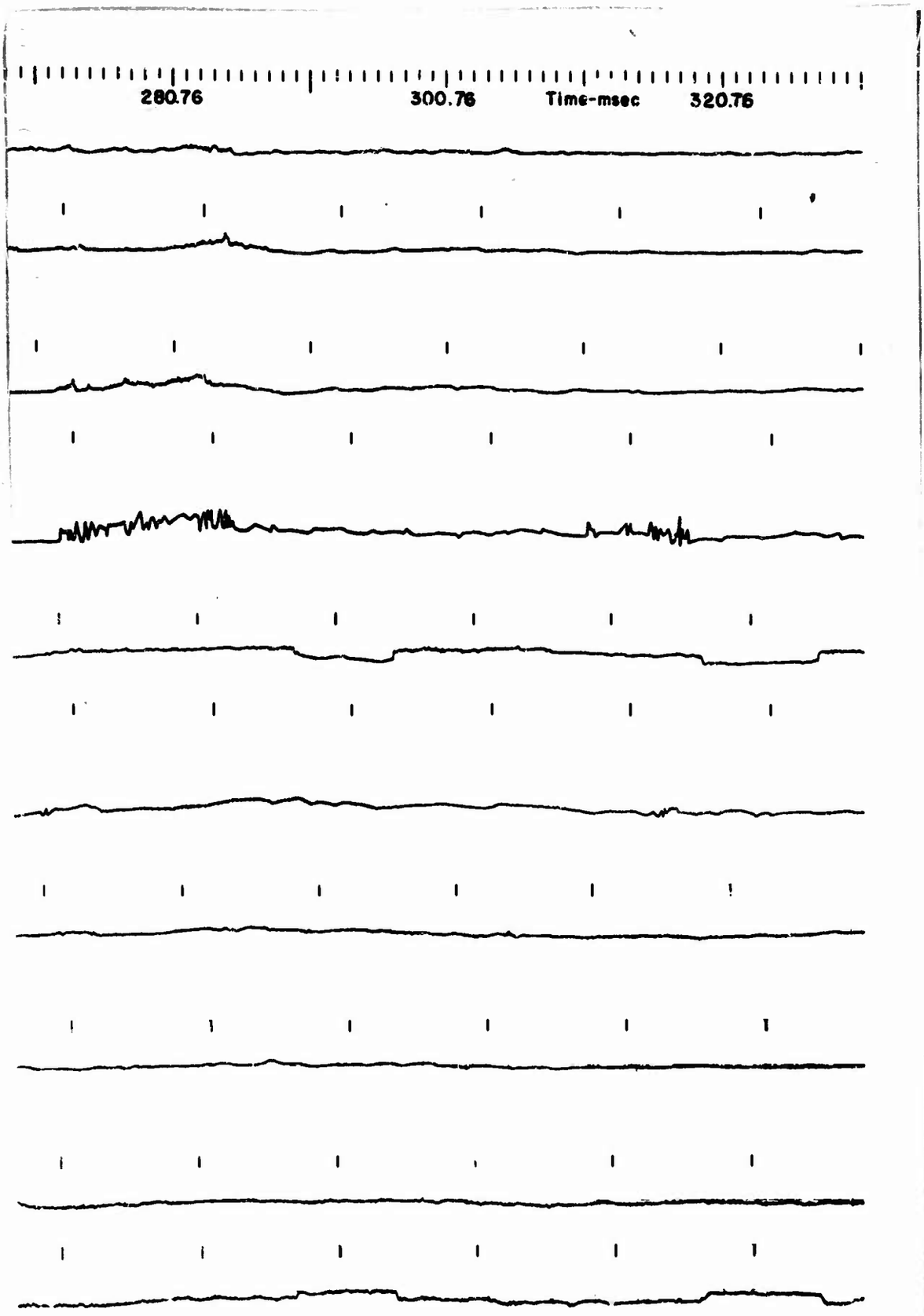

ıre A9 - Pressure Histories - 800-Ft Range from Burst at 50-Ft Depth (Station 7, Test 6)

D

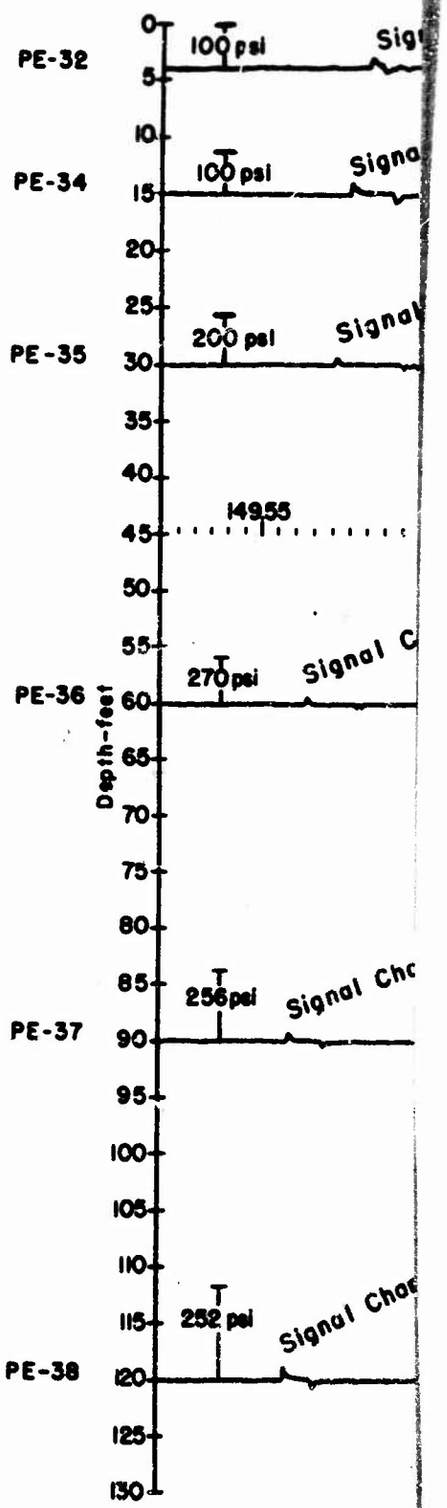
PE-32
100 psi
Sig
PE-34
100 psi
Signa
PE-35
200 psi
Signal
149.55
PE-36
270 psi
Signal C
Depth-feet
0
5
10
15
20
25
30
35
40
45
50
55
60
65
70
75
80
85
90
95
100
105
110
115
120
125
130
PE-37
256 psi
Signal Cha
PE-38
252 psi
Signal Chas

A

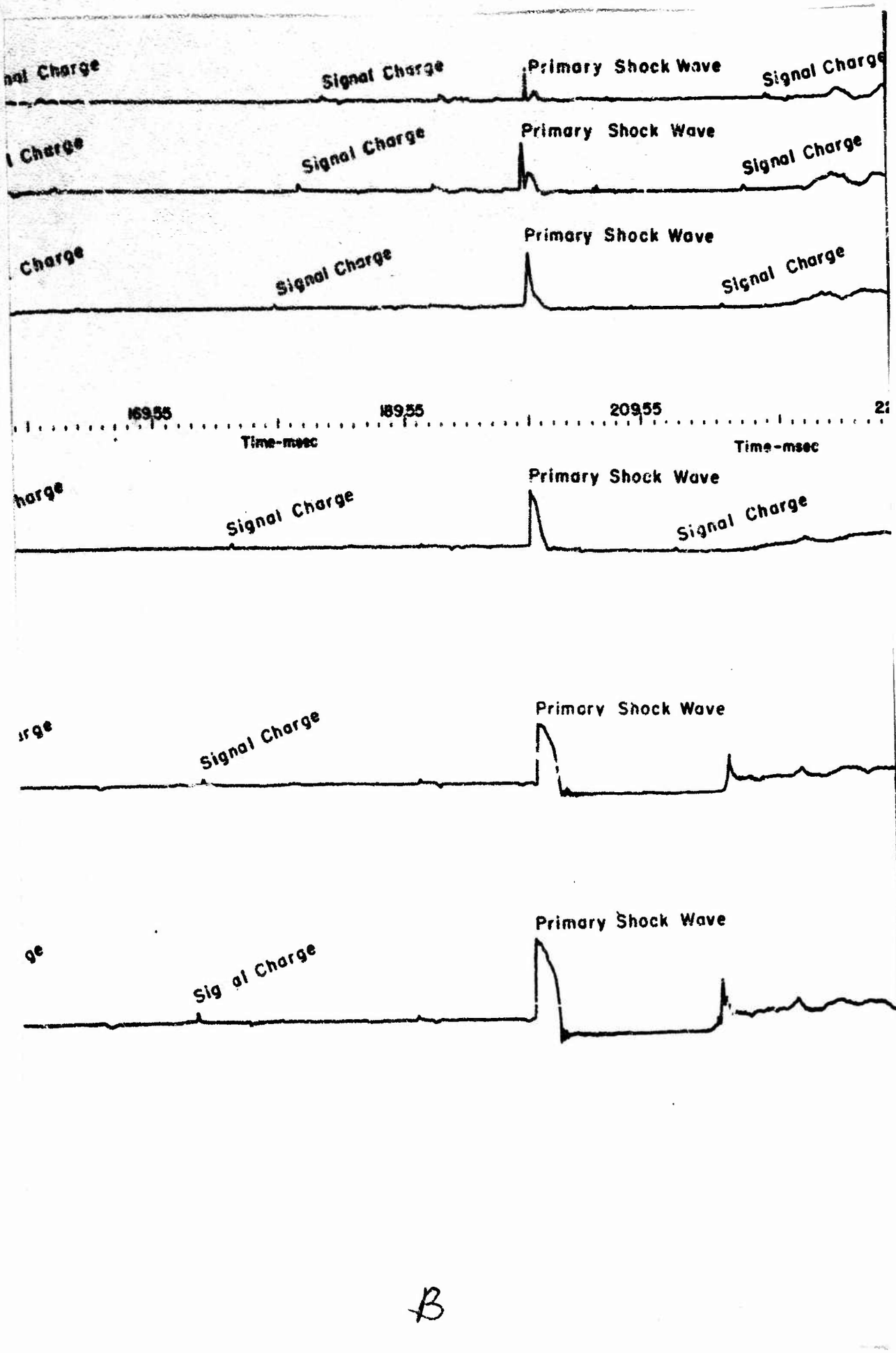
nal Charge
Signal Charge
Primary Shock Wave
Signal Charge
l Charge
Signal Charge
Primary Shock Wave
Signal Charge
Charge
Signal Charge
Primary Shock Wave
Signal Charge
169.55
189.55
209.55
Time-msec
Time-msec
harge
Signal Charge
Primary Shock Wave
Signal Charge
rge
Signal Charge
Primary Shock Wave
ge
Sig al Charge
Primary Shock Wave

B

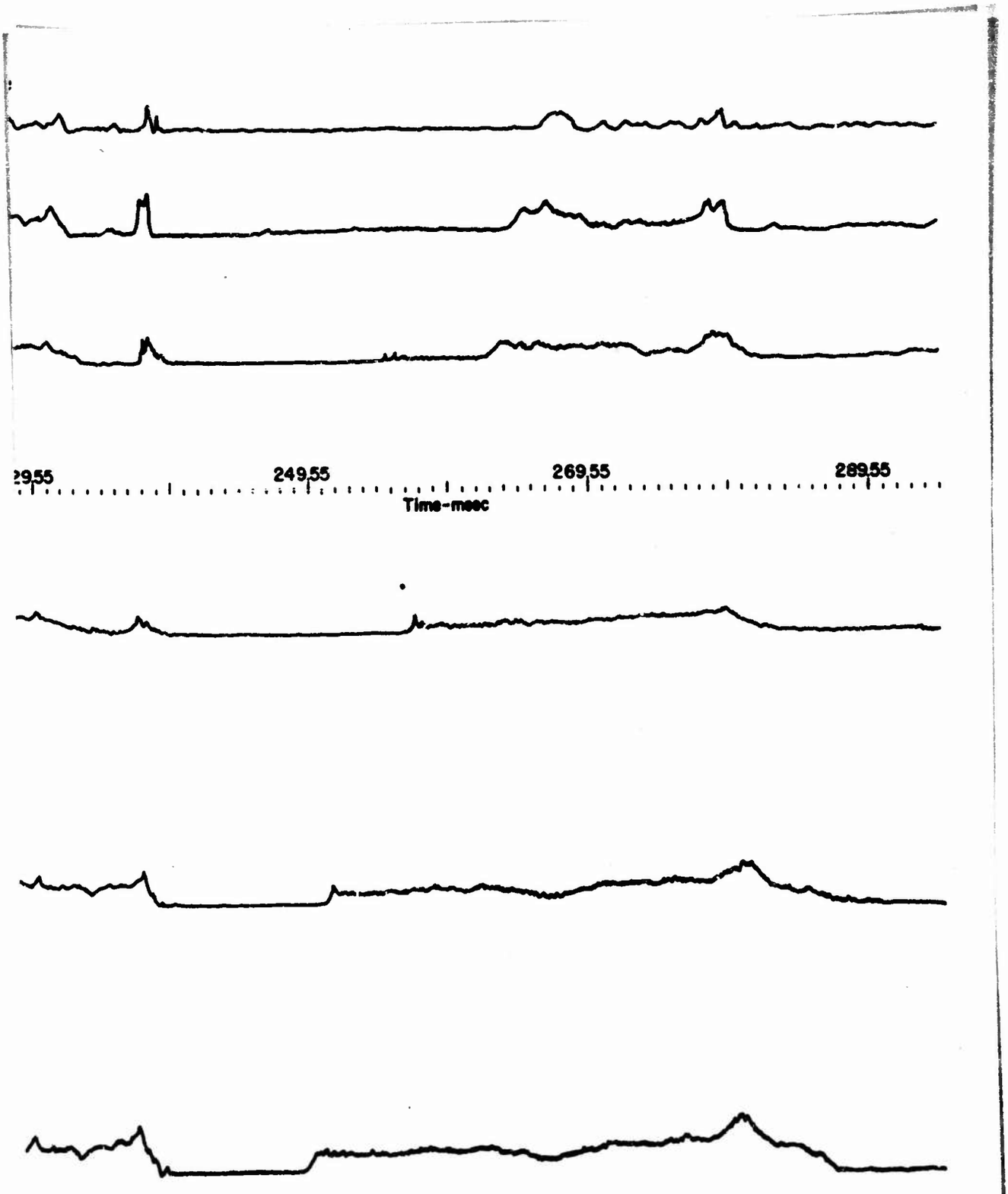

Figure A10 - Pressure Histories - 1000-Ft Range from Burst at 50-Ft Depth (Station 7, Test 1)

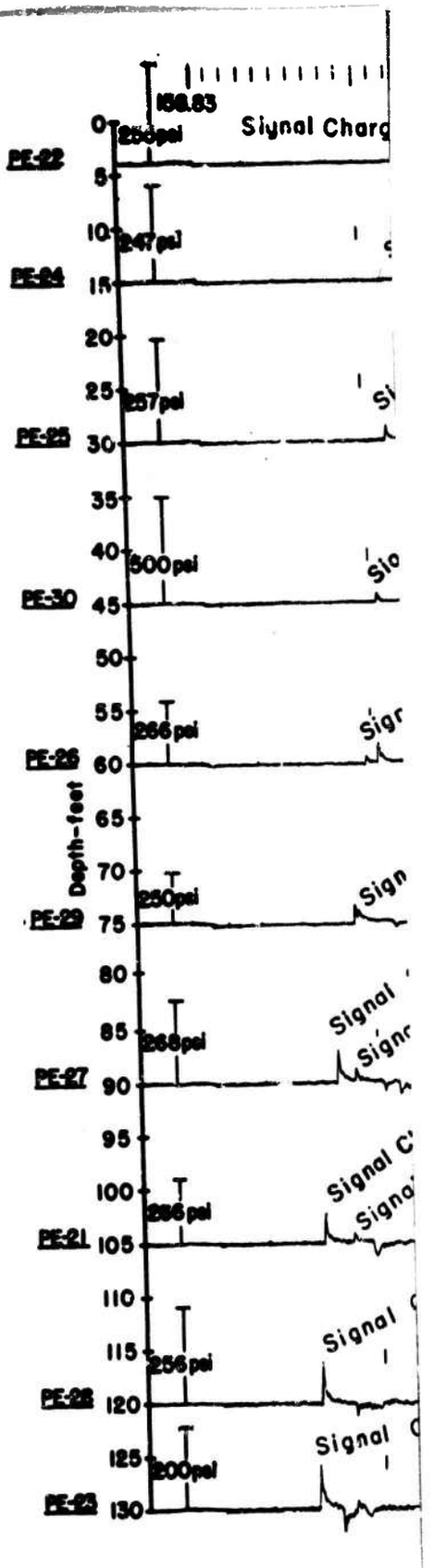
156.83
Signal Charg
250psi
PE-22
247psi
PE-24
257psi
PE-25
300psi
PE-30
266psi
PE-26
Depth-feet
250psi
PE-29
Signal
268psi
PE-27
Signal C
286psi
PE-21
Signal
256psi
PE-28
Signal
200psi
PE-23
0
5
10
15
20
25
30
35
40
45
50
55
60
65
70
75
80
85
90
95
100
105
110
115
120
125
130

A

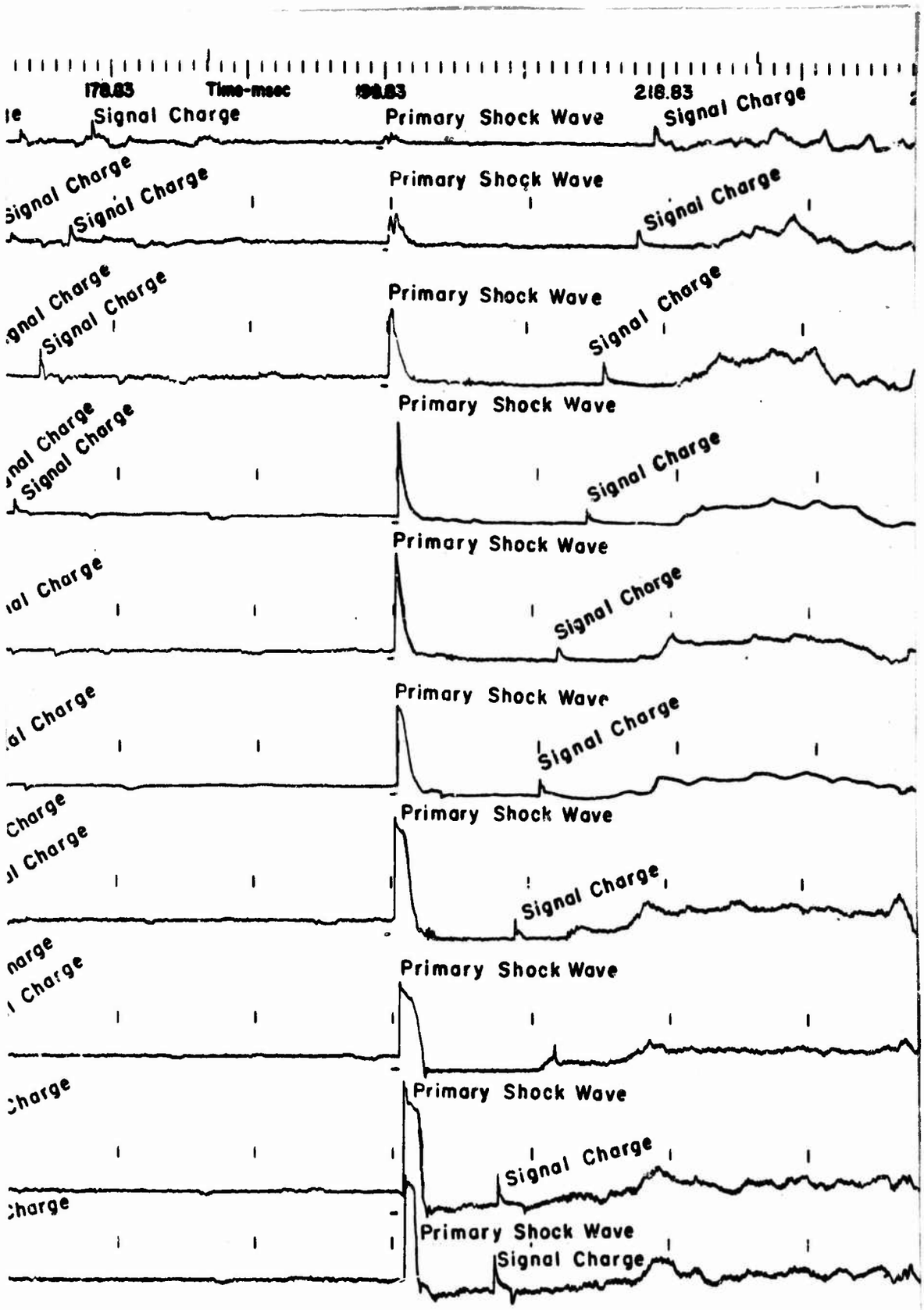
178.83
Time-msec
198.83
218.83
Signal Charge
Primary Shock Wave
Signal Charge
Primary Shock Wave
Signal Charge
Primary Shock Wave
Signal Charge
Primary Shock Wave
Signal Charge
Primary Shock Wave
Signal Charge
Primary Shock Wave
Signal Charge
Primary Shock Wave
Signal Charge
Primary Shock Wave
Signal Charge
Primary Shock Wave
Signal Charge

B

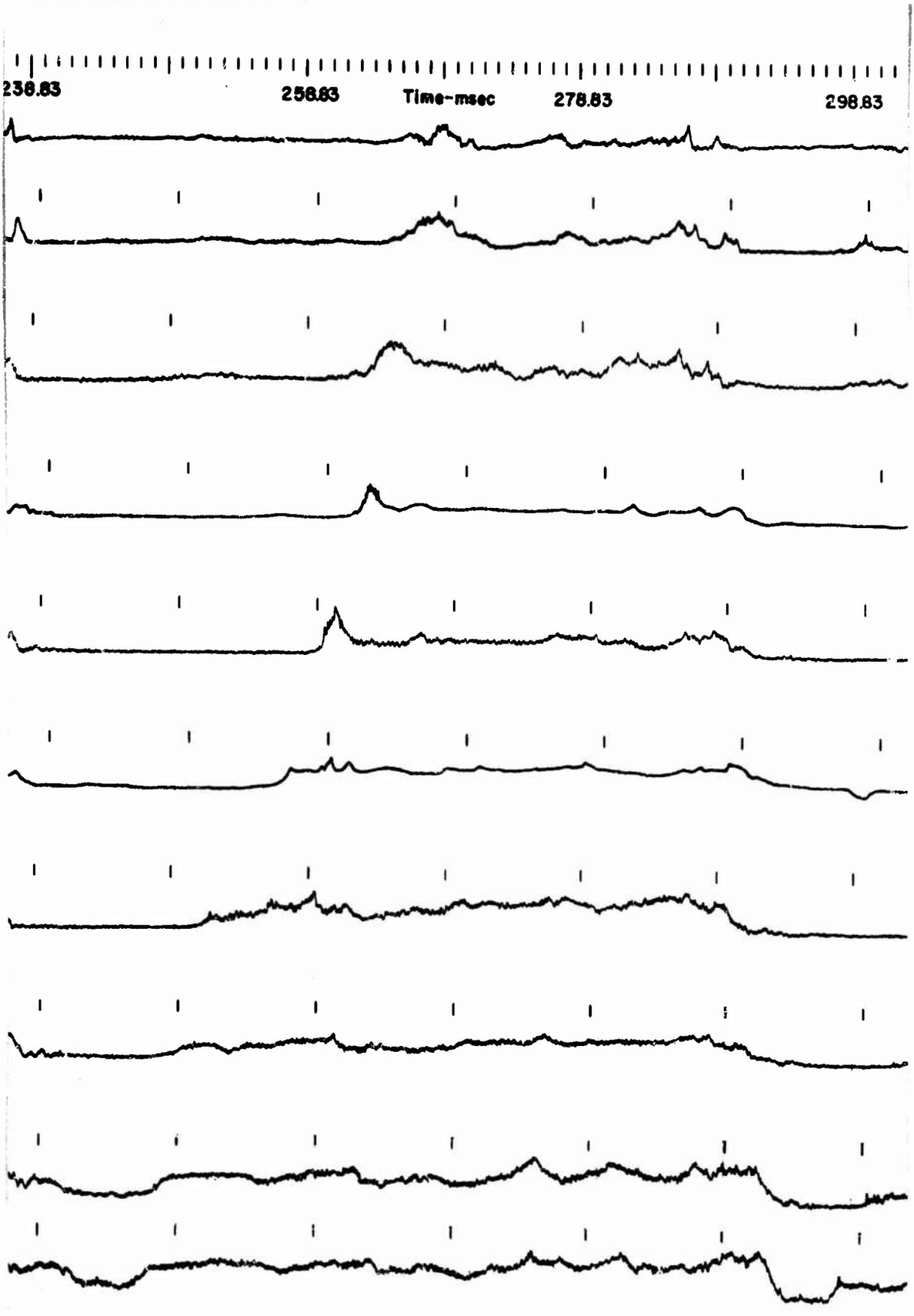

Figur

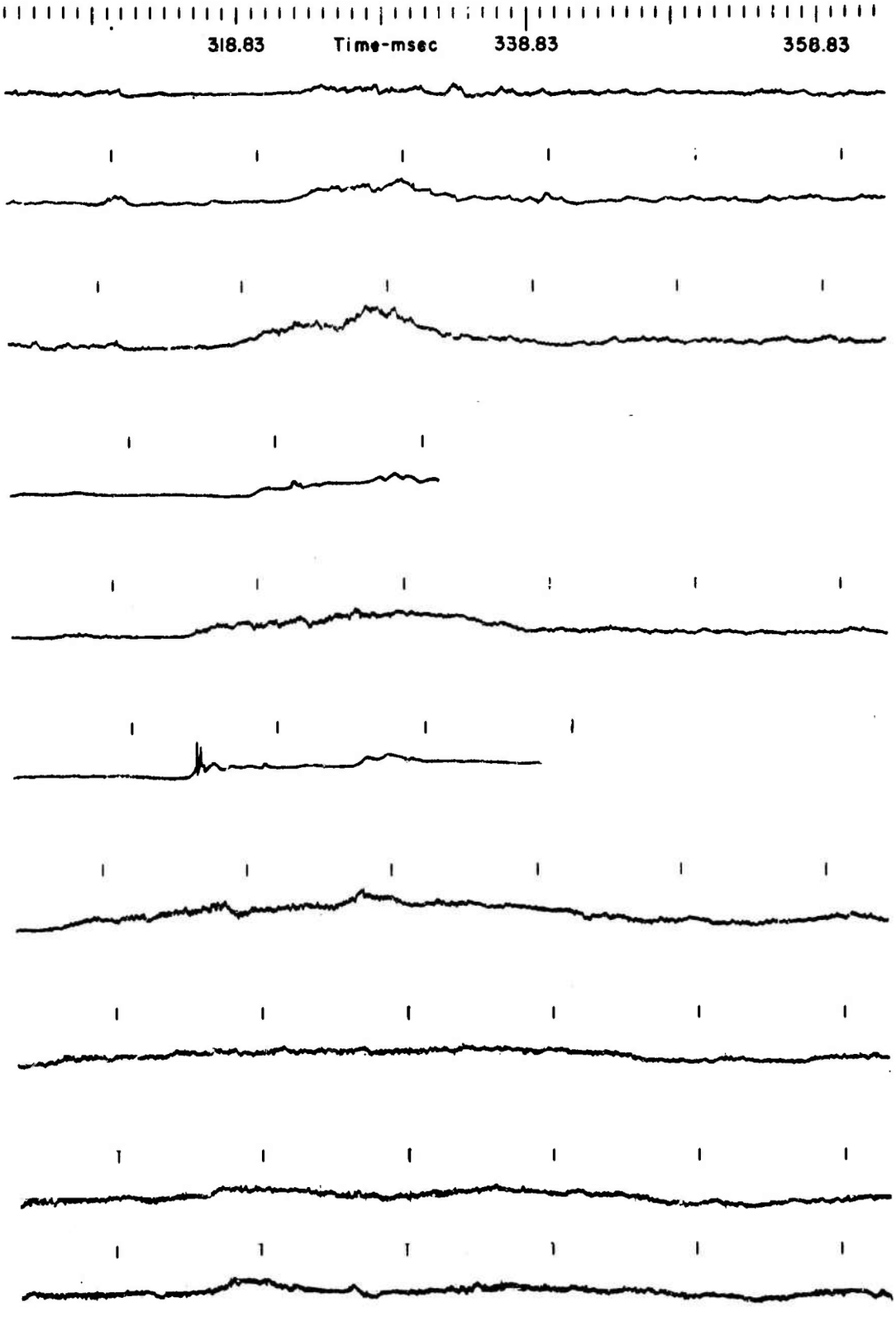

A11- Pressure Histories - 1000-Ft Range from Burst at 50-Ft Depth (Station 5, Test 4)

D

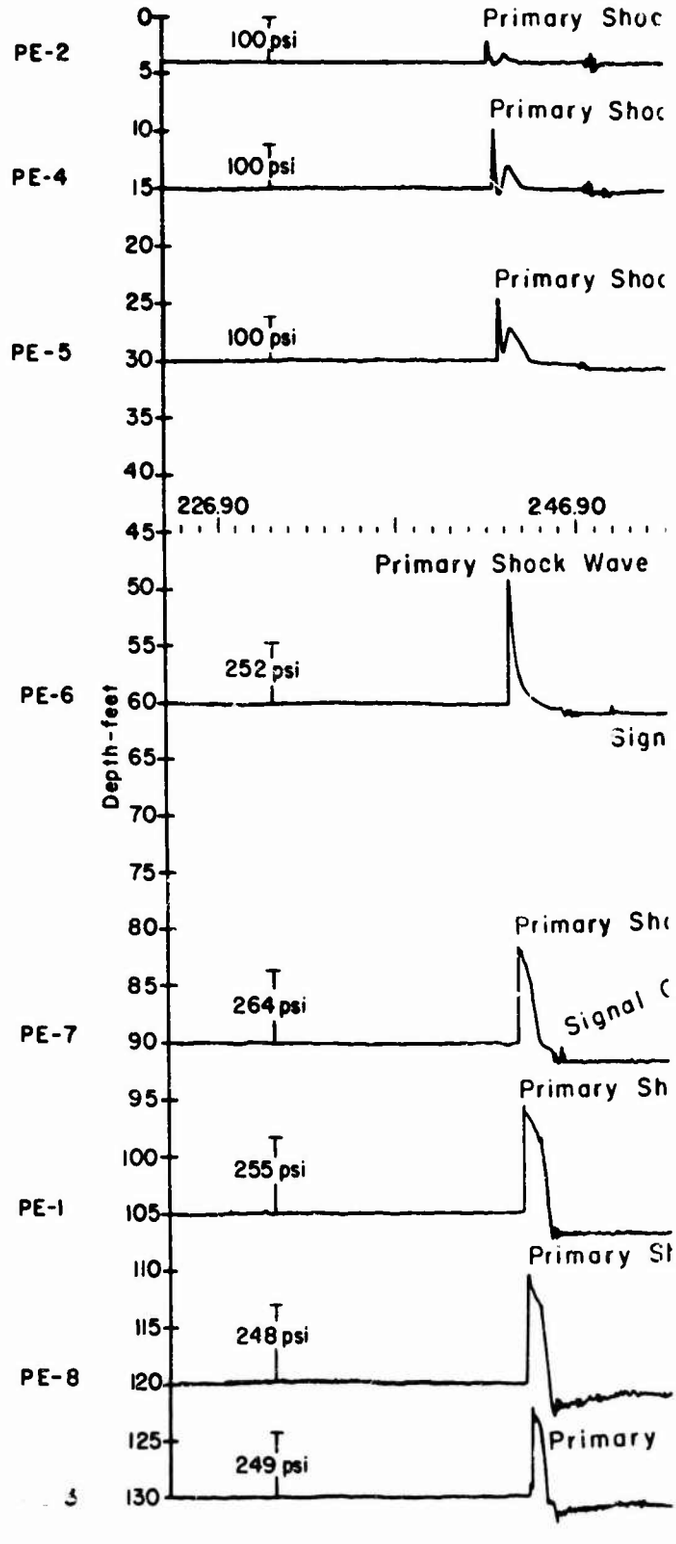
PE-2
100 psi
Primary Shoc
PE-4
100 psi
Primary Shoc
PE-5
100 psi
Primary Shoc
226.90
246.90
Primary Shock Wave
PE-6
252 psi
Sign
Depth-feet
Primary Sh
PE-7
264 psi
Signal
Primary Sh
PE-1
255 psi
Primary Sh
PE-8
248 psi
Primary
249 psi
0
5
10
15
20
25
30
35
40
45
50
55
60
65
70
75
80
85
90
95
100
105
110
115
120
125
130

A

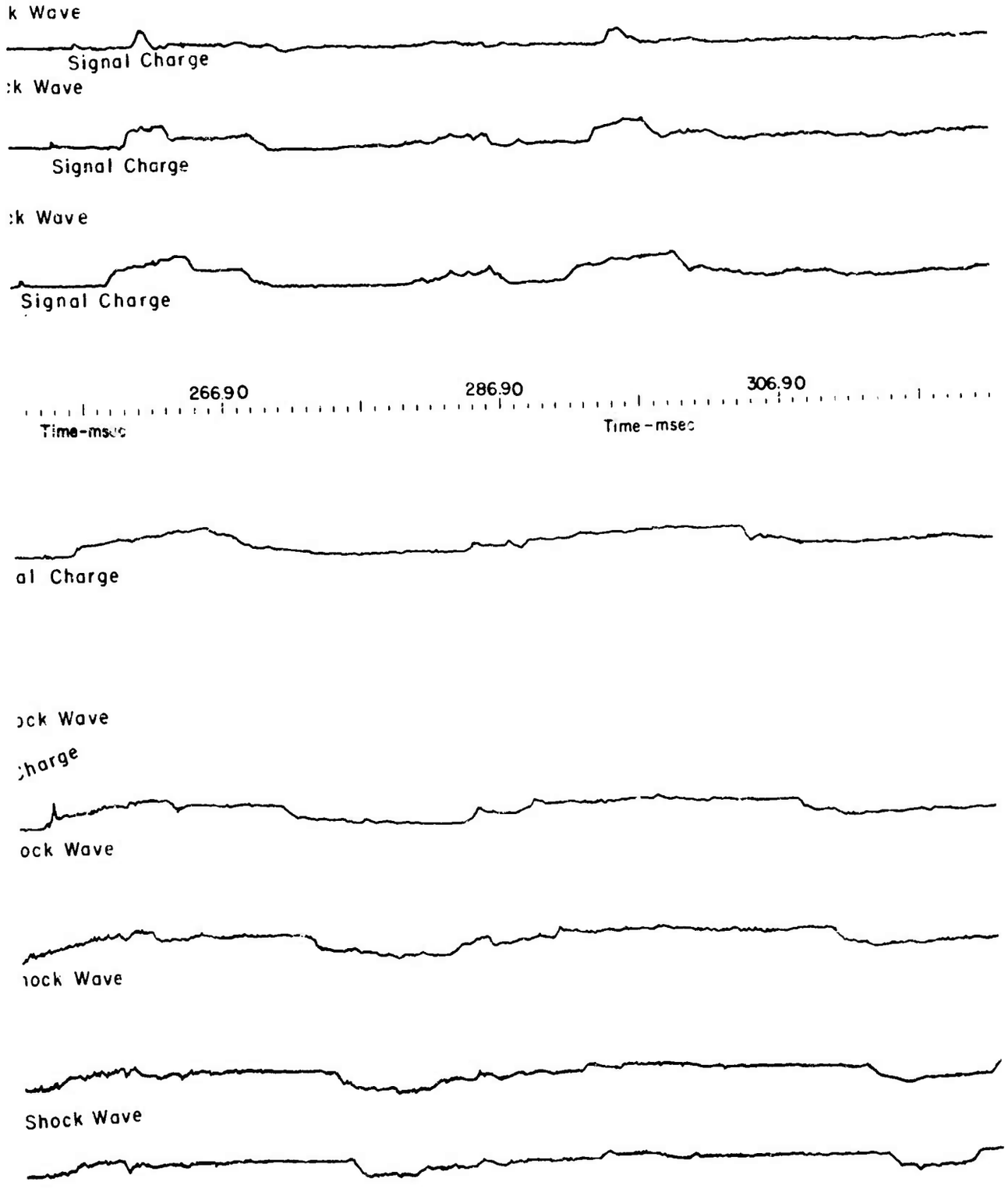
k Wave
Signal Charge
:k Wave
Signal Charge
:k Wave
Signal Charge
266.90
286.90
306.90
Time-msec
Time-msec
al Charge
ɔck Wave
:harge
ock Wave
ıock Wave
Shock Wave

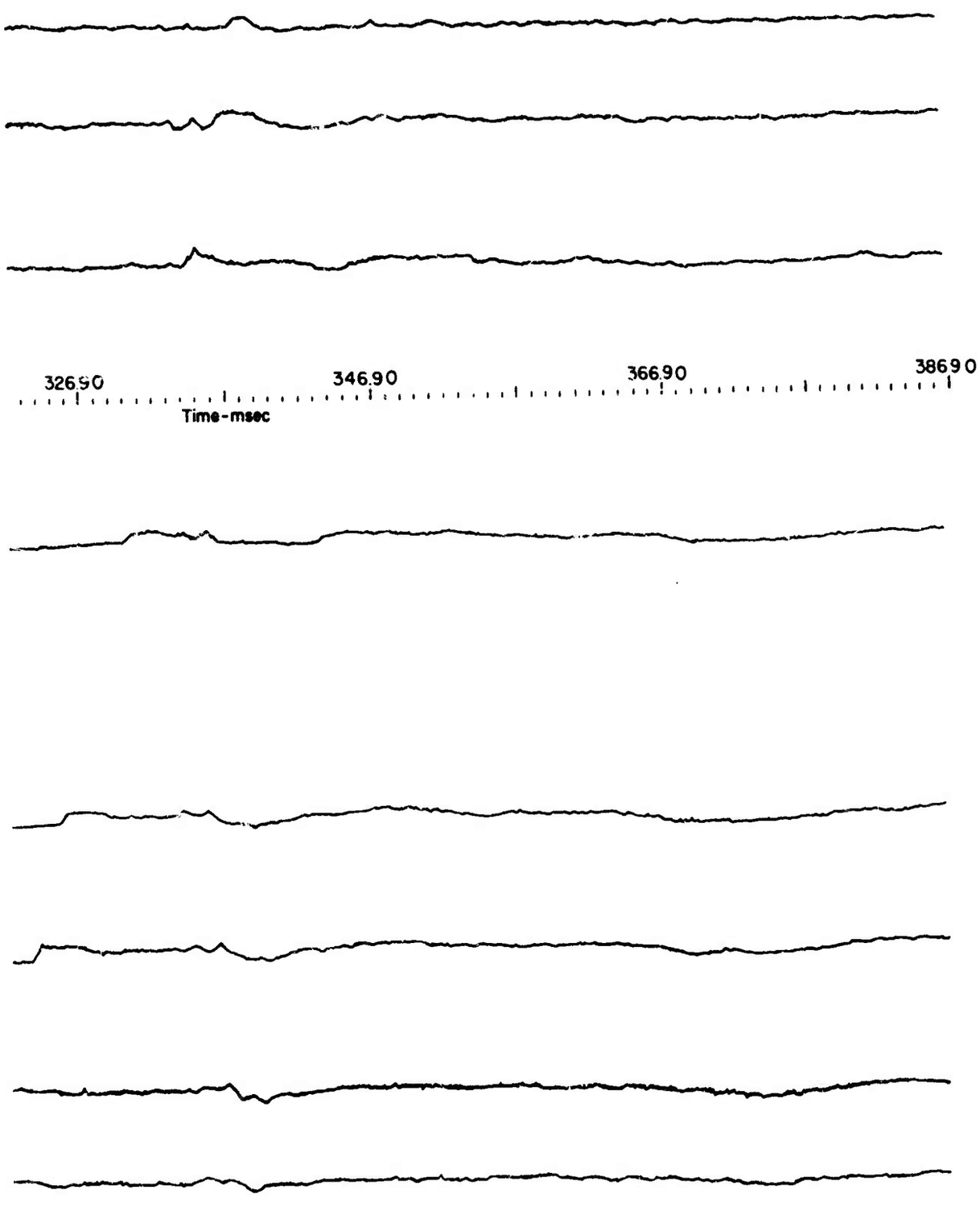

Figure A12 - Pressure Histories - 1200-Ft Range from Burst at 50-Ft Depth (Station 1, Test 2)

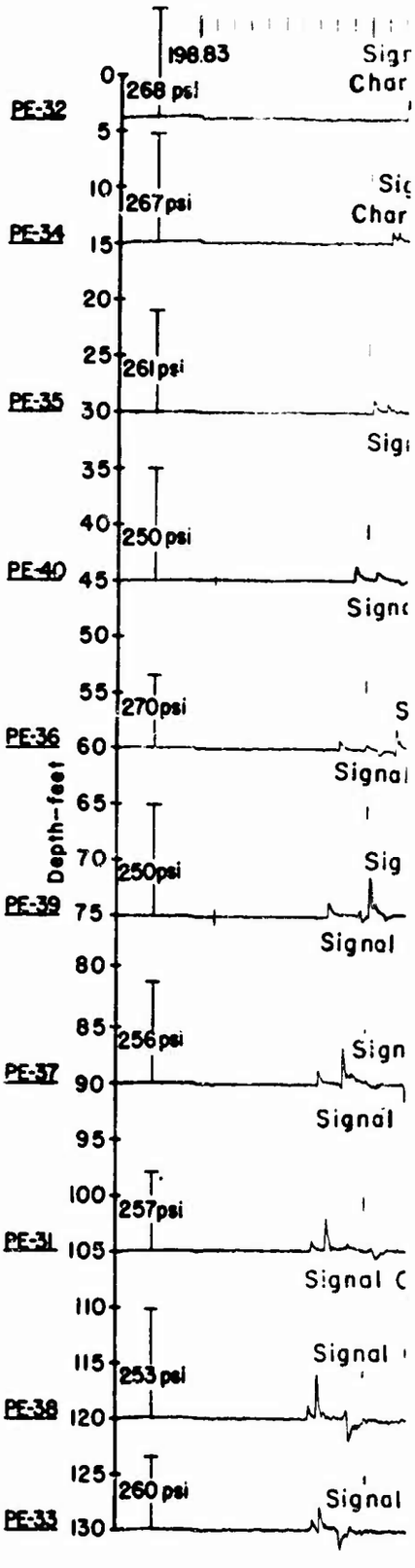
198.83
Sign
Char
0
268 psi
PE-32
5
10
267psi
Sig
Char
PE-34
15
20
25
261psi
PE-35
30
Sig
35
40
250 psi
PE-40
45
Signa
50
55
270psi
S
PE-36
60
Signal
65
Depth-feet
70
250psi
Sig
PE-39
75
Signal
80
85
256psi
Sign
PE-37
90
Signal
95
100
257psi
PE-31
105
Signal C
110
115
Signal
253 psi
PE-38
120
125
260 psi
Signal
PE-33
130

A

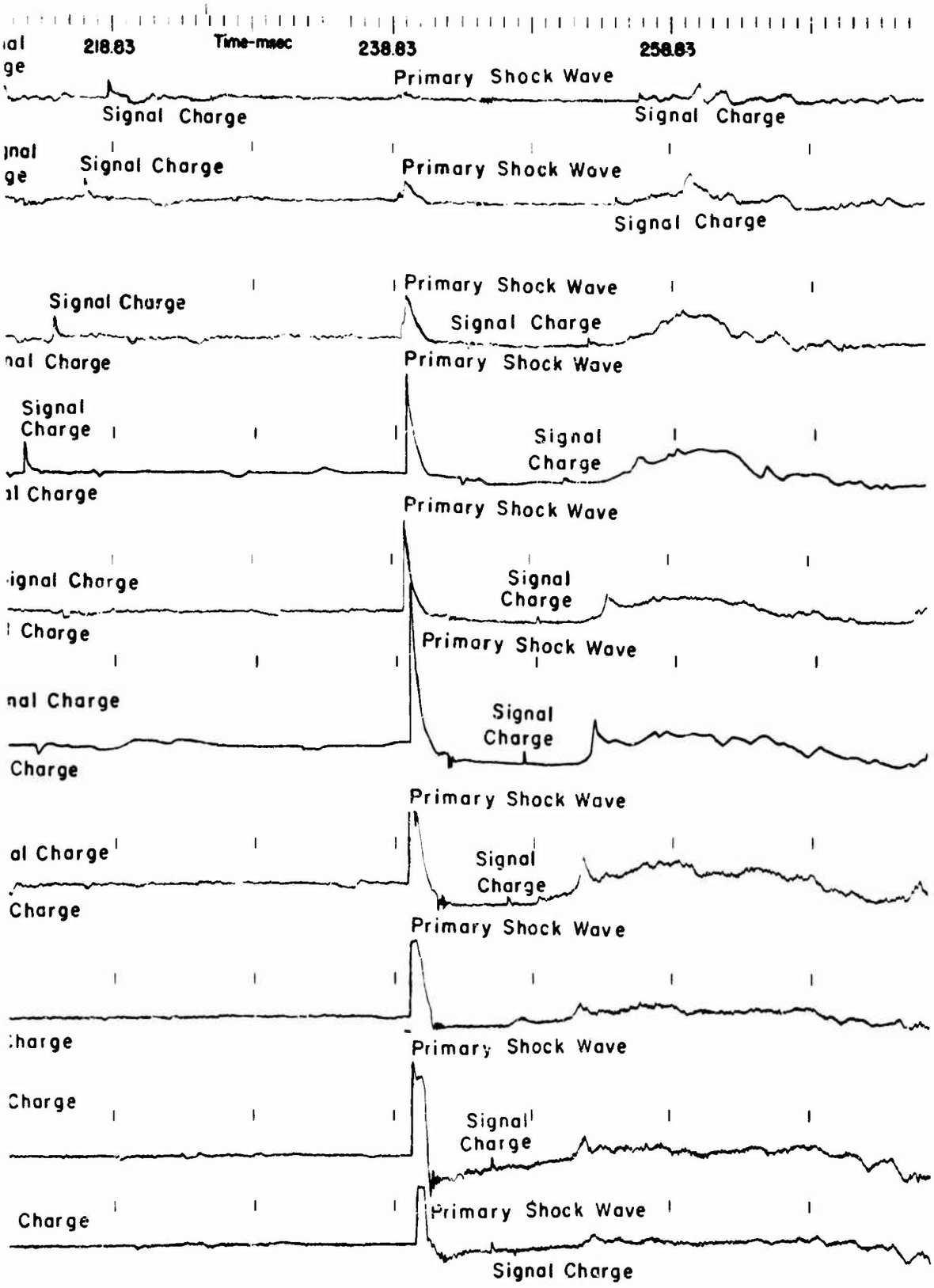
218.83
Time-msec
238.83
258.83
Primary Shock Wave
Signal Charge
Signal Charge
Signal Charge
Primary Shock Wave
Signal Charge
Signal Charge
Primary Shock Wave
Signal Charge
Signal Charge
Primary Shock Wave
Signal Charge
Signal Charge
Primary Shock Wave
Signal Charge
Primary Shock Wave
Signal Charge
Primary Shock Wave
Signal Charge
Primary Shock Wave
Signal Charge
Primary Shock Wave
Signal Charge

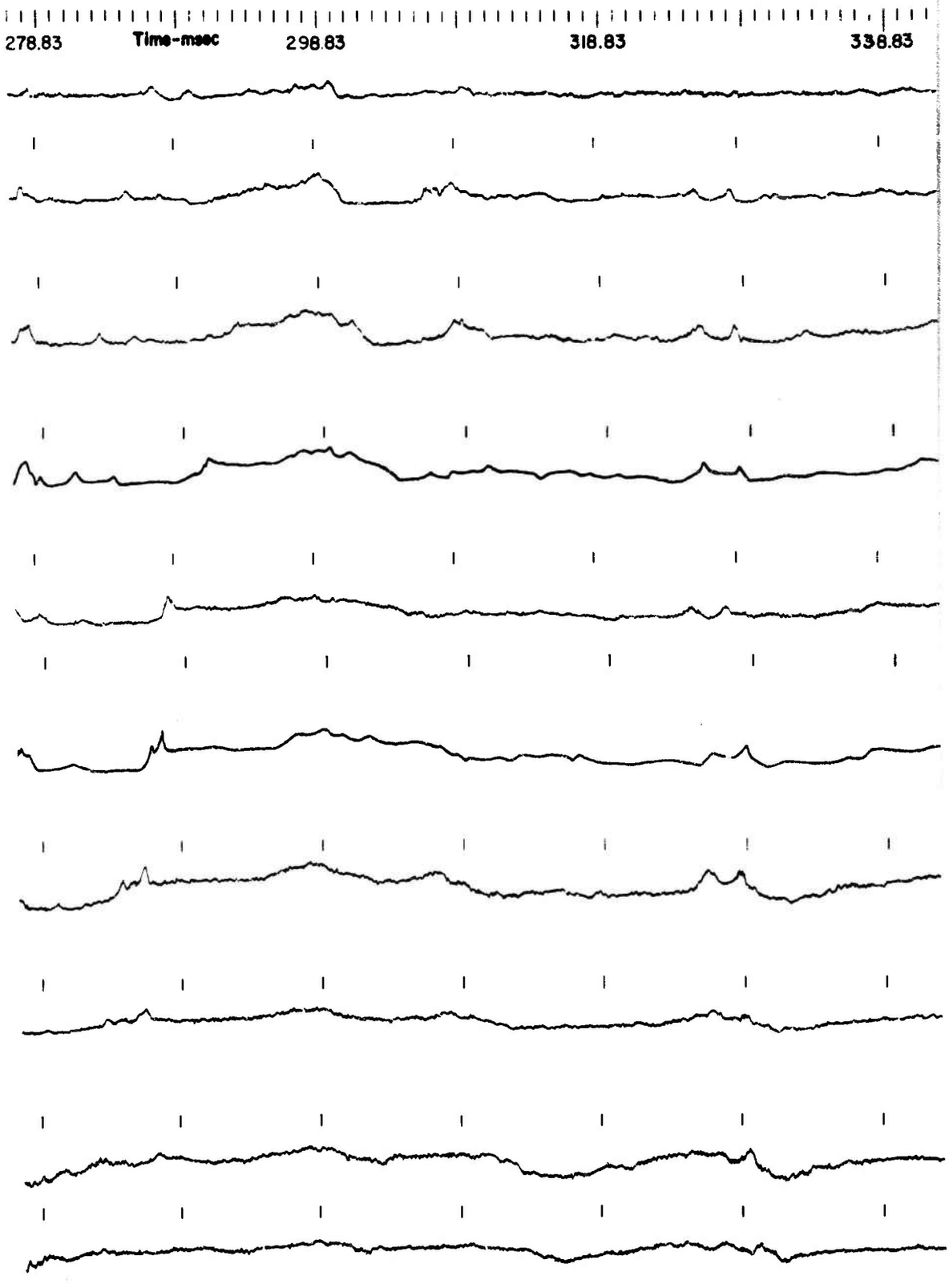

Figur

C

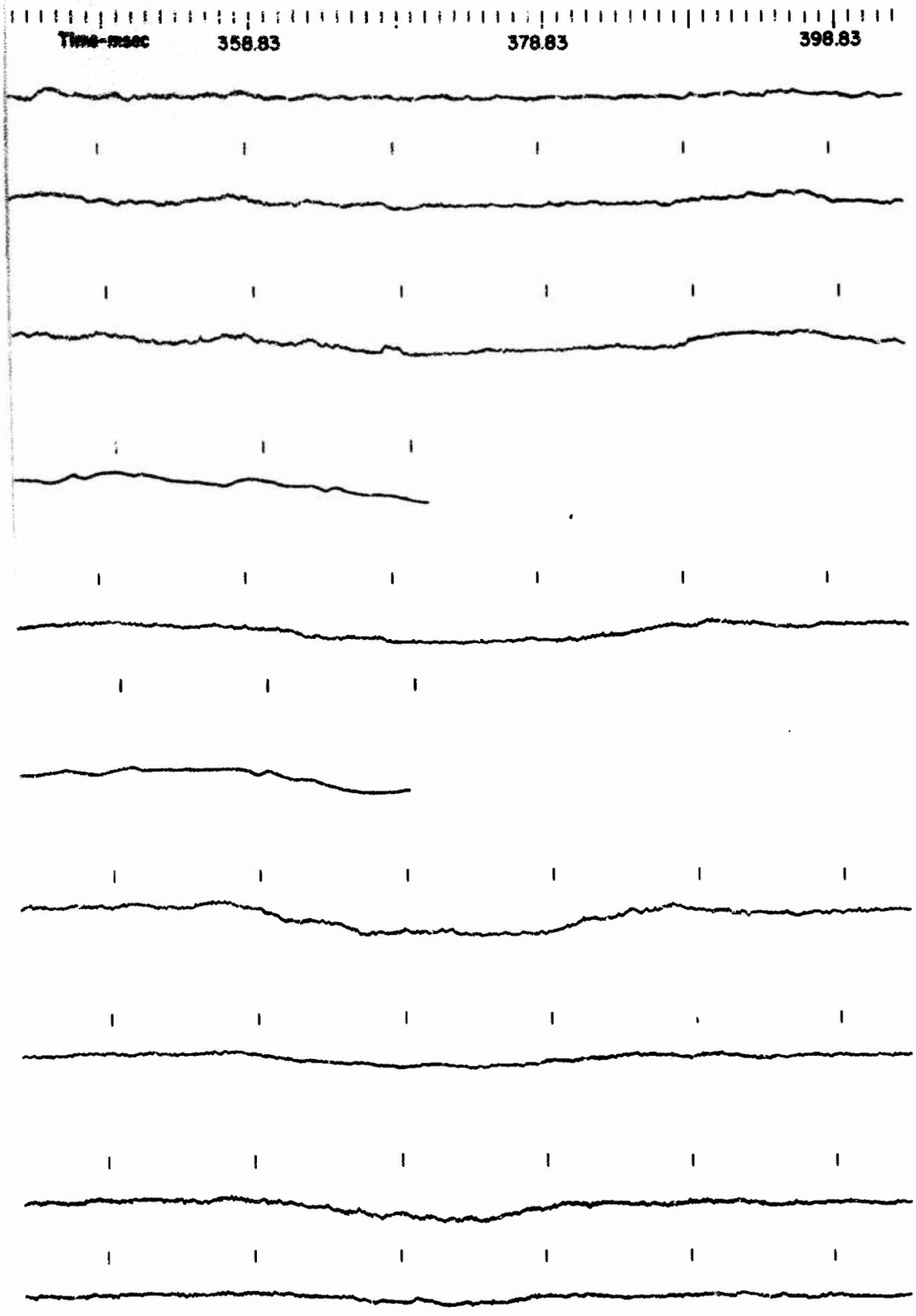

› A13 - Pressure Histories - 1200-Ft Range from Burst at 50-Ft Depth (Station 7, Test 4)

D

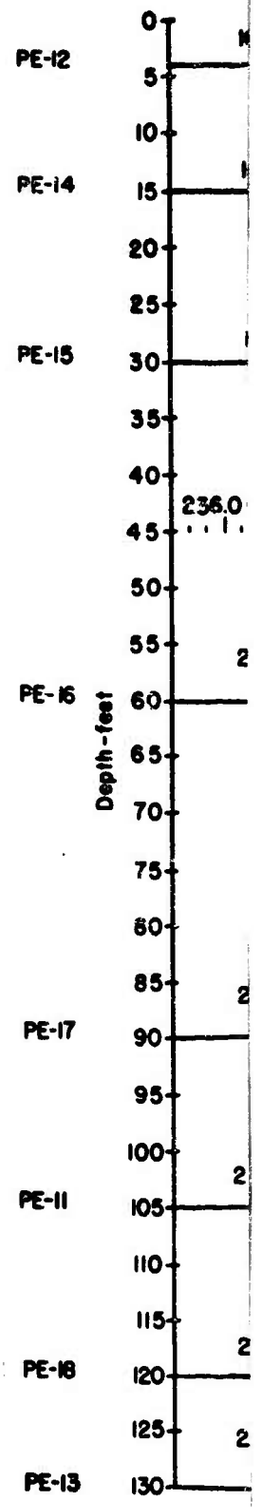
PE-12
PE-14
PE-15
PE-16
PE-17
PE-11
PE-18
PE-13
0
5
10
15
20
25
30
35
40
236.0
45
50
55
60
65
70
75
80
85
90
95
100
105
110
115
120
125
130
Depth-feet

A

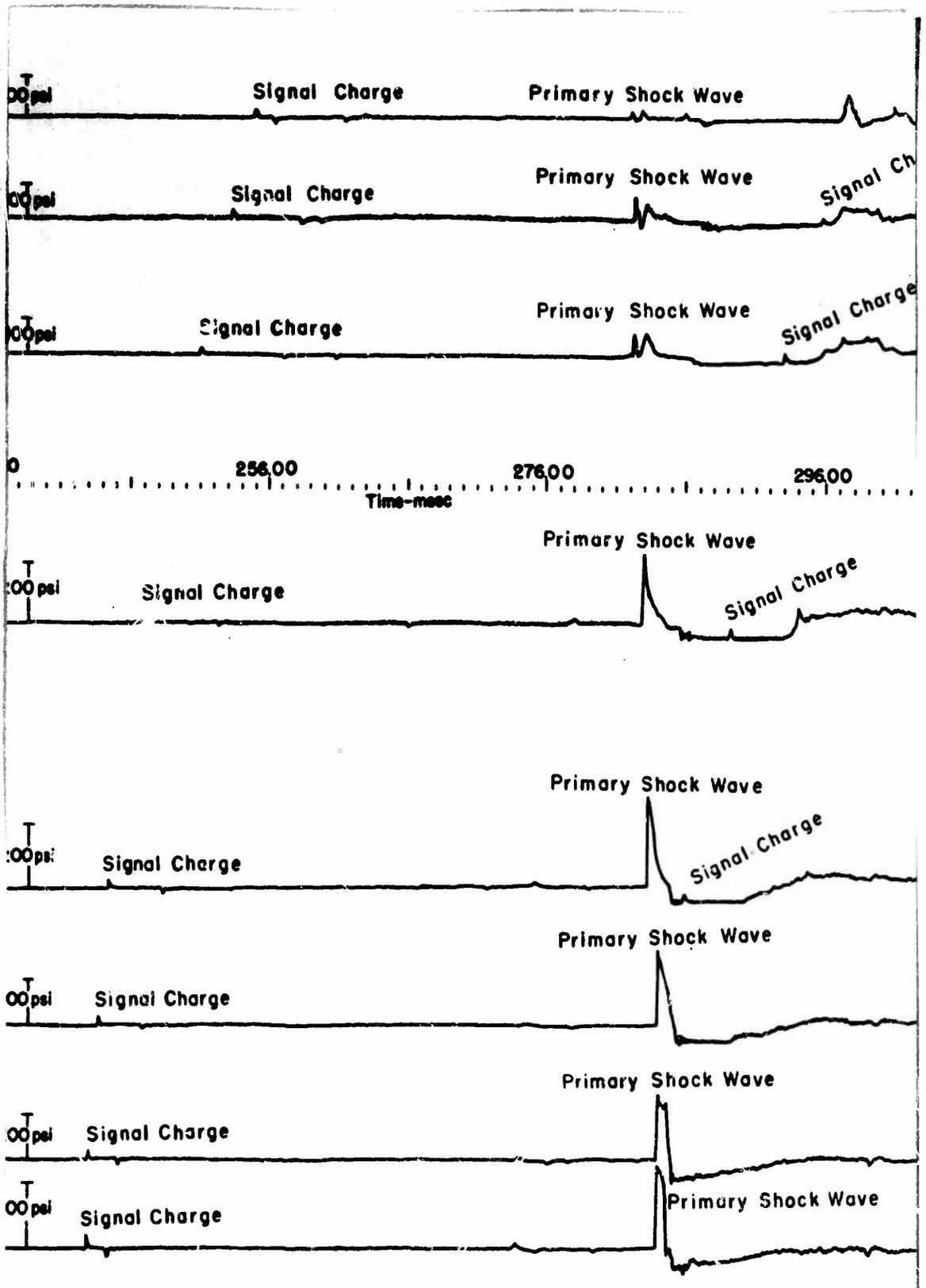
Signal Charge
Primary Shock Wave
Signal Charge
Primary Shock Wave
Signal Charge
Primary Shock Wave
Signal Charge
256.00
276.00
296.00
Time-msec
Primary Shock Wave
Signal Charge
Signal Charge
Primary Shock Wave
Signal Charge
Signal Charge
Primary Shock Wave
Signal Charge
Primary Shock Wave
Signal Charge
Primary Shock Wave

B

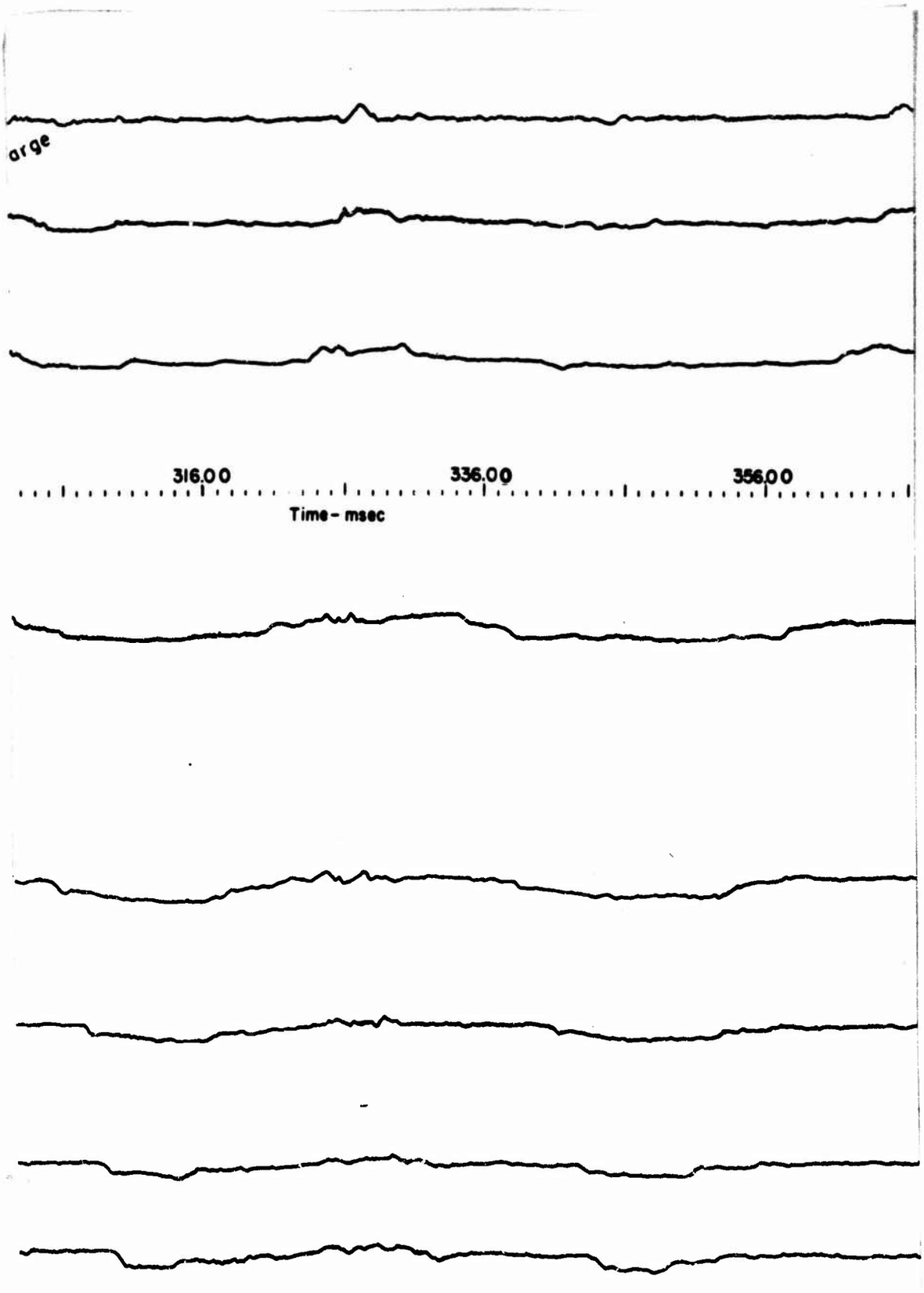

Figur

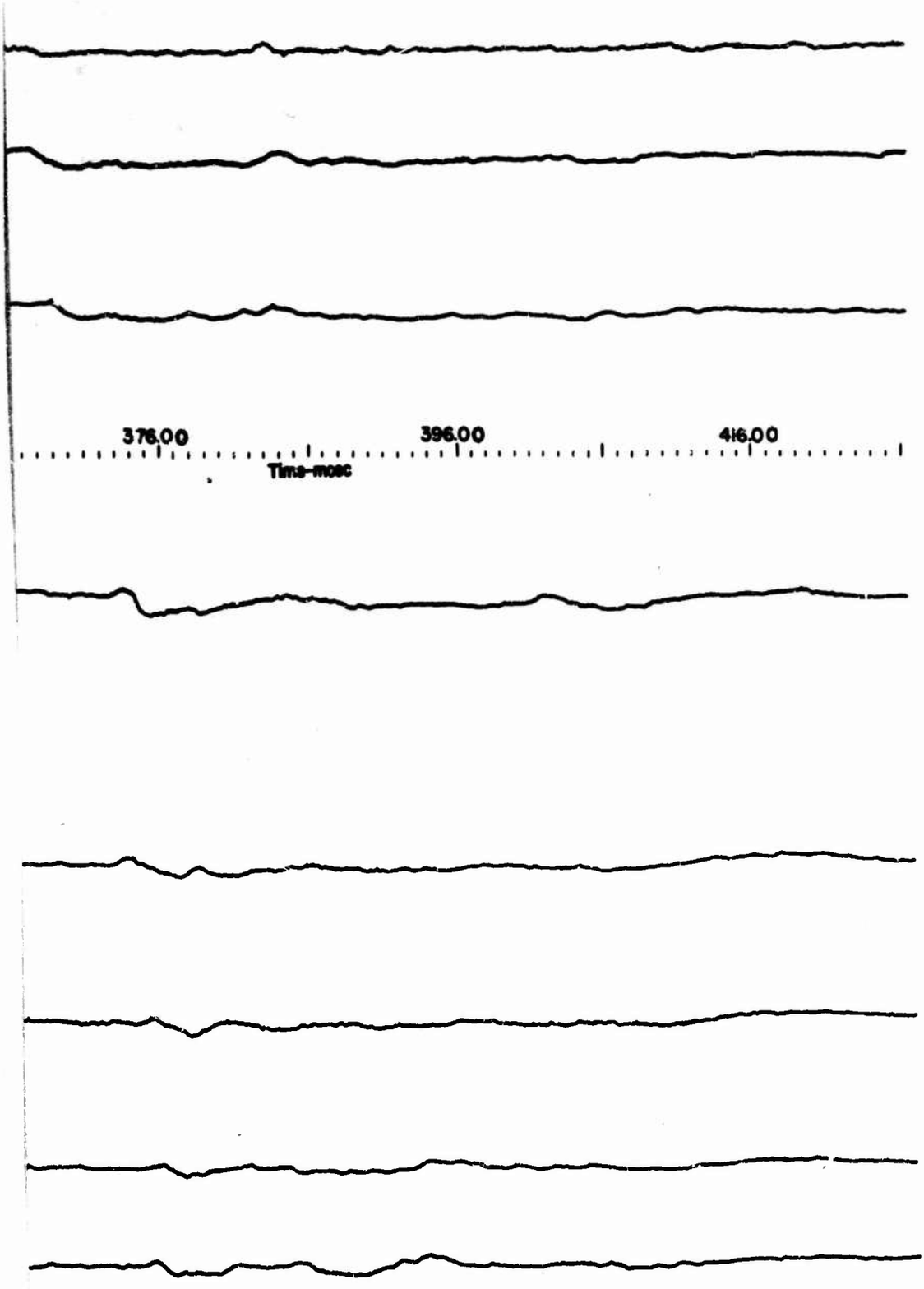

e A14 - Pressure Histories - 1400-Ft Range from Burst at 50-Ft Depth (Station 3, Test 2)

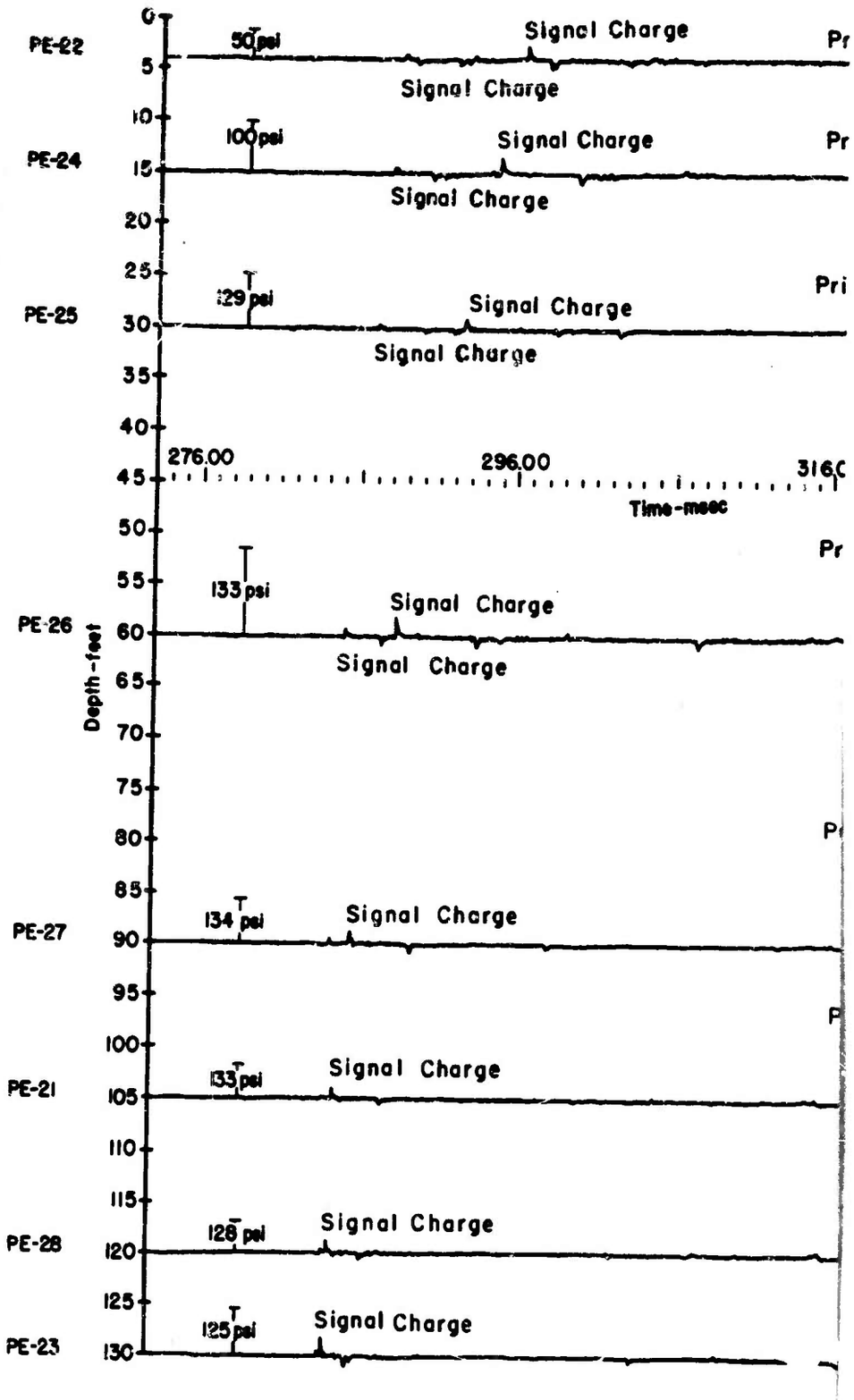
PE-22
50 psi
Signal Charge
Signal Charge
PE-24
100 psi
Signal Charge
Signal Charge
PE-25
129 psi
Signal Charge
Signal Charge
276.00
296.00
Time-msec
PE-26
133 psi
Signal Charge
Signal Charge
Depth-feet
PE-27
134 psi
Signal Charge
PE-21
133 psi
Signal Charge
PE-28
128 psi
Signal Charge
PE-23
125 psi
Signal Charge

A

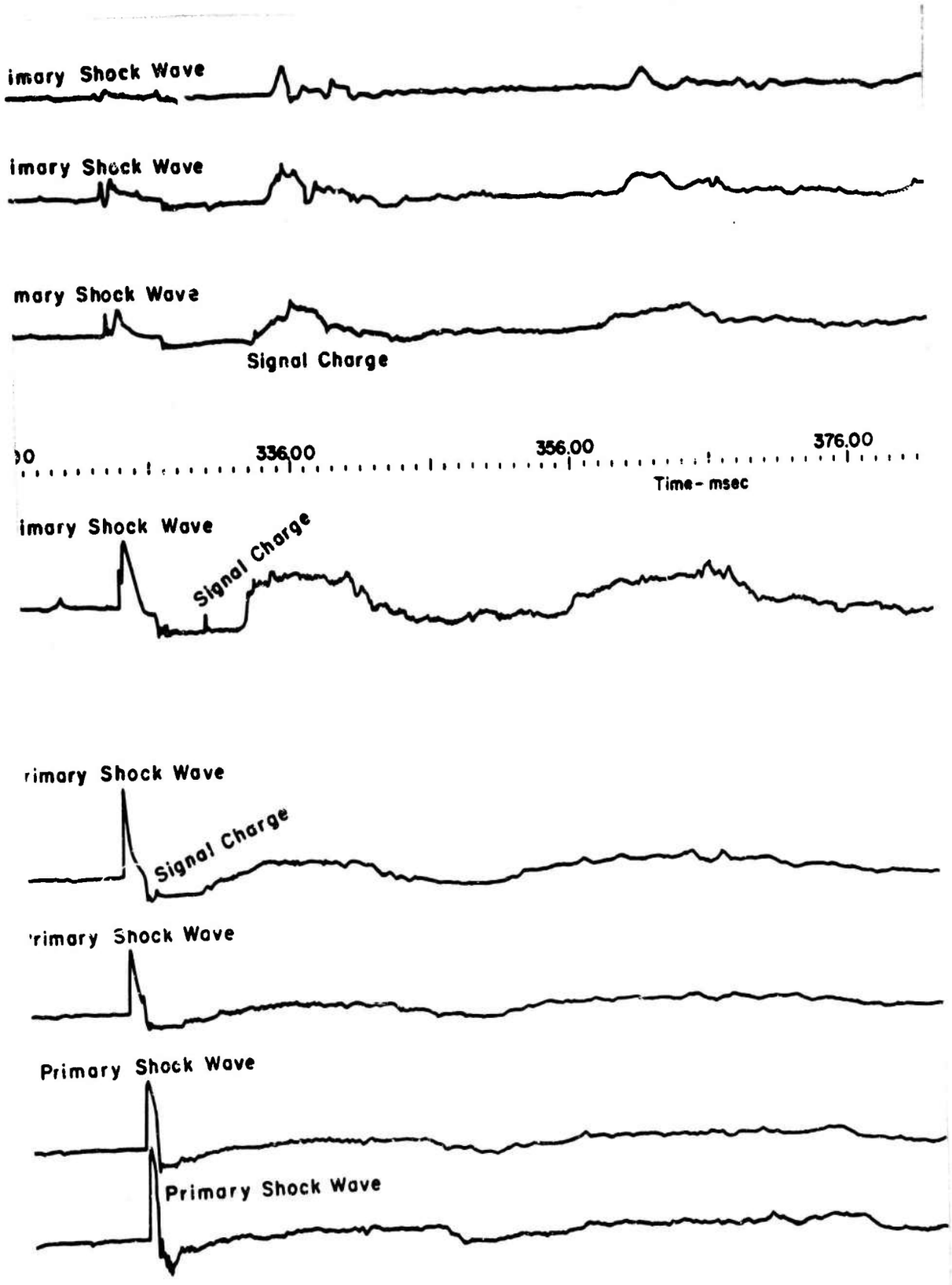
imary Shock Wave
imary Shock Wave
mary Shock Wave
Signal Charge
00
336.00
356.00
376.00
Time - msec
imary Shock Wave
Signal Charge
rimary Shock Wave
Signal Charge
rimary Shock Wave
Primary Shock Wave
Primary Shock Wave

B

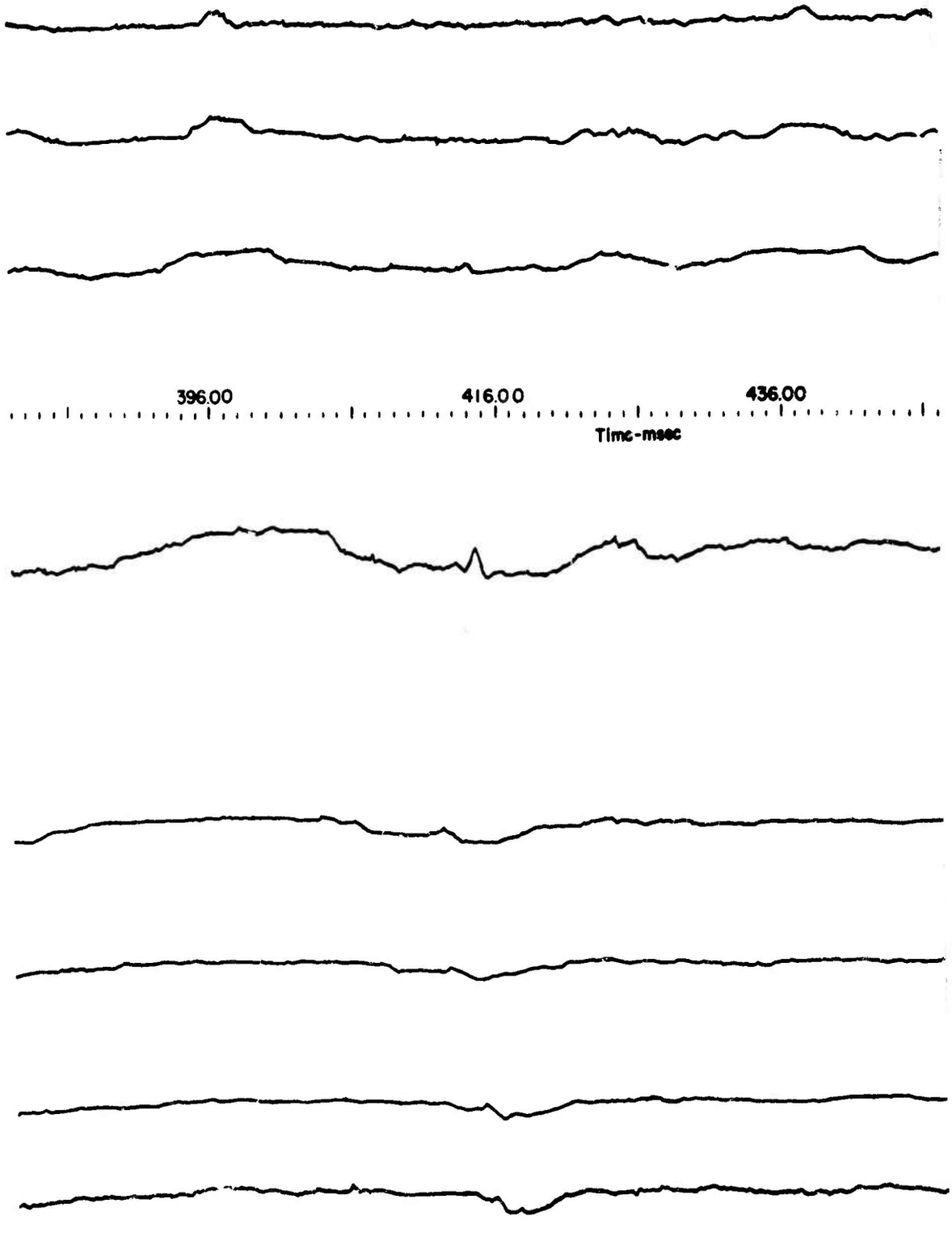

Figure

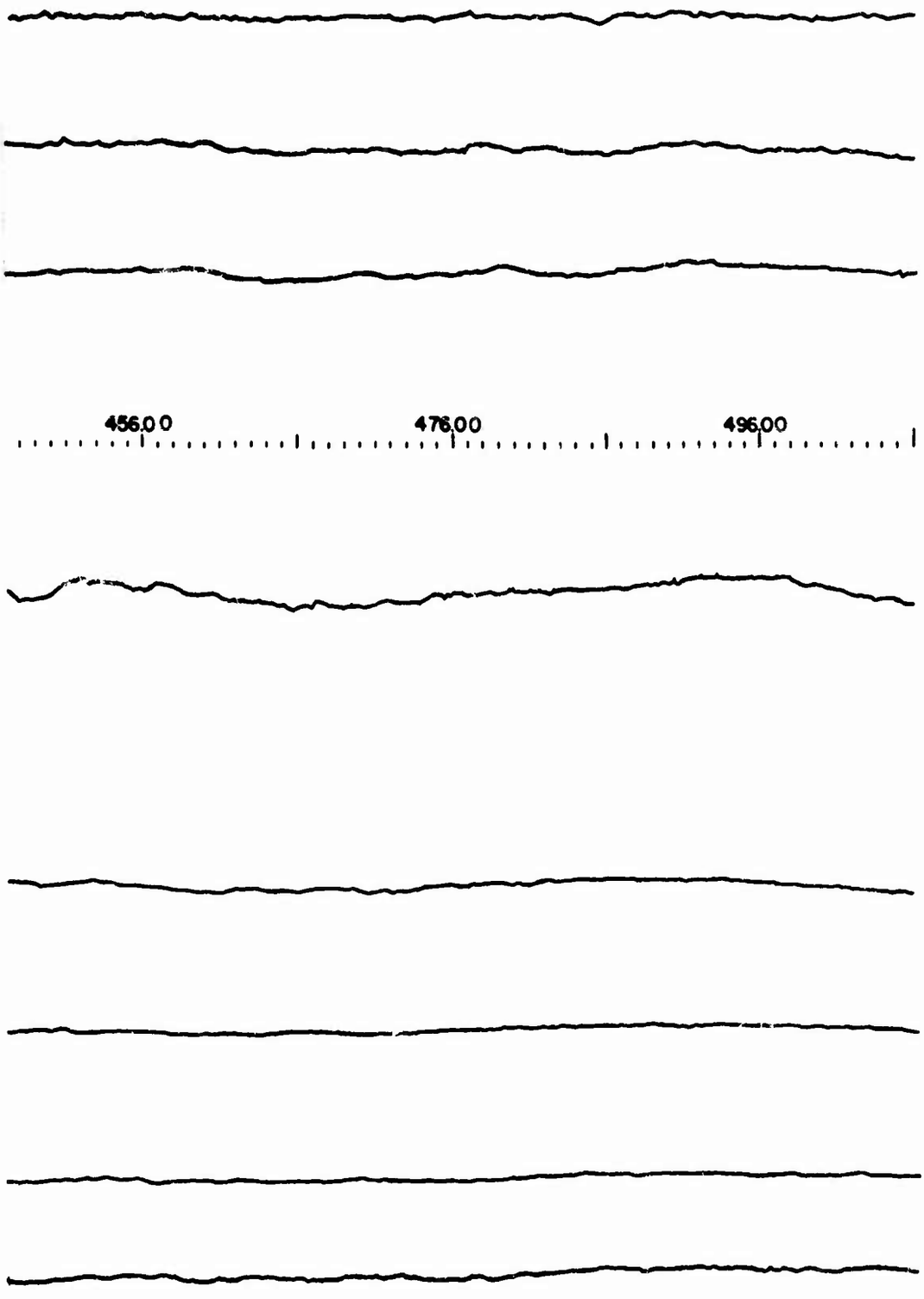

A15 - Pressure Histories - 1600-Ft Range from Burst at 50-Ft Depth (Station 5, Test 2)

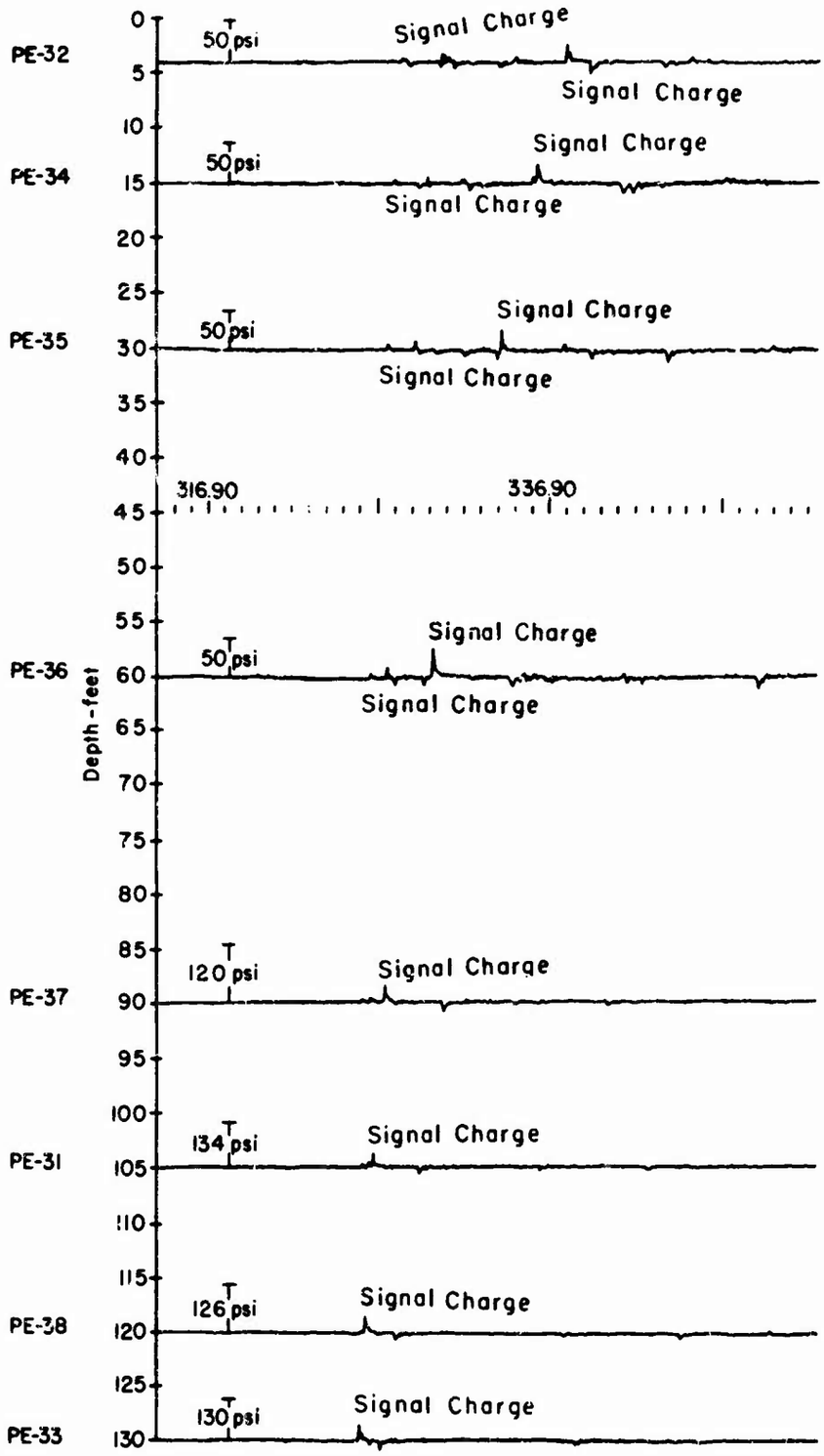
PE-32
PE-34
PE-35
PE-36
PE-37
PE-31
PE-38
PE-33
50 psi
120 psi
134 psi
126 psi
130 psi
Signal Charge
316.90
336.90
Depth - feet
0
5
10
15
20
25
30
35
40
45
50
55
60
65
70
75
80
85
90
95
100
105
110
115
120
125
130

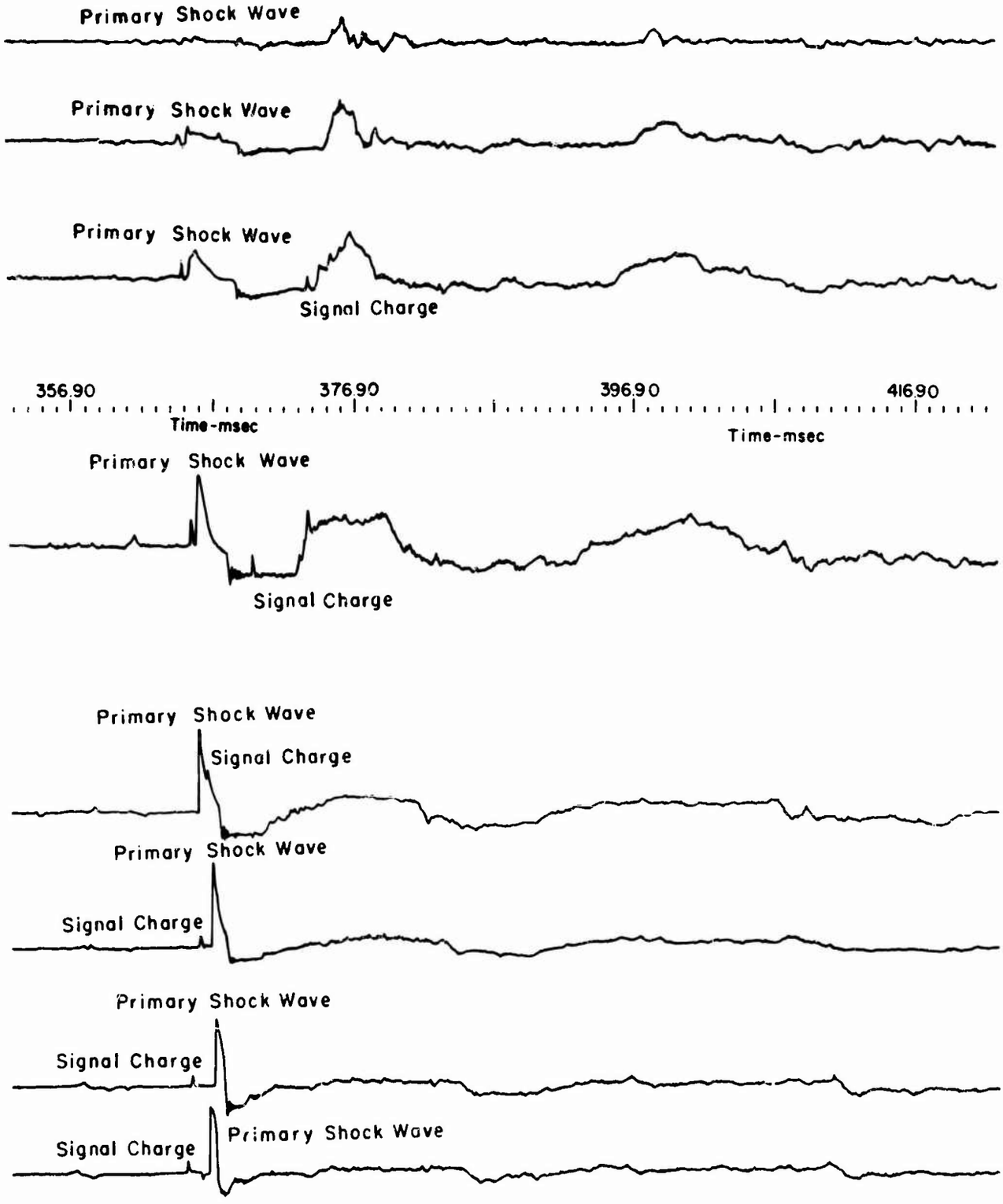
Primary Shock Wave
Primary Shock Wave
Primary Shock Wave
Signal Charge
356.90
376.90
396.90
416.90
Time-msec
Time-msec
Primary Shock Wave
Signal Charge
Primary Shock Wave
Signal Charge
Primary Shock Wave
Signal Charge
Primary Shock Wave
Signal Charge
Primary Shock Wave

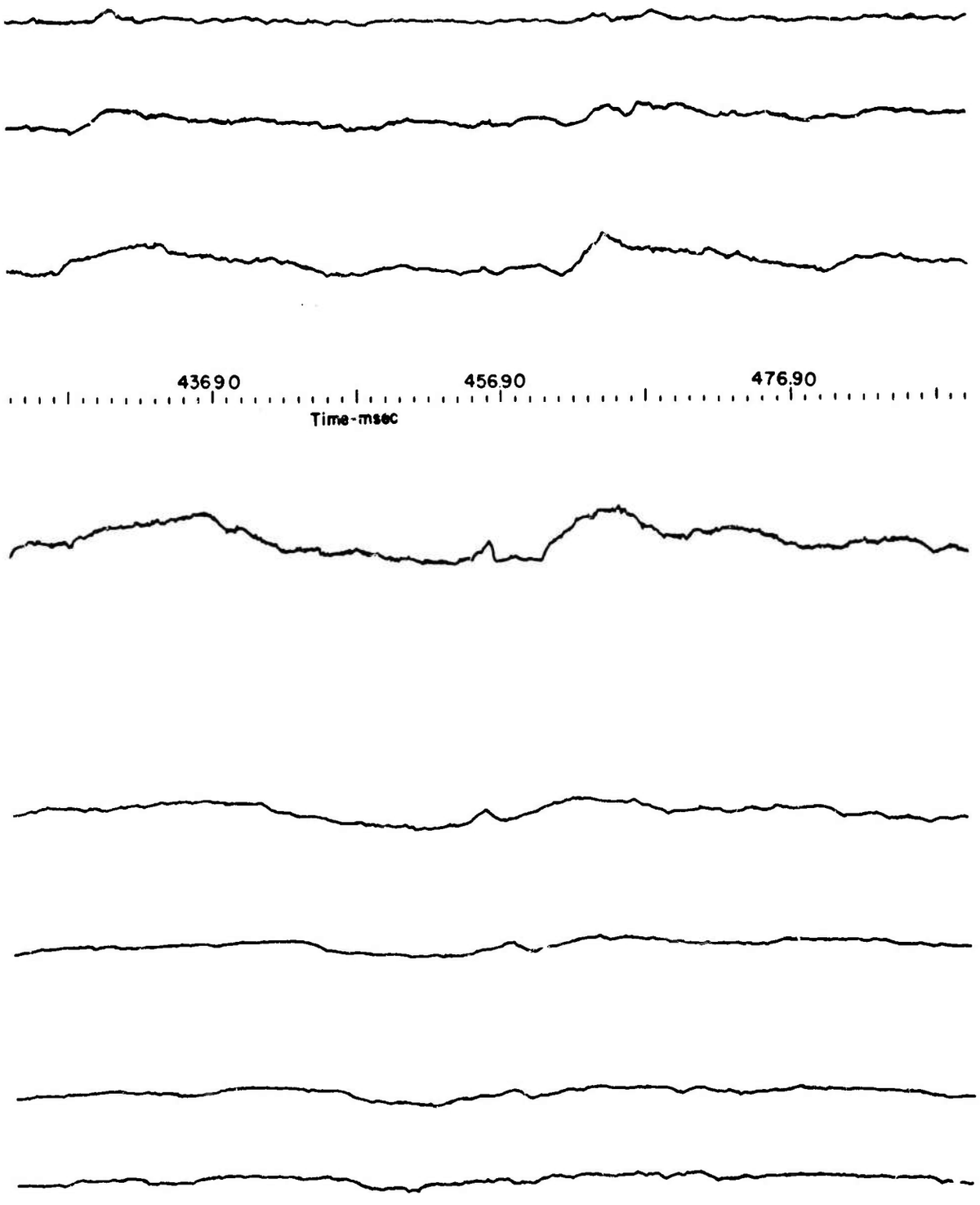

Figure A16 - Pressure Histories - 1800-Ft Range from Burst at 50-Ft Depth (Station 7, Test 2)

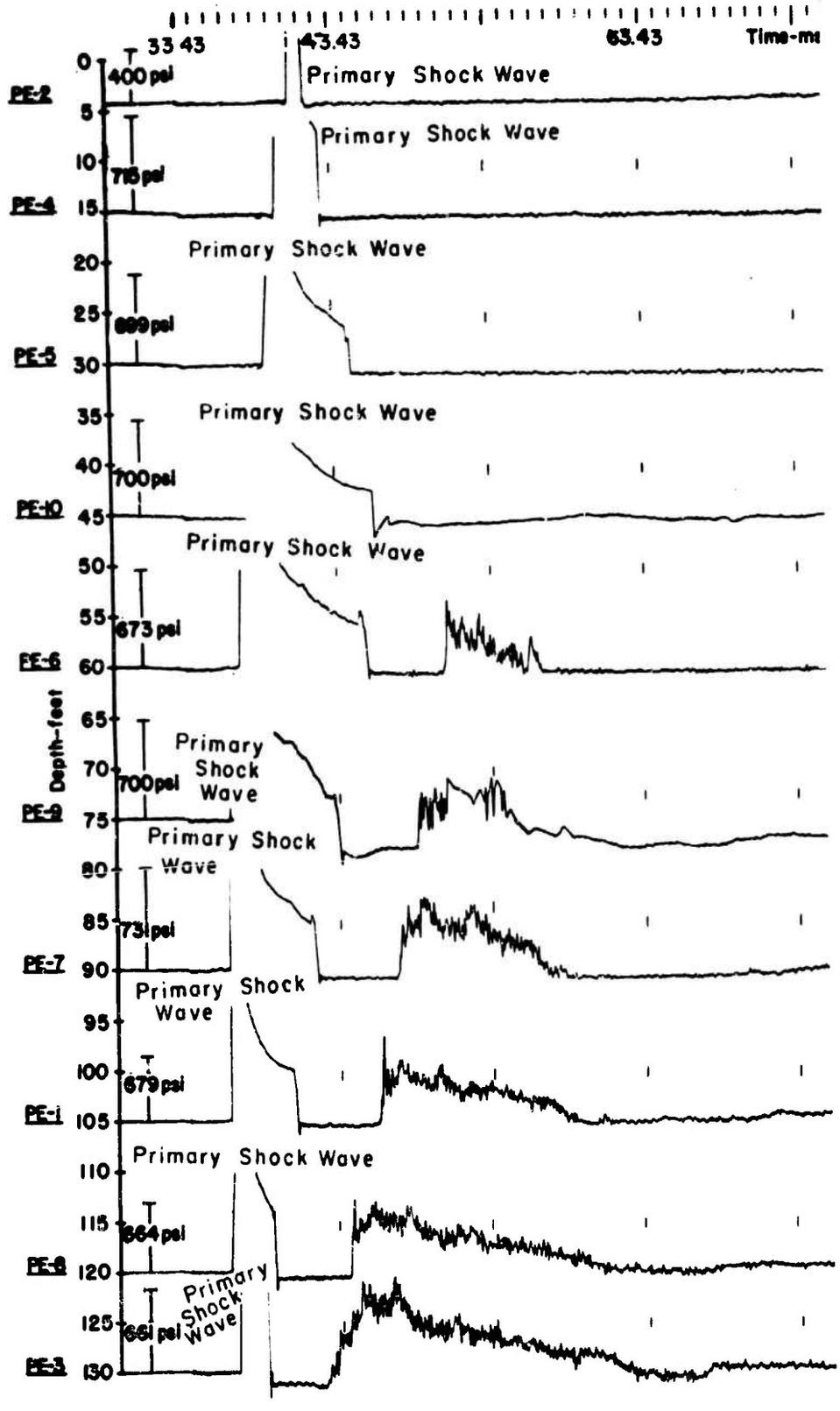
33.43
43.43
63.43
Time-ms
Primary Shock Wave
400 psi
PE-2
715 psi
PE-4
689 psi
PE-5
700 psi
PE-10
673 psi
PE-6
700 psi
PE-9
731 psi
PE-7
679 psi
PE-1
664 psi
PE-8
661 psi
PE-3
Depth-feet
0
5
10
15
20
25
30
35
40
45
50
55
60
65
70
75
80
85
90
95
100
105
110
115
120
125
130

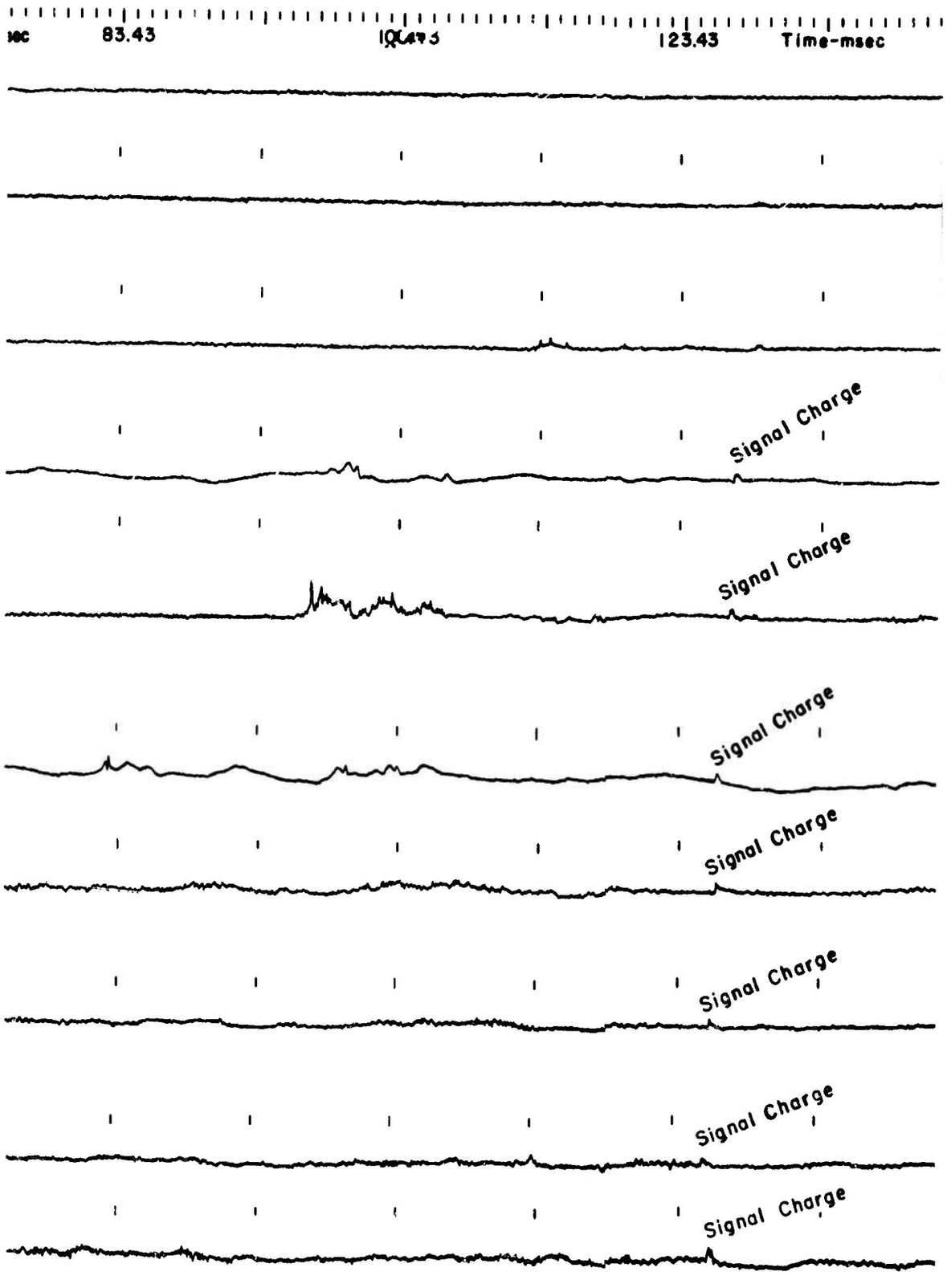
83.43
123.43
Time-msec
Signal Charge
Signal Charge
Signal Charge
Signal Charge
Signal Charge
Signal Charge

B

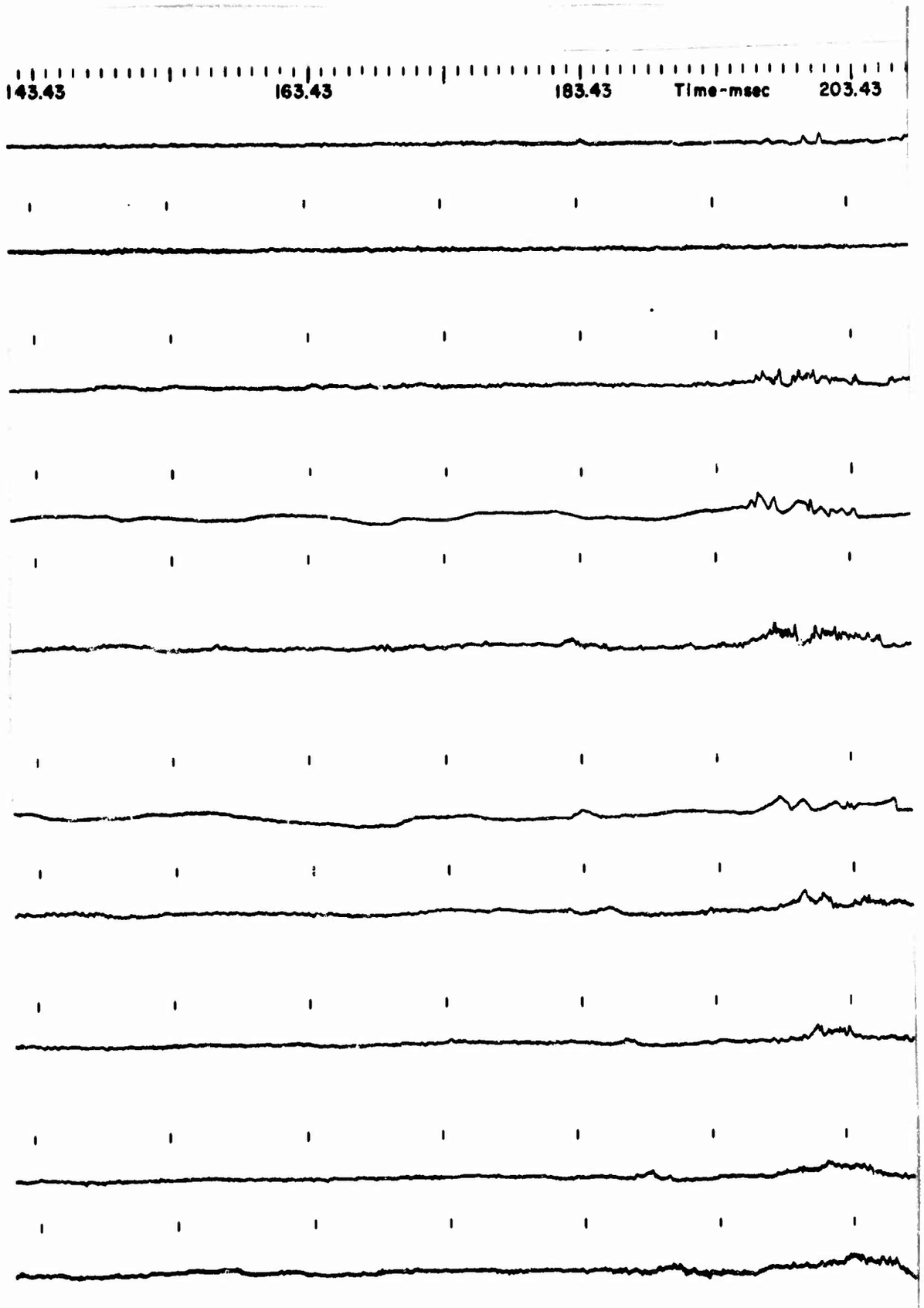

C

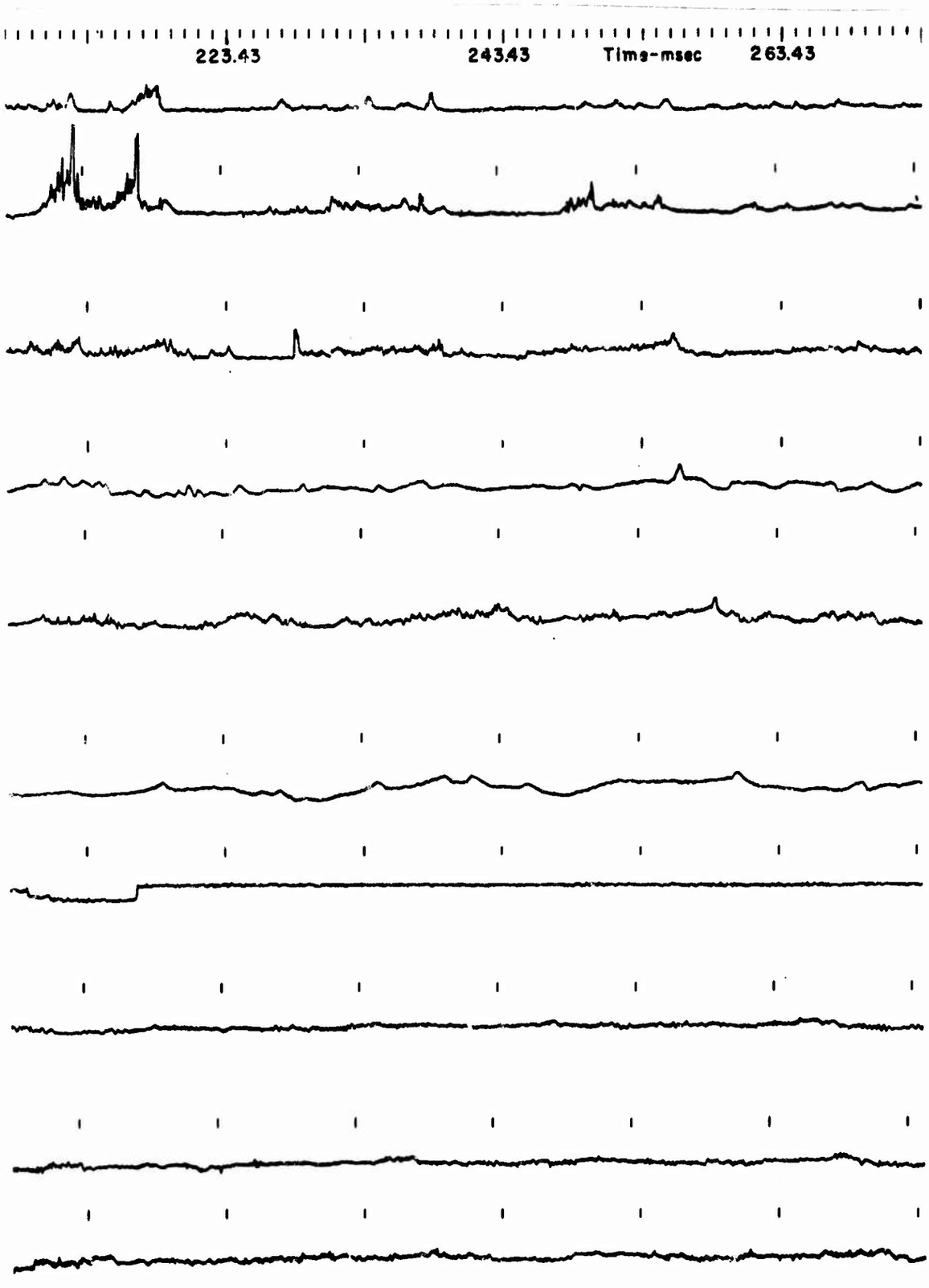

Figu

D

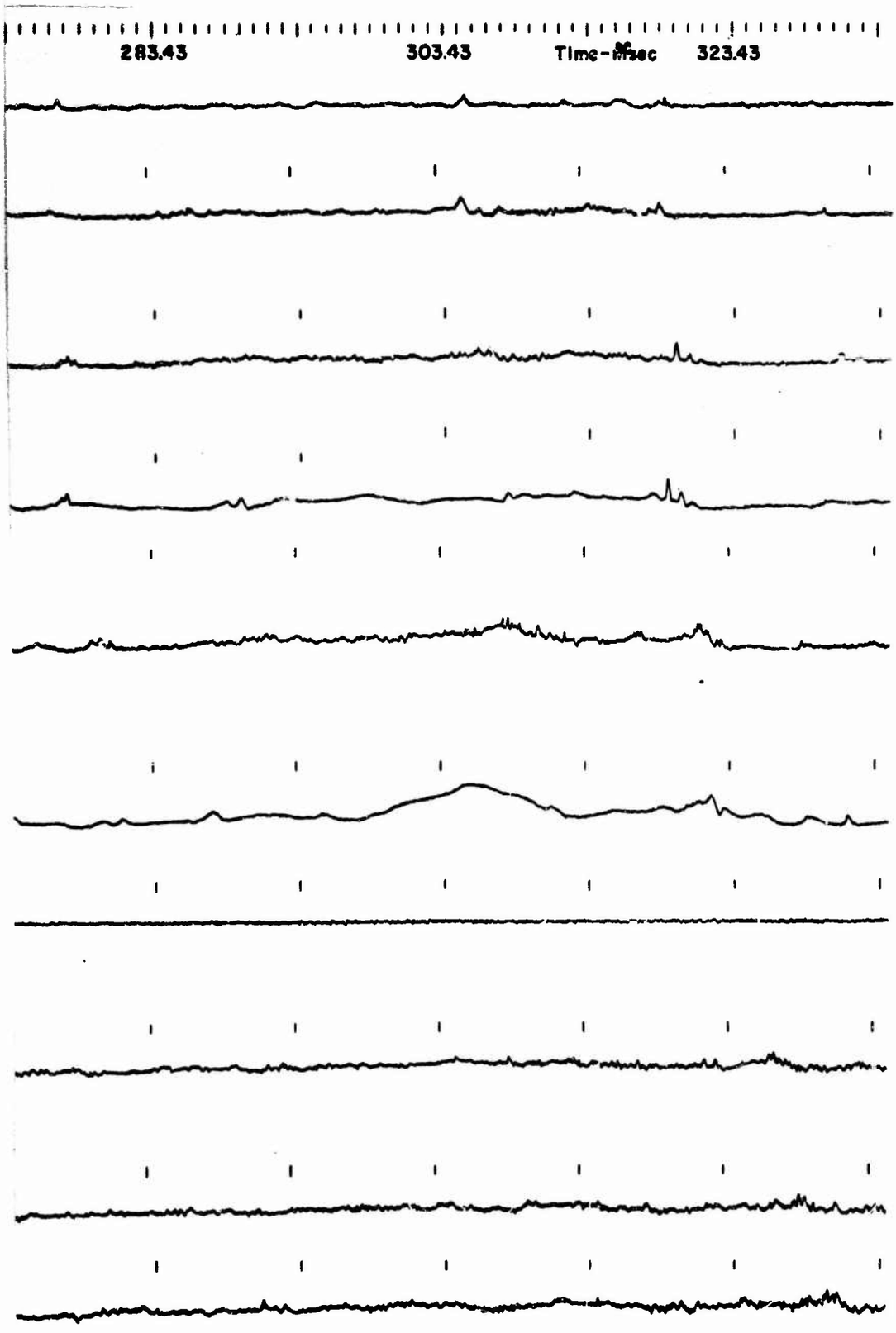

re A17 - Pressure Histories - 200-Ft Range from Burst at 100-Ft Depth (Station 1, Test 7)

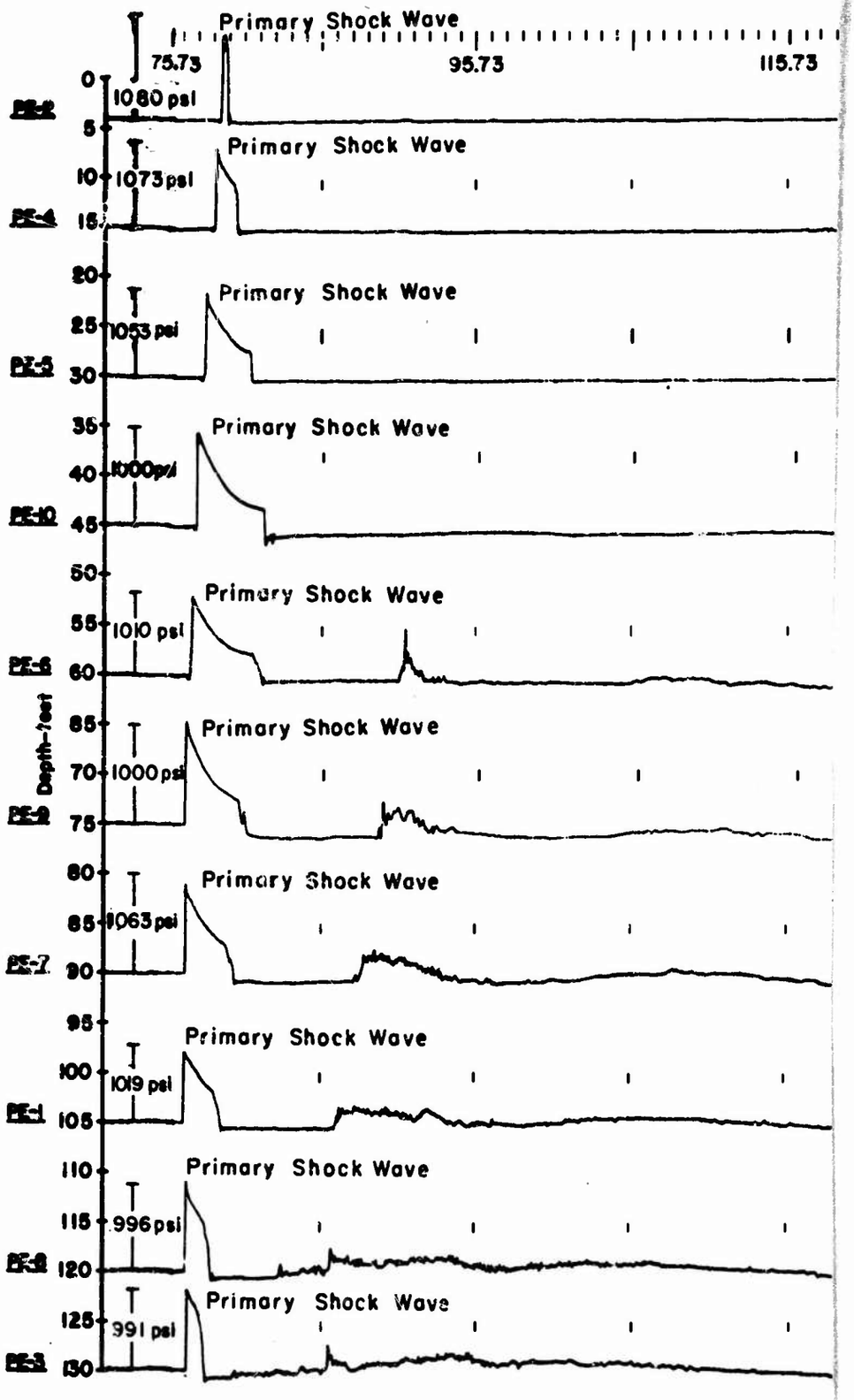
Primary Shock Wave
75.73
95.73
115.73
0
1080 psi
PE-2
5
Primary Shock Wave
10
1073 psi
PE-4
15
20
Primary Shock Wave
25
1053 psi
PE-5
30
35
Primary Shock Wave
40
1000 psi
PE-10
45
50
Primary Shock Wave
55
1010 psi
PE-6
60
Depth-feet
65
Primary Shock Wave
70
1000 psi
PE-9
75
80
Primary Shock Wave
85
1063 psi
PE-7
90
95
Primary Shock Wave
100
1019 psi
PE-1
105
110
Primary Shock Wave
115
996 psi
PE-8
120
125
Primary Shock Wave
991 psi
PE-3
130

A

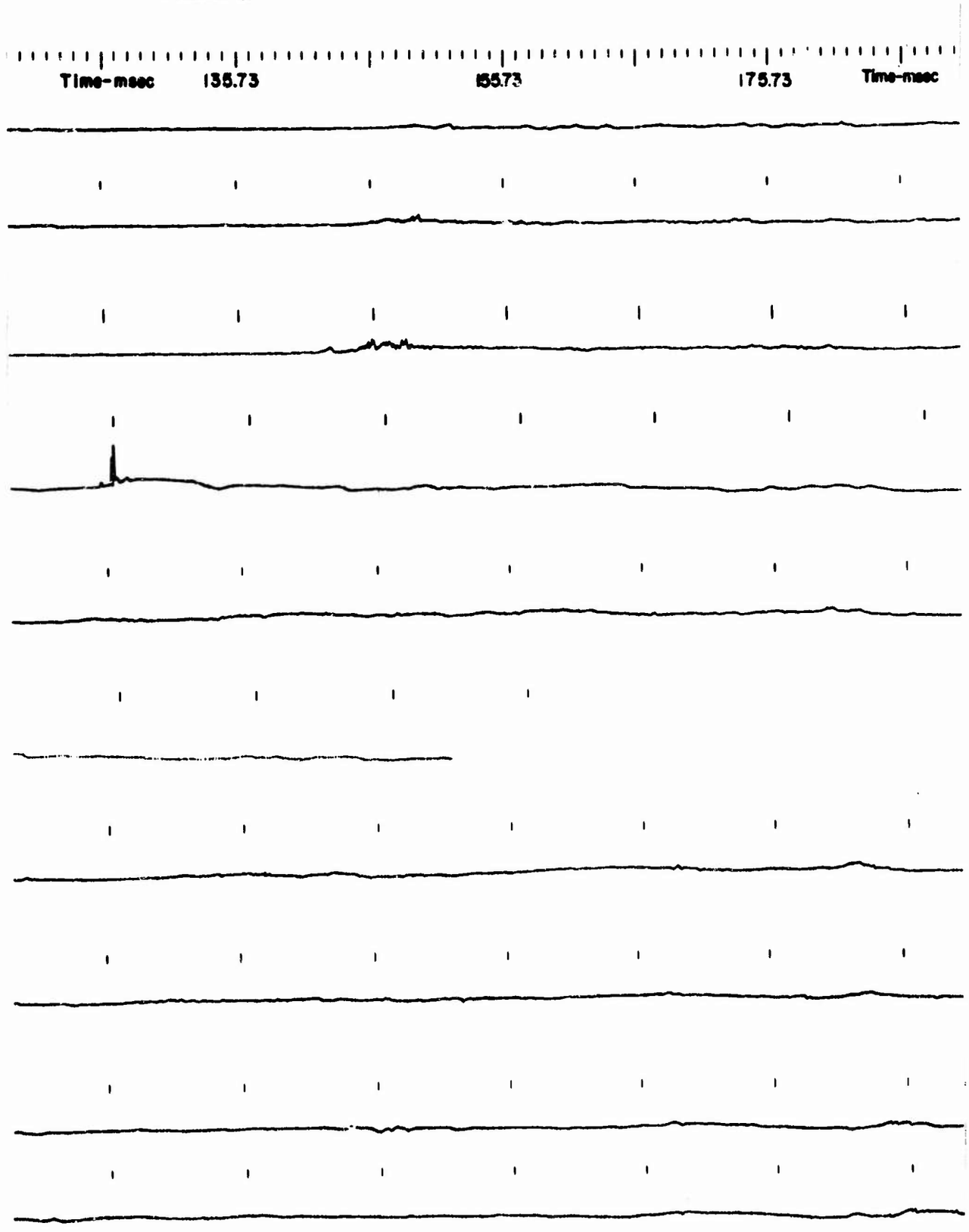

B

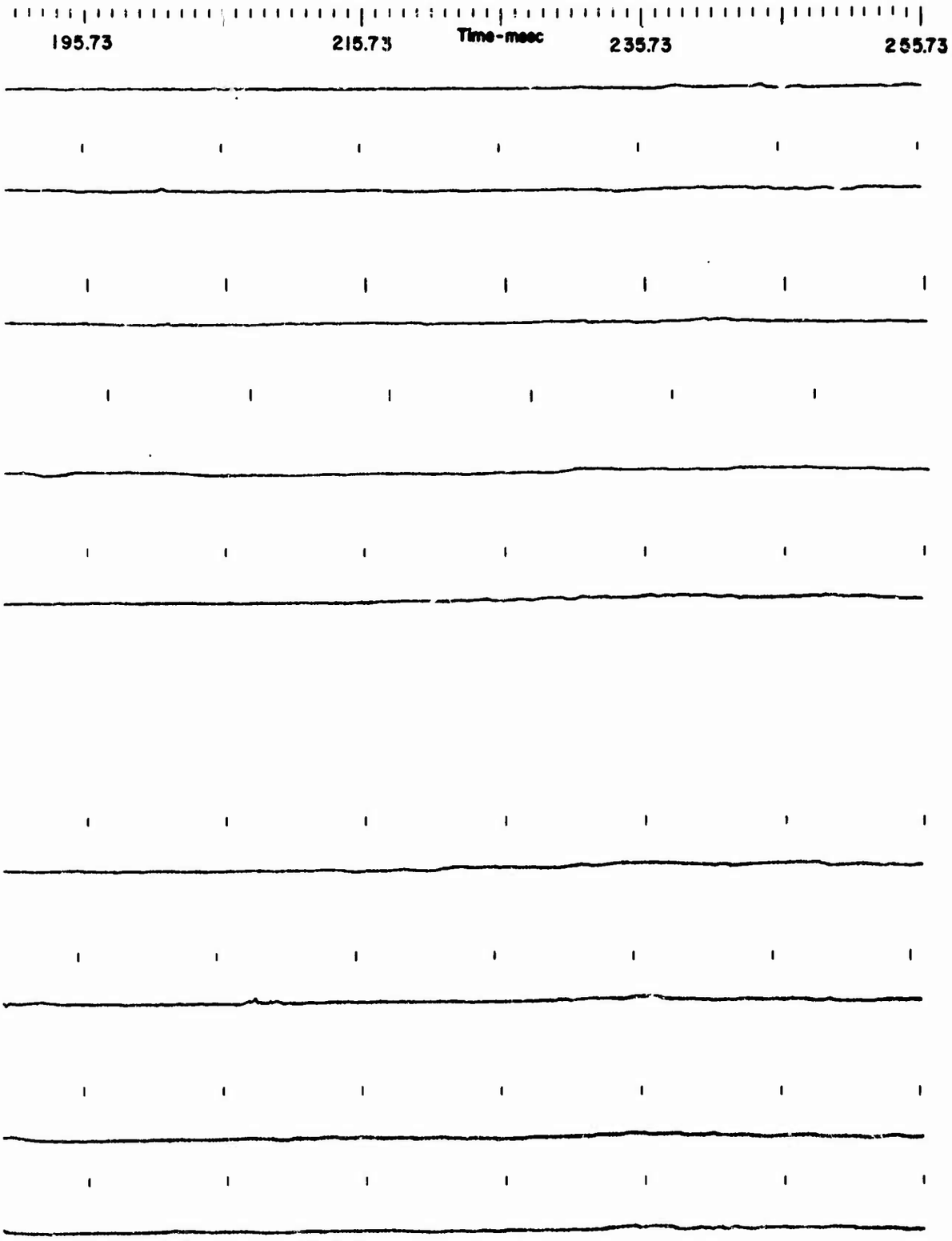

Figure A18 - Pressure Histories - 400-Ft Range from Burst at 100-Ft Depth (Station 1, Test 3)

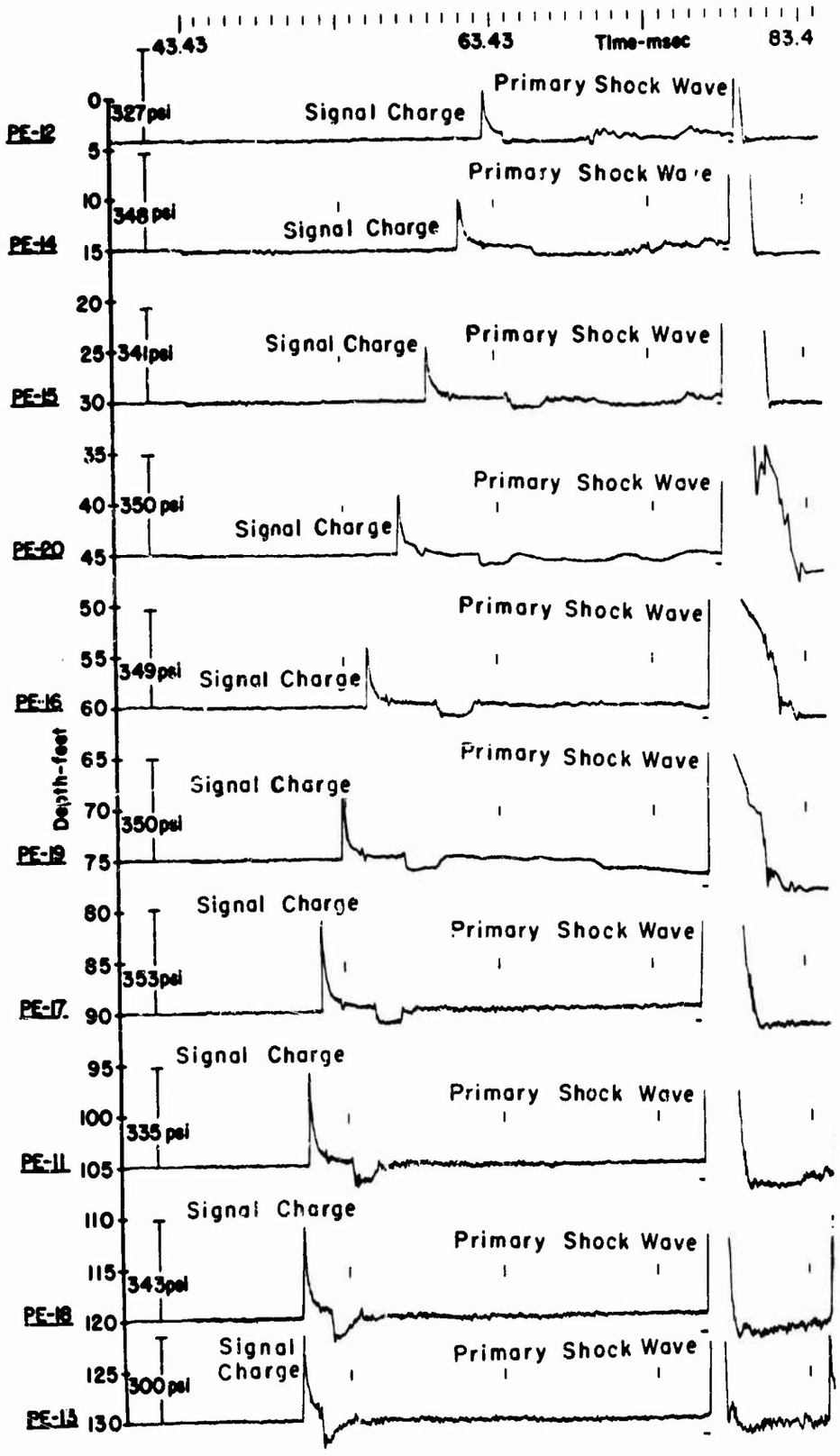
43.43
63.43
Time-msec
83.4
Depth-feet
PE-12
327 psi
Signal Charge
Primary Shock Wave
PE-14
348 psi
Signal Charge
Primary Shock Wave
PE-15
341psi
Signal Charge
Primary Shock Wave
PE-20
350 psi
Signal Charge
Primary Shock Wave
PE-16
349psi
Signal Charge
Primary Shock Wave
PE-19
350psi
Signal Charge
Primary Shock Wave
PE-17
353psi
Signal Charge
Primary Shock Wave
PE-11
335 psi
Signal Charge
Primary Shock Wave
PE-18
343psi
Signal Charge
Primary Shock Wave
PE-13
300psi
Signal Charge
Primary Shock Wave

A

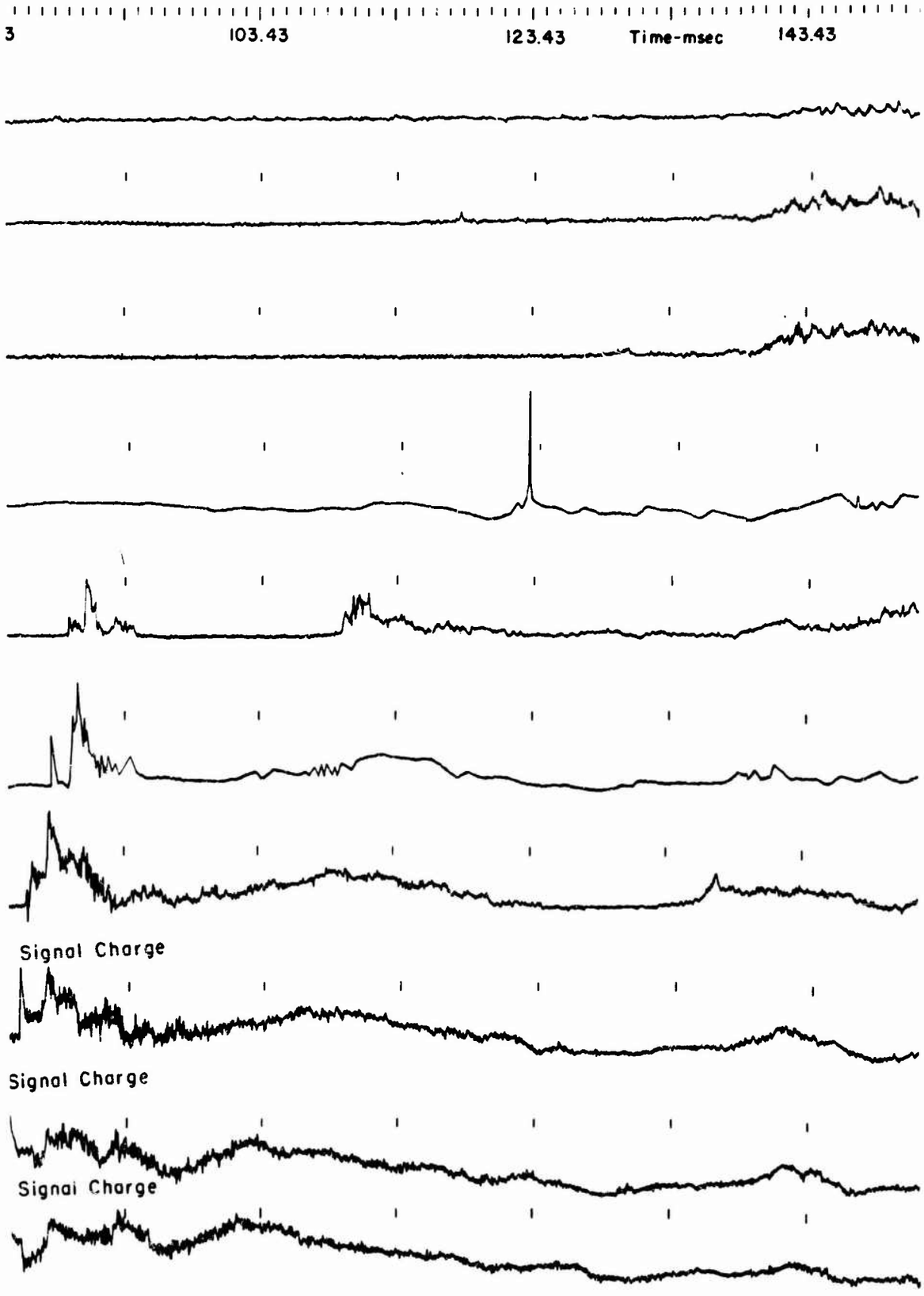
3
103.43
123.43
Time-msec
143.43
Signal Charge
Signal Charge
Signal Charge

B

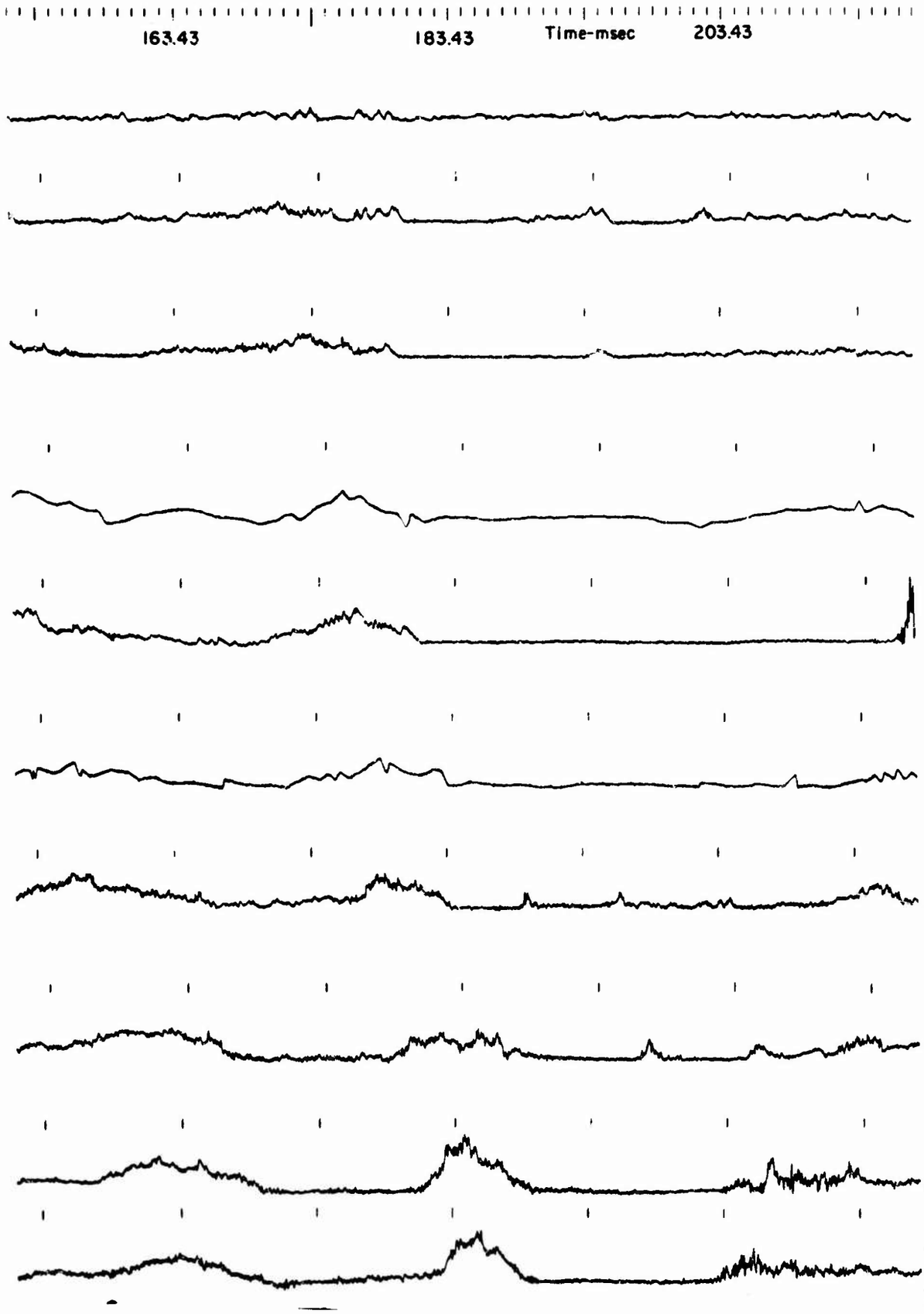

C

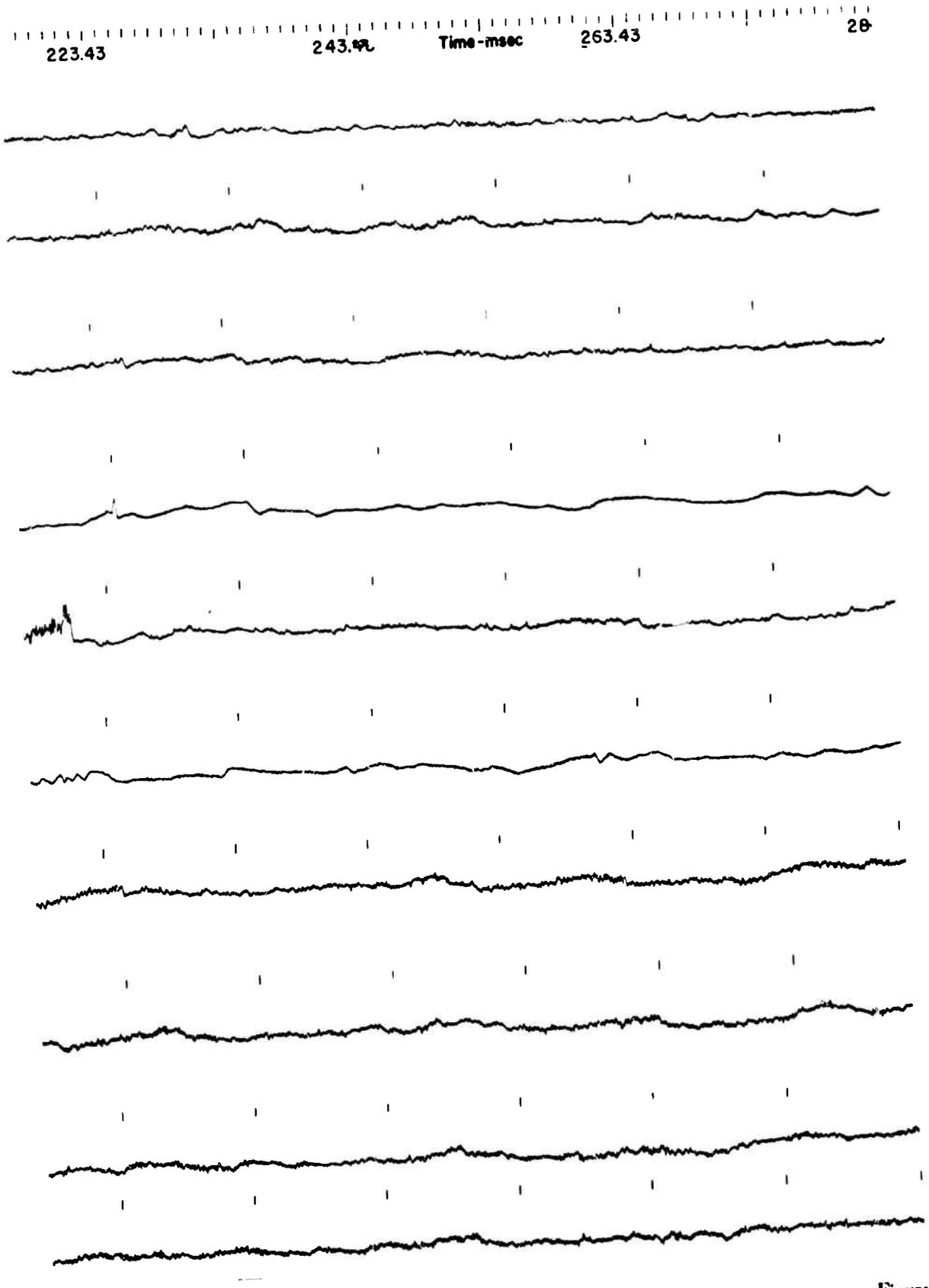

Figure

D

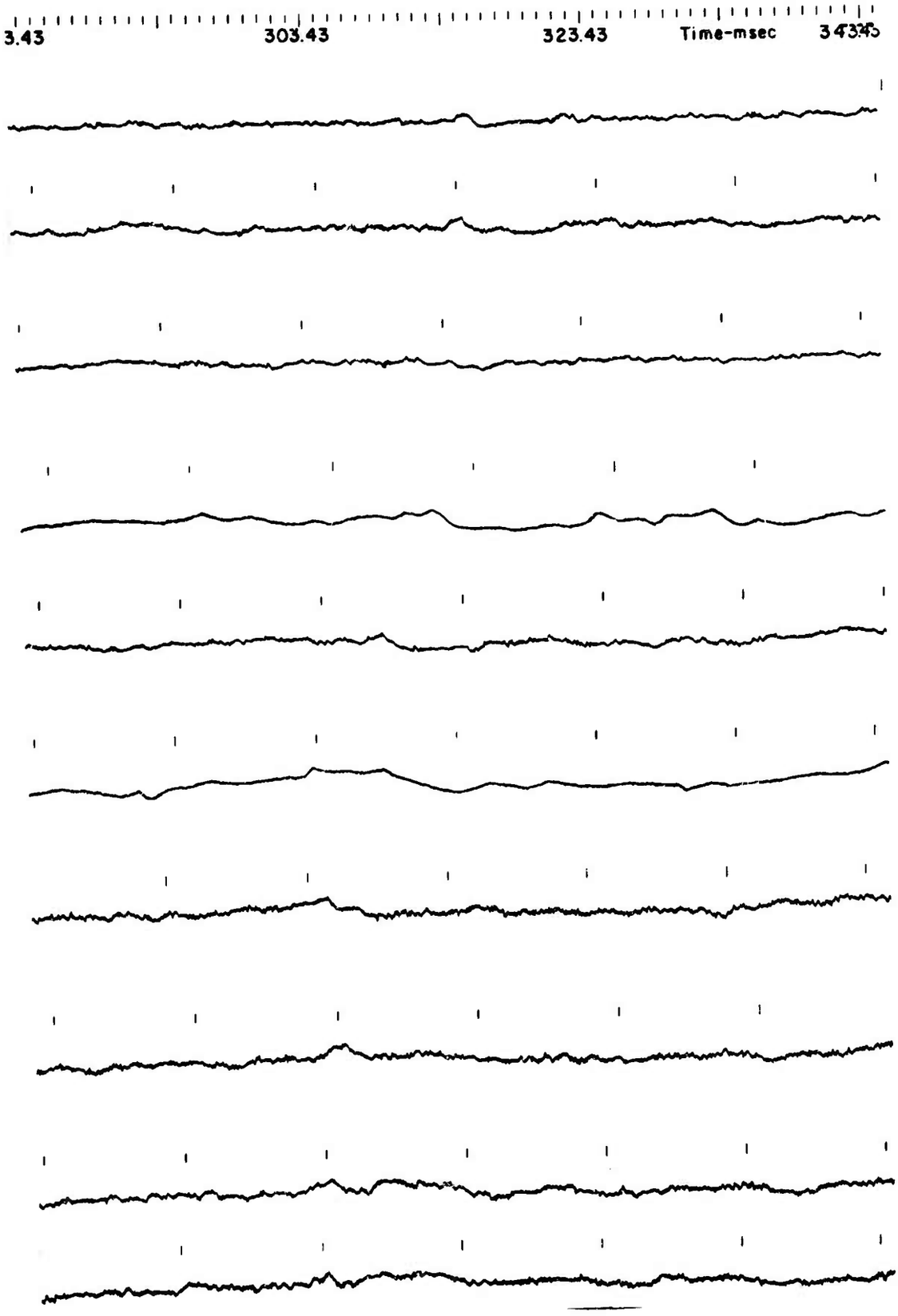

A19 - Pressure Histories - 400-Ft Range from Burst at 100-Ft Depth (Station 3, Test 7)

E

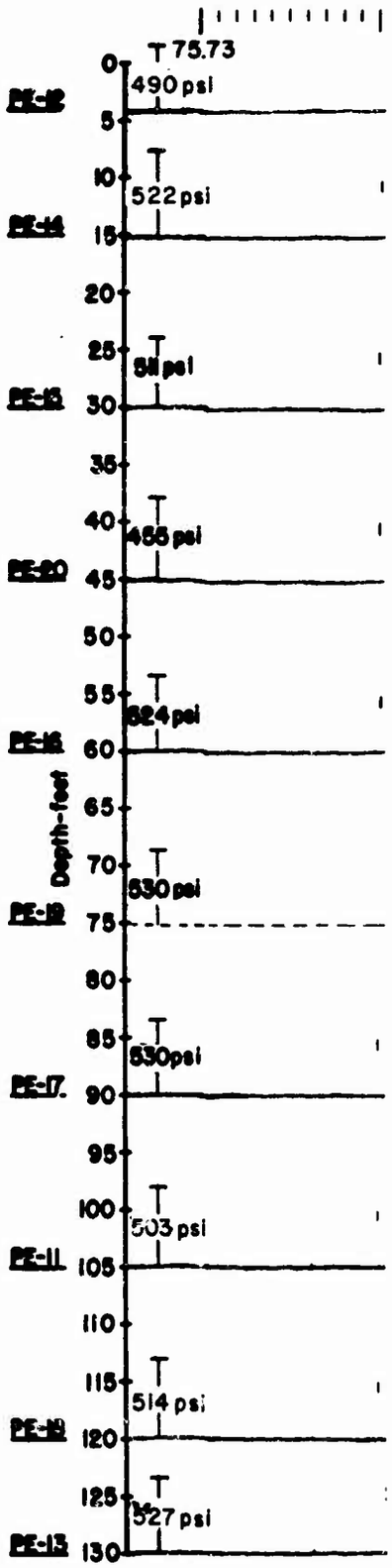
T 75.73
0
490 psi
PE-12
5
10
522 psi
PE-14
15
20
25
511 psi
PE-15
30
35
40
486 psi
PE-20
45
50
55
524 psi
PE-16
60
Depth-feet
65
70
530 psi
PE-18
75
80
85
530 psi
PE-17
90
95
100
503 psi
PE-11
105
110
115
514 psi
PE-19
120
125
527 psi
PE-13
130

A

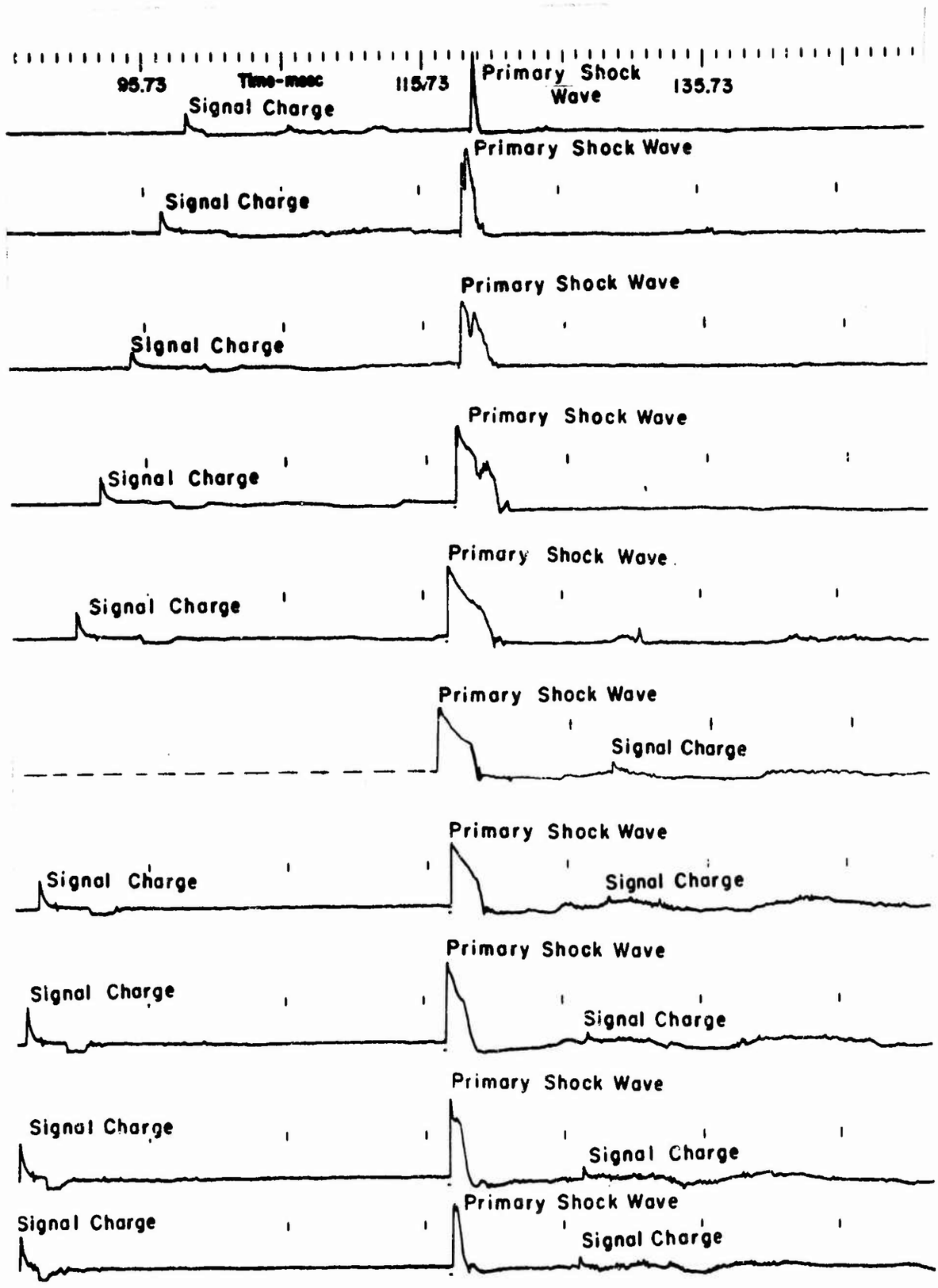
95.73
Time-msec
115.73
Primary Shock Wave
135.73
Signal Charge
Primary Shock Wave
Signal Charge
Primary Shock Wave
Signal Charge
Primary Shock Wave
Signal Charge
Primary Shock Wave
Signal Charge
Primary Shock Wave
Signal Charge
Primary Shock Wave
Signal Charge
Signal Charge
Primary Shock Wave
Signal Charge
Signal Charge
Primary Shock Wave
Signal Charge
Signal Charge
Primary Shock Wave
Signal Charge

B

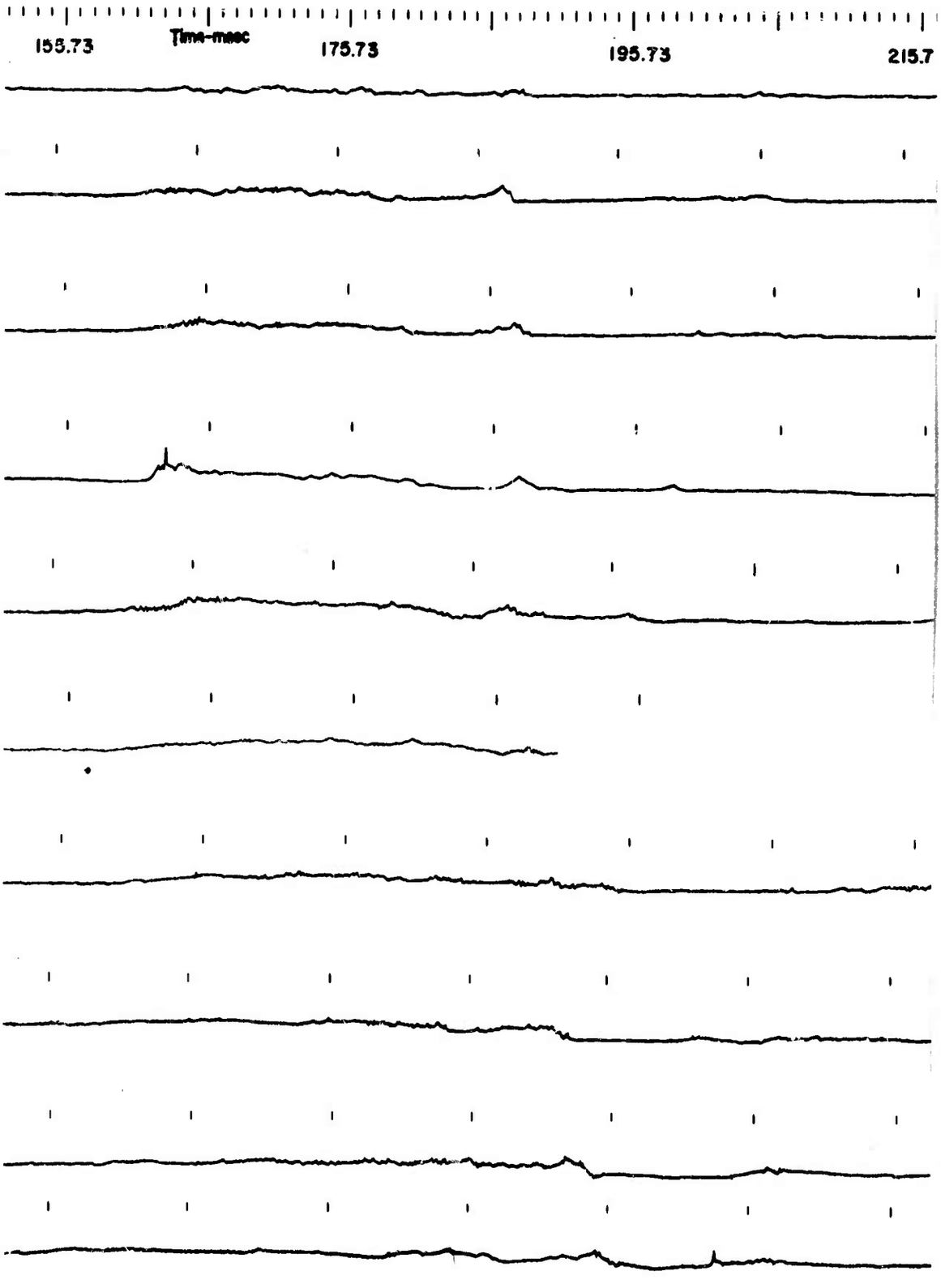

Figu

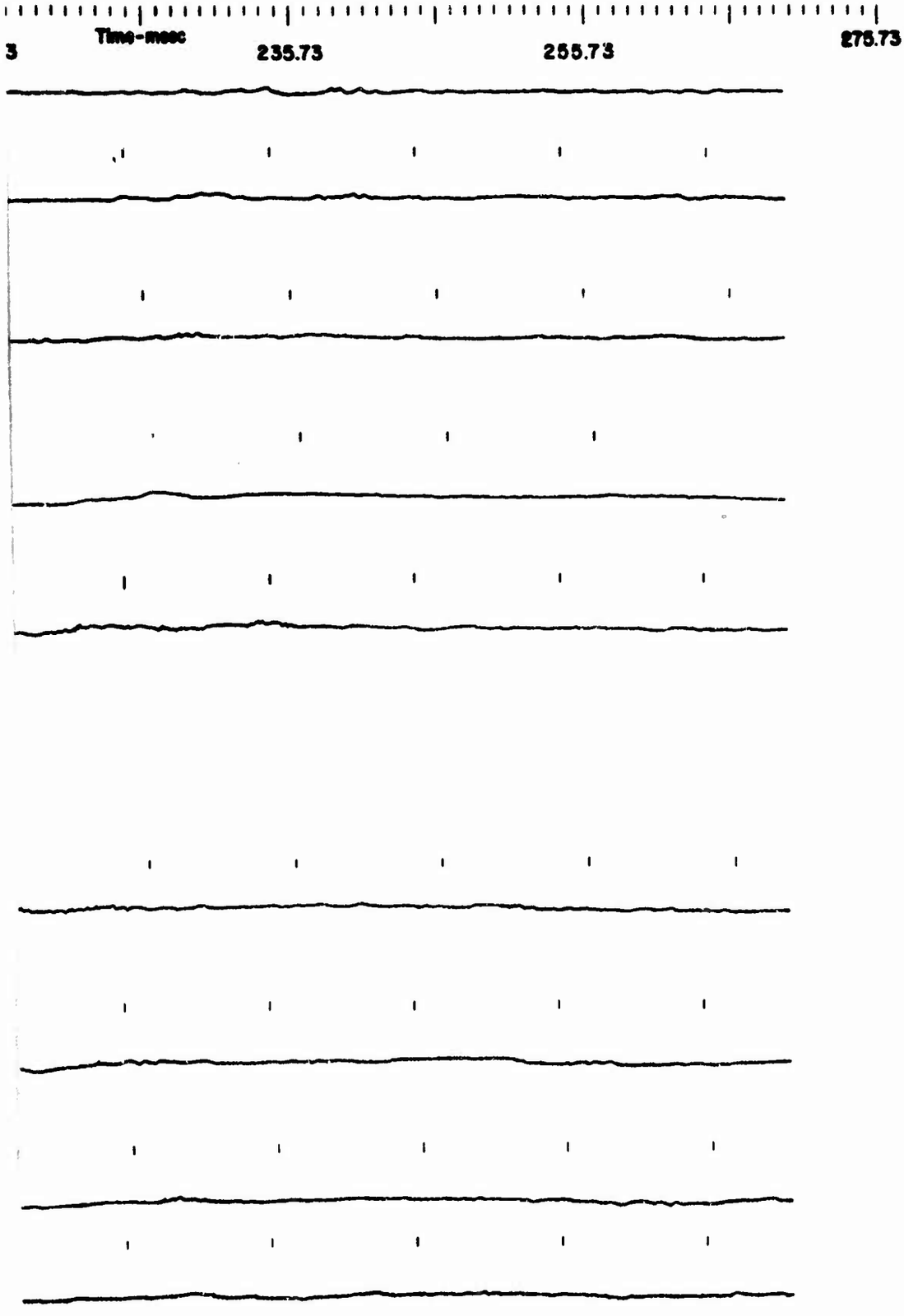

e A20 - Pressure Histories - 600-Ft Range from Burst at 100-Ft Depth (Station 3, Test 3)

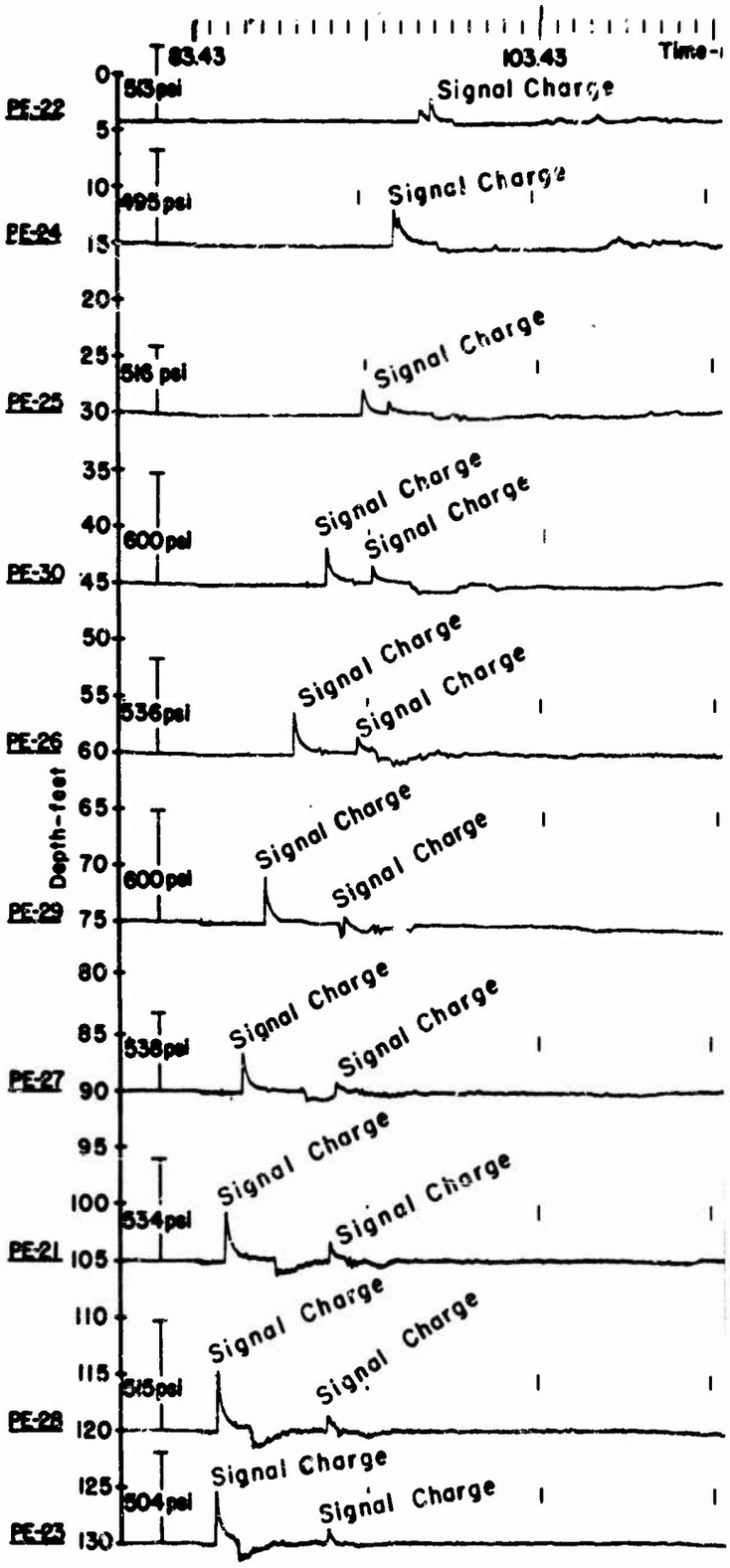
83.43
103.43
Time-
Depth-feet
PE-22
553psi
Signal Charge
PE-24
495psi
Signal Charge
PE-25
516 psi
Signal Charge
PE-30
600psi
Signal Charge
Signal Charge
PE-26
536psi
Signal Charge
Signal Charge
PE-29
600psi
Signal Charge
Signal Charge
PE-27
538psi
Signal Charge
Signal Charge
PE-21
534psi
Signal Charge
Signal Charge
PE-28
515psi
Signal Charge
Signal Charge
PE-23
504psi
Signal Charge
Signal Charge

A

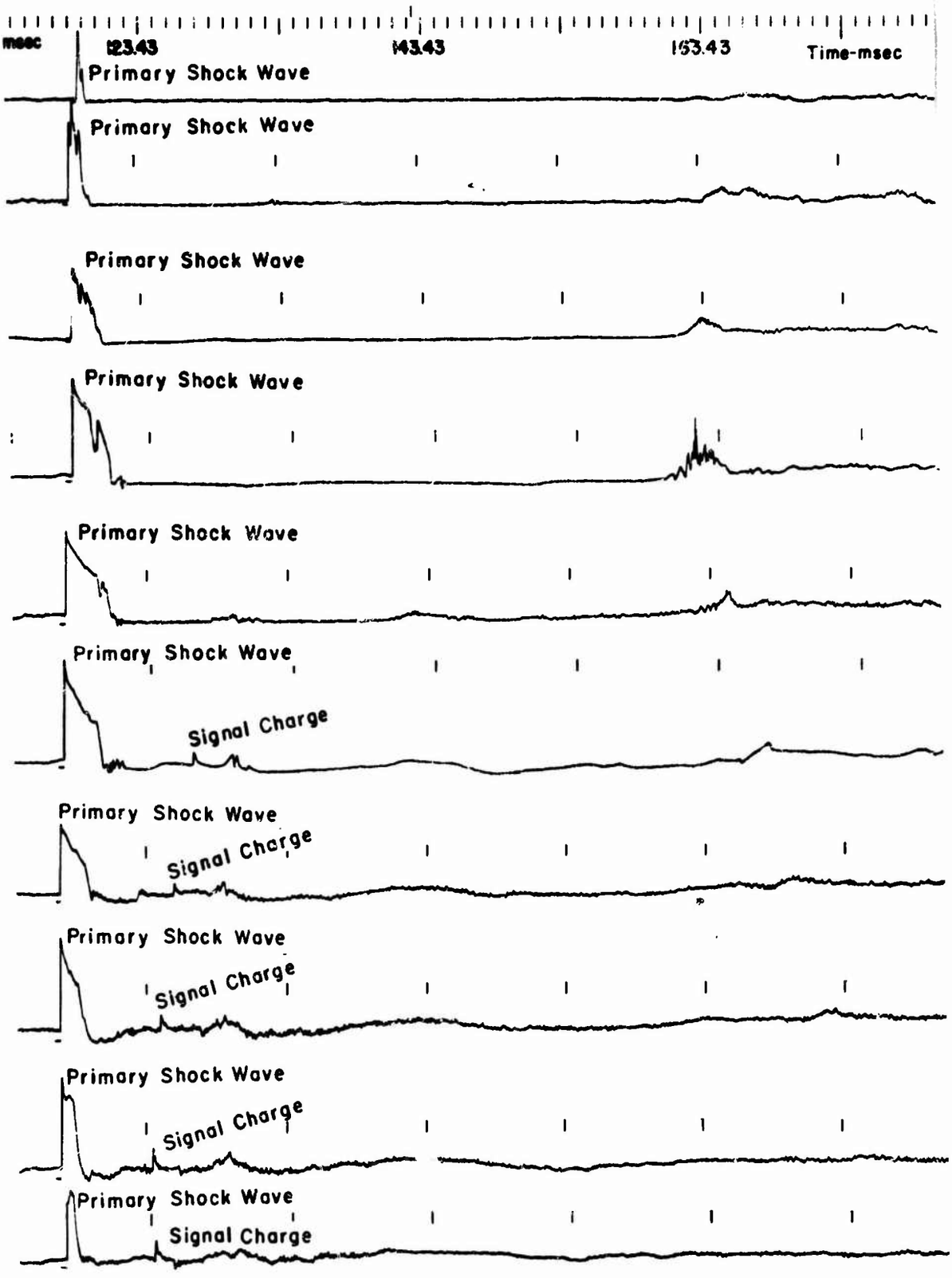
msec
123.43
143.43
163.43
Time-msec
Primary Shock Wave
Primary Shock Wave
Primary Shock Wave
Primary Shock Wave
Primary Shock Wave
Primary Shock Wave
Signal Charge
Primary Shock Wave
Signal Charge
Primary Shock Wave
Signal Charge
Primary Shock Wave
Signal Charge
Primary Shock Wave
Signal Charge

B

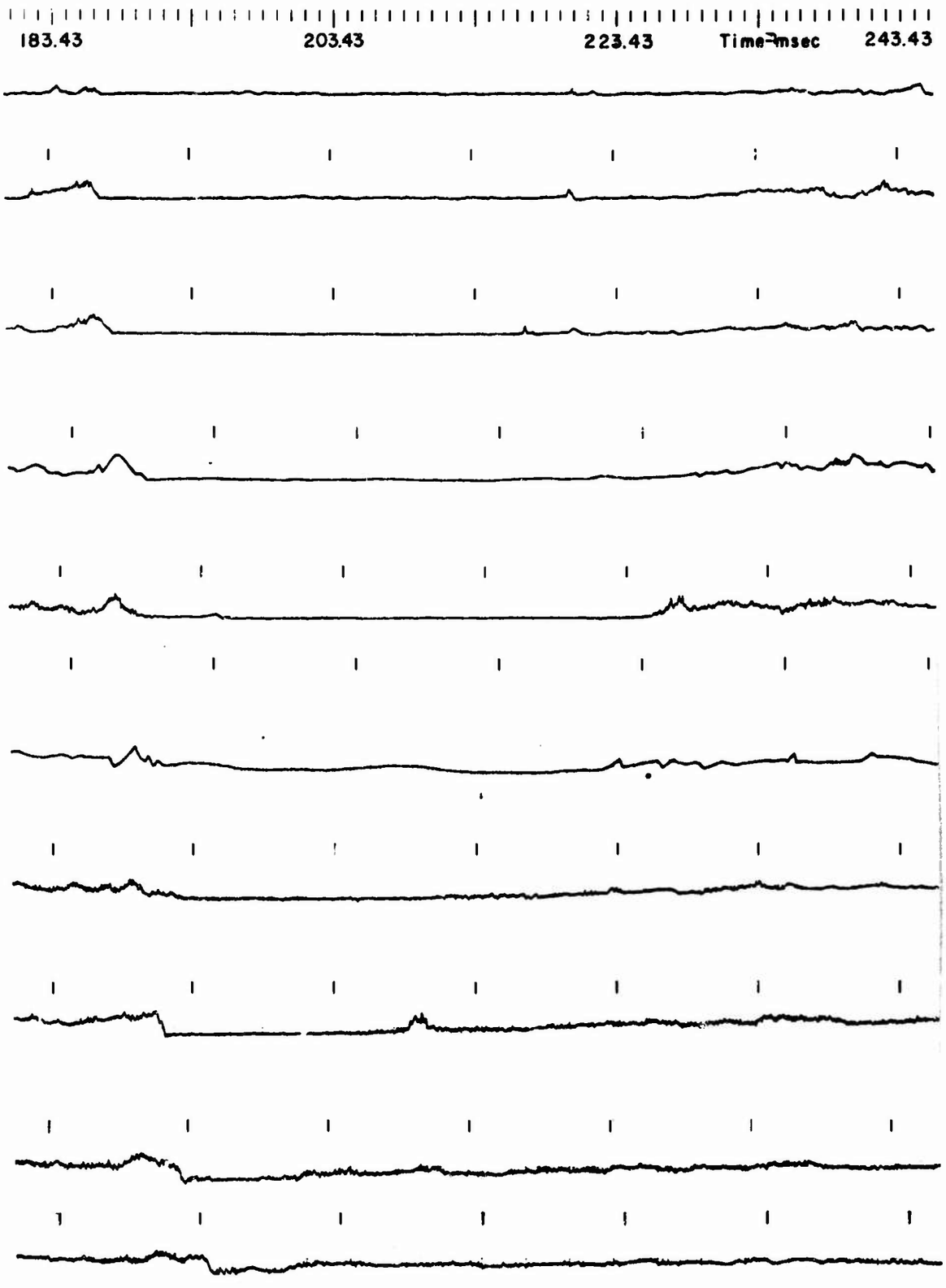

Figur

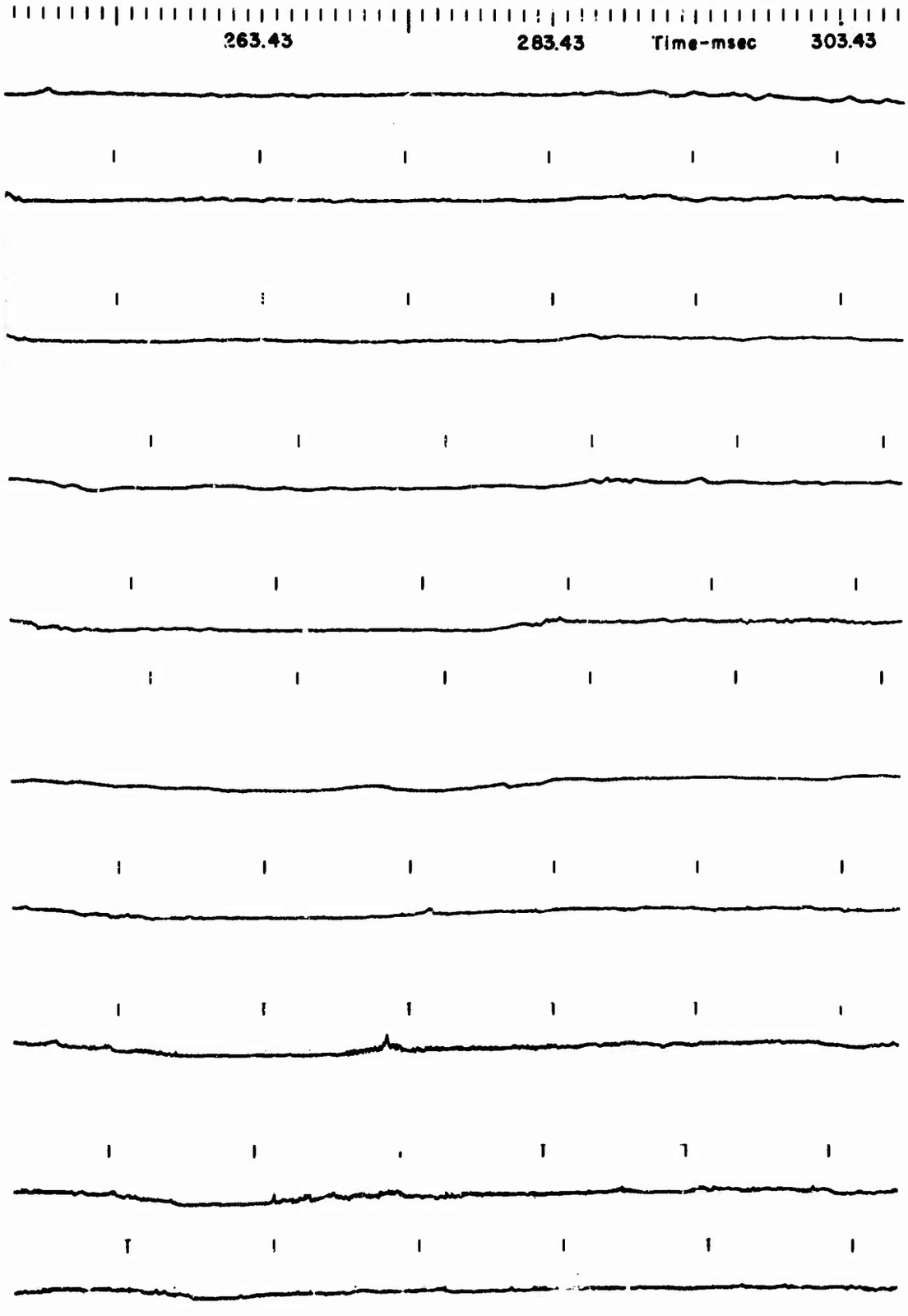

e A21 - Pressure Histories - 600-Ft Range from Burst at 100-Ft Depth (Station 5, Test 7)

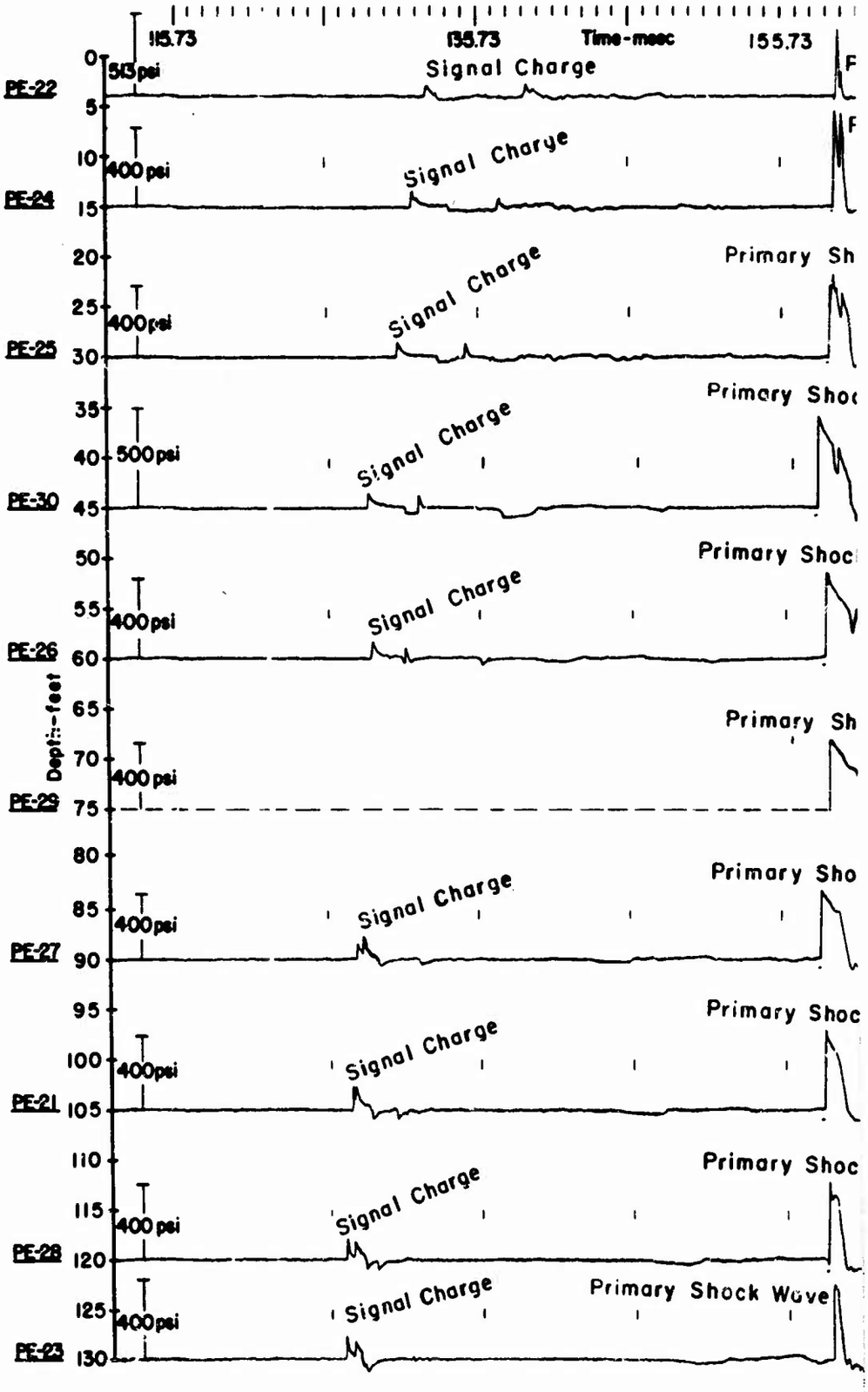
115.73
135.73
Time-msec
155.73
PE-22
515psi
Signal Charge
PE-24
400psi
Signal Charge
PE-25
400psi
Signal Charge
Primary Sh
PE-30
500psi
Signal Charge
Primary Shoc
PE-26
400psi
Signal Charge
Primary Shoc
Depth-feet
PE-29
400psi
Primary Sh
PE-27
400psi
Signal Charge
Primary Sho
PE-21
400psi
Signal Charge
Primary Shoc
PE-28
400psi
Signal Charge
Primary Shoc
PE-23
400psi
Signal Charge
Primary Shock Wave

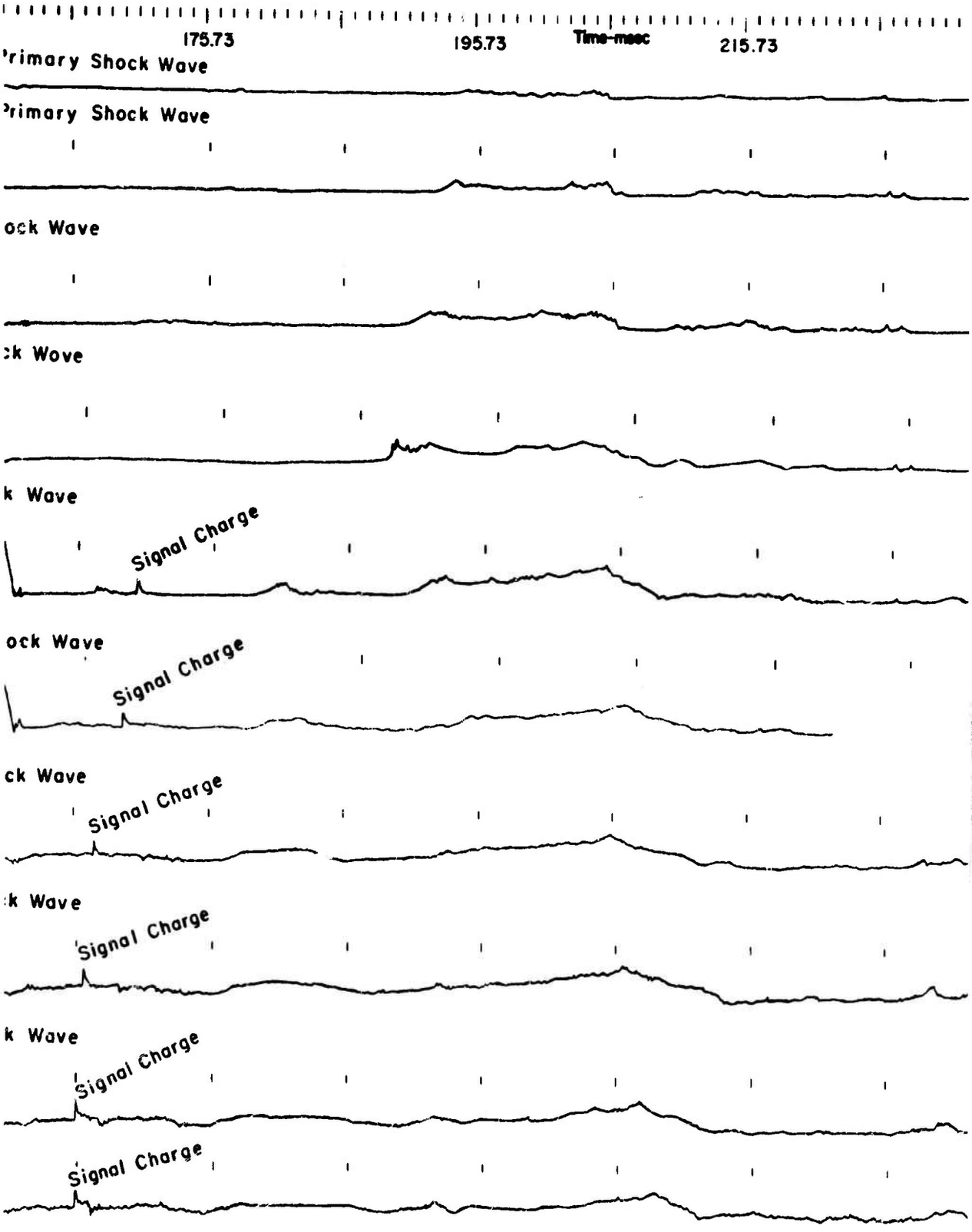
175.73
195.73
Time-msec
215.73
Primary Shock Wave
Primary Shock Wave
ock Wave
ck Wove
k Wave
Signal Charge
ock Wave
Signal Charge
ck Wave
Signal Charge
k Wave
'Signal Charge
k Wave
Signal Charge
Signal Charge

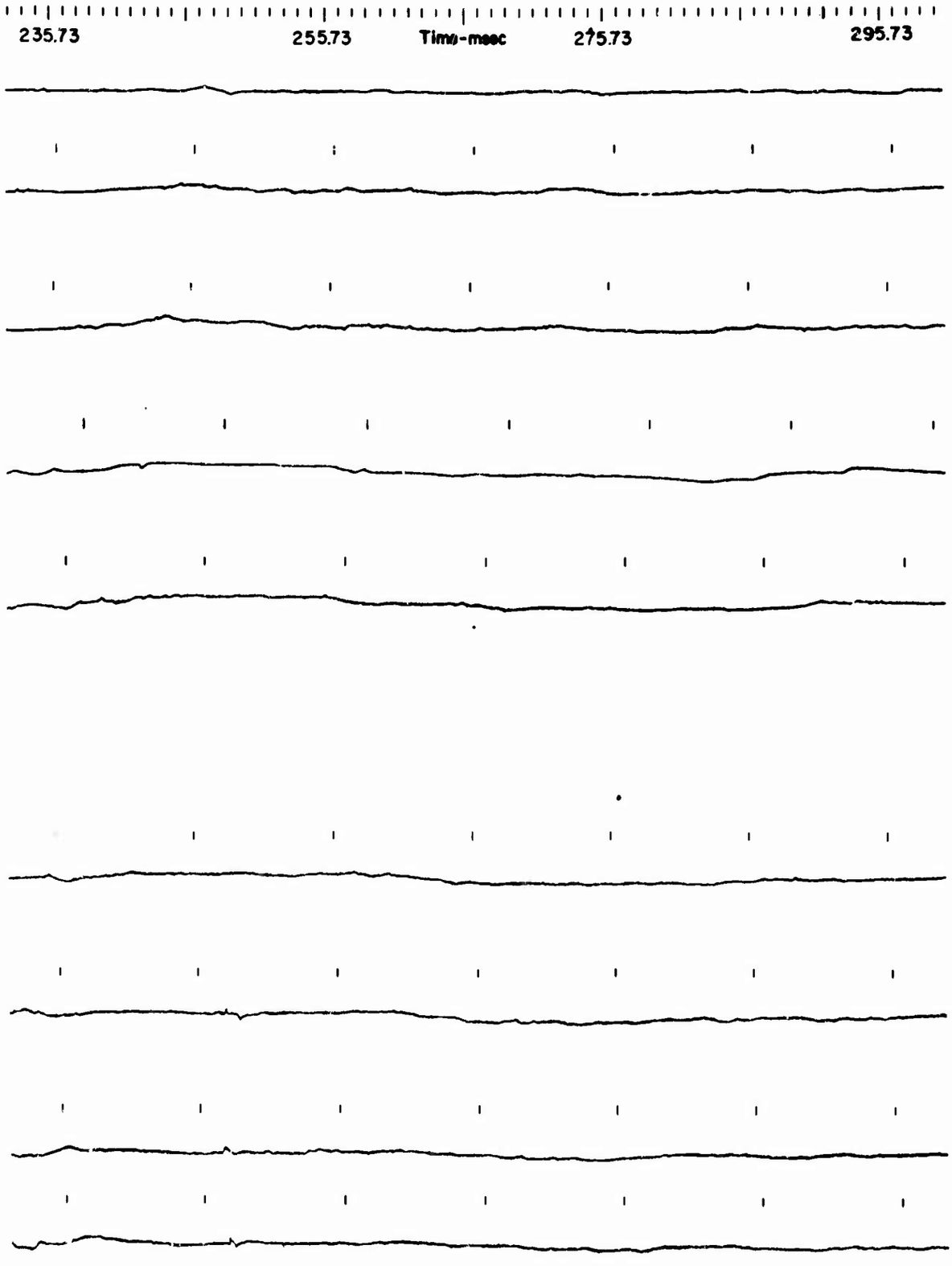

Figure A22 - Pressure Histories - 800-Ft Range from Burst at 100-Ft Depth (Station 5, Test 3)

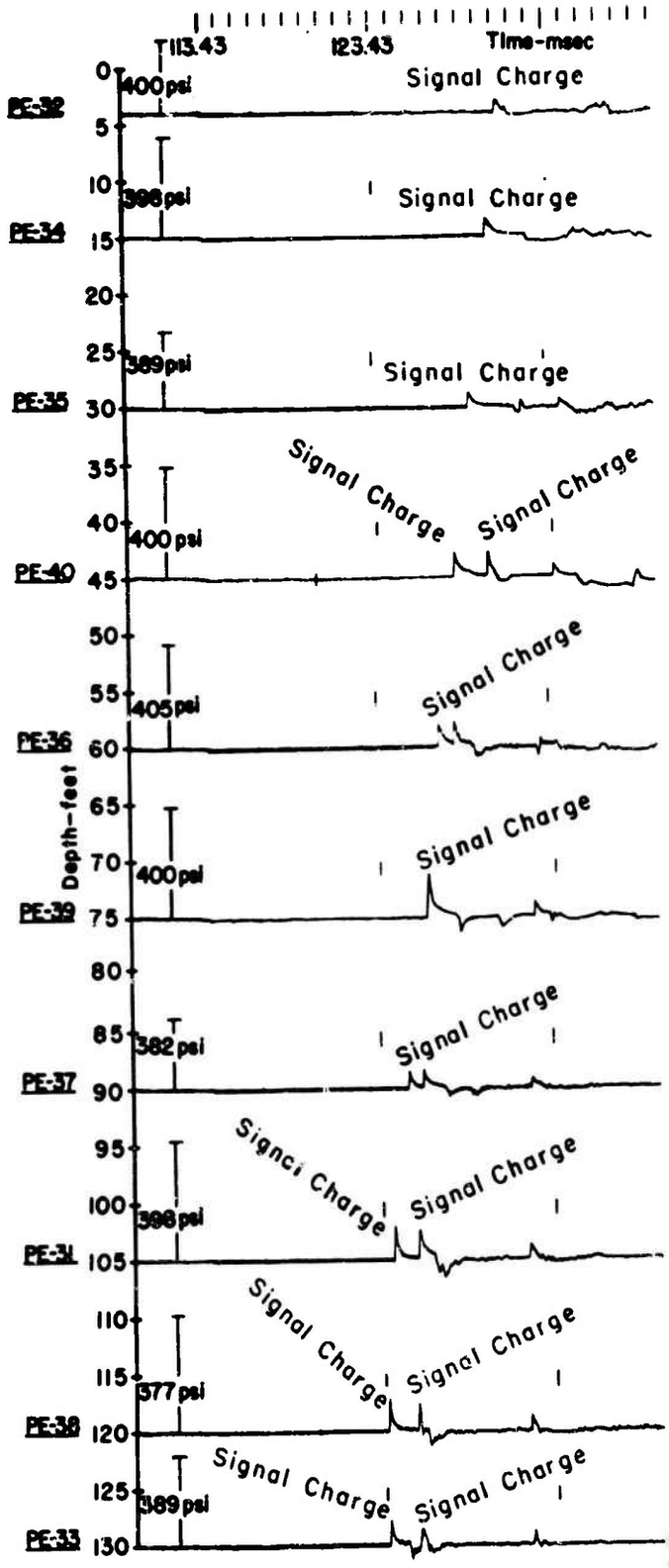
113.43
123.43
Time-msec
Depth-feet
PE-32
400 psi
Signal Charge
PE-34
398 psi
Signal Charge
PE-35
389 psi
Signal Charge
PE-40
400 psi
Signal Charge
Signal Charge
PE-36
405 psi
Signal Charge
PE-39
400 psi
Signal Charge
PE-37
382 psi
Signal Charge
PE-31
398 psi
Signal Charge
Signal Charge
PE-38
377 psi
Signal Charge
Signal Charge
PE-33
389 psi
Signal Charge
Signal Charge

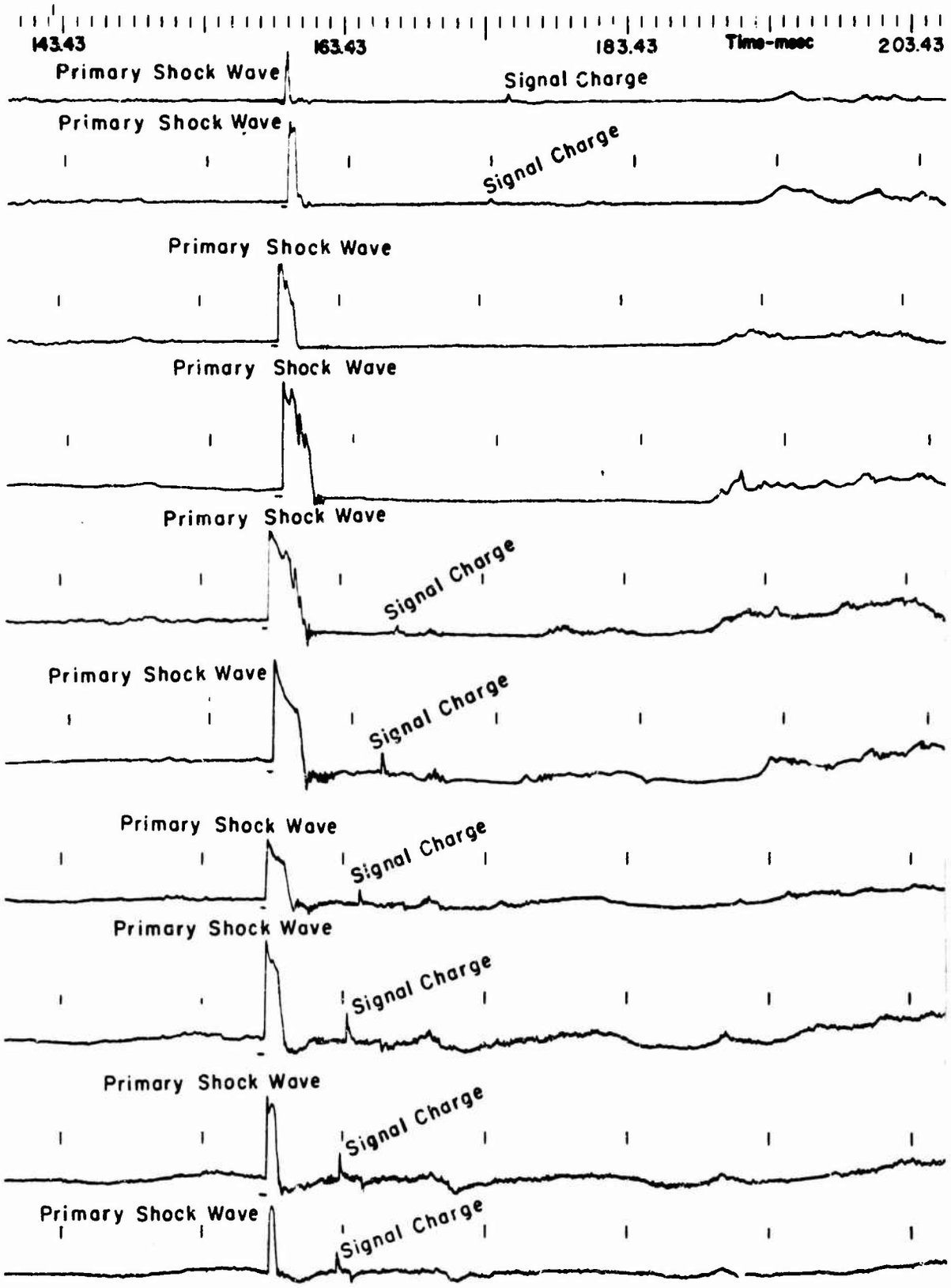
143.43
163.43
183.43
Time-msec
203.43
Primary Shock Wave
Signal Charge
Primary Shock Wave
Signal Charge
Primary Shock Wave
Primary Shock Wave
Primary Shock Wave
Signal Charge
Primary Shock Wave
Signal Charge
Primary Shock Wave
Signal Charge
Primary Shock Wave
Signal Charge
Primary Shock Wave
Signal Charge
Primary Shock Wave
Signal Charge

B

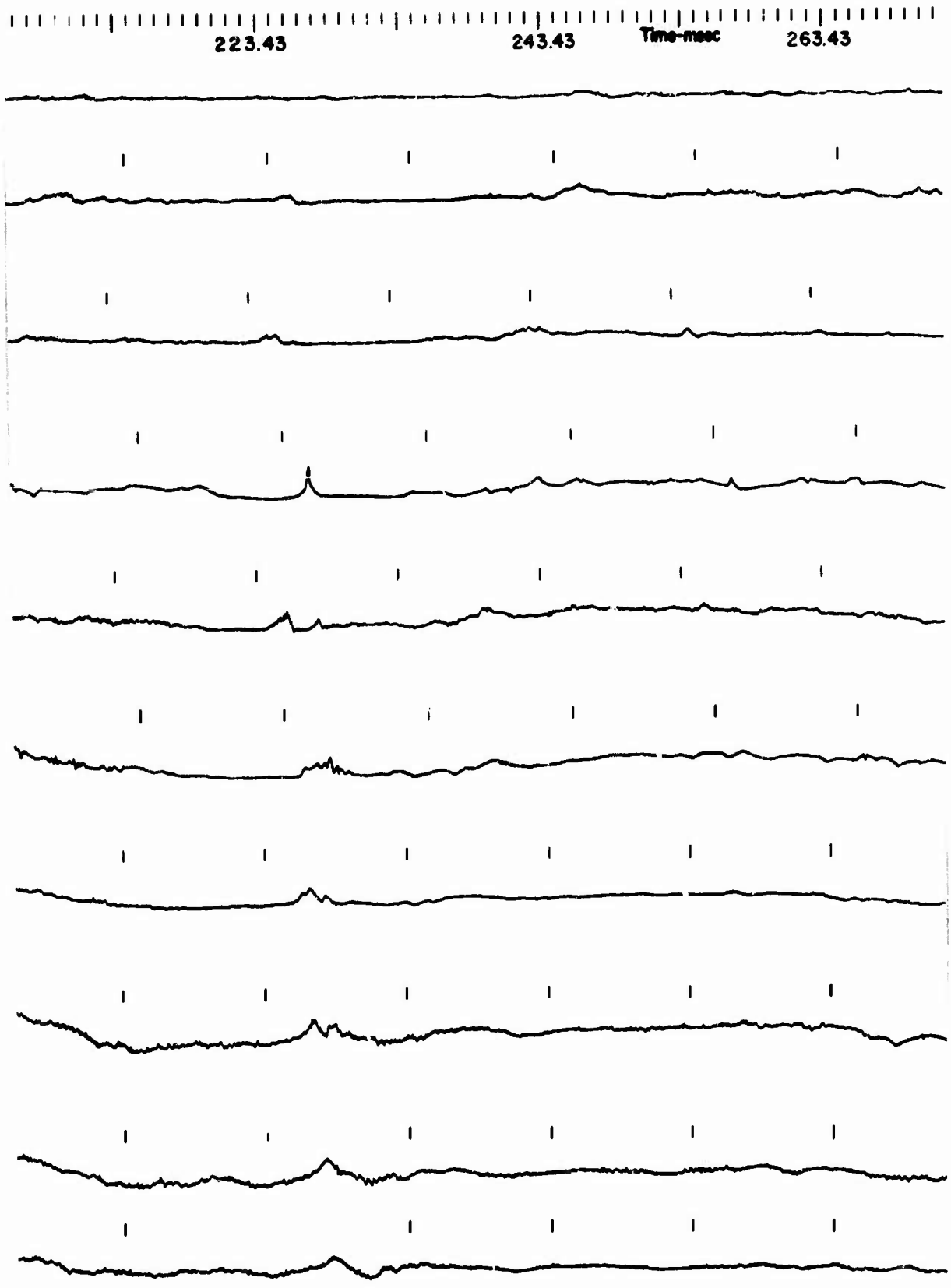

Figur

C

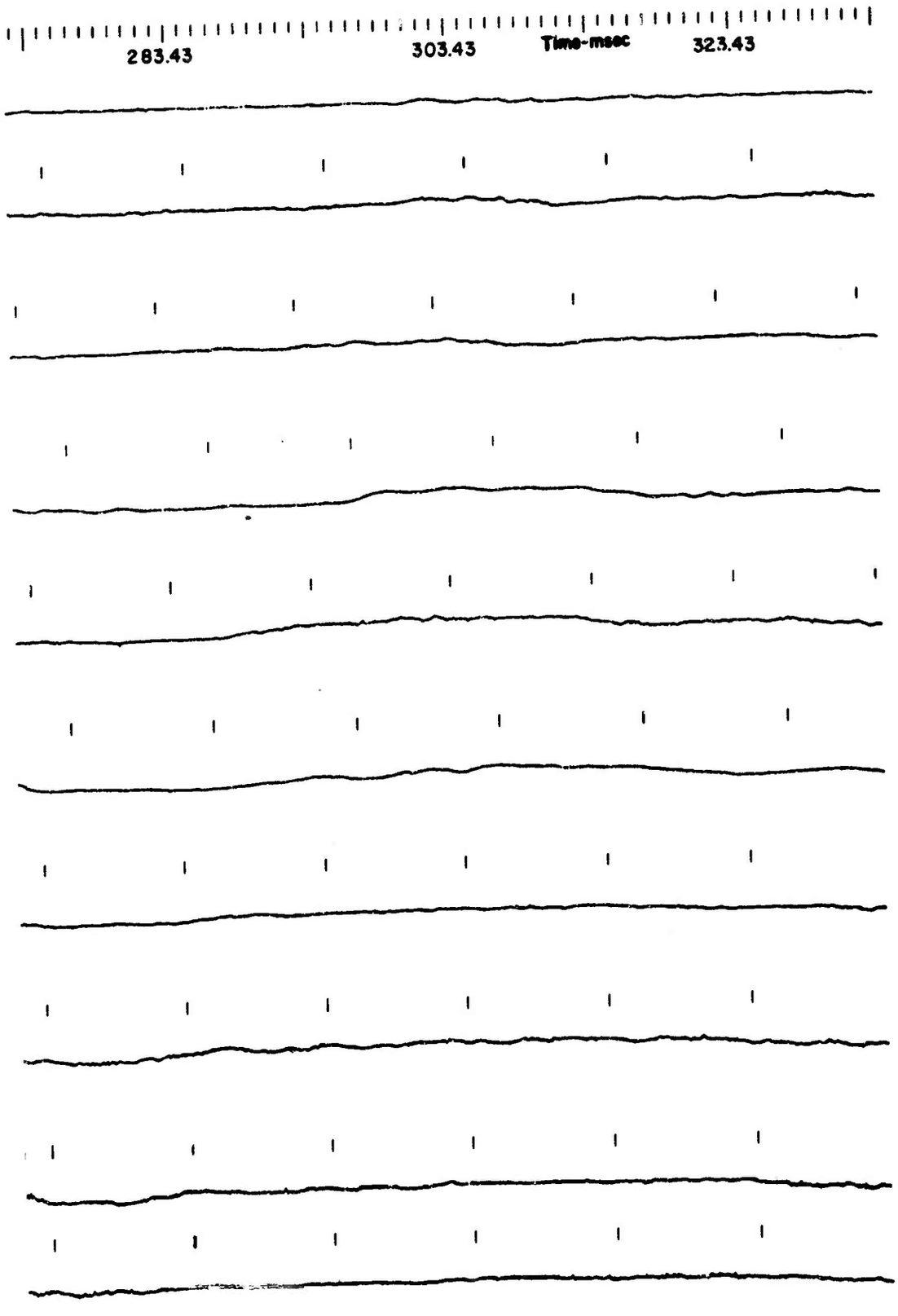

e A23 - Pressure Histories - 800-Ft Range from Burst at 100-Ft Depth (Station 7, Test 7)

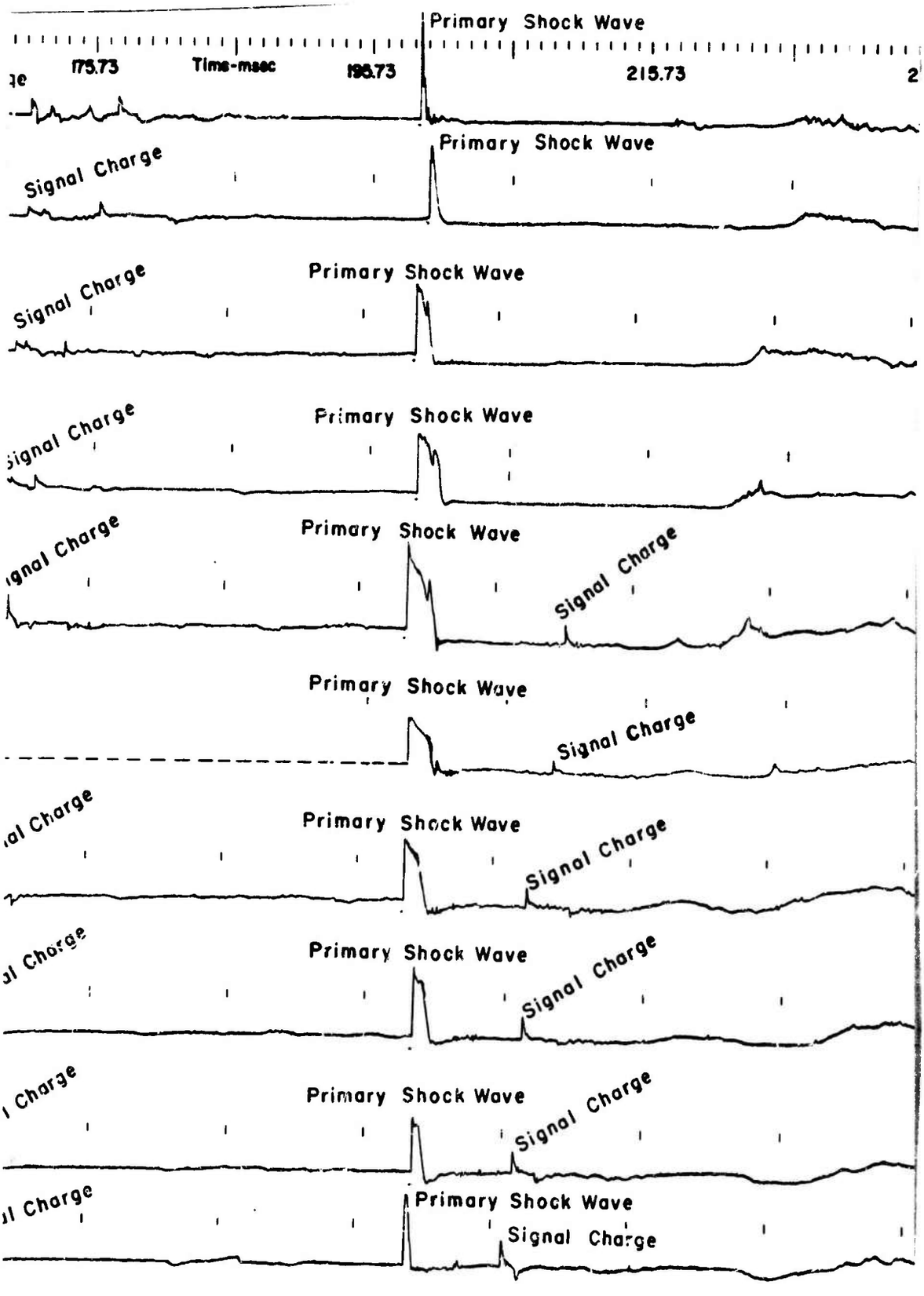
Primary Shock Wave
175.73
Time-msec
195.73
215.73
Signal Charge
Primary Shock Wave
Signal Charge
Primary Shock Wave
Primary Shock Wave
Signal Charge
Primary Shock Wave
Signal Charge
Primary Shock Wave
Signal Charge
Primary Shock Wave
Signal Charge
Primary Shock Wave
Signal Charge
Primary Shock Wave
Signal Charge
Primary Shock Wave
Signal Charge

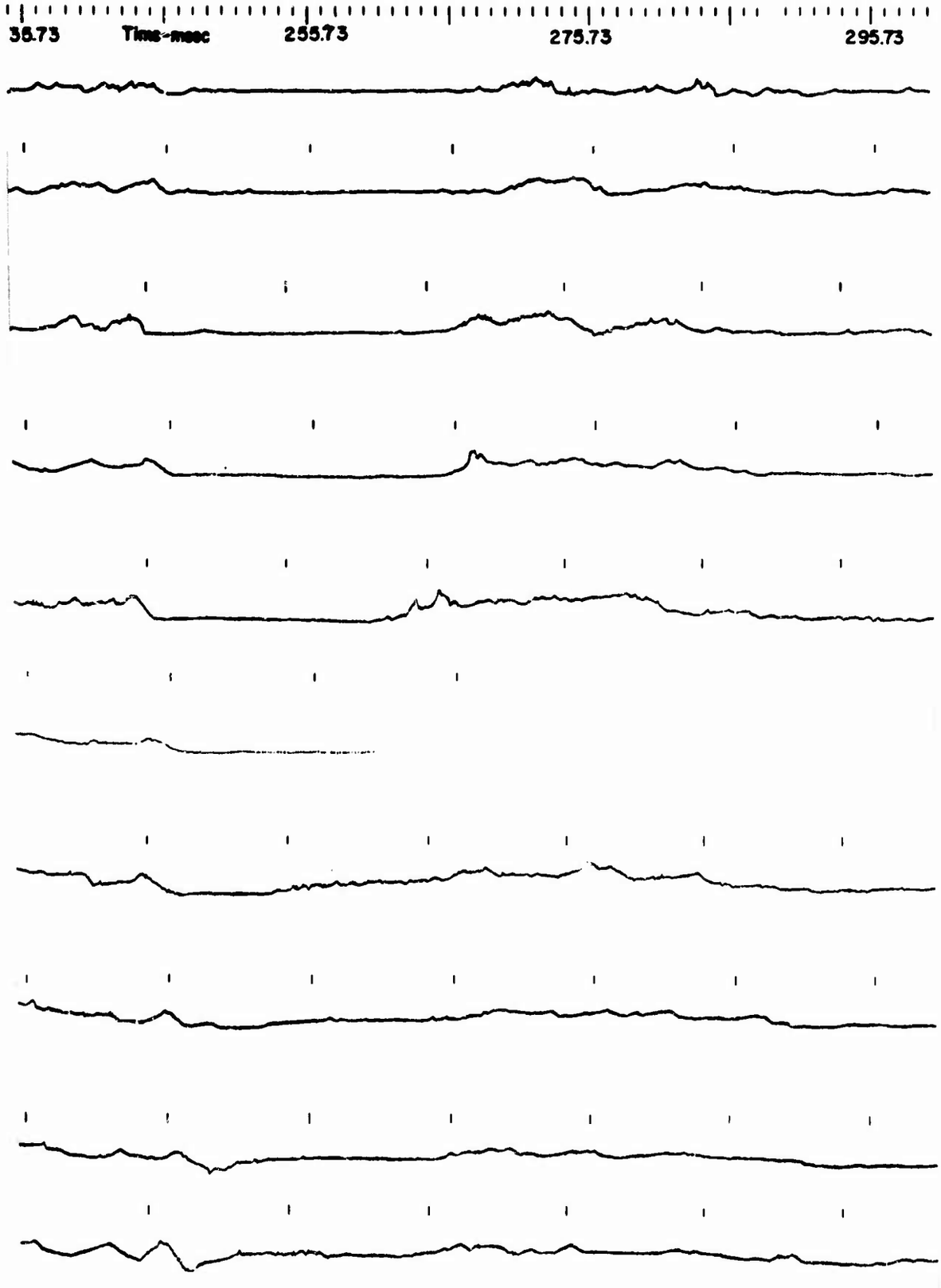

Figu

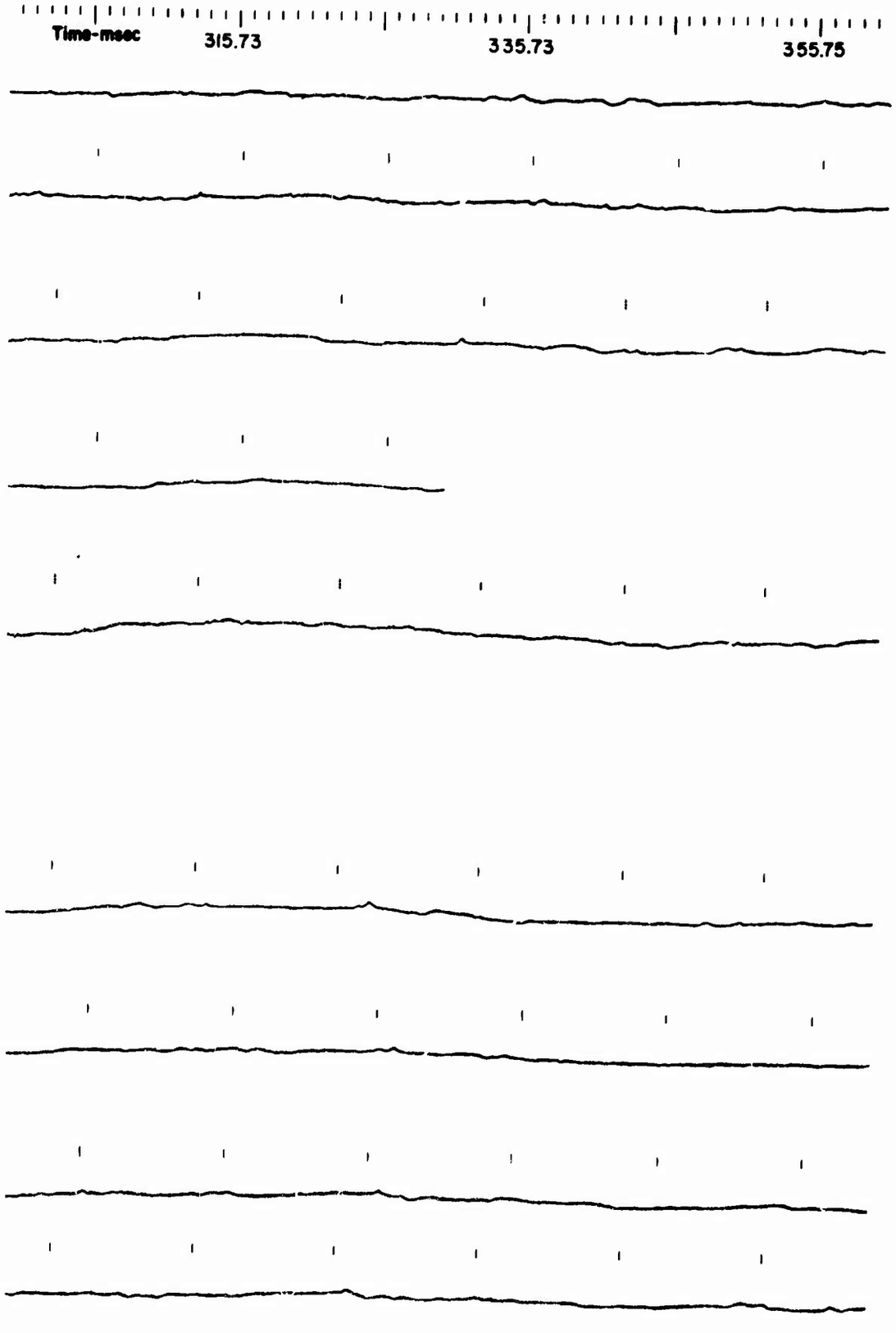

ıre A24 - Pressure Histories - 1000-Ft Range fr on Burst at 100-Ft Depth (Station 7, Test 3)

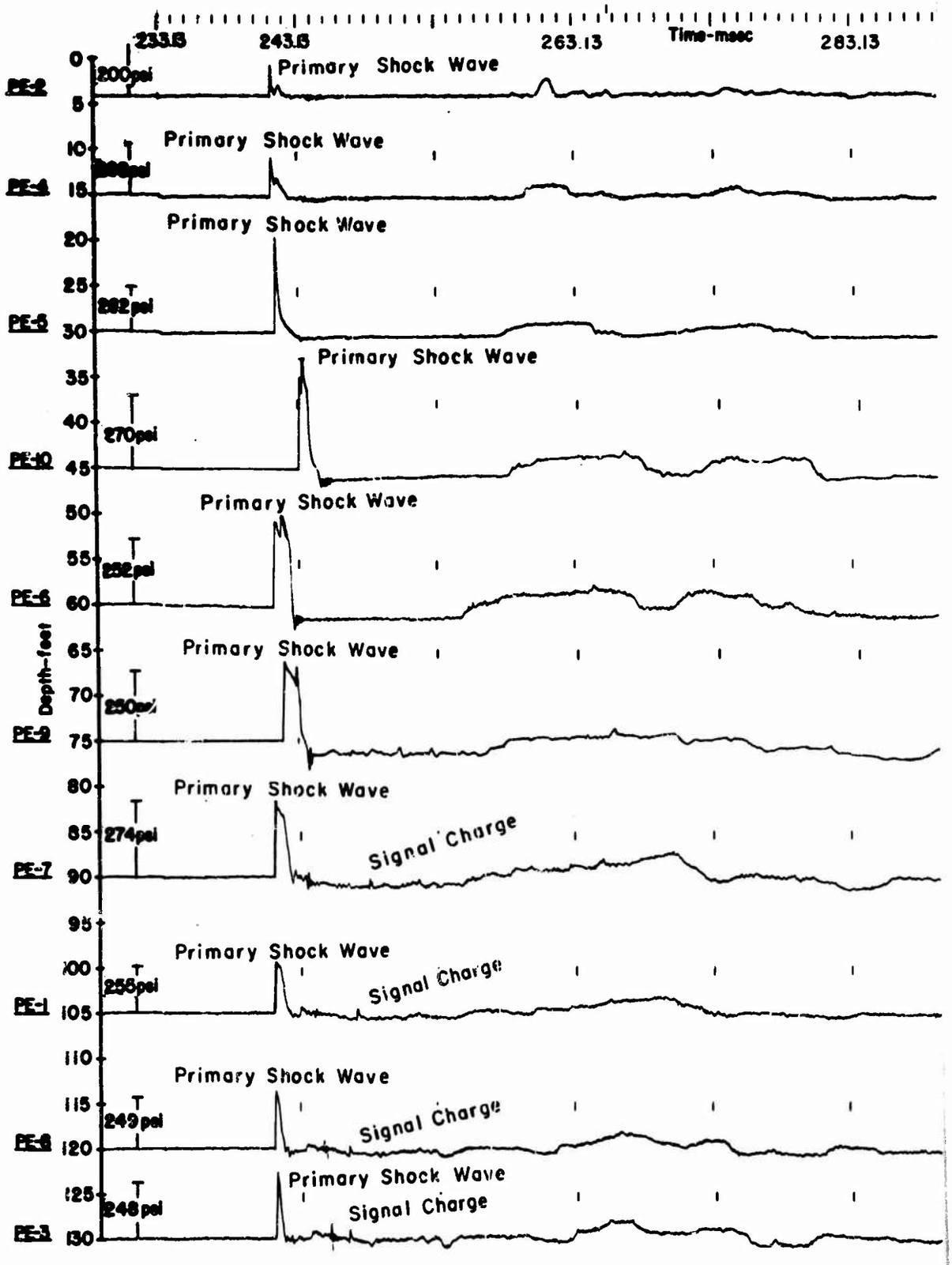
233.13
243.13
263.13
Time-msec
283.13
Depth-feet
0
5
10
15
20
25
30
35
40
45
50
55
60
65
70
75
80
85
90
95
100
105
110
115
120
125
130
PE-2
PE-4
PE-5
PE-10
PE-6
PE-9
PE-7
PE-1
PE-8
PE-3
200psi
282psi
270psi
252psi
274psi
256psi
249psi
248psi
Primary Shock Wave
Signal Charge

A

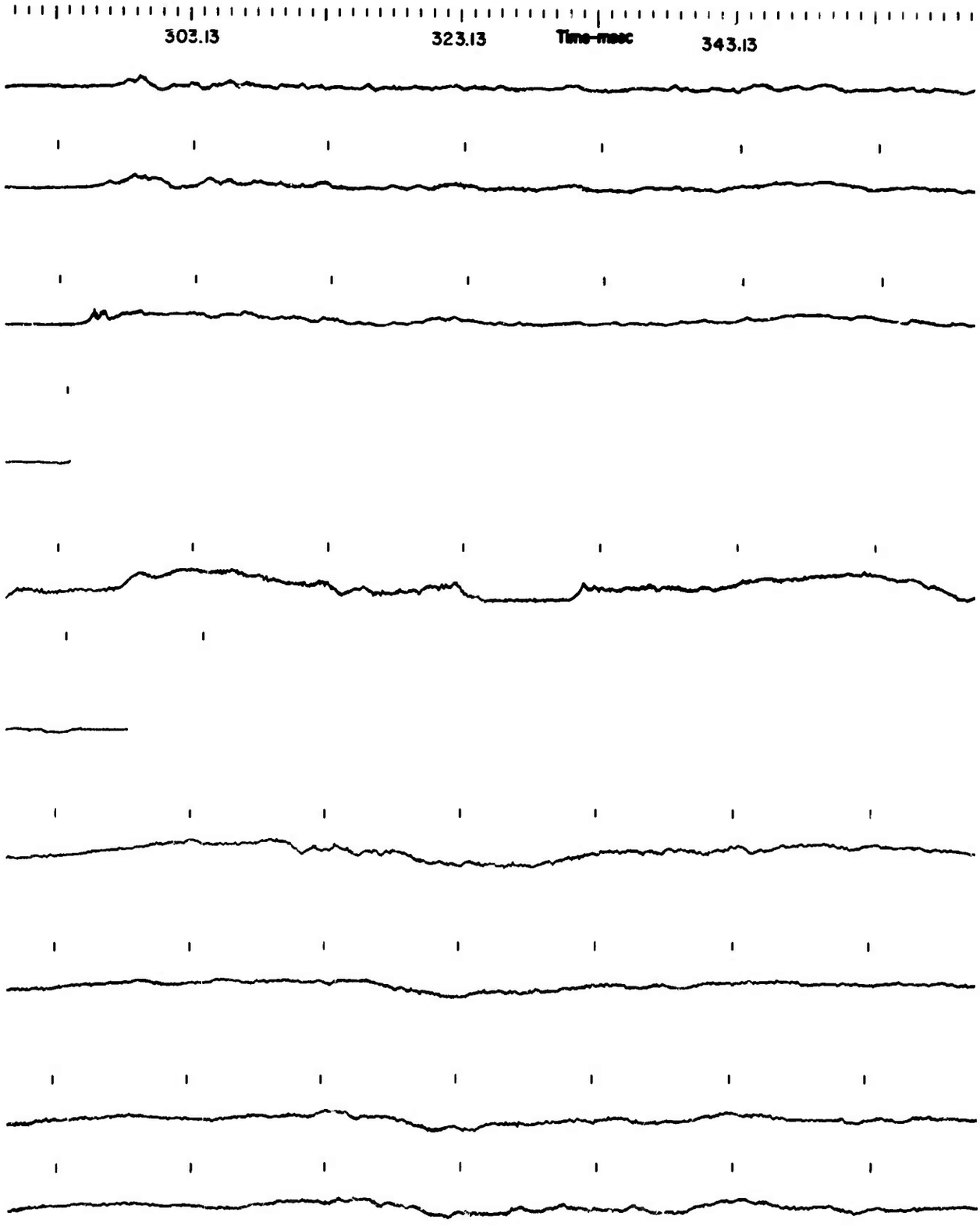

B

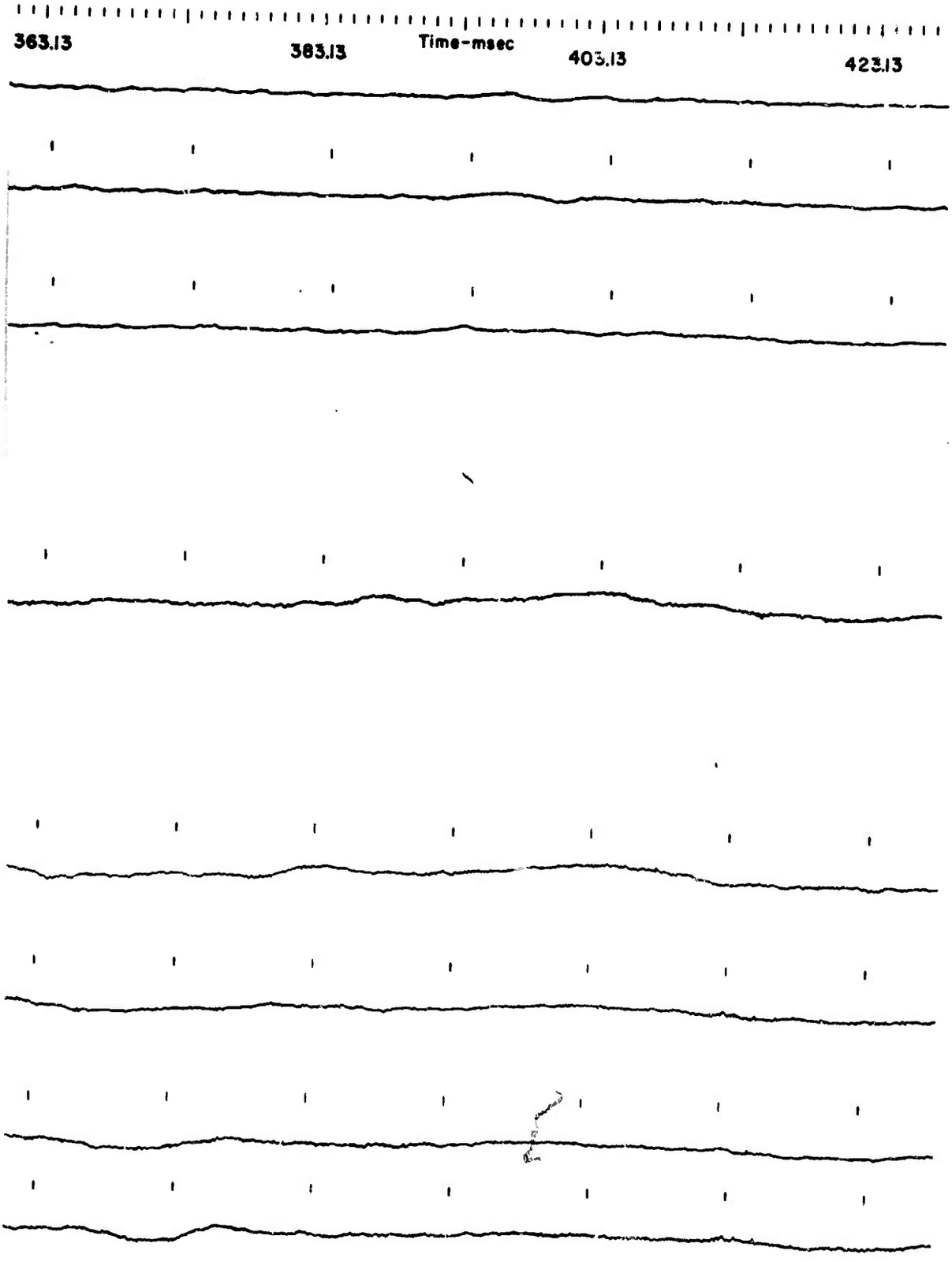

Figure A25 - Pressure Histories - 1200-Ft Range from Burst at 100-Ft Depth (Station 1, Test 5)

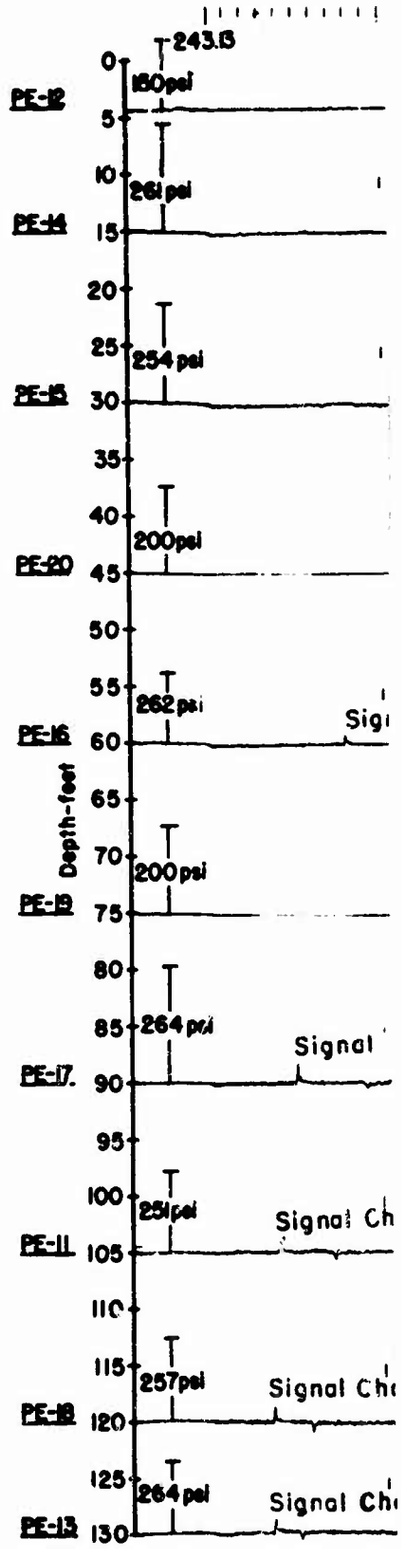
243.15
0
150psi
PE-12
5
10
261psi
PE-14
15
20
25
254psi
PE-15
30
35
40
200psi
PE-20
45
50
55
262psi
Sig
PE-16
60
Depth-feet
65
70
200psi
PE-19
75
80
85
264psi
Signal
PE-17.
90
95
100
251psi
Signal Ch
PE-11
105
110
115
257psi
Signal Ch
PE-18
120
125
264psi
Signal Ch
PE-13
130

A

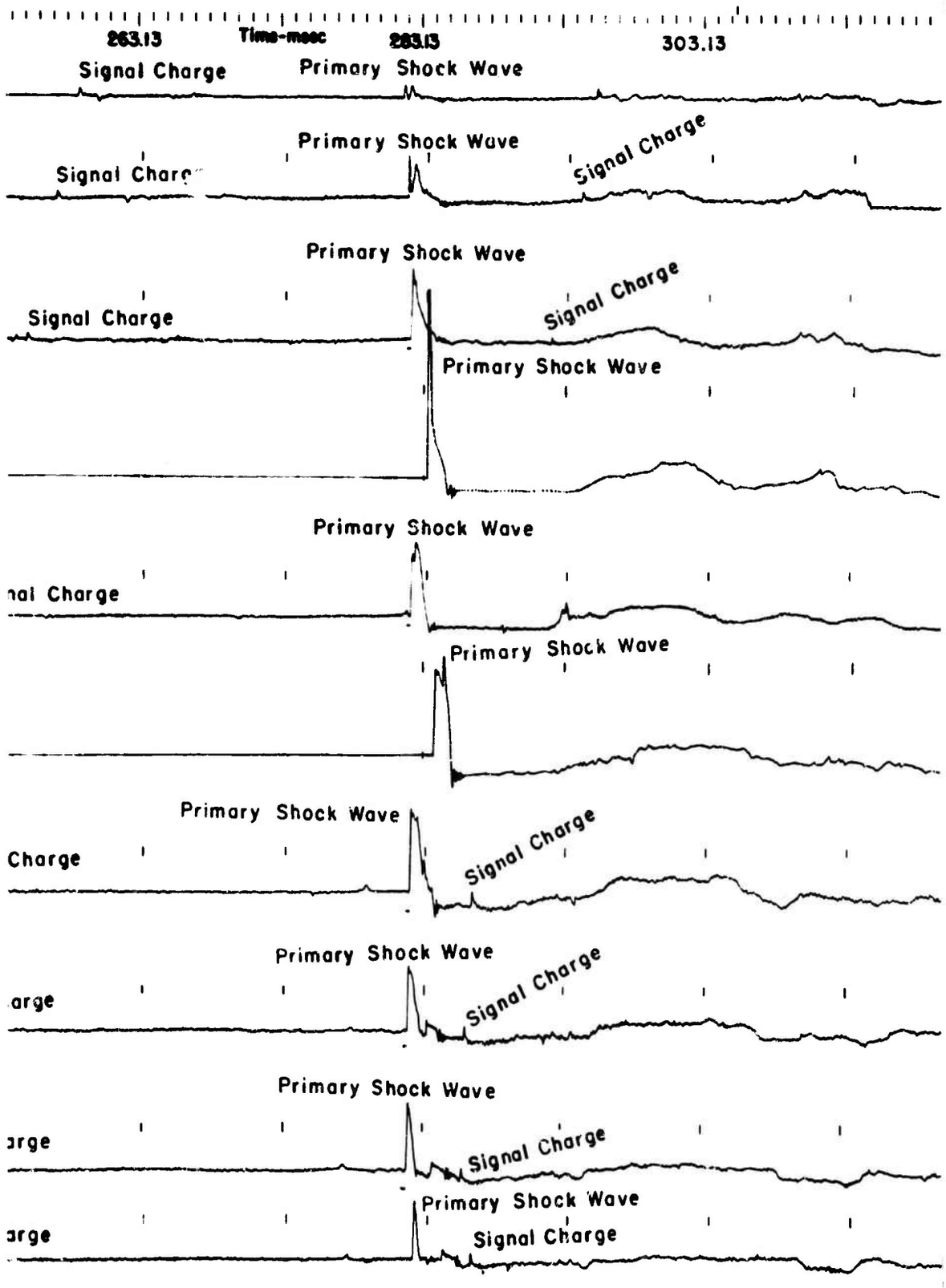
263.13
Time-msec
283.13
303.13
Signal Charge
Primary Shock Wave
Primary Shock Wave
Signal Charge
Primary Shock Wave
Signal Charge
Signal Charge
Primary Shock Wave
Primary Shock Wave
Primary Shock Wave
Charge
Signal Charge
Primary Shock Wave
Signal Charge
Primary Shock Wave
Signal Charge
Primary Shock Wave
Signal Charge

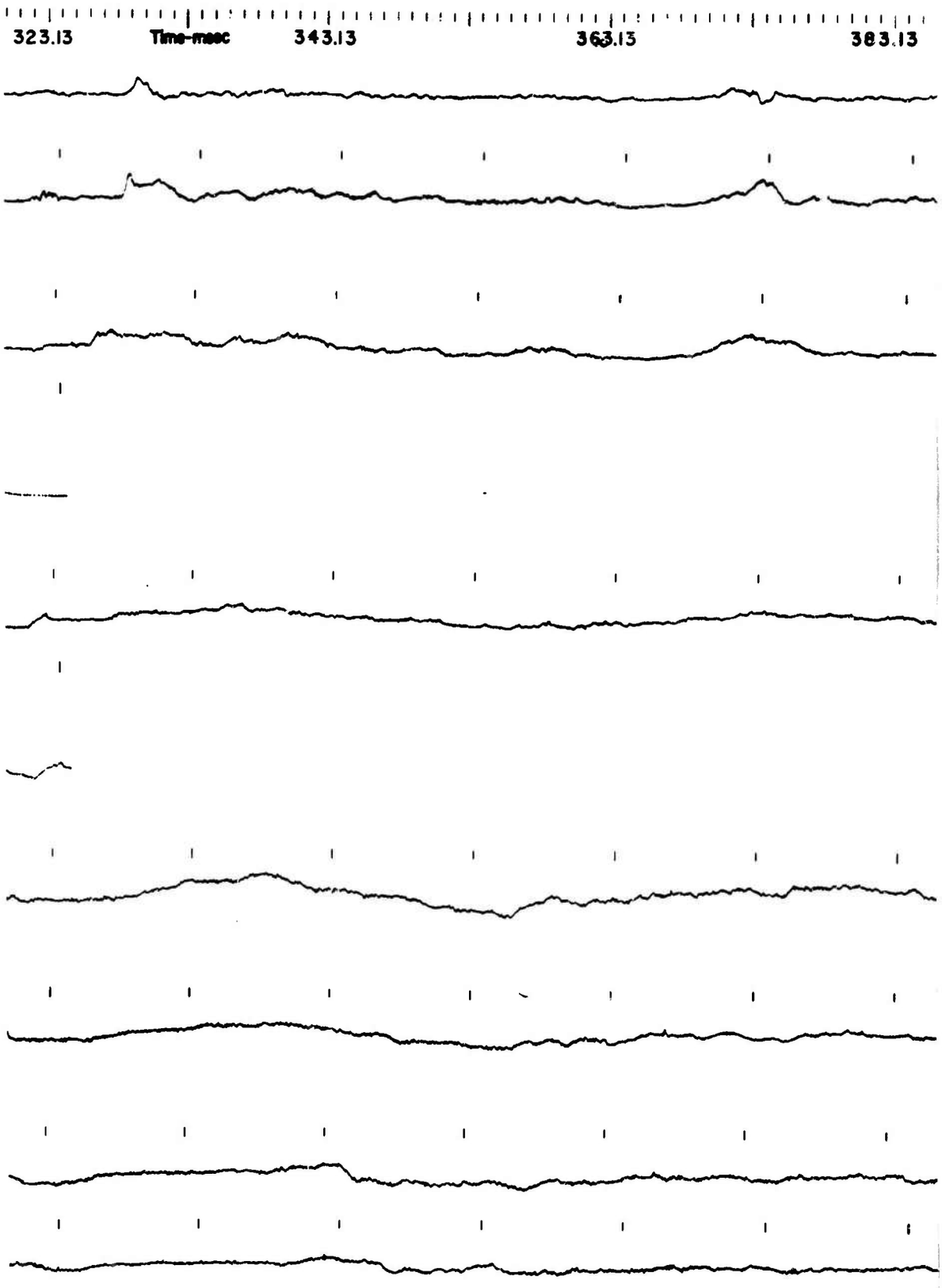

Figur

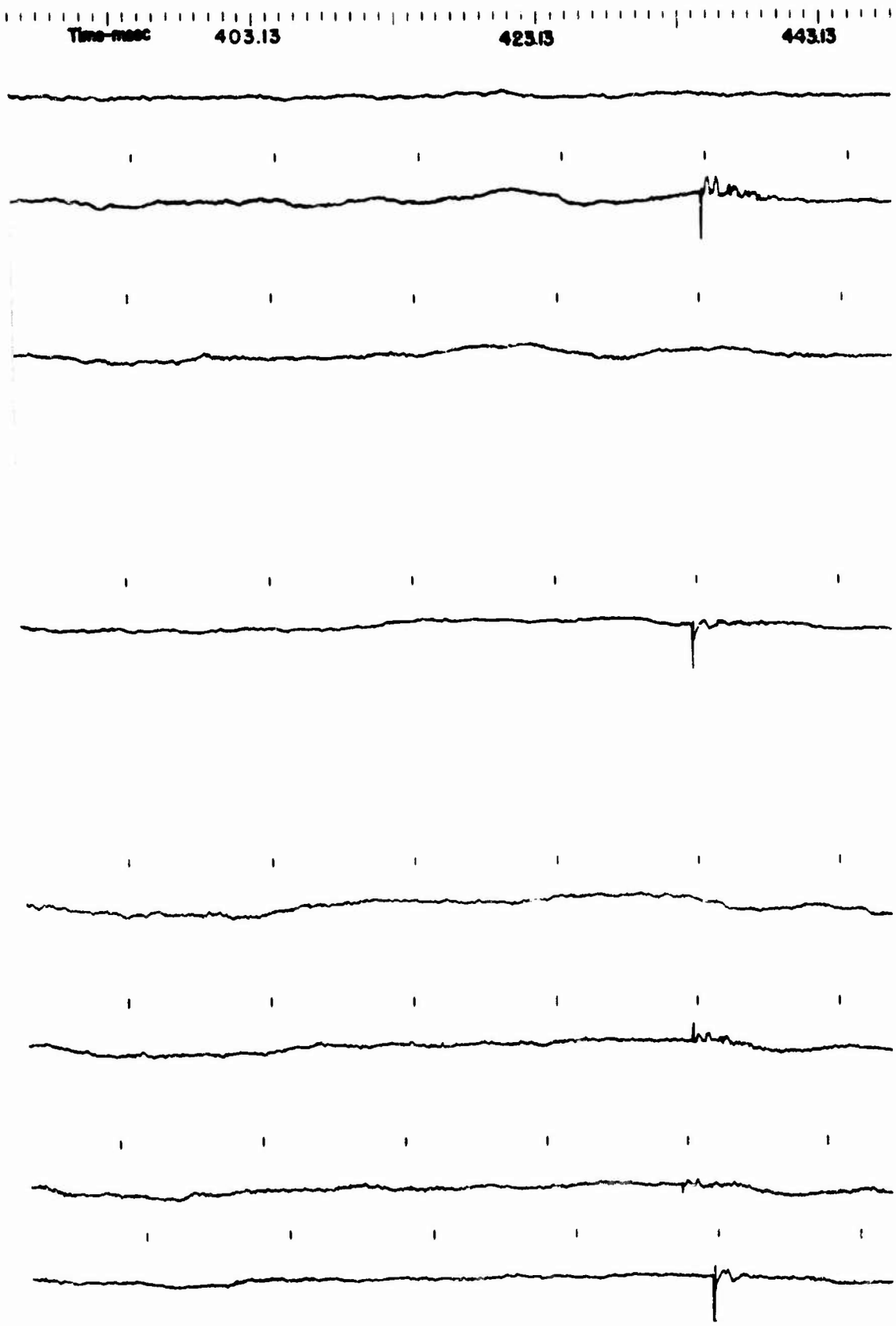

e A26 - Pressure Histories - 1400-Ft Range from Burst at 100-Ft Depth (Station 3, Test 5)

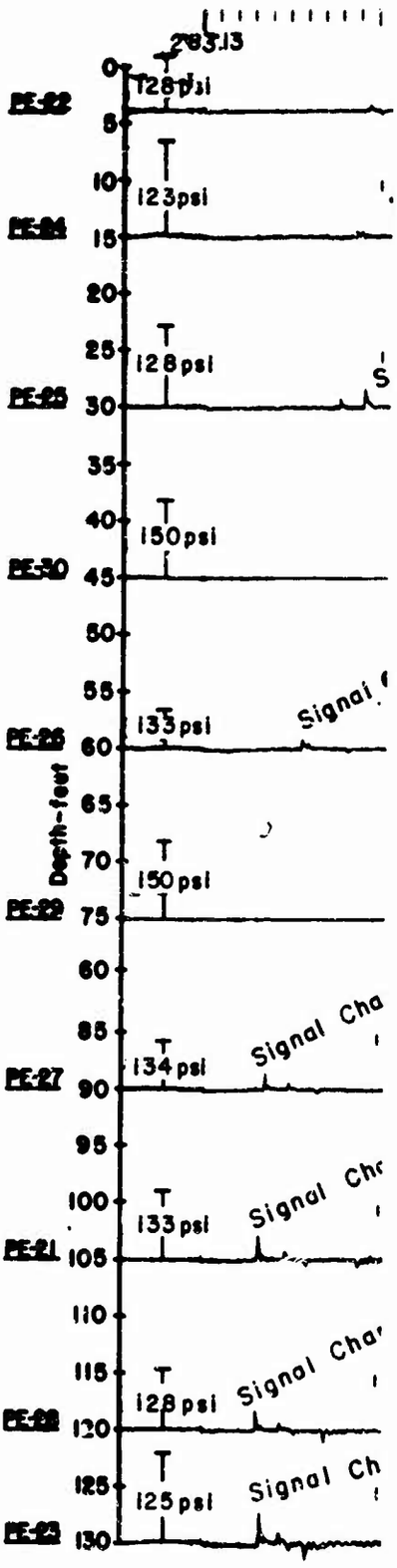
2633.13
0
5
10
15
20
25
30
35
40
45
50
55
60
65
70
75
80
85
90
95
100
105
110
115
120
125
130
Depth-feet
PE-22
T 128 psi
PE-24
T 123psi
PE-25
T 128psi
S
PE-30
T 150psi
PE-26
T 133psi
Signal
PE-29
T 150psi
PE-27
T 134psi
Signal Cha
PE-21
T 133psi
Signal Cha
PE-28
T 128psi
Signal Cha
PE-23
T 125psi
Signal Ch

A

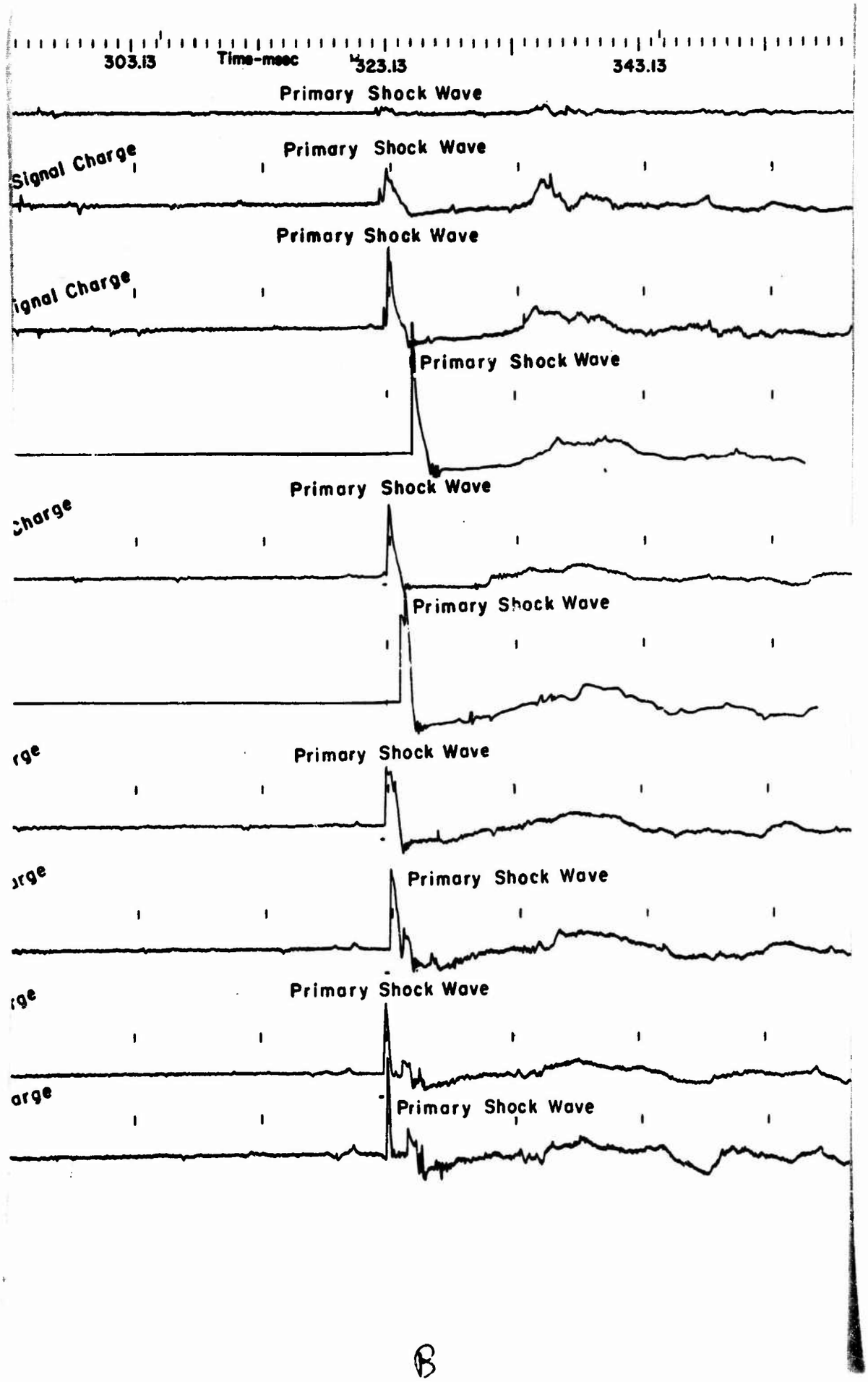
303.13
Time-msec
323.13
343.13
Primary Shock Wave
Signal Charge
Primary Shock Wave
Primary Shock Wave
ignal Charge
Primary Shock Wave
Primary Shock Wave
Charge
Primary Shock Wave
rge
Primary Shock Wave
arge
Primary Shock Wave
rge
Primary Shock Wave
arge
Primary Shock Wave

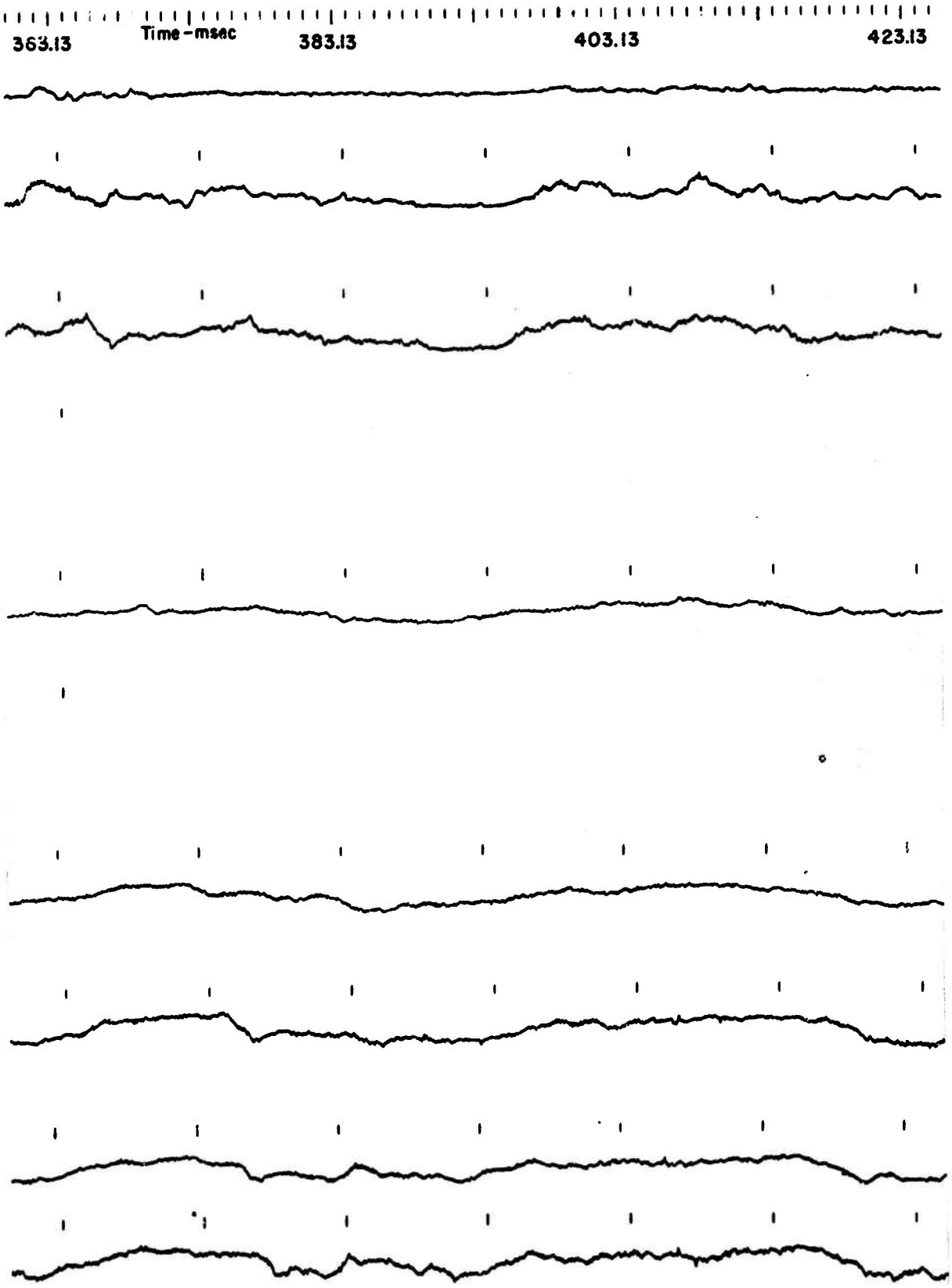

Fig.

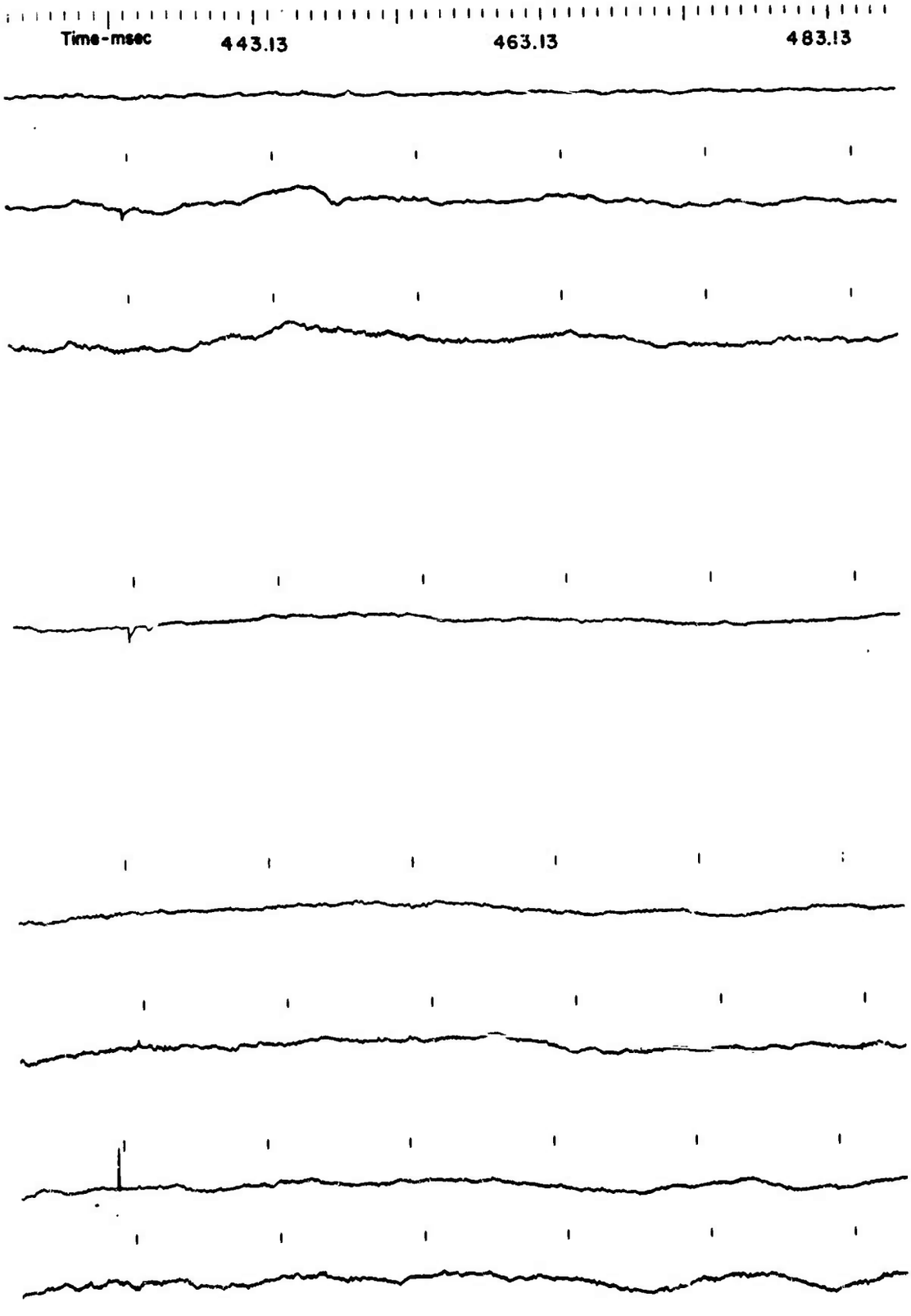

ıre A27- Pressure Histories - 1600-Ft Range from Burst at 100-Ft Depth (Station 5, Test 5)

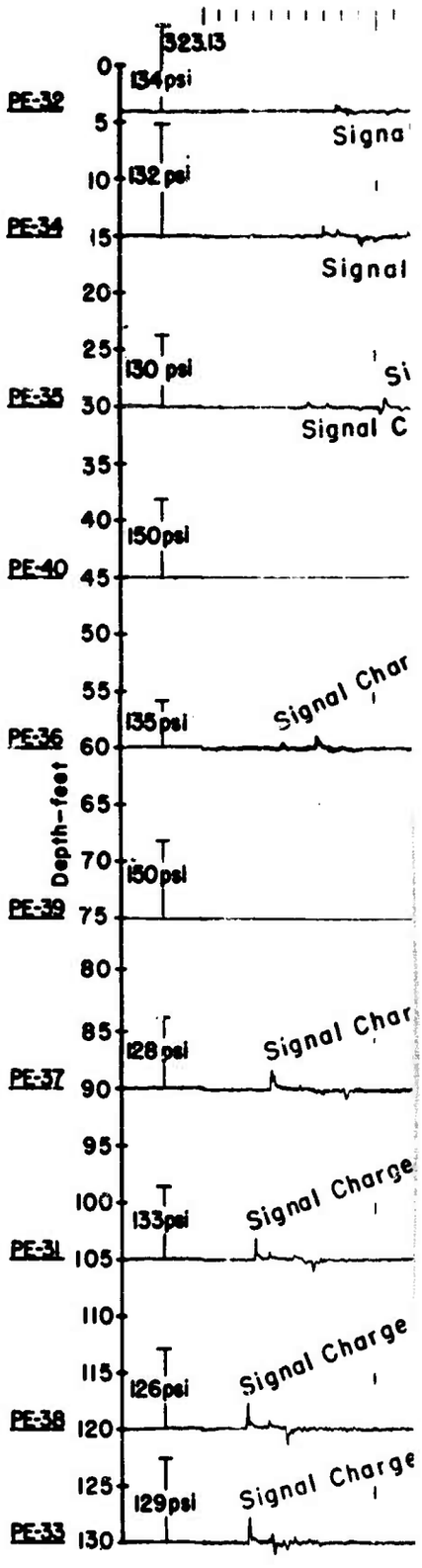
323.13
0
134psi
PE-32
5
Signa
10
132 psi
PE-34
15
Signal
20
25
130 psi
Si
PE-35
30
Signal C
35
40
150psi
PE-40
45
50
55
135psi
Signal Char
PE-36
60
Depth-feet
65
70
150psi
PE-39
75
80
85
128 psi
Signal Char
PE-37
90
95
100
133psi
Signal Charge
PE-31
105
110
115
126psi
Signal Charge
PE-38
120
125
129psi
Signal Charge
PE-33
130

A

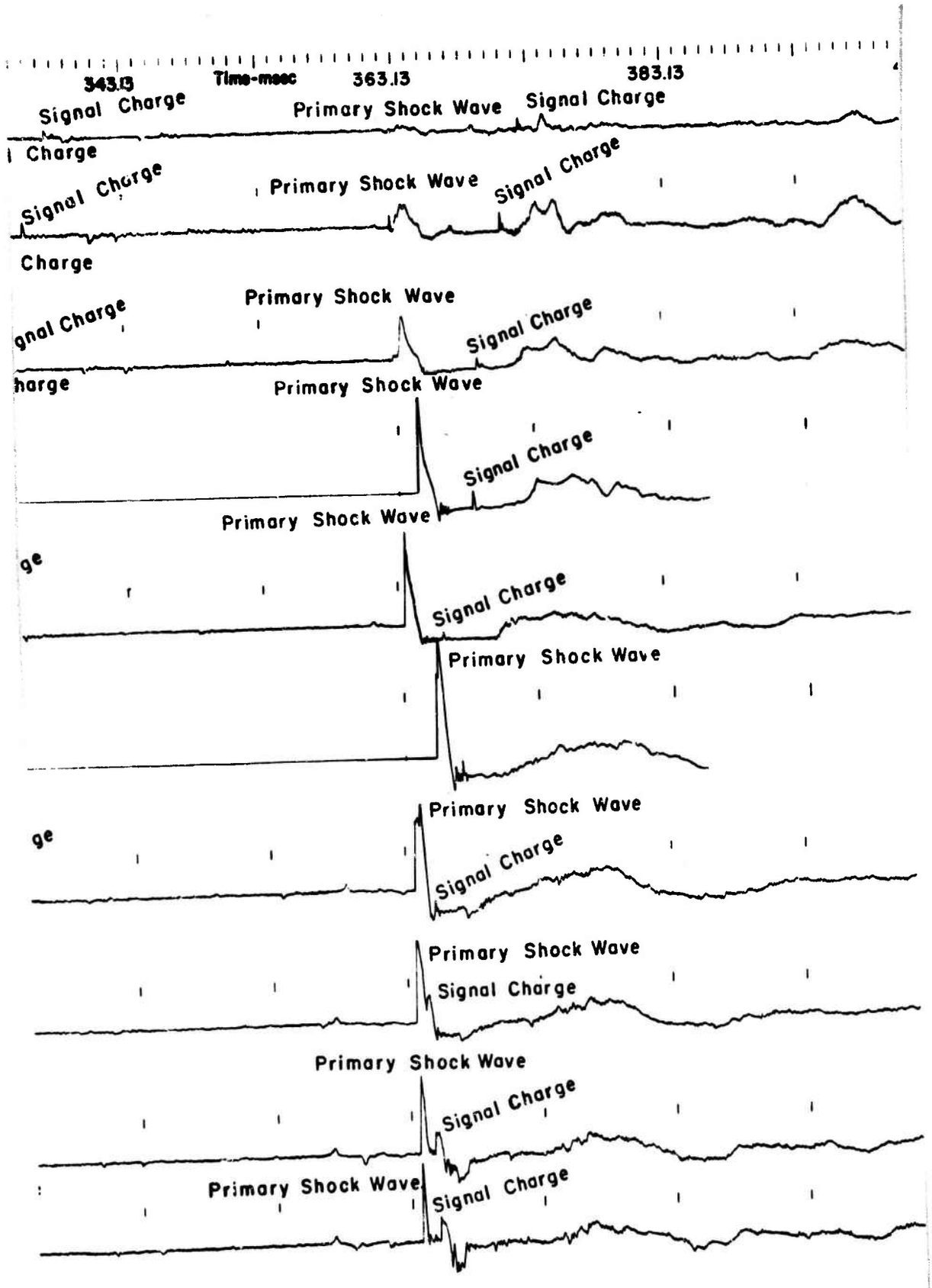
343.13
Time-msec
363.13
383.13
Signal Charge
Primary Shock Wave
Signal Charge
Charge
Signal Charge
Primary Shock Wave
Signal Charge
Charge
gnal Charge
Primary Shock Wave
Signal Charge
harge
Primary Shock Wave
Signal Charge
Primary Shock Wave
ge
Signal Charge
Primary Shock Wave
Primary Shock Wave
ge
Signal Charge
Primary Shock Wave
Signal Charge
Primary Shock Wave
Signal Charge
Primary Shock Wave
Signal Charge

B

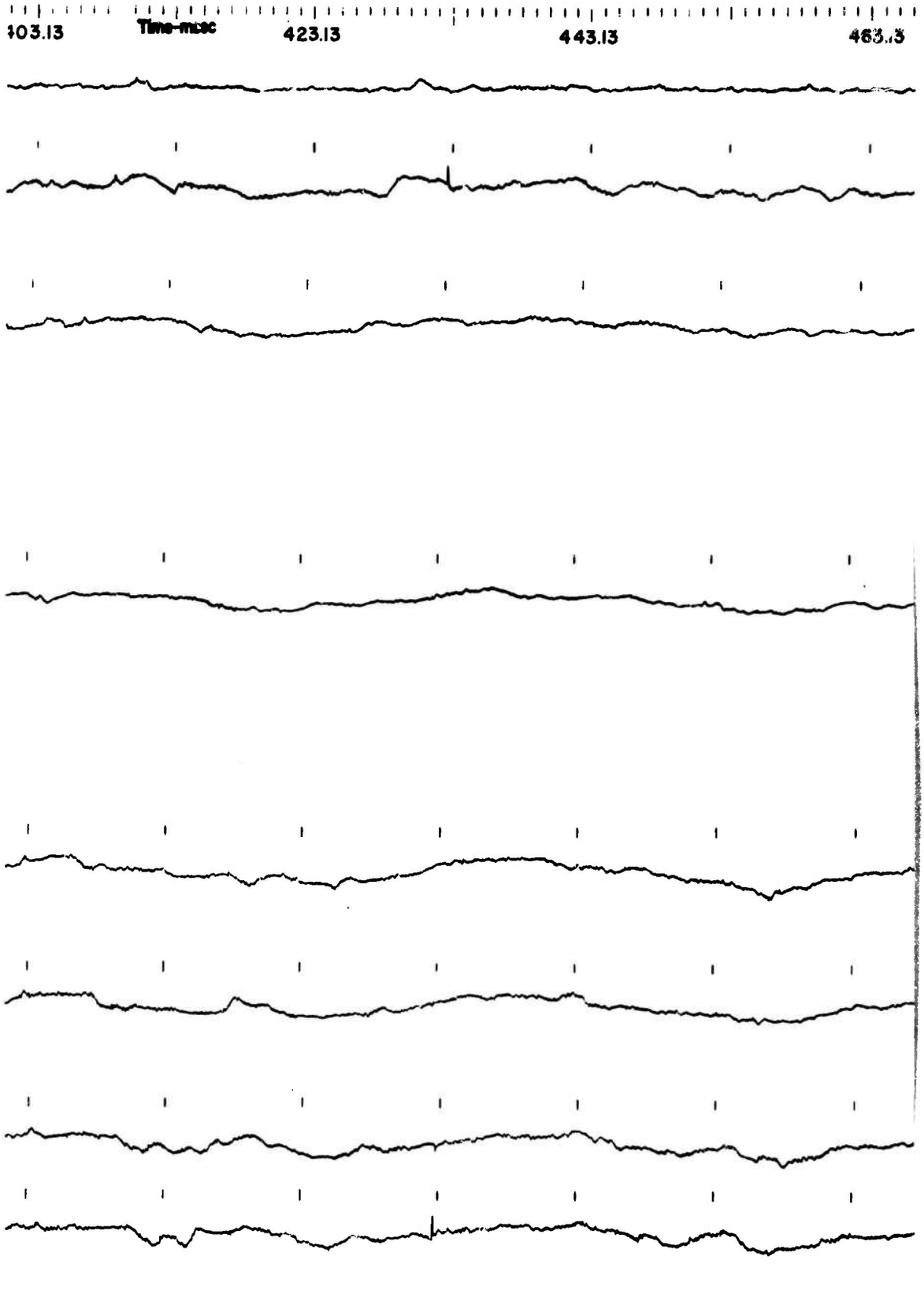

Figu

C

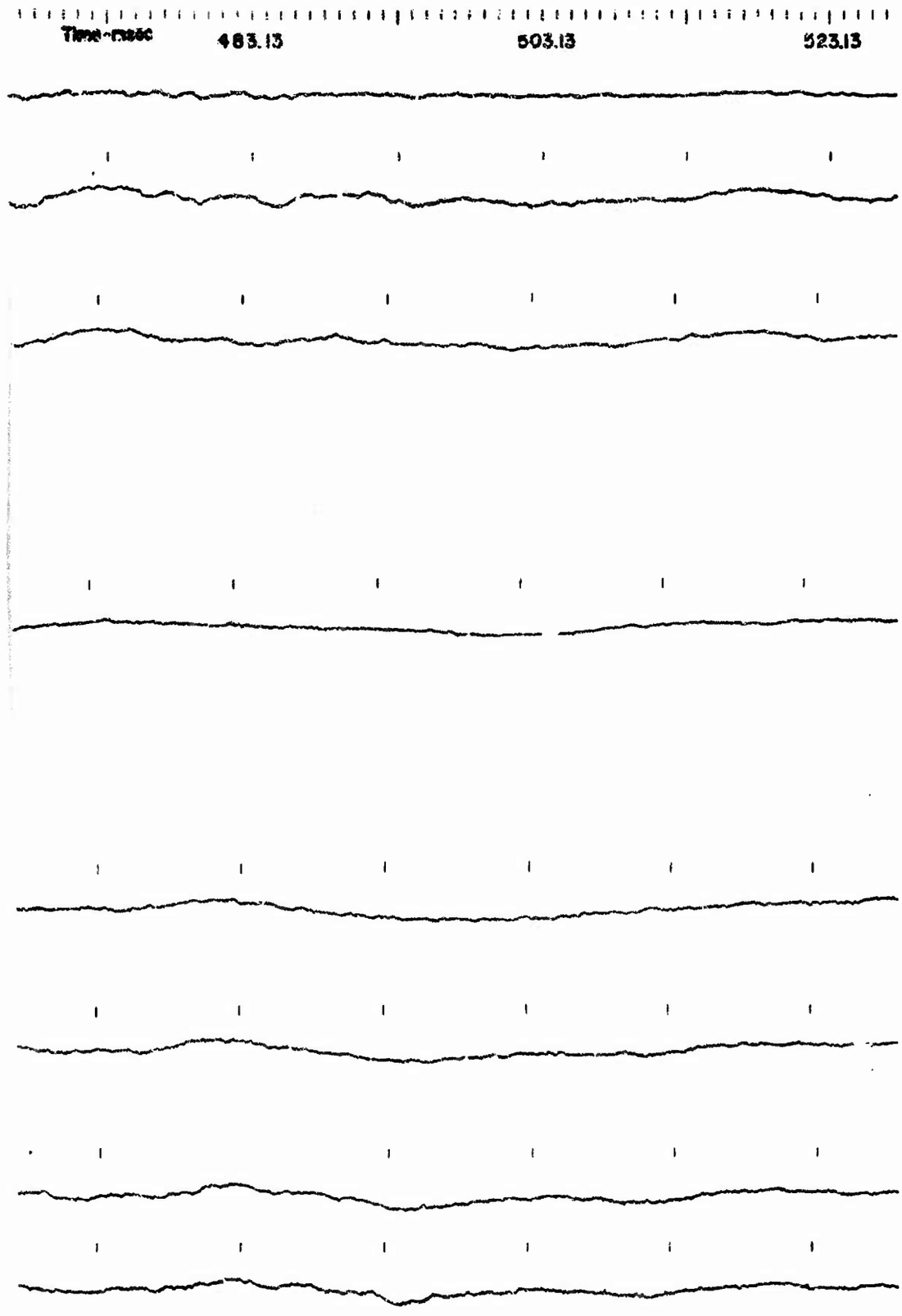

e A28 - Pressure Histories - 1860-Ft Range from Burst at 100-Ft Depth (Station 7, Test 5)

D

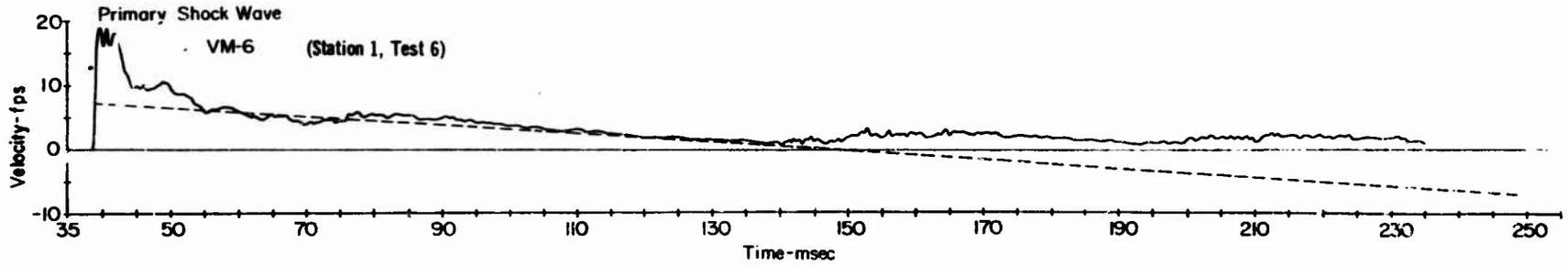

Figure A29 - Velocity Histories - 200-Ft Range from Burst at 50-Ft Depth

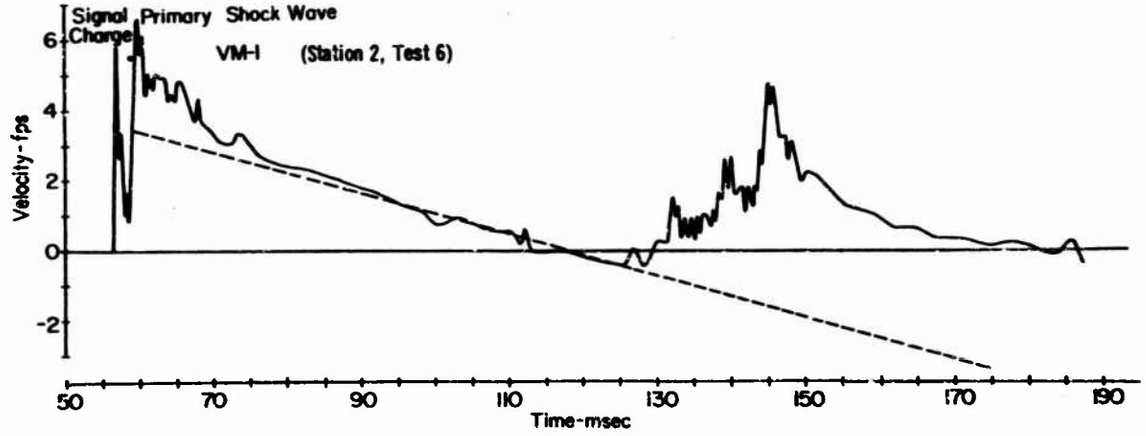

Figure A30 - Velocity Histories - 300-Ft Range from Burst at 50-Depth

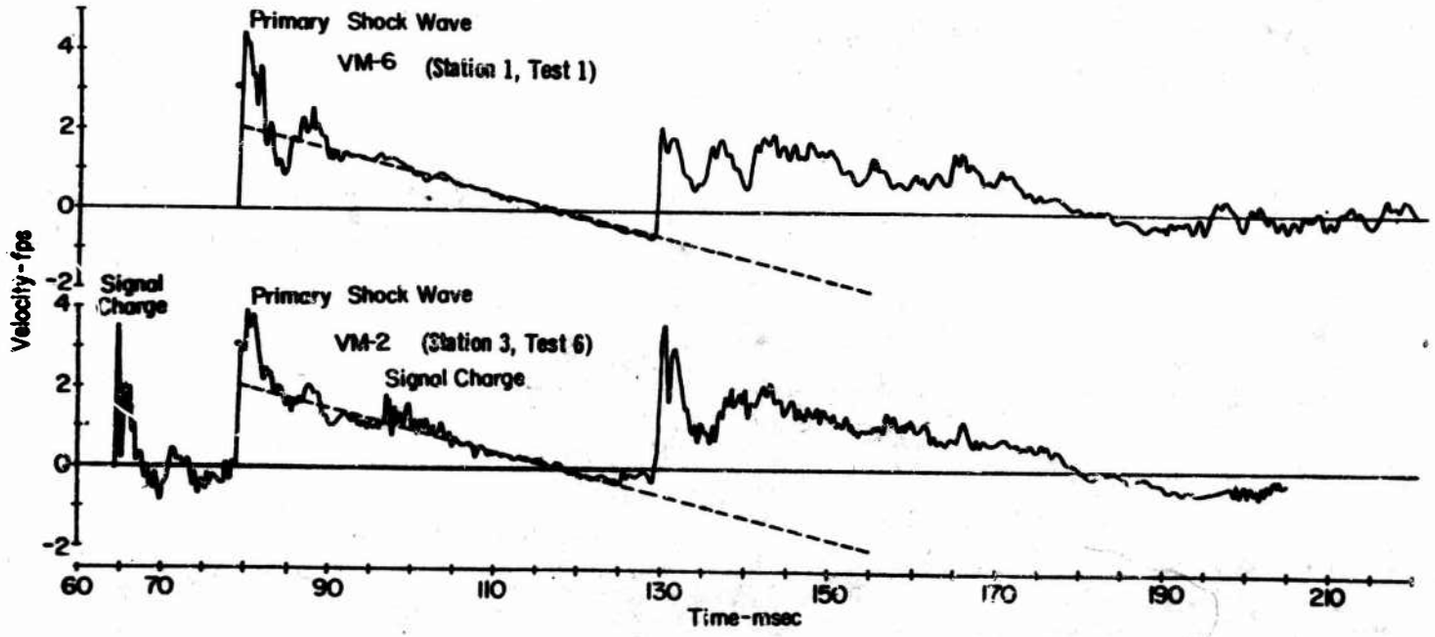

Figure A31 - Velocity Histories - 400-Ft Range from Burst at 50-Ft Depth

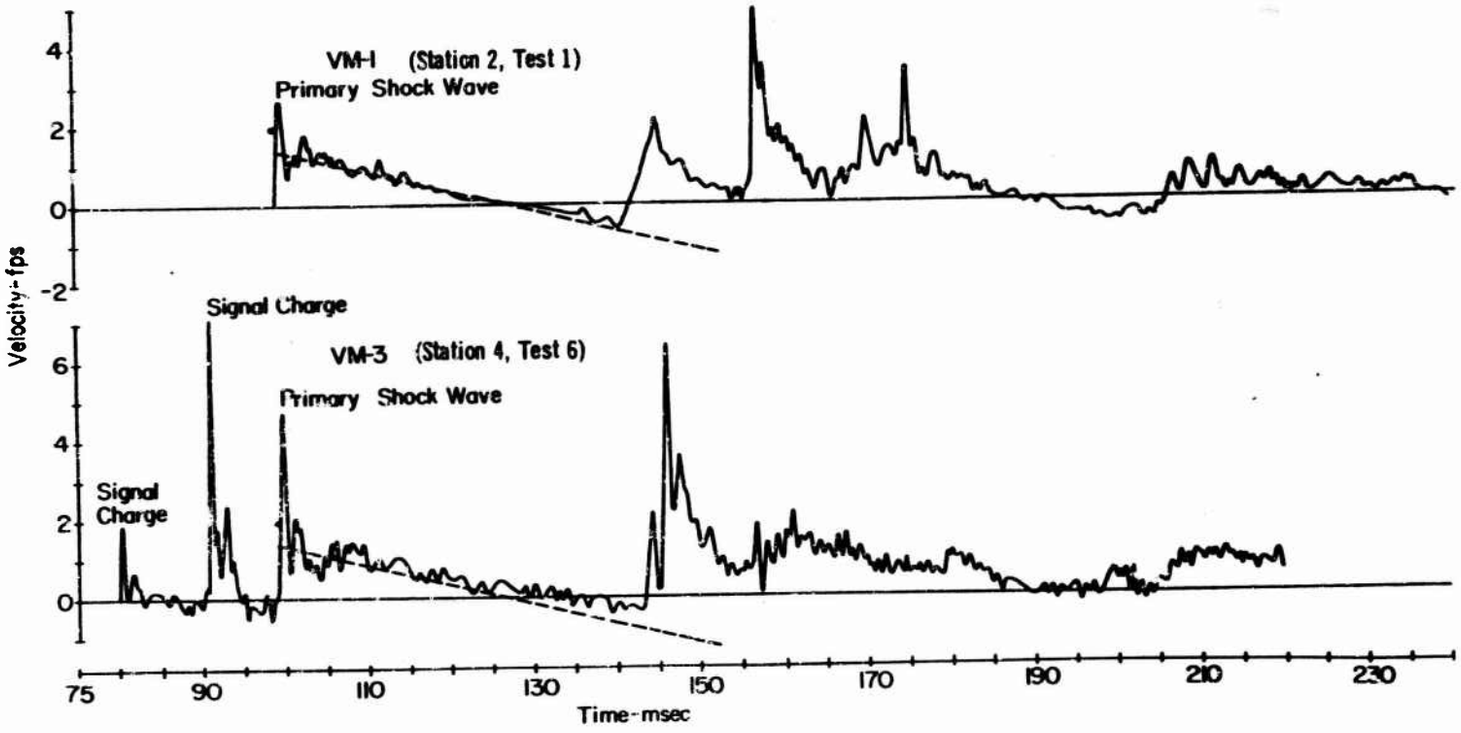

Figure A32 - Velocity Histories - 500-Ft Range from Burst at 50-Ft Depth

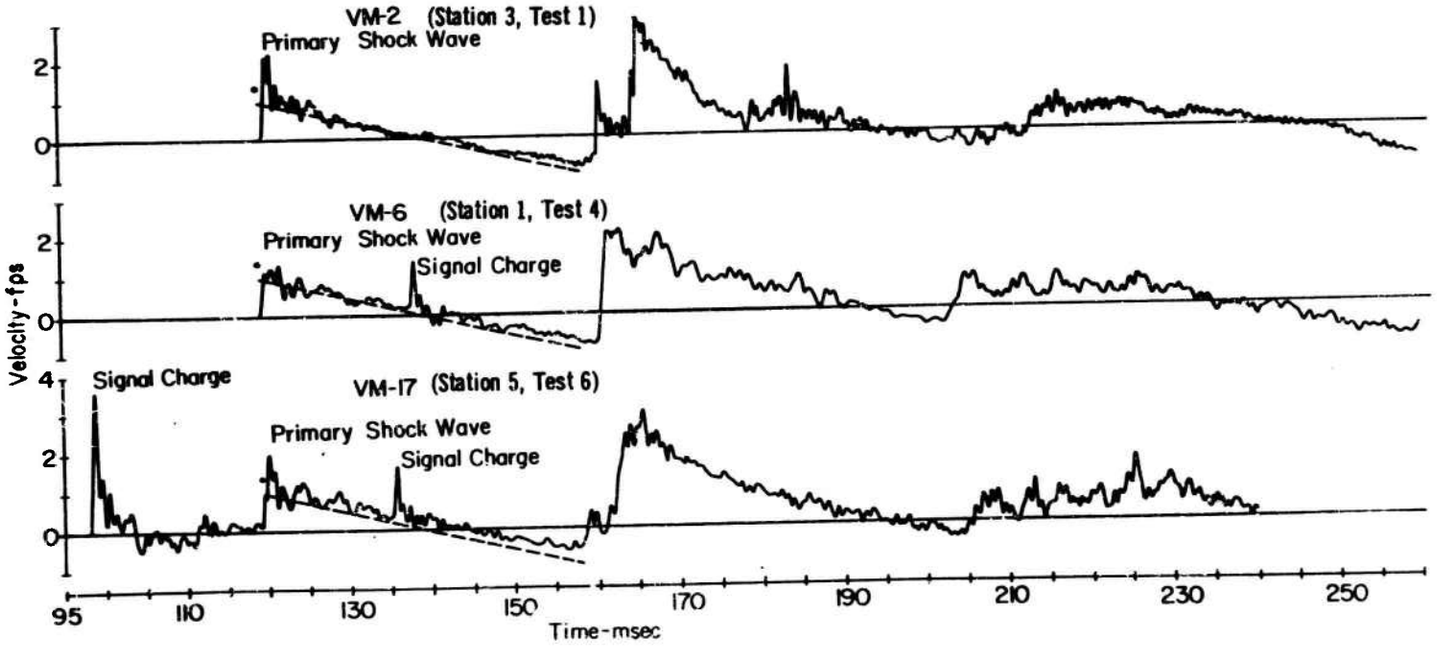

Figure A33 - Velocity Histories - 600-Ft Range from Burst at 50-Ft Depth

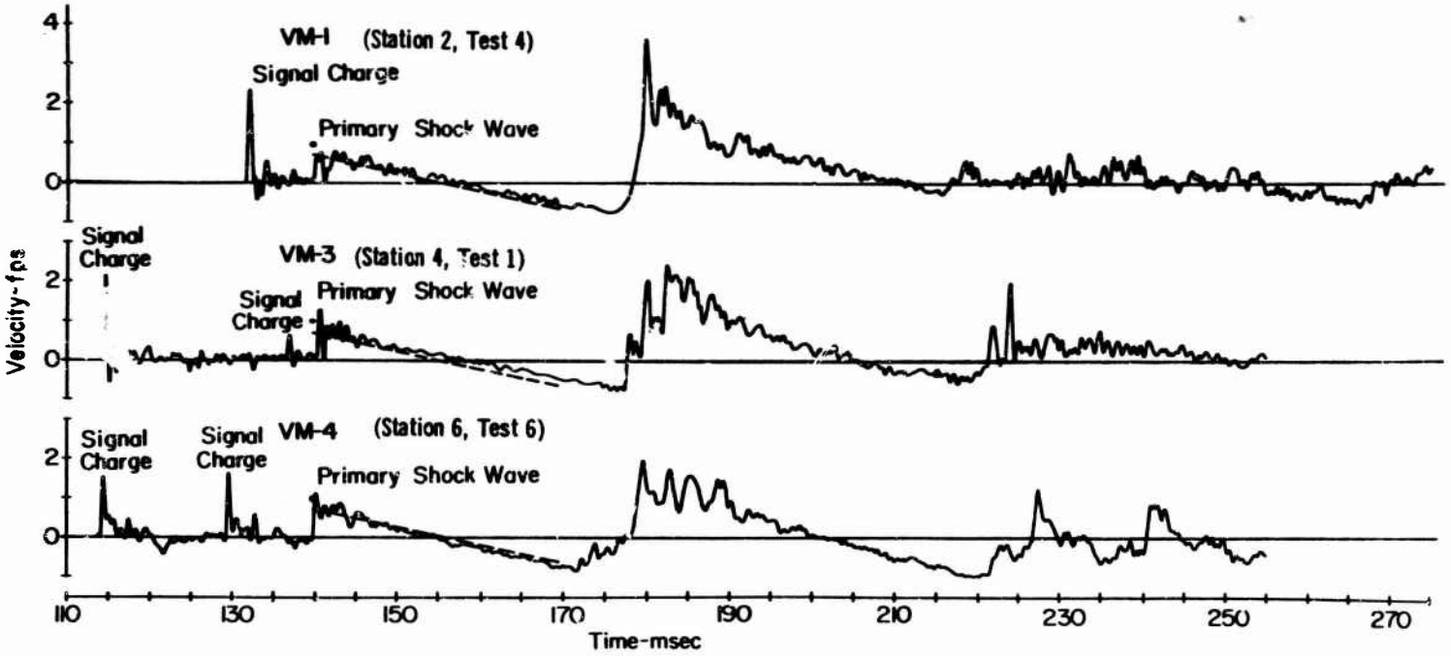

Figure A34 - Velocity Histories - 700- Ft Range from Burst at 50-Ft Depth

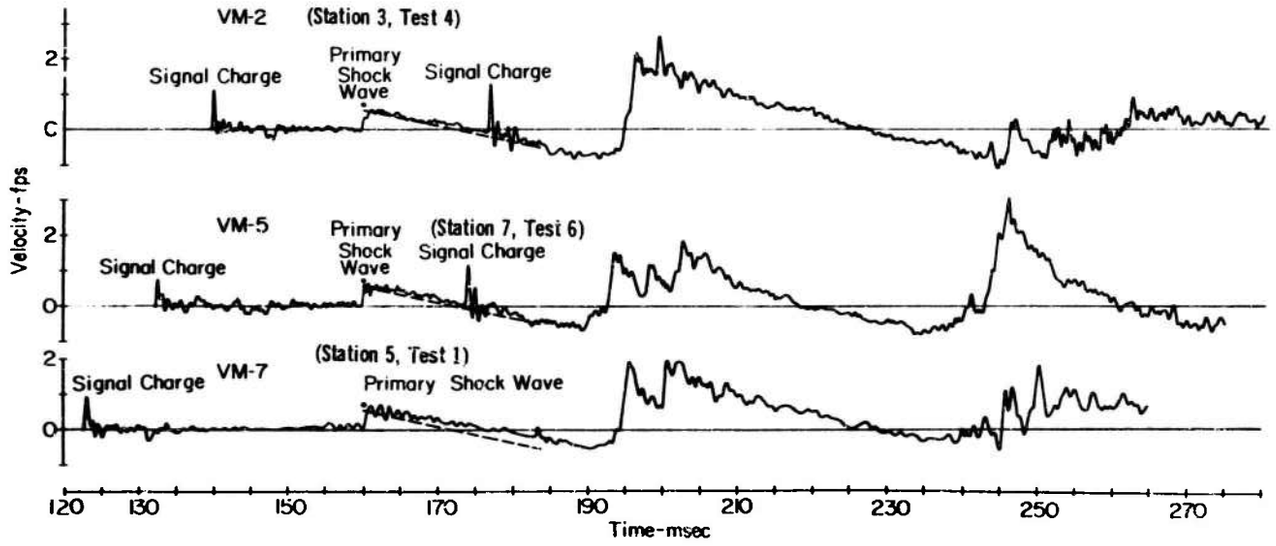

Figure A35 - Velocity Histories - 800-Ft Range from Burst at 50-Ft Depth

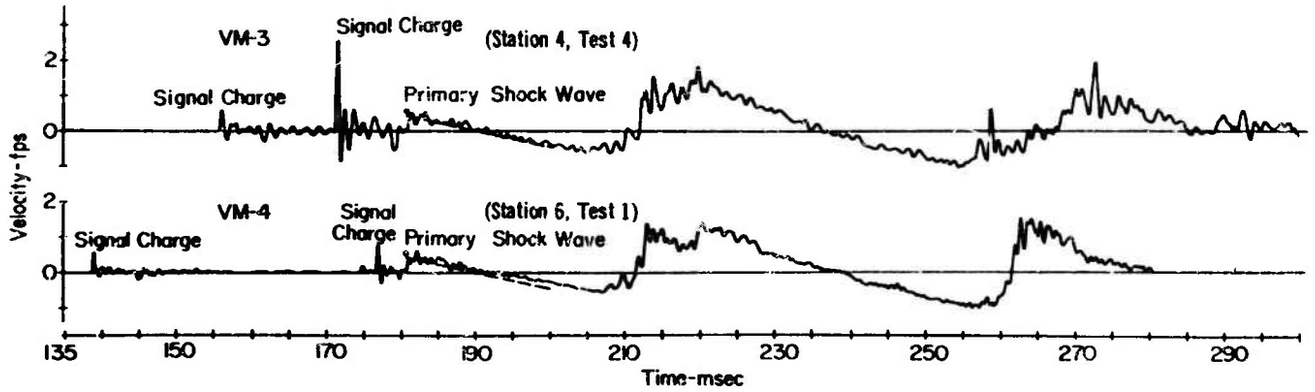

Figure A36 - Velocity Histories - 900-Ft Range from Burst at 50-Ft Depth

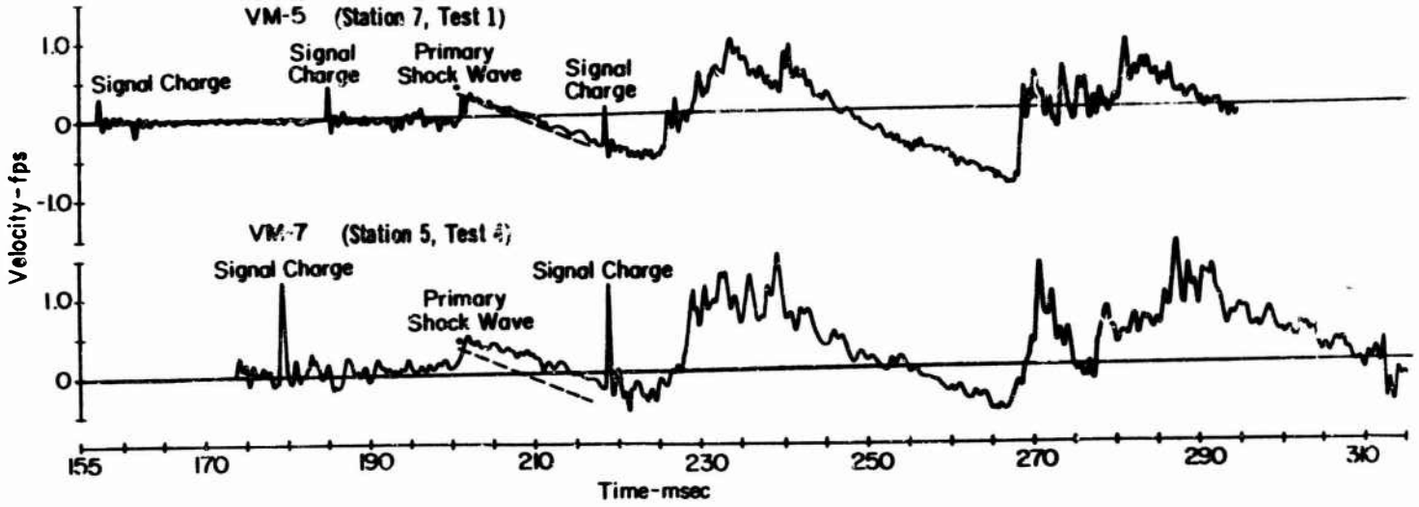

Figure A37 - Velocity Histories - 1000-Ft Range from Burst at 50-Ft Depth

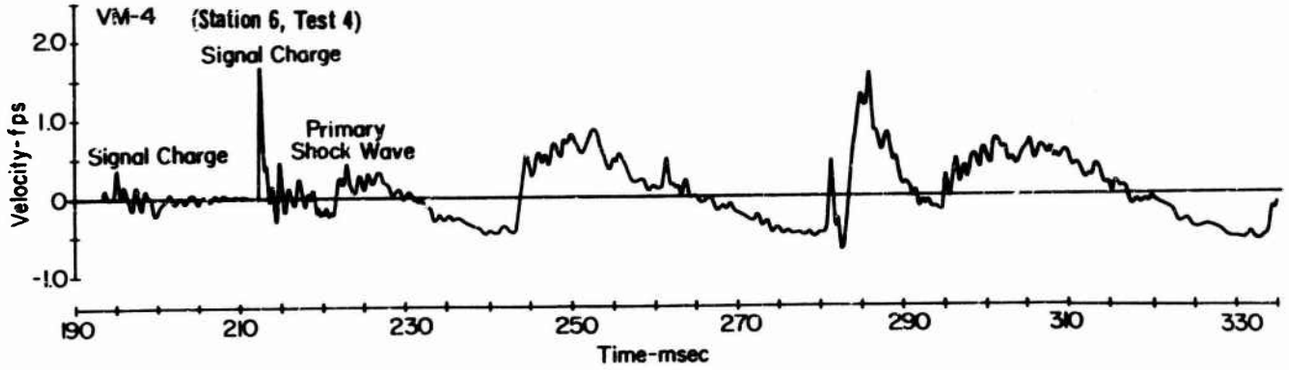

Figure A38 - Velocity History - 1100-Ft Range from Burst at 50-Ft Depth

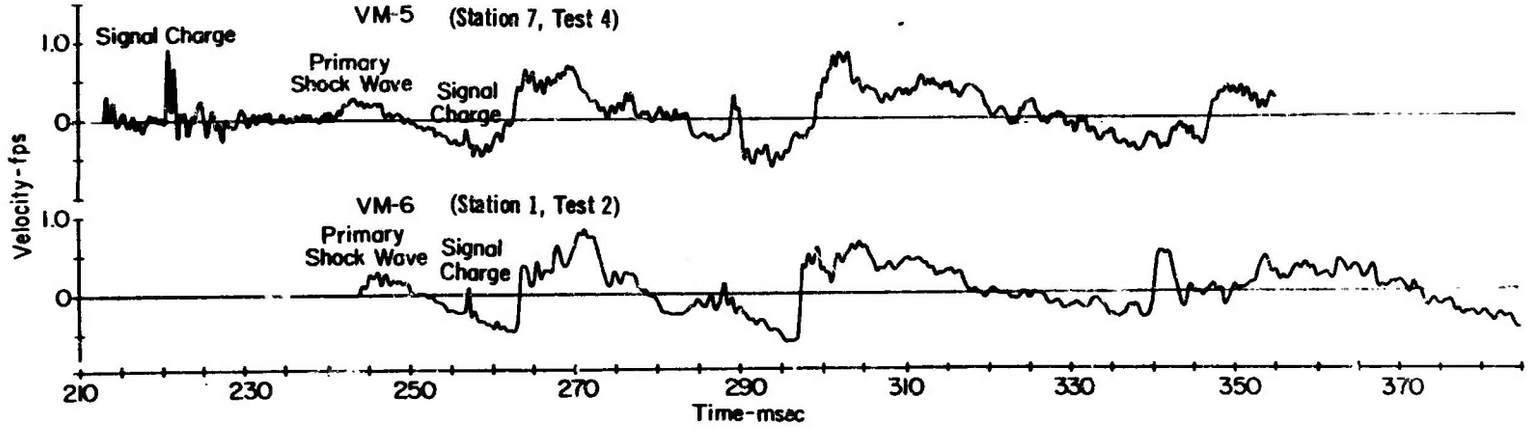

Figure A39 - Velocity Histories - 1200-Ft Range from Burst at 50-Ft Depth

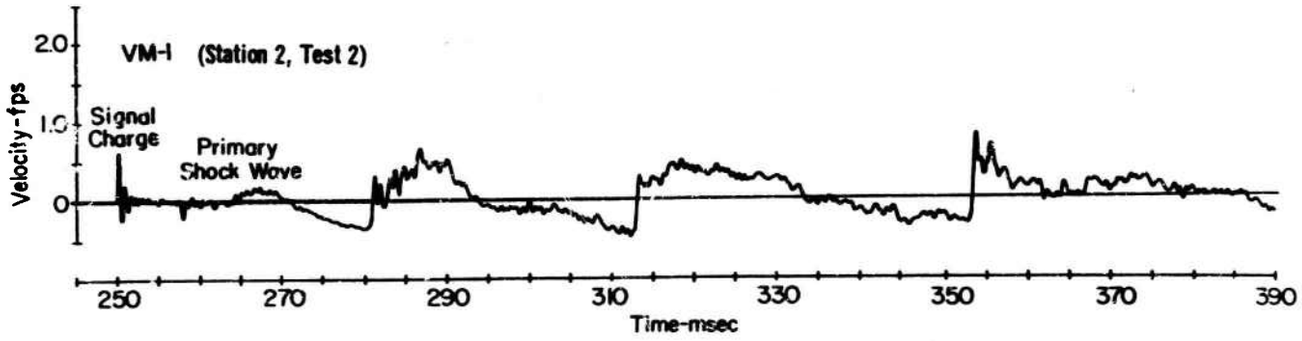

Figure A40 - Velocity History - 1300-Ft Range from Burst at 50-Ft Depth

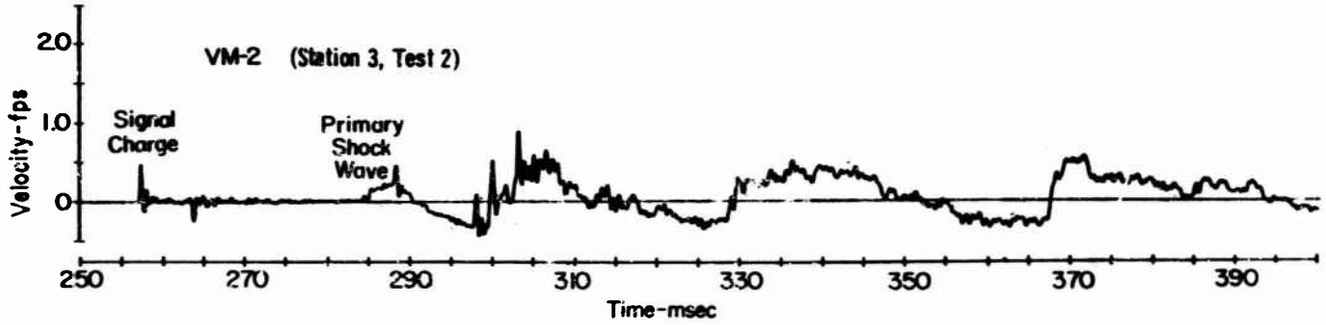

Figure A41 - Velocity History - 1400-Ft Range from Burst at 50-Ft Depth

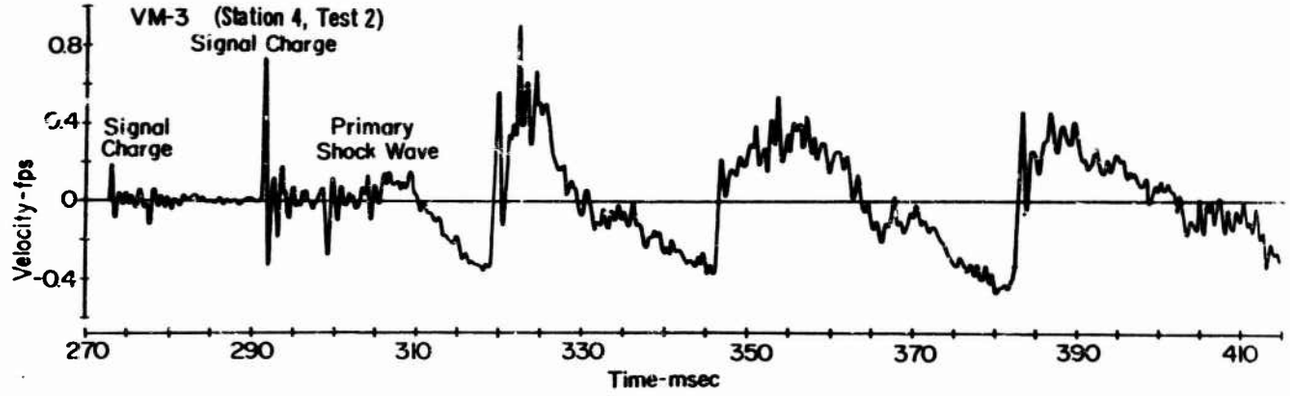

Figure A42 - Velocity History - 1500-Ft Range from Burst at 50-Ft Depth

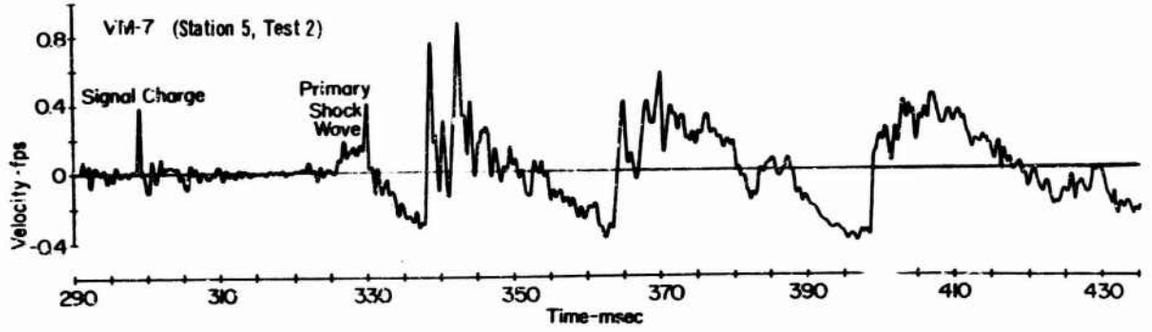

Figure A43 - Velocity History - 1600-Ft Range from Burst at 50-Ft Depth

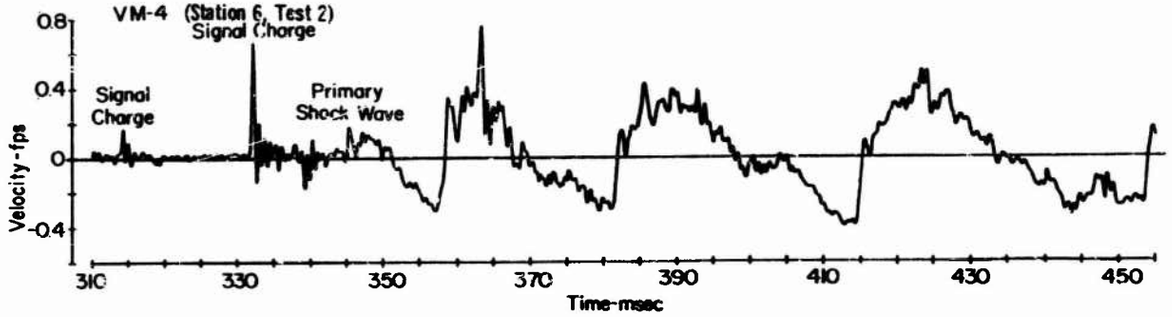

Figure A44 - Velocity History - 1700-Ft Range from Burst at 50-Ft Depth

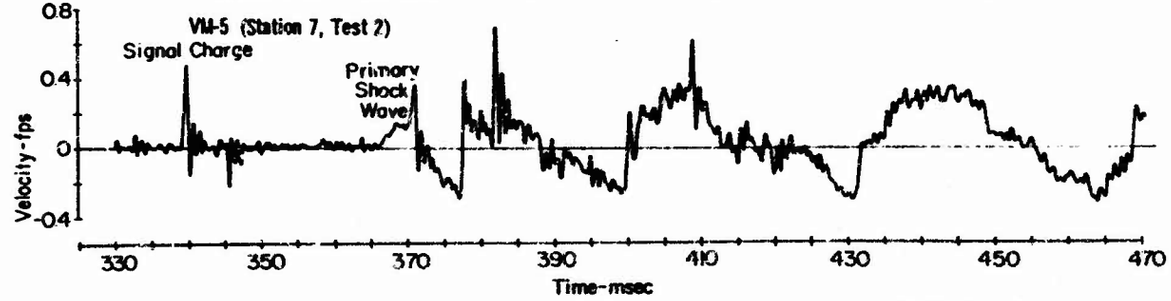

Figure A45 - Velocity History - 1800-Ft Range from Burst at 50-Ft Depth

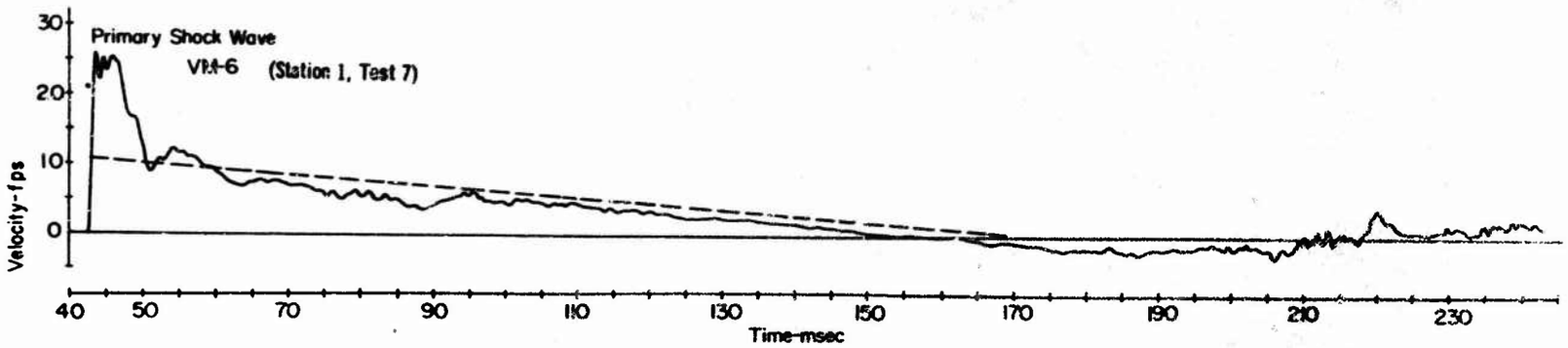

Figure A46 - Velocity Histories - 200-Ft Range from Burst at 100-Ft Depth

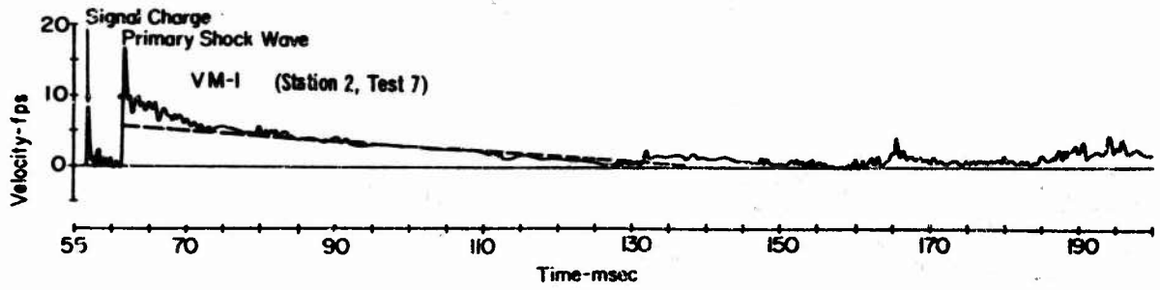

Figure A47 - Velocity Histories - 300-Ft Range from Burst at 100-Ft Depth

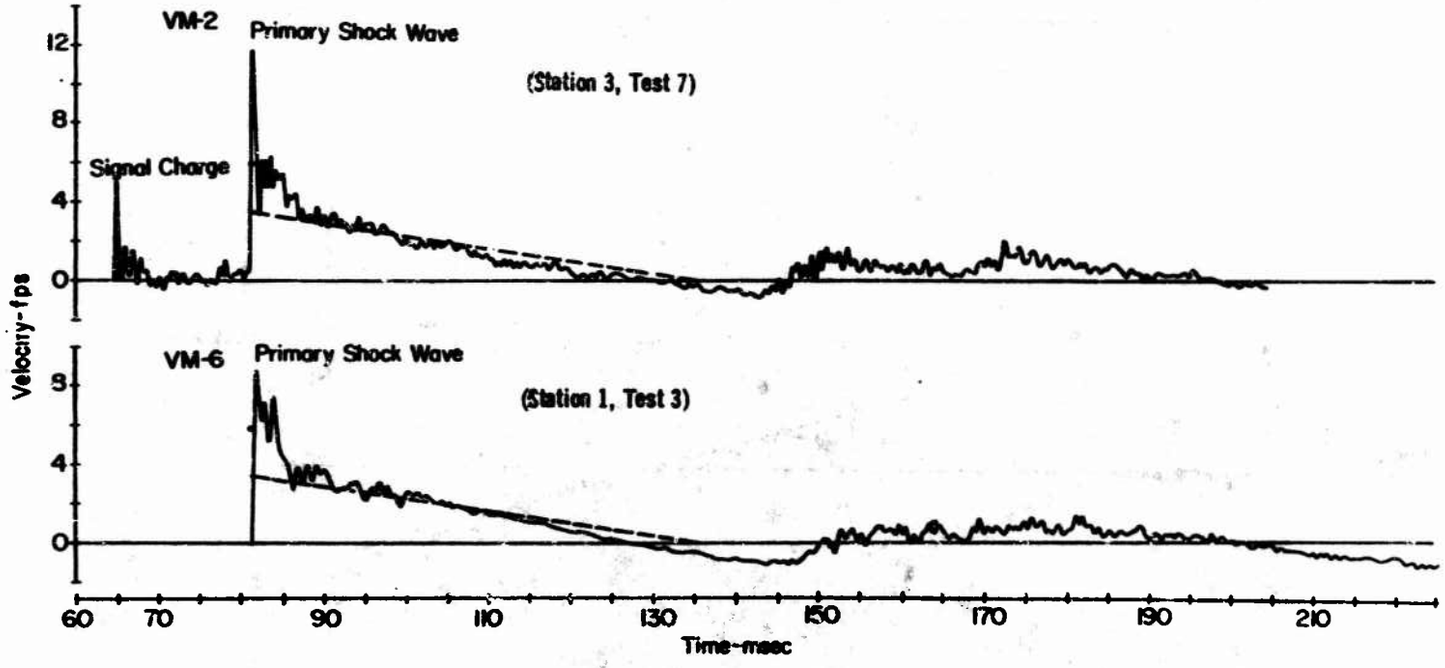

Figure A48 - Velocity Histories - 400-Ft Range from Burst at 100-Ft Depth

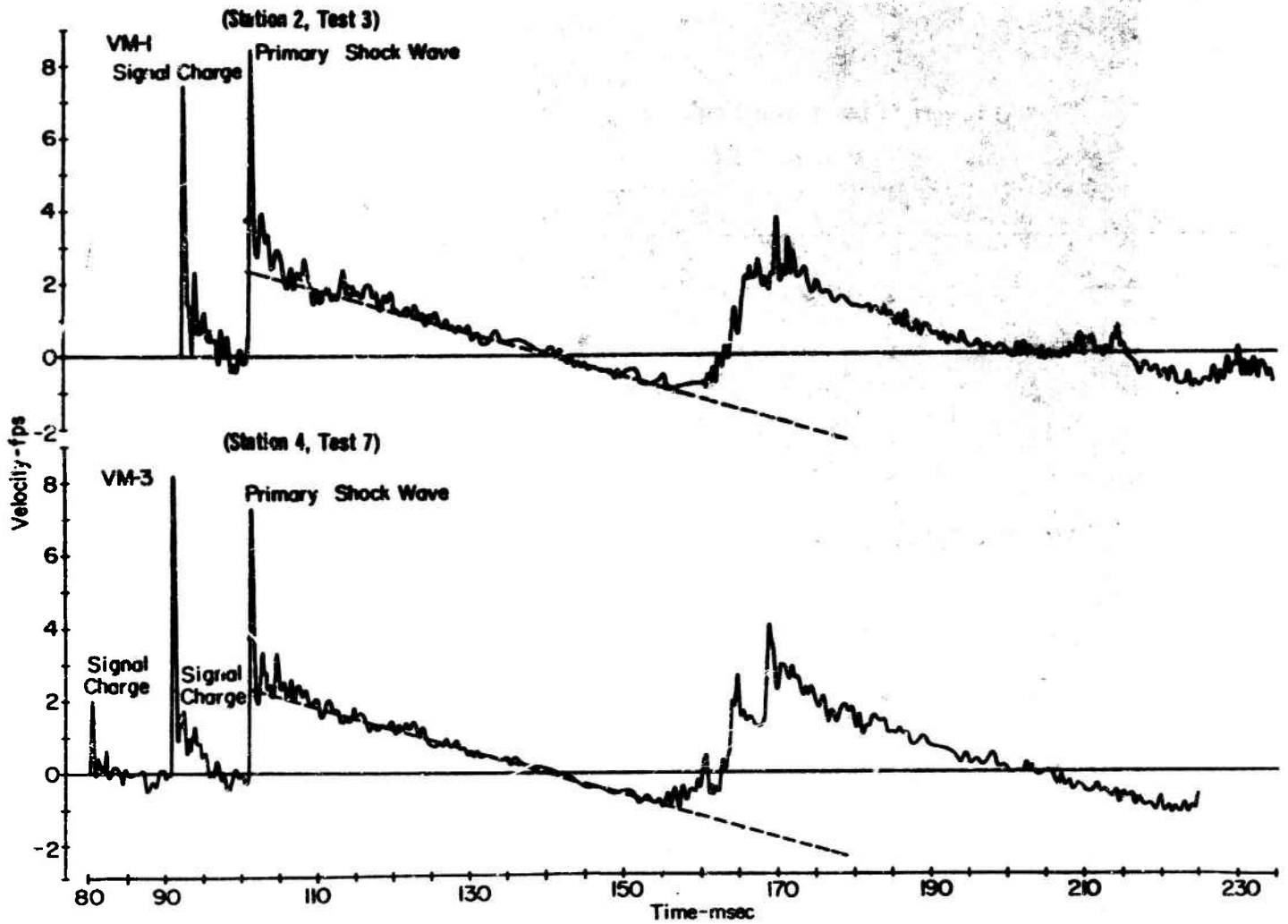

Figure A49 - Velocity Histories - 500-Ft Range from Burst at 100-Ft Depth

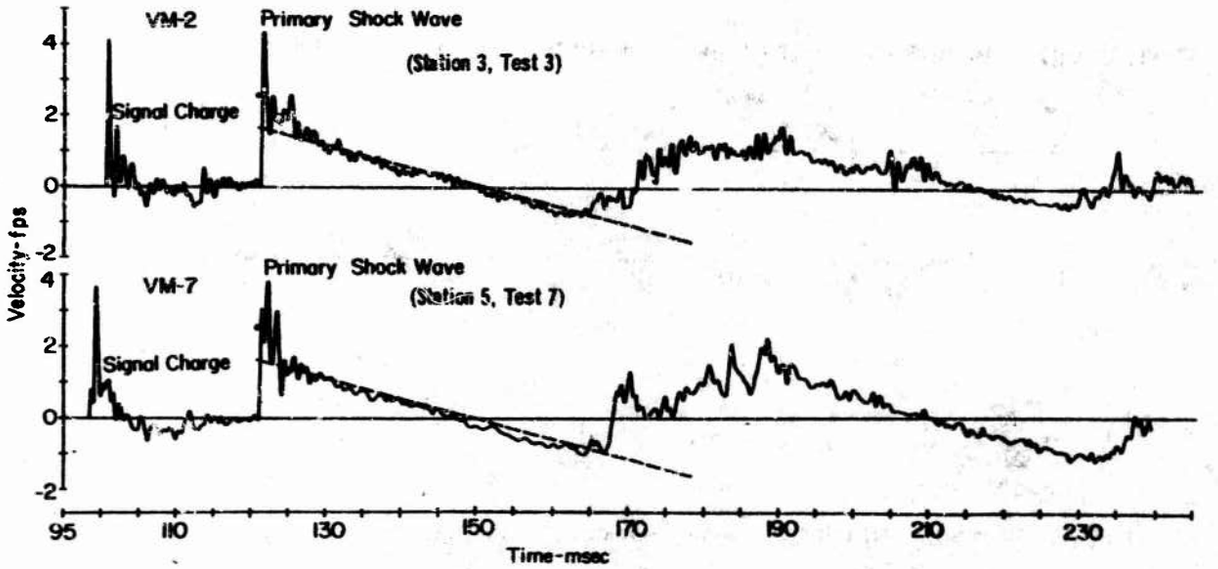

Figure A50 - Velocity Histories - 600-Ft Range from Burst at 100-Ft Depth

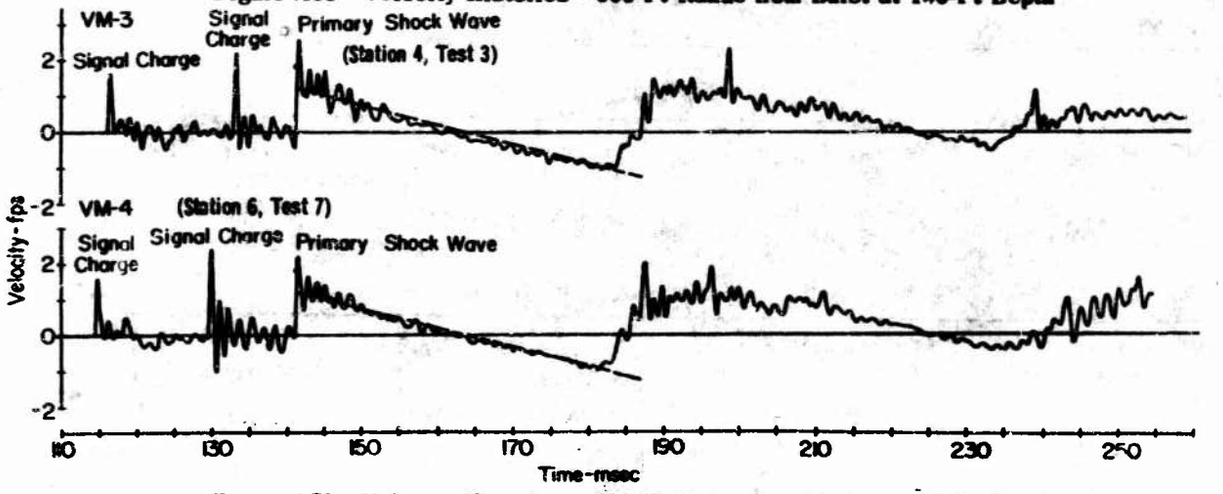

Figure A51 - Velocity Histories - 700-Ft Range from Burst at 100-Ft Depth

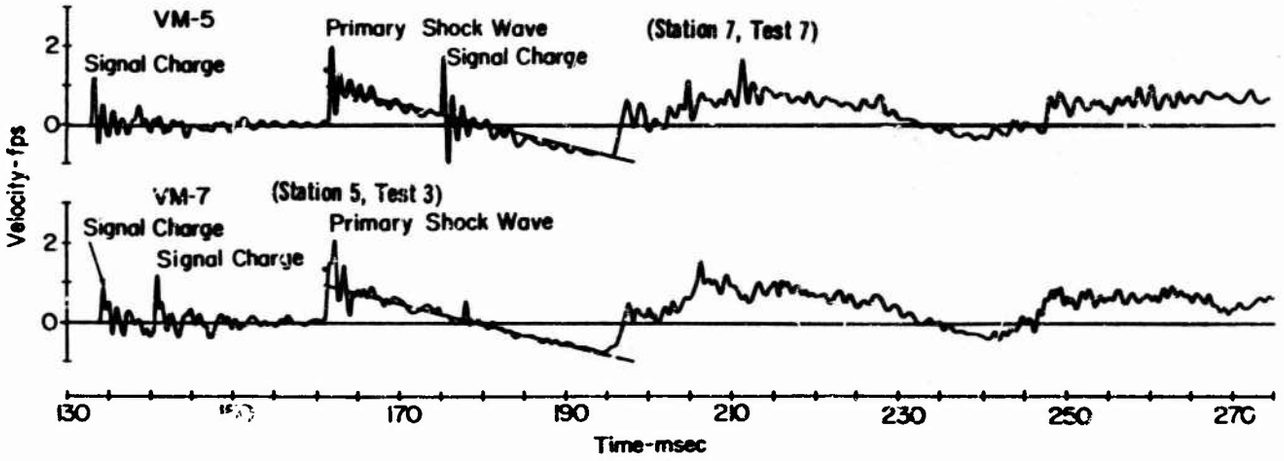

Figure A52 - Velocity Histories - 800-Ft Range from Burst at 100-Ft Depth

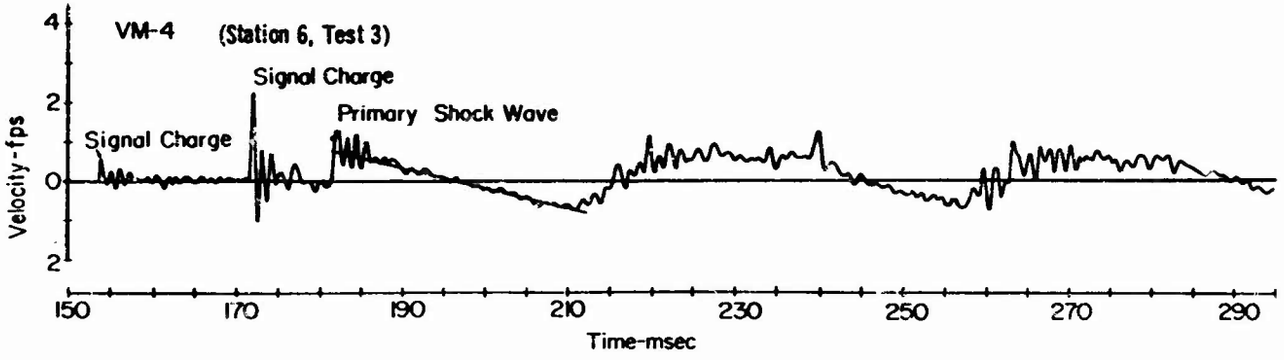

Figure A53 - Velocity Histories - 900-Ft Range from Burst at 100-Ft Depth

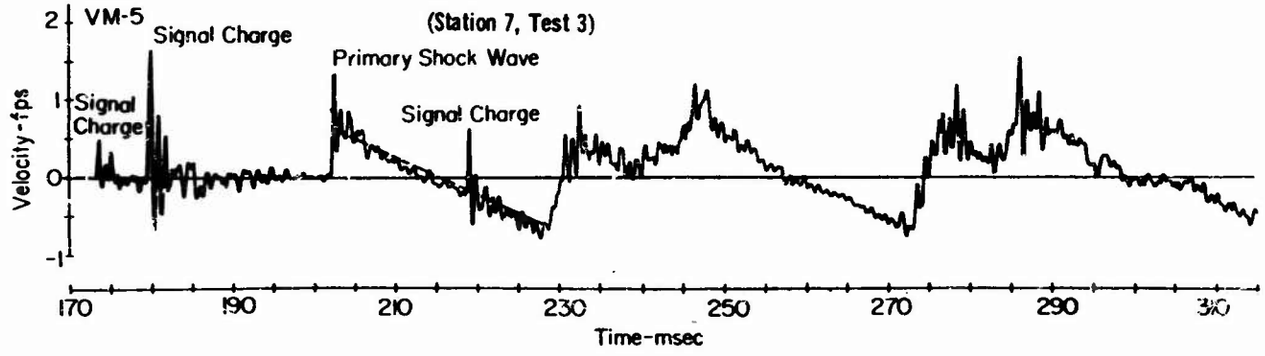

Figure A54 - Velocity Histories - 1000-Ft Range from Burst at 100-Ft Depth

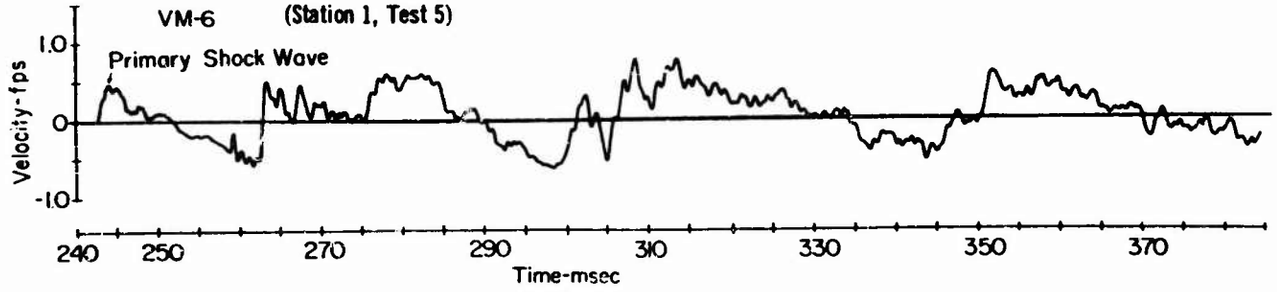

Figure A55 - Velocity History - 1200-Ft Range from Burst at 100-Ft Depth

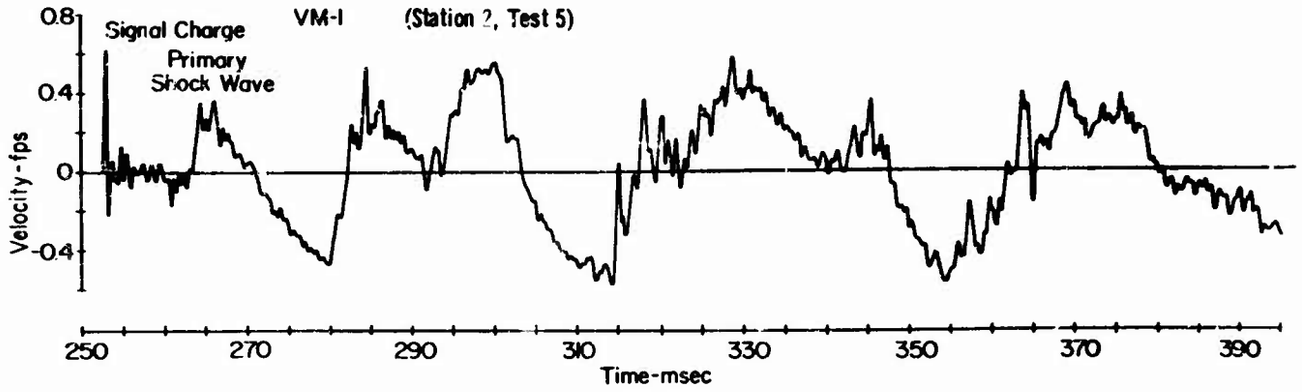

Figure A56 - Velocity History - 1300-Ft Range from Burst at 100-Ft Depth

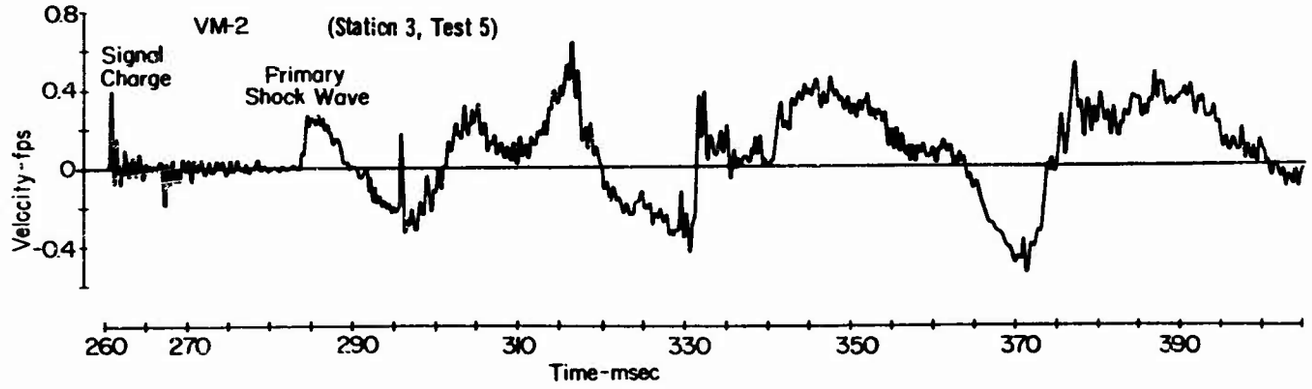

Figure A57 - Velocity History - 1400-Ft Range from Burst at 100-Ft Depth

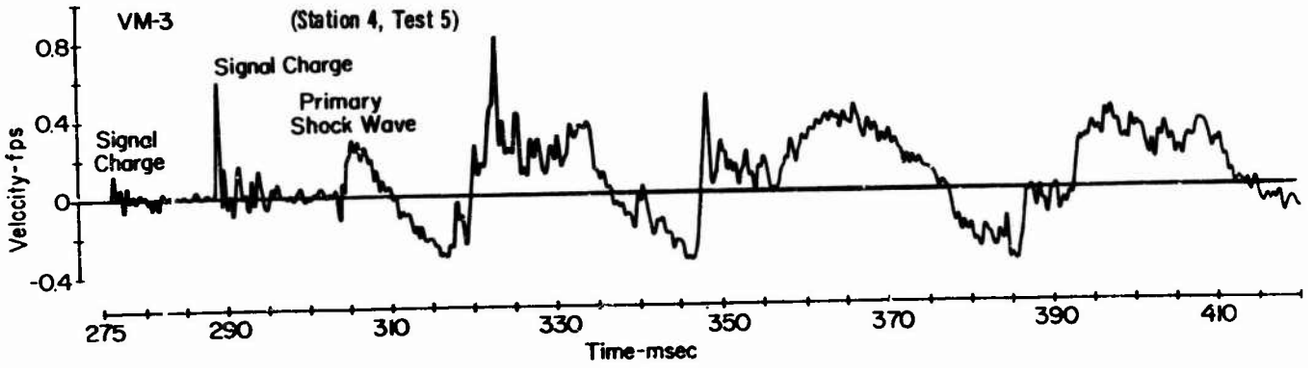

Figure A58 - Velocity History - 1500-Ft Range from Burst at 100-Ft Depth

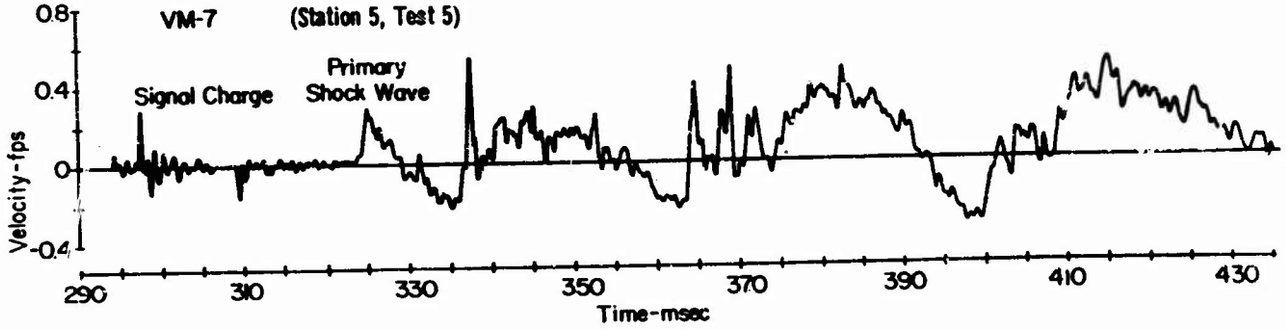

Figure A59 - Velocity History - 1600-Ft Range from Burst at 100-Ft Depth

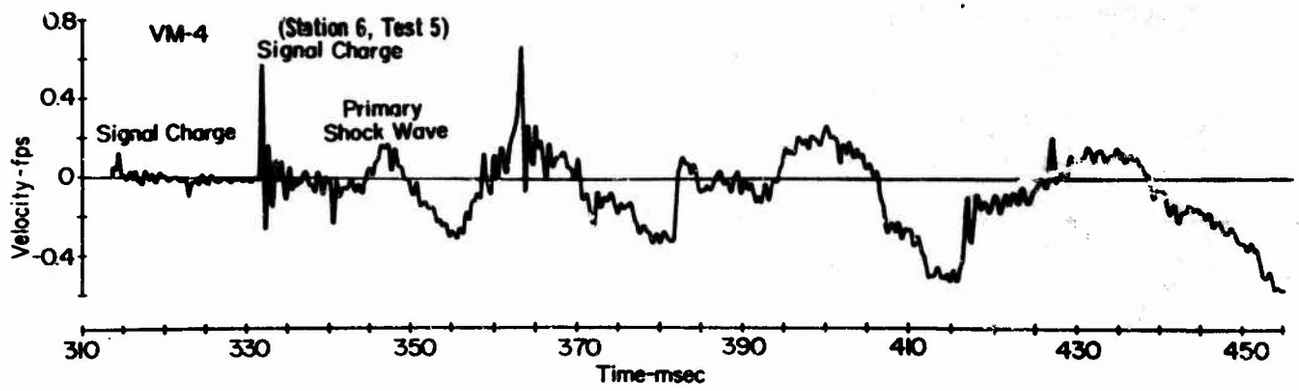

Figure A60 - Velocity History - 1700-Ft Range from Burst at 100-Ft Depth

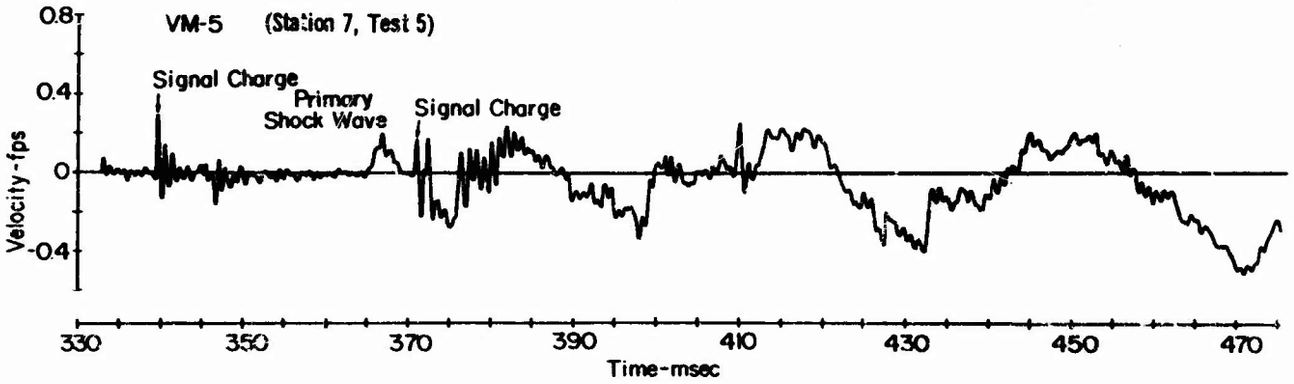

Figure A61 - Velocity History - 1800-Ft Range from Burst at 100-Ft Depth

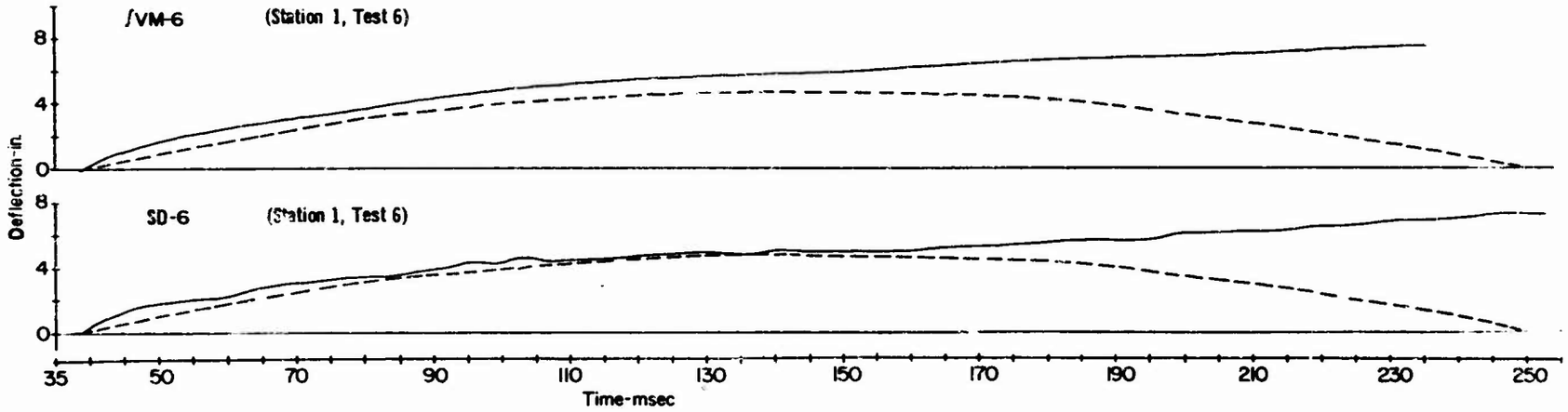

Figure A62 - Displacement Histories - 200-Ft Range from Burst at 50-Ft Depth

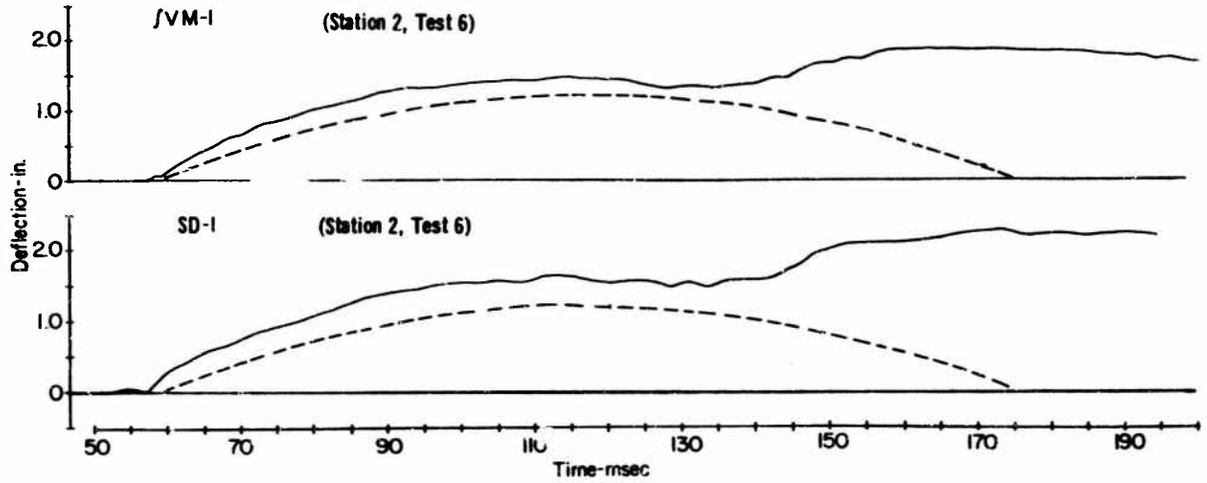

Figure A63 - Displacement Histories - 300-Ft Range from Burst at 50-Ft Depth

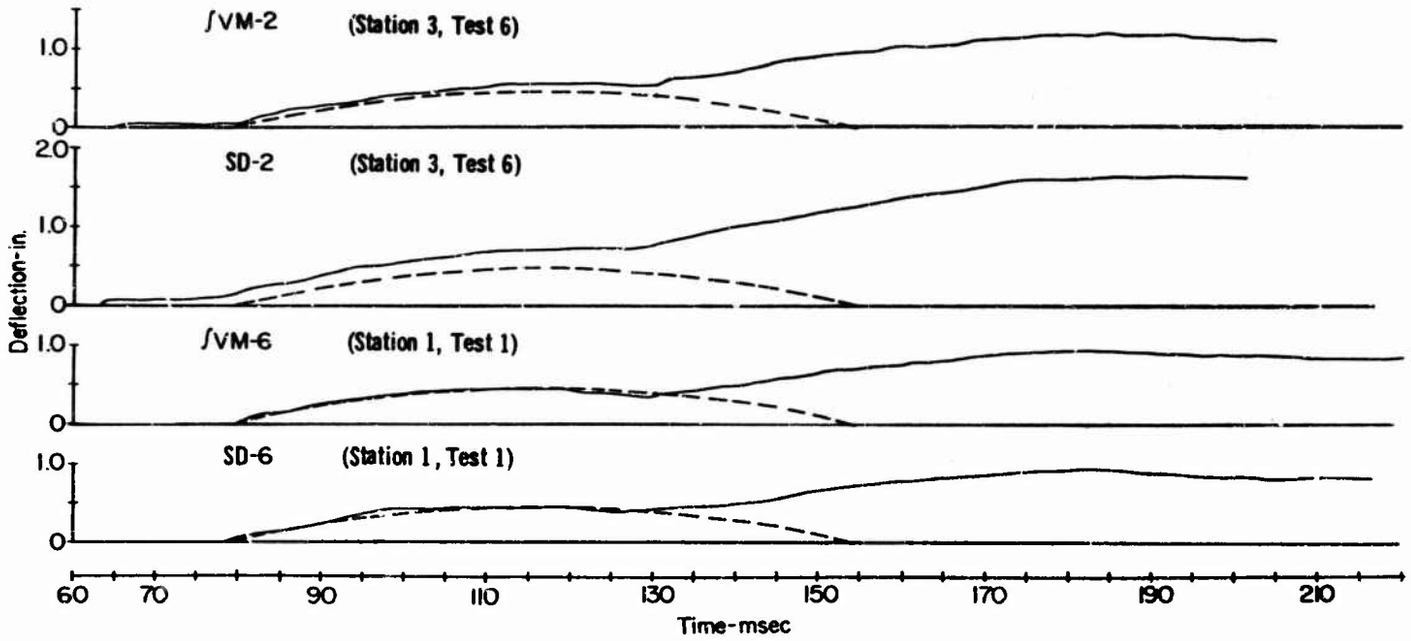

Figure A64 - Displacement Histories - 400-Ft Range from Burst at 50-Ft Depth

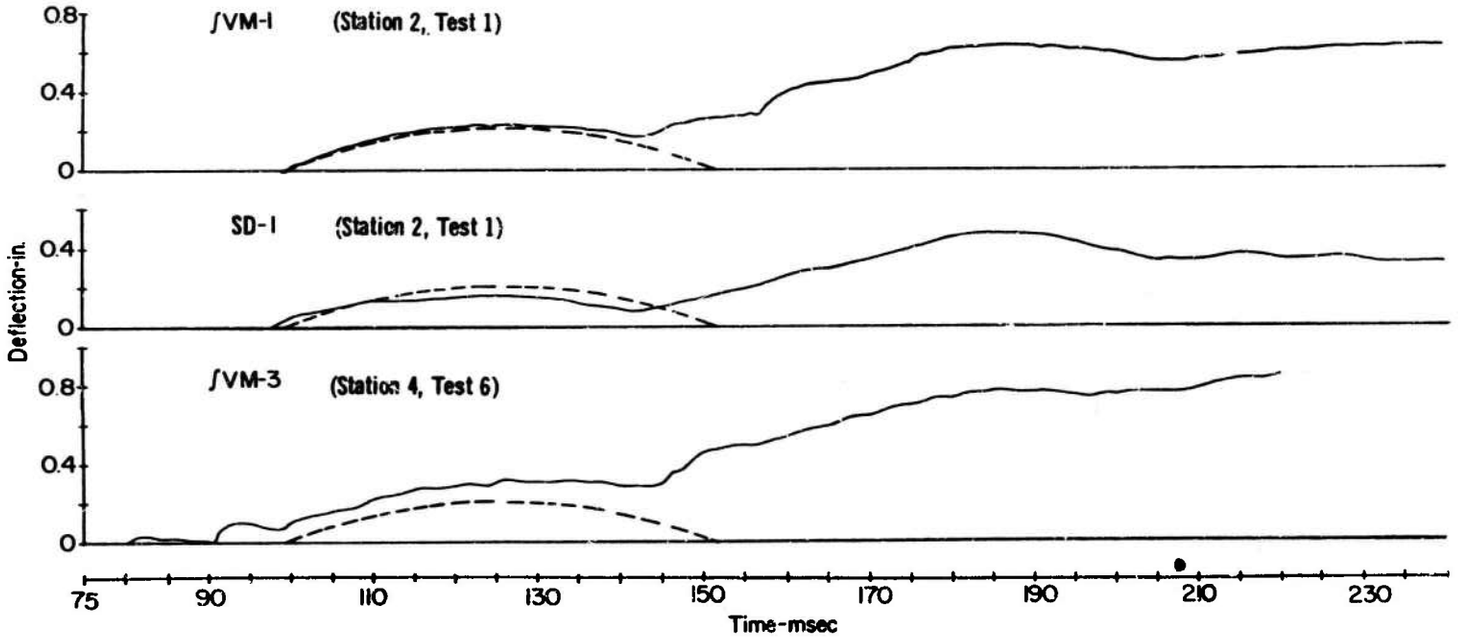

Figure A65 - Displacement Histories - 500-Ft Range from Burst at 50-Ft Depth

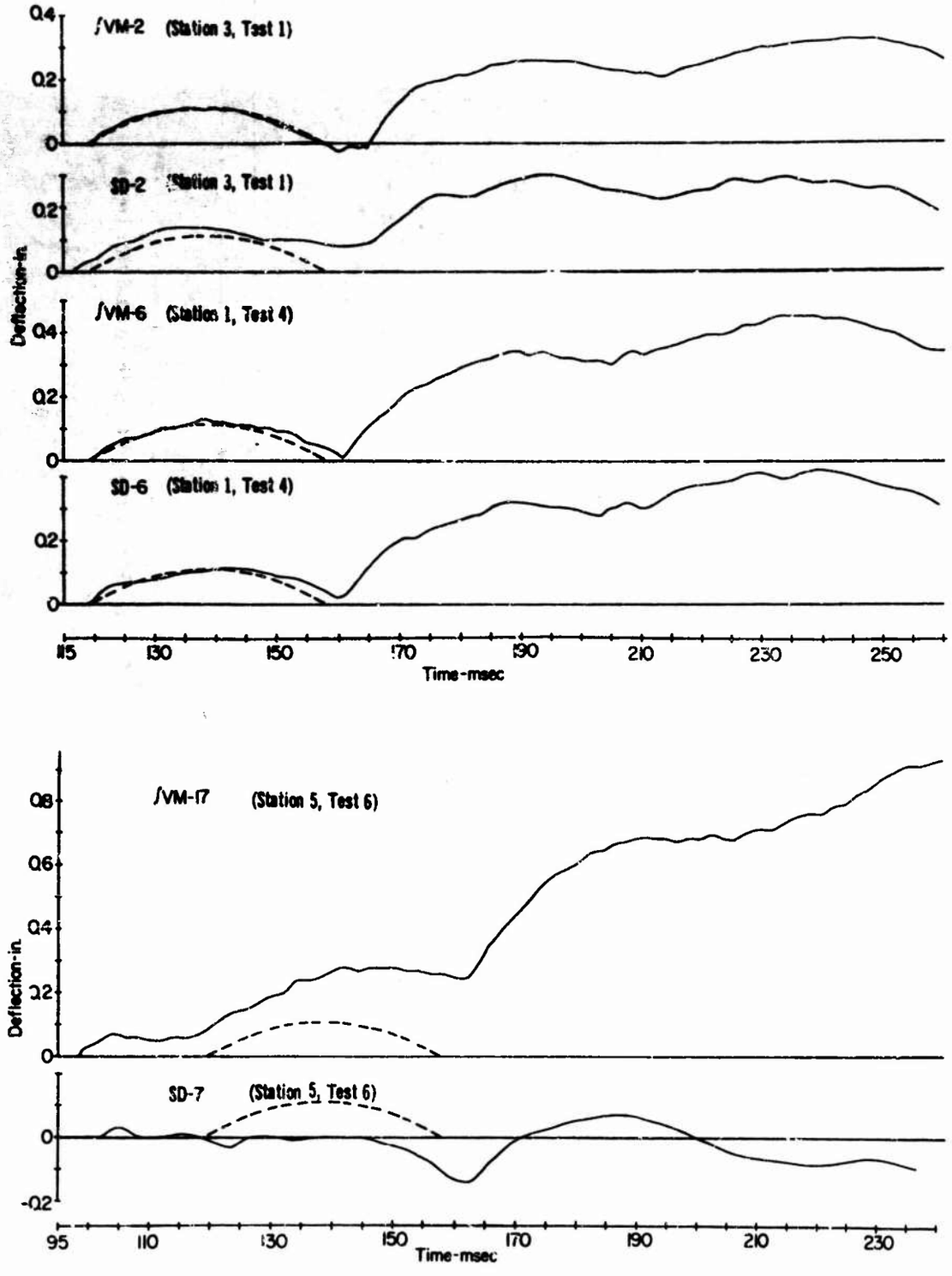

Figure A66 - Displacement Histories - 600-Ft Range from Burst at 50-Ft Depth

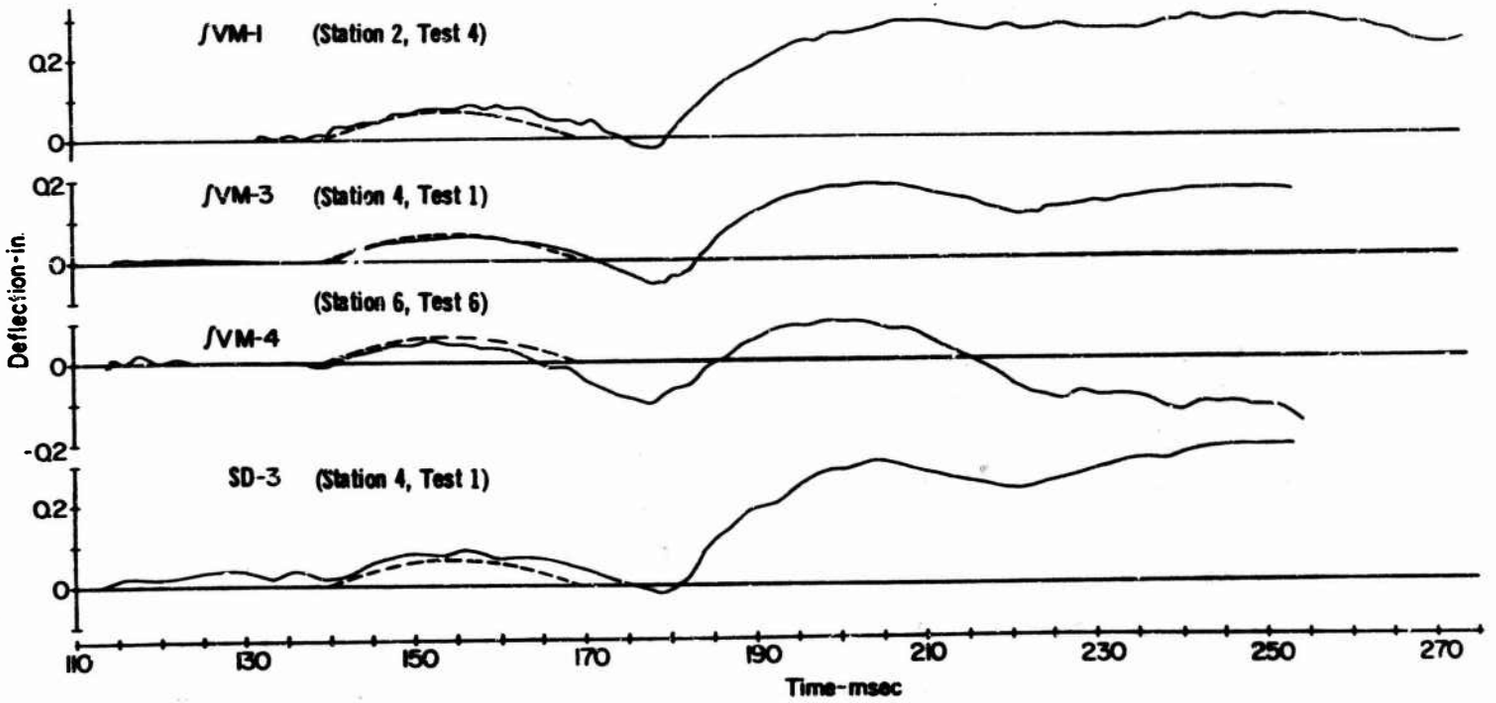

Figure A67 - Displacement Histories - 700-Ft Range from Burst at 50-Ft Depth

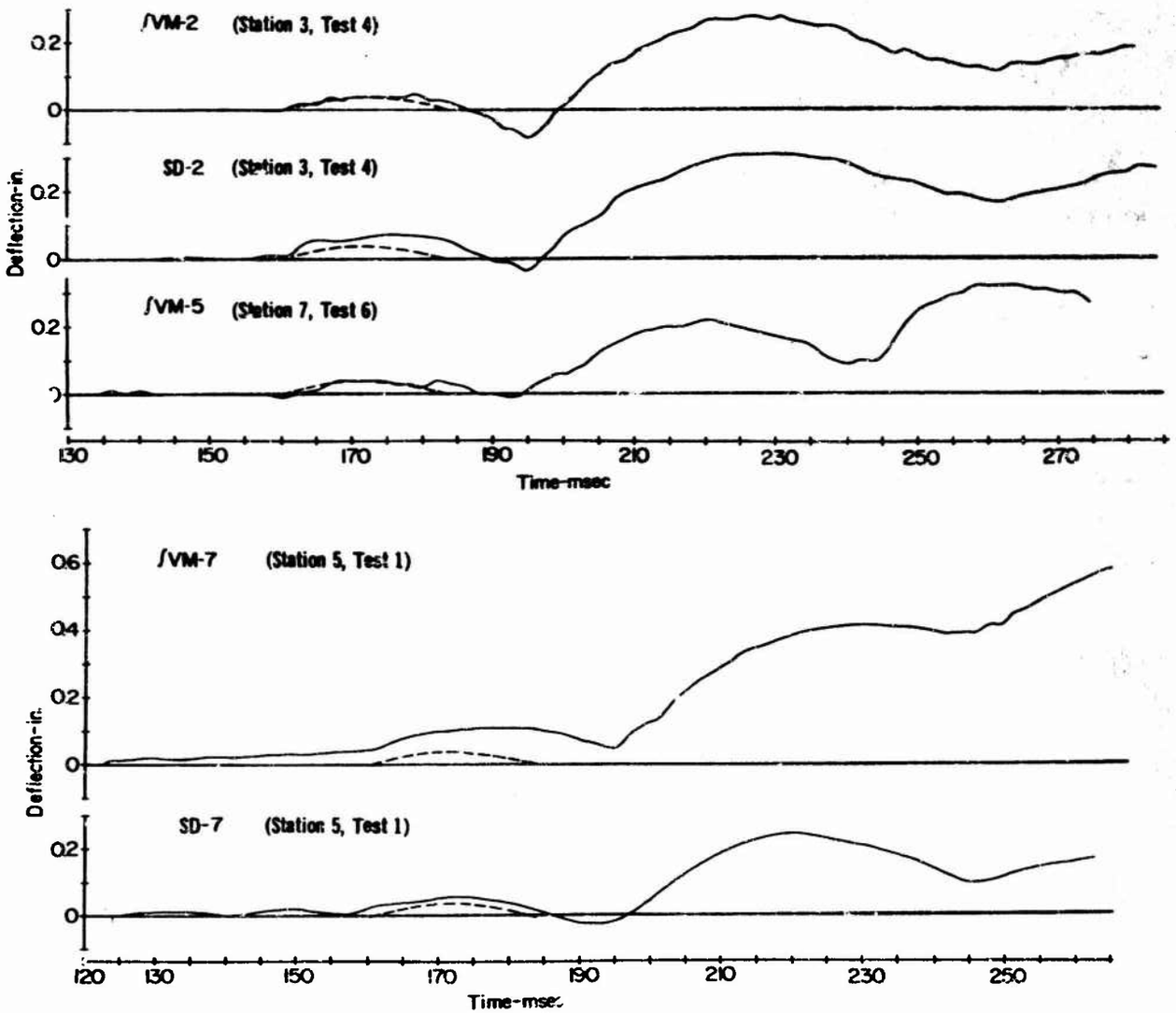

Figure A68 - Displacement Histories - 860-Ft Range from Burst at 50-Ft Depth

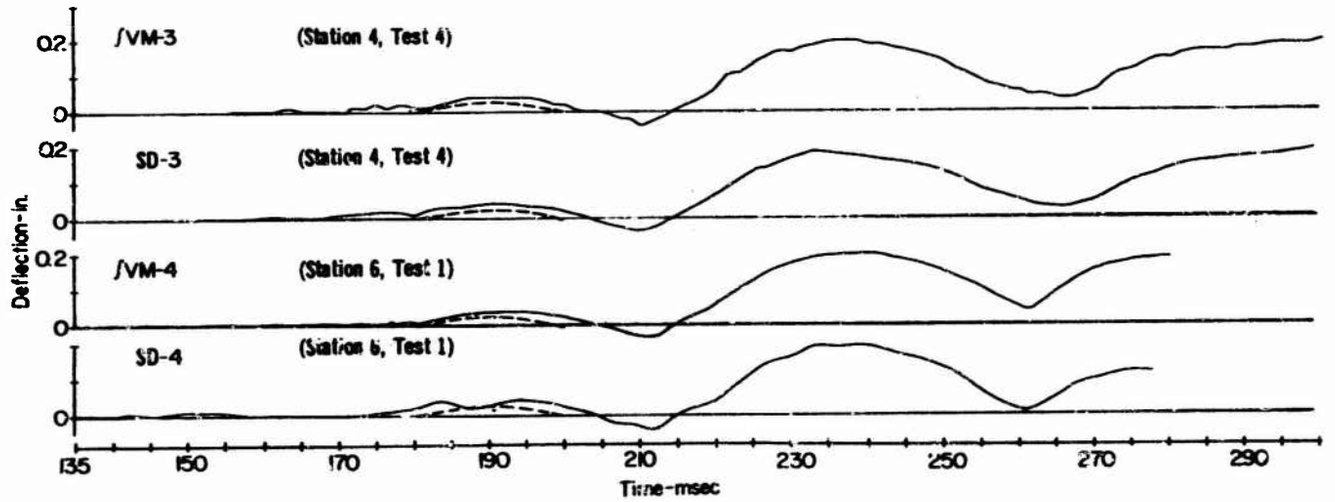

Figure A69 - Displacement Histories - 900-Ft Range from Burst at 50-Ft Depth

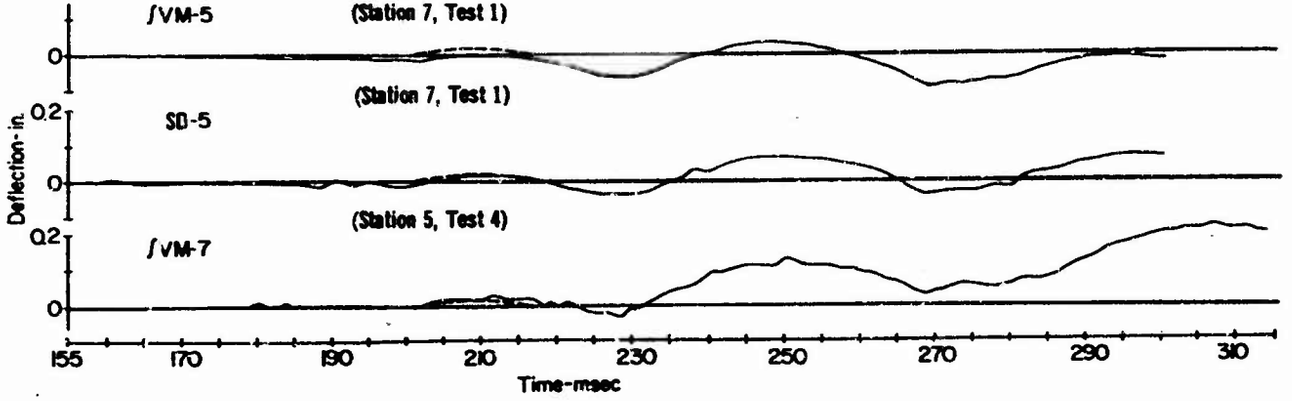

Figure A70 - Displacement Histories - 1000-Ft Range from Burst at 50-Ft Depth

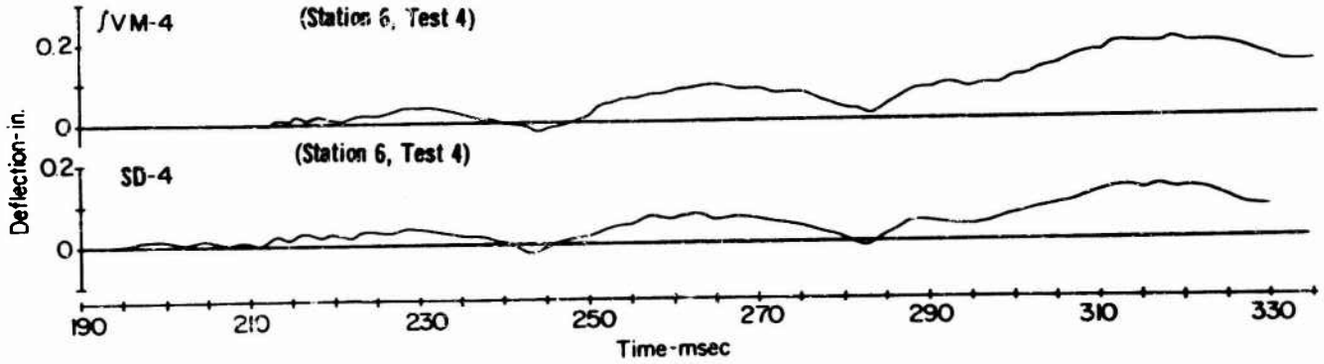

Figure A71 - Displacement Histories - 1100-Ft Range from Burst at 50-Ft Depth

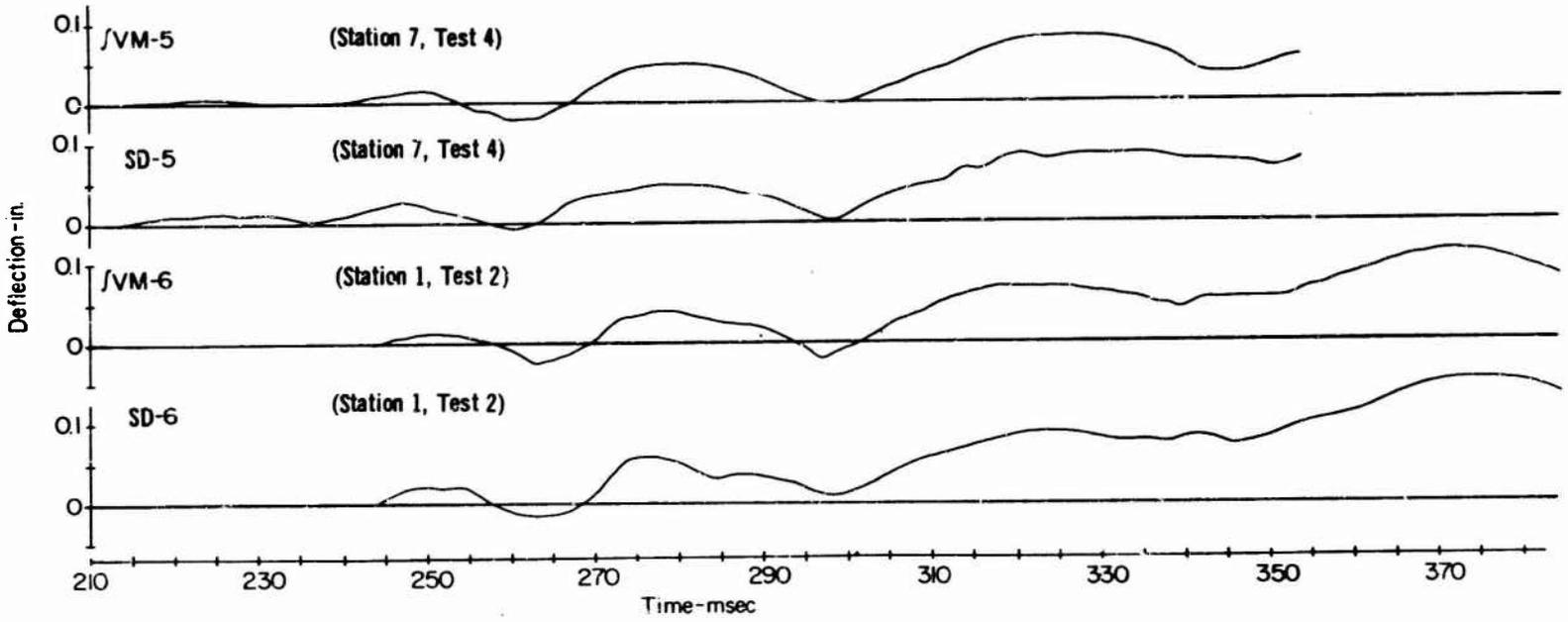

Figure A72 --Displacement Histories - 1200-Ft Range from Burst at 50-Ft Depth

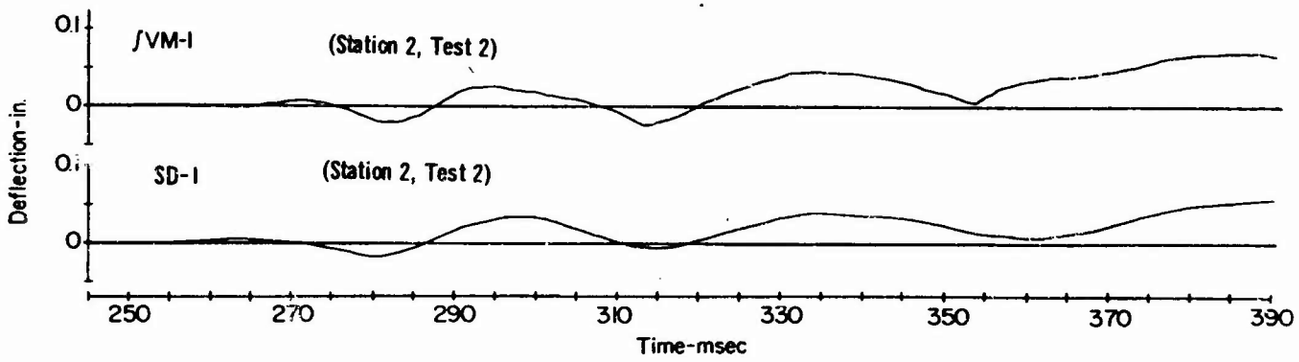

Figure A73 - Displacement Histories - 1300-Ft Range from Burst at 50-Ft Depth

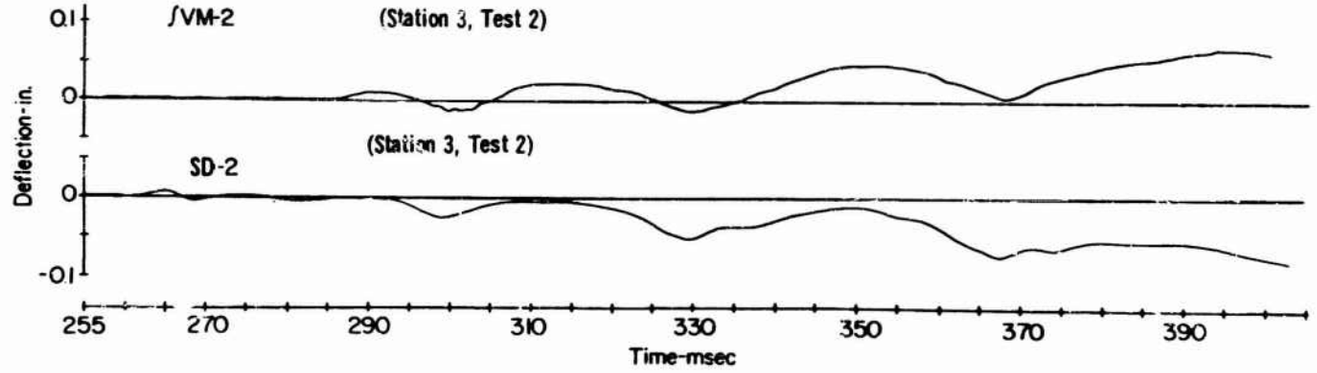

Figure A74 - Displacement Histories - 1400-Ft Range from Burst at 50-Ft Depth

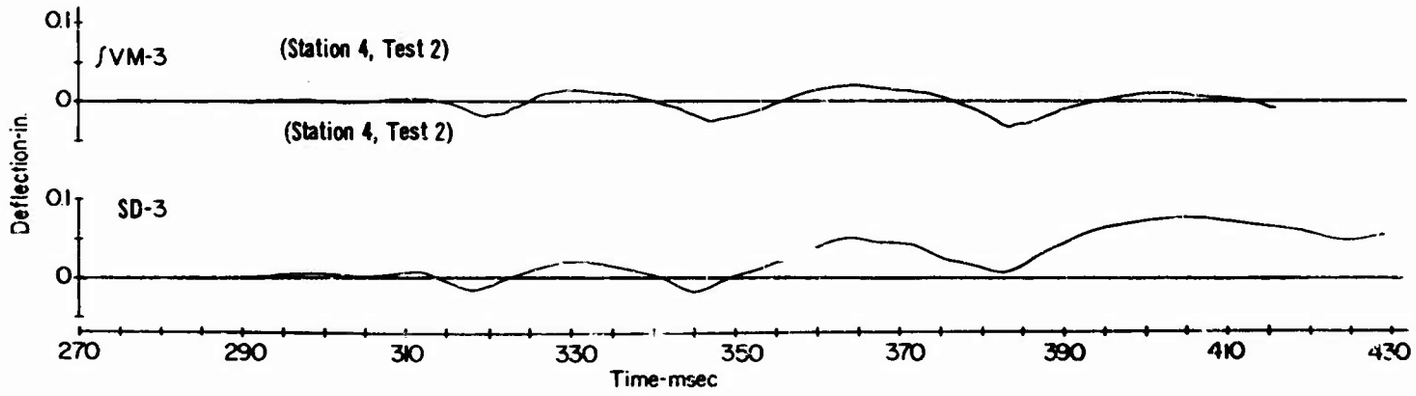

Figure A75 - Displacement Histories - 1500-Ft Range from Burst at 50-Ft Depth

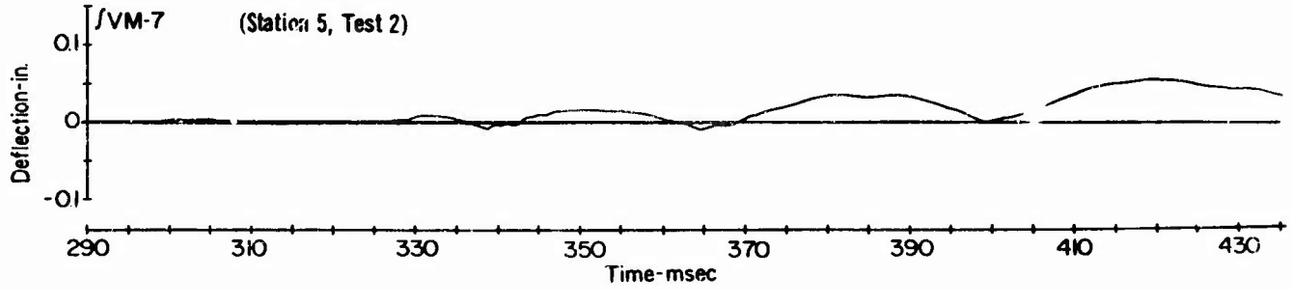

Figure A76 - Displacement History - 1600-Ft Range from Burst at 50-Ft Depth

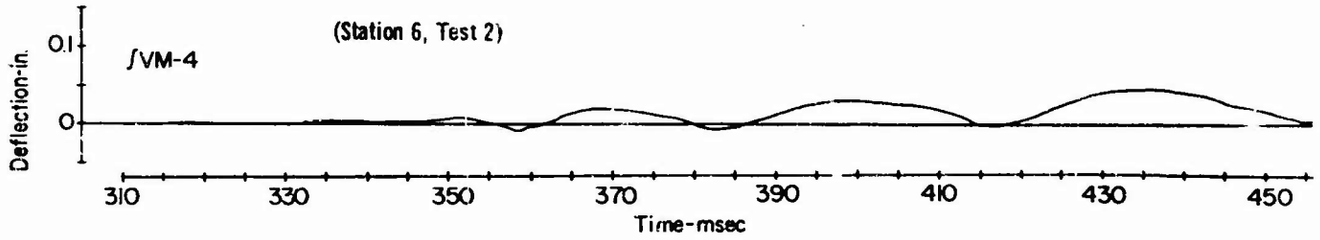

Figure A77 - Displacement History - 1700-Ft Range from Burst at 50-Ft Depth

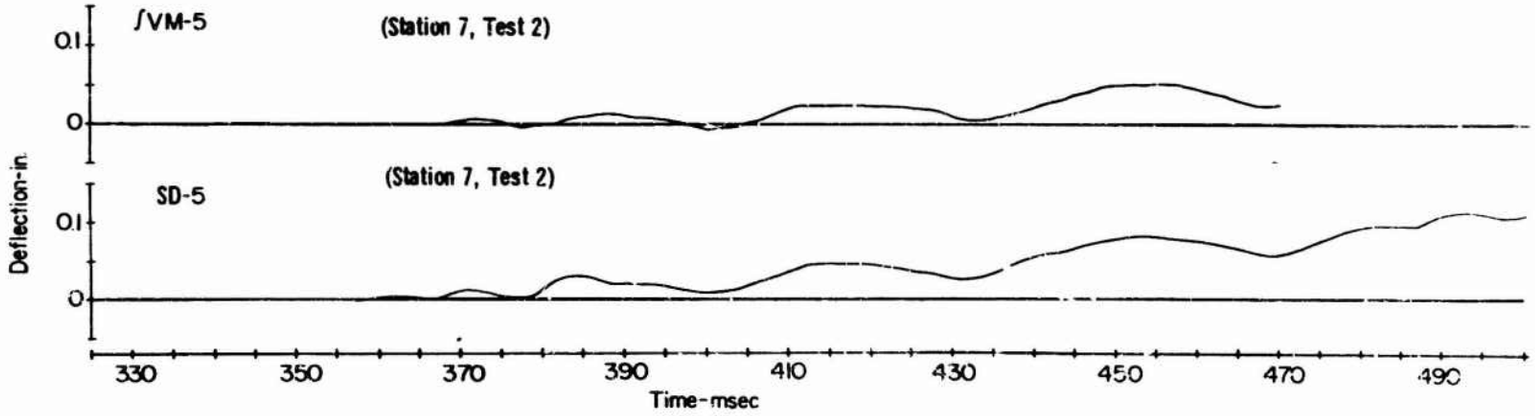

Figure A78 - Displacement Histories - 1800-Ft Range from Burst at 50-Ft Depth

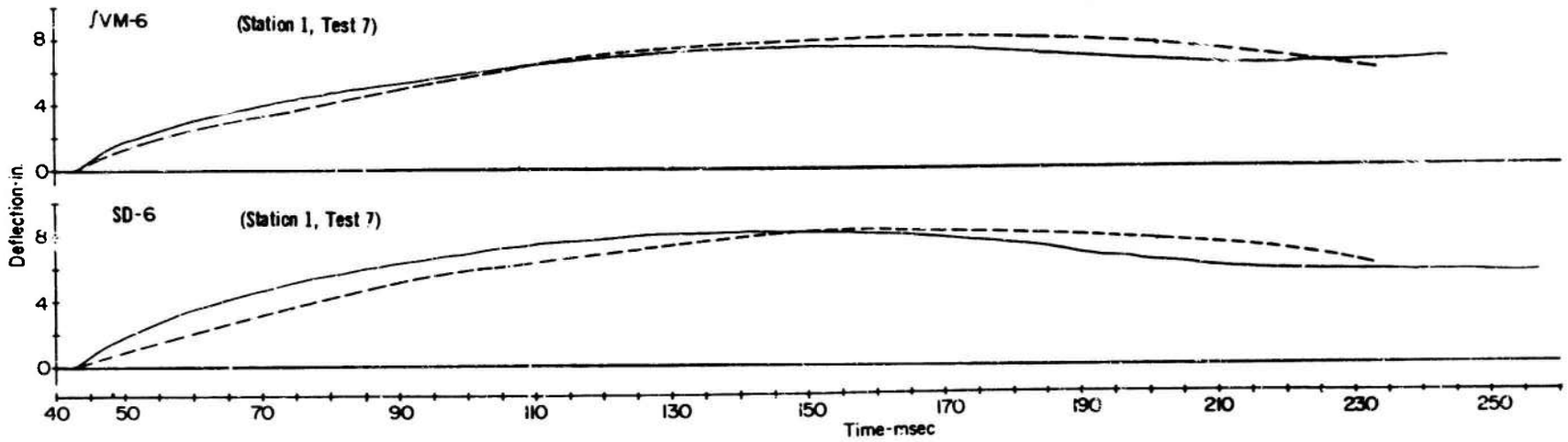

Figure A79 - Displacement Histories - 200-Ft Range from Burst at 100-Ft Depth

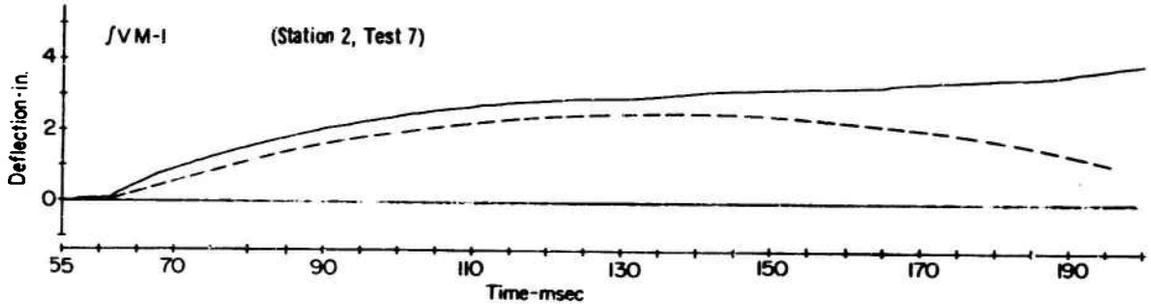

Figure A80 - Displacement Histories - 300-Ft Range from Burst at 100-Ft Depth

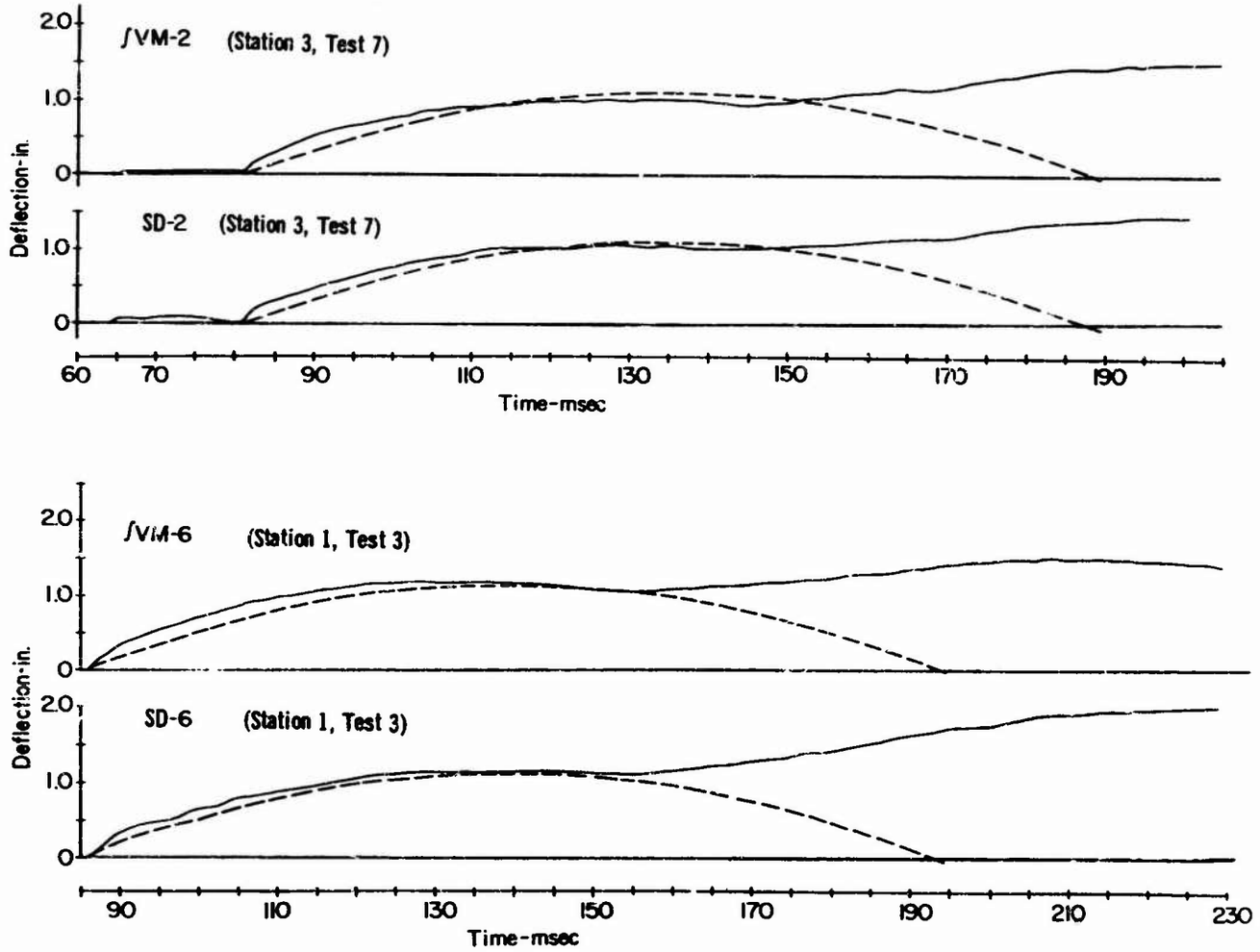

Figure A81 - Displacement Histories - 400-Ft Range from Burst at 100-Ft Depth

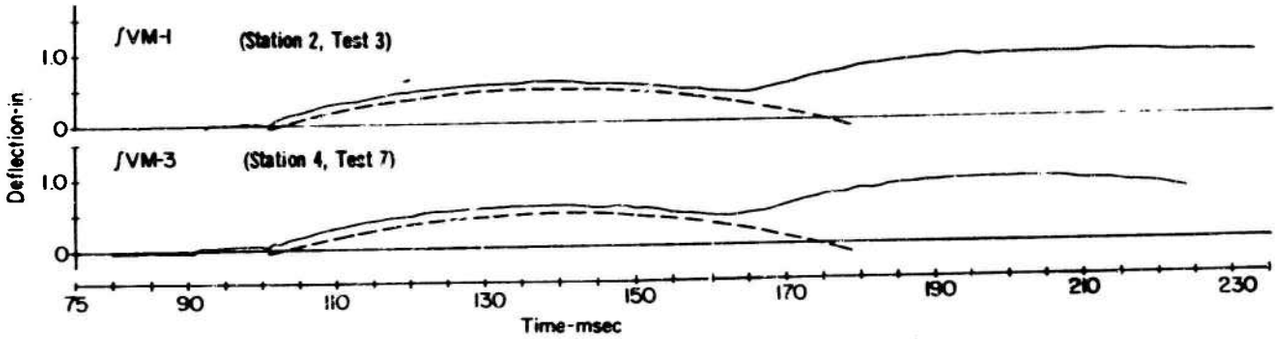

Figure A82 - Displacement Histories - 500-Ft Range from Burst a 100-Ft Depth

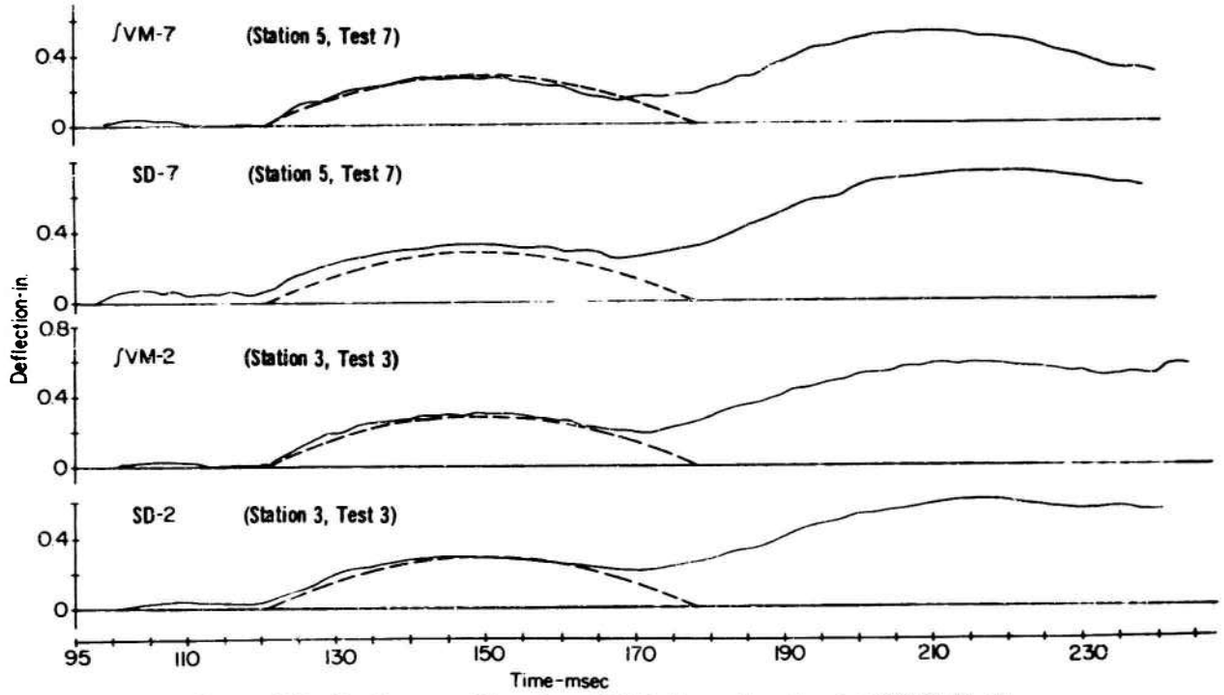

Figure A83 - Displacement Histories - 600-Ft Range from Burst at 100-Ft Depth

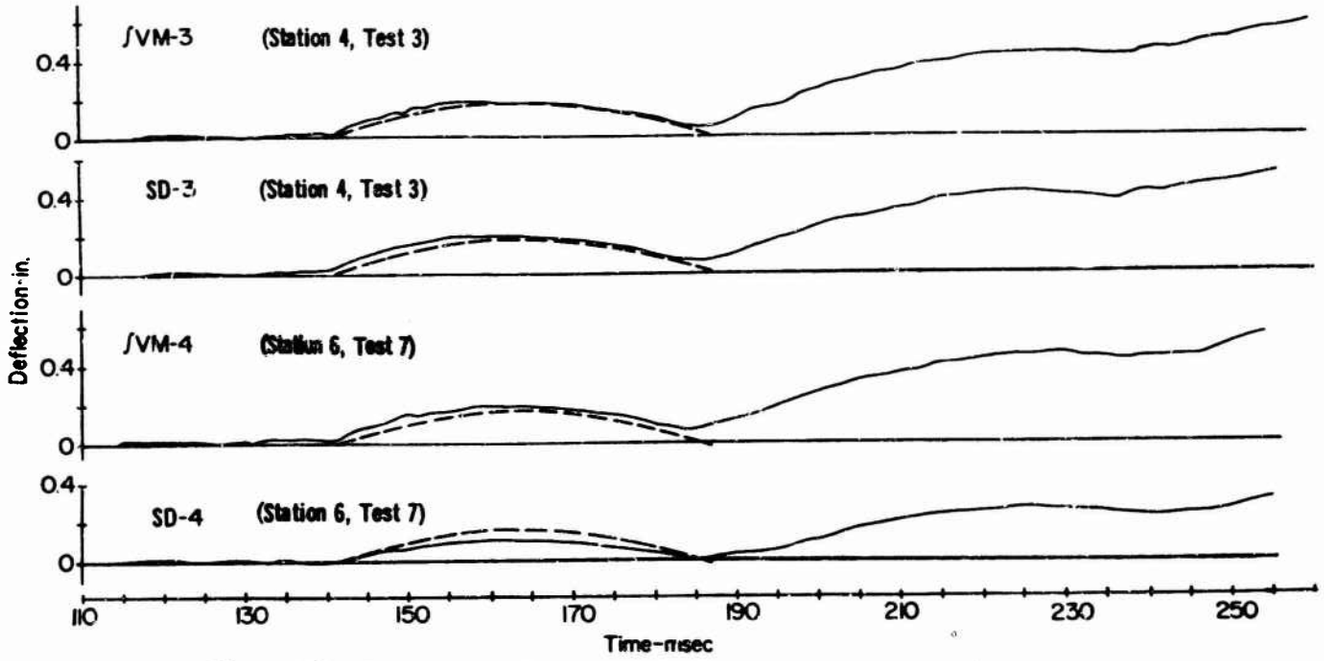

Figure A84 - Displacement Histories - 700-Ft Range from Burst at 100-Ft Depth

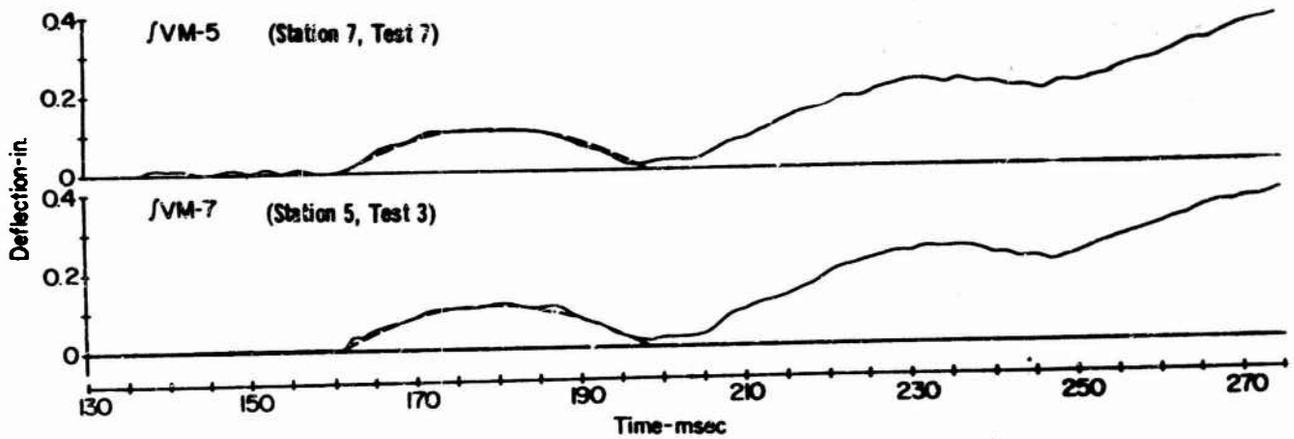

Figure A85 - Displacement Histories - 800-Ft Range from Burst at 100-Ft Depth

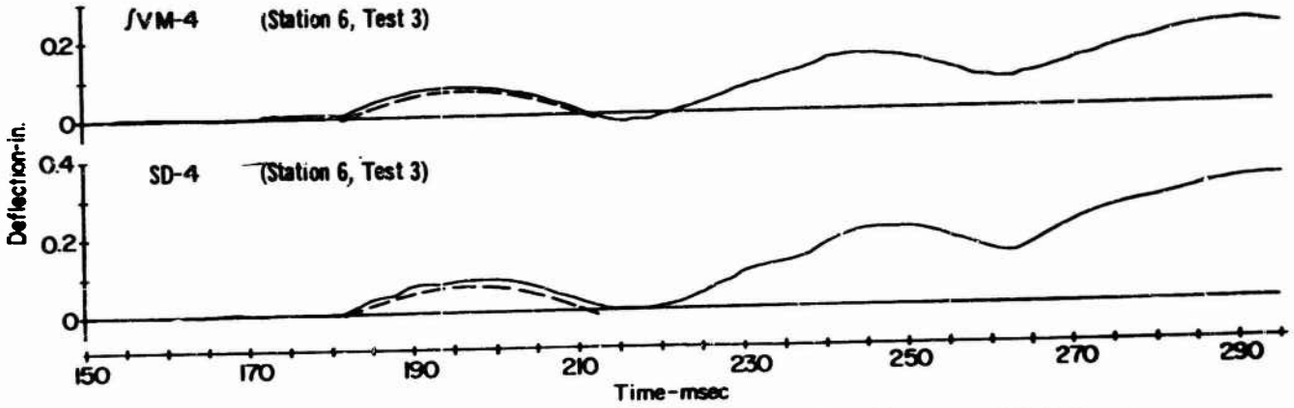

Figure A86 - Displacement Histories - 900-Ft Range from Burst at 100-Ft Depth

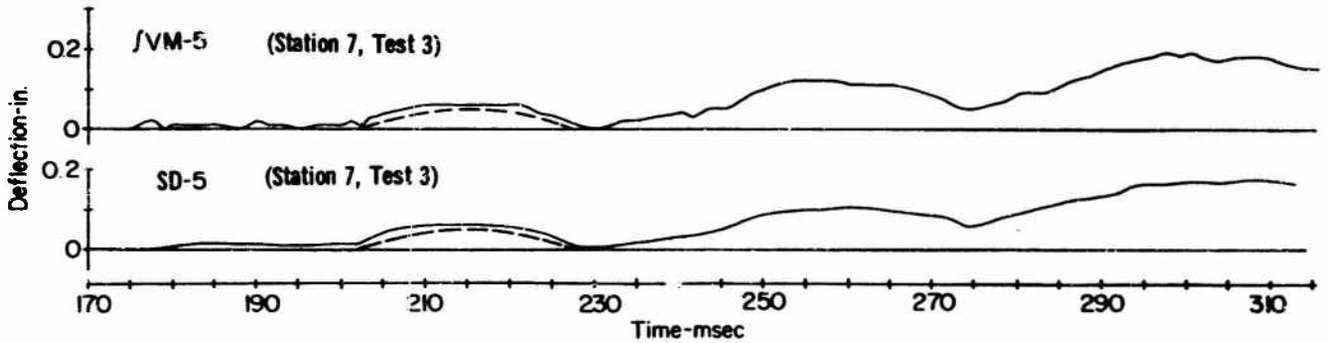

Figure A87 - Displacement Histories - 1000-Ft Range from Burst at 100-Ft Depth

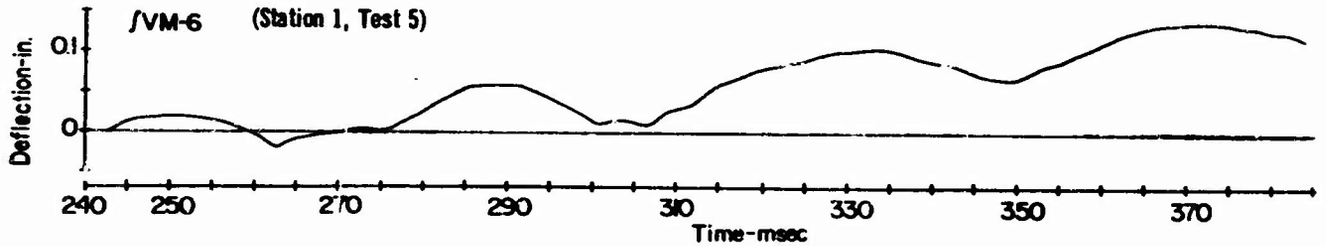

Figure A88 - Displacement History - 1200-Ft Range from Burst at 100-Ft Depth

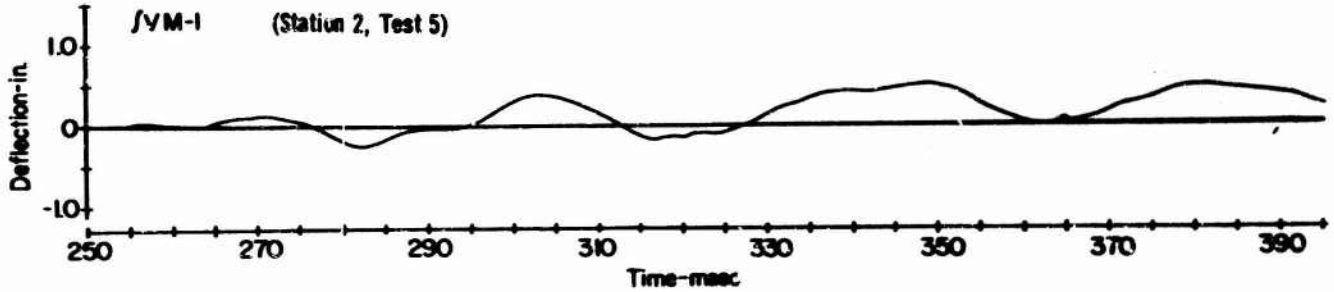

Figure A89 - Displacement History - 1300-Ft Range from Burst at 100-Ft Depth

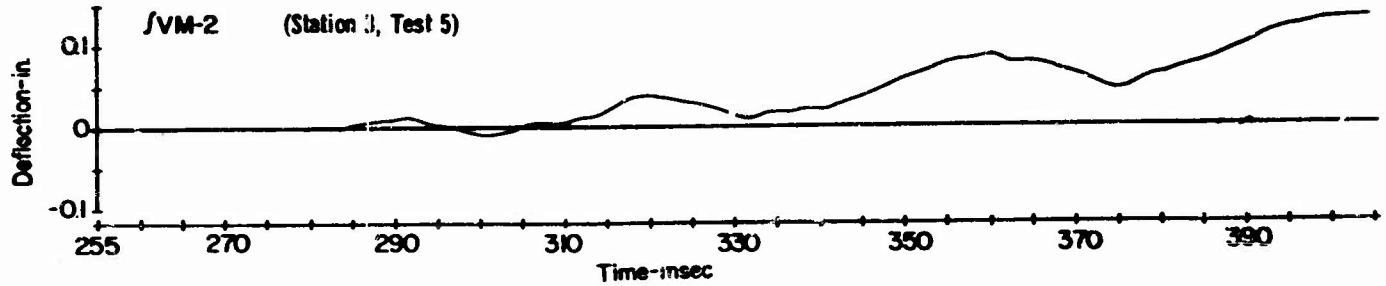

Figure A90 - Displacement History - 1400-Ft Range from Burst at 100-Ft Depth

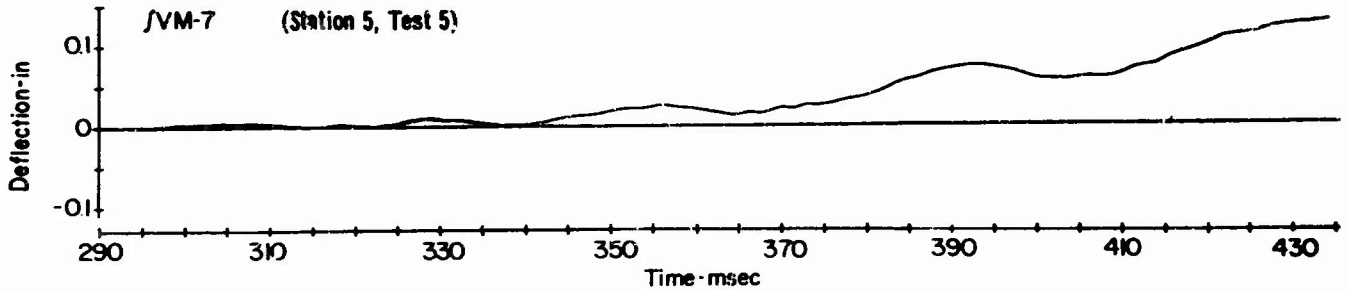

Figure A91 - Displacement History - 1600-Ft Range from Burst at 100-Ft Depth

UNCLASSIFIED
Security Classification

DOCUMENT CONTROL DATA - R&D

(Security classification of title, body of abstract and indexing annotation must be entered when the overall report is classified)

1. ORIGINATING ACTIVITY (Corporate author) Underwater Explosions Research Division David Taylor Model Basin Portsmouth, Virginia	2a. REPORT SECURITY CLASSIFICATION UNCLASSIFIED 2b. GROUP

3. REPORT TITLE

A STUDY OF THE BULK CAVITATION CAUSED BY UNDERWATER EXPLOSIONS

4. DESCRIPTIVE NOTES (Type of report and inclusive dates)

5. AUTHOR(S) (Last name, first name, initial)

Walker, R. R. and Gordon, J. D.

6. REPORT DATE	7a. TOTAL NO. OF PAGES	7b. NO. OF REFS
September 1966	100	3

8a. CONTRACT OR GRANT NO. b. PROJECT NO. DASA Web No. 14.055 c. d.	9a. ORIGINATOR'S REPORT NUMBER(S) 1896 9b. OTHER REPORT NO(S) (Any other numbers that may be assigned this report)

10. AVAILABILITY/LIMITATION NOTICES

DISTRIBUTION OF THIS DOCUMENT IS UNLIMITED.

11. SUPPLEMENTARY NOTES	12. SPONSORING MILITARY ACTIVITY
	Naval Ship Engineering Center, Navy Department Washington, D. C.

13. ABSTRACT

The detailed theoretical models of bulk cavitation derived in studies conducted by the Engineering-Physics Company of Rockville, Maryland, under contract of the Office of Naval Research and bulk cavitation data obtained from tests conducted by the David Taylor Model Basin are used to develop simple calculations for predicting bulk cavitation phenomena. Several reasonable mathematical approximations describing these phenomena are derived. The mathematical treatments have, as a foundation, concepts derived in the theoretical study; however they are modified and simplified in this study where experimental results indicate that such modifications and simplifications are justified. With these approximate mathematical models, estimations can be made of the boundaries, depths and durations of cavitation as well as the motion of the water surface for a wide variety of conditions without employing a computer.

Other findings derived from the experimental test data are: (1) for the closer regions extending even beyond the ring of first impact, the bubble expansion causes the water below the closure depth to rise and thus causes closure to occur at a much earlier time, since the layer does not have to fall to its original position, (2) when the draft of a floating structure is small compared to the thickness of the water layer, the bodily motions of that structure are essentially the same as the water layer, and these motions are relatively independent of the cross sectional shape of the structure; and (3) negative reflections from the bottom strong enough to produce cutoff are quite possible even with relatively large pressure amplitudes, and are capable of considerably modifying the region of cavitation.

DD FORM 1 JAN 64 1473

UNCLASSIFIED
Security Classification

14. KEY WORDS	LINK A		LINK B		LINK C	
	ROLE	WT	ROLE	WT	ROLE	WT
Underwater Explosion - Effects						
Water surface phenomena						
Cavitation process						
Boundaries, bulk cavitation						
Surface velocity						
Surface displacements						
Pressure field						
Theory						
Experiment						

INSTRUCTIONS

1. **ORIGINATING ACTIVITY:** Enter the name and address of the contractor, subcontractor, grantee, Department of Defense activity or other organization *(corporate author)* issuing the report.

2a. **REPORT SECURITY CLASSIFICATION:** Enter the overall security classification of the report. Indicate whether "Restricted Data" is included. Marking is to be in accordance with appropriate security regulations.

2b. **GROUP:** Automatic downgrading is specified in DoD Directive 5200.10 and Armed Forces Industrial Manual. Enter the group number. Also, when applicable, show that optional markings have been used for Group 3 and Group 4 as authorized.

3. **REPORT TITLE:** Enter the complete report title in all capital letters. Titles in all cases should be unclassified. If a meaningful title cannot be selected without classification, show title classification in all capitals in parenthesis immediately following the title.

4. **DESCRIPTIVE NOTES:** If appropriate, enter the type of report, e.g., interim, progress, summary, annual, or final. Give the inclusive dates when a specific reporting period is covered.

5. **AUTHOR(S):** Enter the name(s) of author(s) as shown on or in the report. Enter last name, first name, middle initial. If military, show rank and branch of service. The name of the principal author is an absolute minimum requirement.

6. **REPORT DATE:** Enter the date of the report as day, month, year, or month, year. If more than one date appears on the report, use date of publication.

7a. **TOTAL NUMBER OF PAGES:** The total page count should follow normal pagination procedures. I.e., enter the number of pages containing information.

7b. **NUMBER OF REFERENCES:** Enter the total number of references cited in the report.

8a. **CONTRACT OR GRANT NUMBER:** If appropriate, enter the applicable number of the contract or grant under which the report was written.

8b, 8c, & 8d. **PROJECT NUMBER:** Enter the appropriate military department identification, such as project number, subproject number, system numbers, task number, etc.

9a. **ORIGINATOR'S REPORT NUMBER(S):** Enter the official report number by which the document will be identified and controlled by the originating activity. This number must be unique to this report.

9b. **OTHER REPORT NUMBER(S):** If the report has been assigned any other report numbers *(either by the originator or by the sponsor)*, also enter this number(s).

10. **AVAILABILITY/LIMITATION NOTICES:** Enter any limitations on further dissemination of the report, other than those imposed by security classification, using standard statements such as:

(1) "Qualified requesters may obtain copies of this report from DDC."

(2) "Foreign announcement and dissemination of this report by DDC is not authorized."

(3) "U. S. Government agencies may obtain copies of this report directly from DDC. Other qualified DDC users shall request through _____."

(4) "U. S. military agencies may obtain copies of this report directly from DDC. Other qualified users shall request through _____."

(5) "All distribution of this report is controlled. Qualified DDC users shall request through _____."

If the report has been furnished to the Office of Technical Services, Department of Commerce, for sale to the public, indicate this fact and enter the price, if known.

11. **SUPPLEMENTARY NOTES:** Use for additional explanatory notes.

12. **SPONSORING MILITARY ACTIVITY:** Enter the name of the departmental project office or laboratory sponsoring *(paying for)* the research and development. Include address.

13. **ABSTRACT:** Enter an abstract giving a brief and factual summary of the document indicative of the report, even though it may also appear elsewhere in the body of the technical report. If additional space is required, a continuation sheet shall be attached.

It is highly desirable that the abstract of classified reports be unclassified. Each paragraph of the abstract shall end with an indication of the military security classification of the information in the paragraph, represented as (TS), (S), (C), or (U).

There is no limitation on the length of the abstract. However, the suggested length is from 150 to 225 words.

14. **KEY WORDS:** Key words are technically meaningful terms or short phrases that characterize a report and may be used as index entries for cataloging the report. Key words must be selected so that no security classification is required. Identifiers, such as equipment model designation, trade name, military project code name, geographic location, may be used as key words but will be followed by an indication of technical context. The assignment of links, roles, and weights is optional.